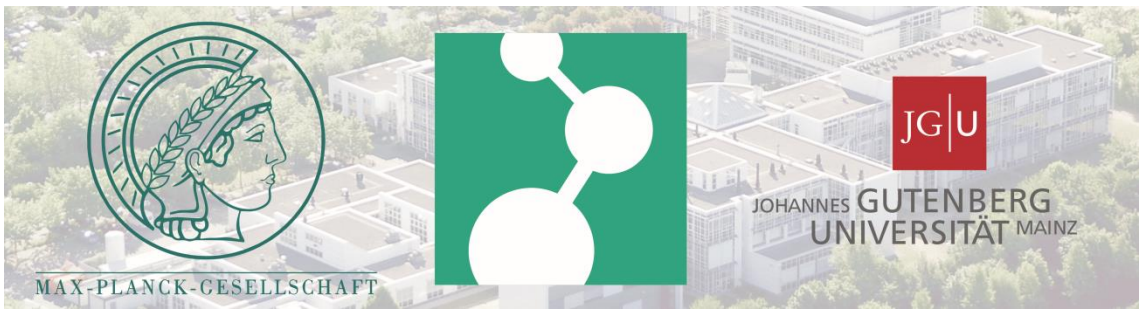

Guanidinium group-bearing polymers as nonviral delivery agents for polynucleotides

Dissertation

zur Erlangung des Grades

„Doktor der Naturwissenschaften“

– Dr. rer. nat. –

im Promotionsfach Chemie

am Fachbereich Chemie, Pharmazie und Geowissenschaften

der Johannes Gutenberg-Universität Mainz

Vorgelegt von Diplom Chemiker

Ilja Tabujew

geb. in Karaganda, Kasachstan

Mainz, 2019

1. Berichterstatter:

2. Berichterstatter:

Tag der mündlichen Prüfung:

Die vorliegende Arbeit wurde in der Zeit von Januar 2014 und August 2018 in der Arbeitsgruppe von Herrn Prof. Dr. Klaus Müllen und unter der Betreuung von Prof. Dr. Kalina Peneva im Max-Planck-Institut für Polymerforschung in Mainz angefertigt.

Ich widme diese Arbeit meinen Eltern

-

Johann und Karoline Tabujew.

Ihr habt mir immer den Rücken gestärkt und mir geholfen, den richtigen Weg zu finden. Für eure liebevolle und tatkräftige Unterstützung werde ich euch mein Leben lang aus tiefstem Herzen dankbar sein.

List of most used abbreviations

ACN	Acetonitrile
APMA	N-(3-Aminopropyl) methacrylamide
AUC	Analytical ultracentrifugation
Boc	tert-butyloxycarbonyl group
CMP	Cytidine monophosphate
CTA	Chain transfer agent
δ	Chemical shift [ppm]
DCM	Dichlormethane
Da	Dalton
DIPEA	N,N-Diisopropylethylamine
DMF	N,N-Dimethylformamide
DMSO	Dimethylsulfoxide
DNA	Deoxyribonucleic acid
DPBS	Dulbecco's phosphate-buffered saline
FCS	Fluorescence correlation spectroscopy
GFP	Green fluorescent protein
GPC	Gel permeation chromatography
GPMA	N-(3-guanidinopropyl) methacrylamide
HPLC	High performance liquid chromatography
HPMA	N-(2-Hydroxypropyl) methacrylamide
IR	Infrared
IC_{50}	half maximal inhibitory concentration
K_d	Dissociation constant
m	Mass
MeOH	Methanol
min	Minute
MST	Microscale thermophoresis
MWCO	molecular weight cut-off
NCL	Native chemical ligation

NHS	N-Hydroxysuccinimide
nm	Nanometer
NMR	Nuclear magnetic resonance
PBS	phosphate-buffered saline
PEG	Polyethylene glycol
Ph	Phenyl
ppm	parts per million
RNA	Ribonucleic acid
R_h	Hydrodynamic radius
R_T	Room temperature
SEC	Size exclusion chromatography
T	Temperature [K]
TLC	Thin-layer chromatography
THF	Tetrahydrofuran
Trp	Tryptophan
UV	Ultra violet
ν	Wave number [cm^{-1}]
z	Charge

Table of contents

1 Introduction

The potential of gene therapy enticed numerous scientists to devote themselves to its research leading up to the postulation by Tatum in 1966, who specified the importance of this treatment approach for the future of medicine.[1] However, the challenges of this field cannot be shouldered by molecular biology alone. The creativity of chemists is required to find solutions to the problematic delivery of genes.

1.1 Gene therapy

The therapy of widespread diseases of our modern society, such as diabetes, cancer and cardiovascular sicknesses, which are either caused or promoted by an unhealthy lifestyle and closely associated with missing, mutated or overexpressed genes, is usually limited to invasive, symptomatic or even chemotherapeutic treatment.[2-4] Addressing a genetic defect would be more advantageous, but it is only possible, if the affected gene can be targeted specifically.[5] The idea of treating genetic disorders by regulating the transcription or translation of genes inside of pathogenic cells was developed half a century ago and it can be accredited to the works of Griffith[6] (1928), Avery *et al.*[7] (1943) and Zinder *et al.*[8] (1952), who were able to identify mechanisms for gene transfer even before the DNA molecule was identified as the carrier of our genetic information.[9, 10] This initial theory was proven applicable by the first human gene transfer into tumor-infiltrating lymphocytes in 1989.[11] In the following year, the first clinically reported gene therapy was performed, in which the transfer of functional genes via a viral carrier helped to successfully combat adenosine deaminase deficiency.[12] Additional support was obtained during the simultaneously performed clinical trial, in which patients with advanced melanoma were treated by using the same method.[11] Due to this early success, the tremendous potential of gene therapy, which offers treatment for AIDS, cancer or other diseases that are associated with a derailed gene expression, was vastly recognized, research was stimulated, and numerous formulations were tested clinically in regard to their ability to combat lung cancer[13], brain tumors[14], sarcoma[15] or ovarian carcinoma[16].[17] However, human gene therapy is currently limited to somatic cells, since the use of germlines is ethically forbidden. Polynucleotides can be utilized in different ways to achieve a therapeutic effect. Depending on their structure, they can either promote the expression of a certain gene or inhibit its translation (Figure 1.1). If endogenous genes are poorly, wrongly or even not at all expressed due to inherited or ac-

quired defects, it is possible to treat the resultant condition of the patient by using gene therapy.[18] Double stranded DNA (dsDNA), such as plasmid DNA molecules (pDNA), which are usually 100 to 1000 base pairs long and include not only the therapeutic gene, but also their own promoters and enhancers for transcription, can be utilized to combat monogenetic disorders.[19] The introduction of these external genes into the nucleus leads to autonomous extrachromosomal transcription and translation of the therapeutic gene, which alleviates the effects of the disorder.[20] Overexpressed genes, on the other hand, represent an equally important group of disorders, but they need to be addressed by inhibiting their translation. This approach relies on reducing the concentration of messenger RNA molecules (mRNA), which play a crucial role in the bio-synthesis of proteins. The RNA interference pathway (RNAi), which relies on small interfering RNA molecules (siRNA), can be utilized for that purpose. Other RNA structures, such as short hairpin RNA (shRNA) or micro RNA (miRNA), can trigger this pathway as well. shRNA is a single stranded RNA molecule (ssRNA), but it contains self-complementary ends of 25 to 29 base pairs, which are separated by loop region of 4 to 23 base pairs. The endoribonuclease Dicer removes the loop region in the catosol leaving a fully functional siRNA molecule. The single stranded miRNA, on the other hand, does not require further processing inside the cell. These RNA molecules are 20 to 24 base pairs long and their whole sequence is complementary to the targeted mRNA. Hence, they can be directly utilized for the RNAi pathway.

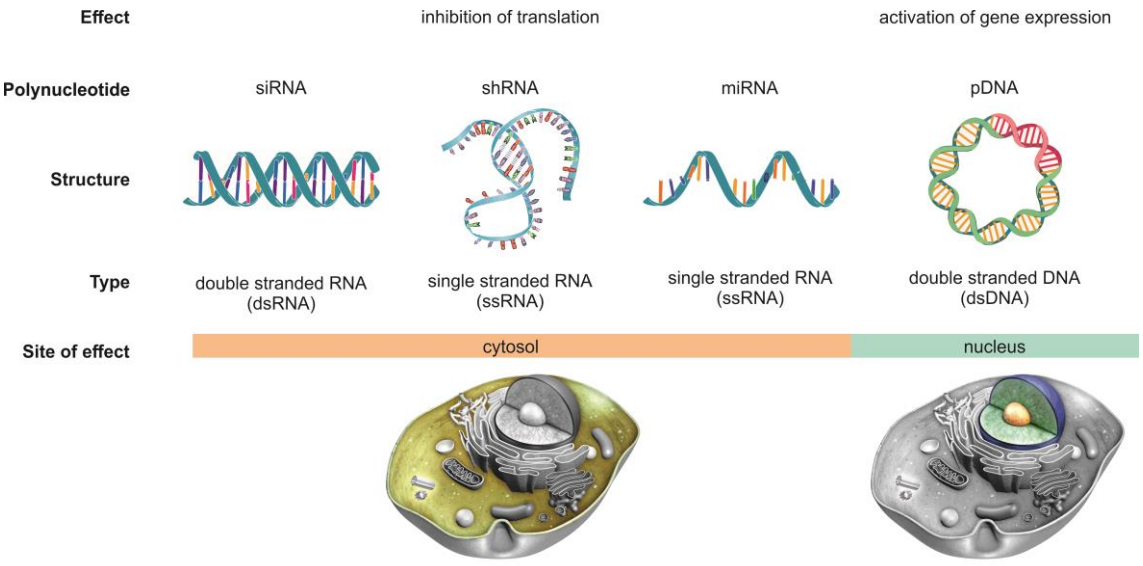

Figure 1.1 Differences of therapeutic polynucleotides

Although this approach of treating otherwise incurable diseases has high potential, the successful utilization of gene therapy remains a great challenge in modern medicine. The large, negatively charged RNA and DNA molecules, which cannot bypass cellular membranes by themselves and are quickly degraded inside a patient's body due to ubiquitous nucleases (RNase, DNase), must be introduced into cells without affecting their intended activity. In addition, the successful application of gene therapy also requires not only concerted, but also directed transfection of a large number of cells (e.g. a certain tissue or an organ). Delivering the cargo into the wrong cells could lead to an acute health risk for the patient (short term) or even affect his progeny, if the therapeutic gene were to be incorporated into a patient's germline (long term). These reasons make the search for safe and efficient delivery system necessary. For the successful implementation of gene therapy a number of requirements must be fulfilled. Besides (1) the protection of the transgene against breakdown by nucleases and (2) the successful transport of RNA or DNA into the right cell, other challenges must be met, which encompass not only (3) biocompatibility by minimizing interactions with blood constituents, but also (4) an efficient intracellular release in the appropriate cellular compartment (e.g. cytosol or nucleus).[21, 22]

The known methods for gene transfer are classified into two principal groups: viral and nonviral. The nonviral approach can be further differentiated into physical- and chemical methods.[23] Physical methods such as electroporation, sonoporation, gene gun and microinjection rely on mechanical, electrical, ultrasonic, hydrodynamic, or laser-based energy to penetrate the cell membrane. They are often employed to transfect cells, but they lead to poor results due to reduced cellular viability and inconsistent transfection efficacy.[24] They also offer limited opportunity for in vivo applications, since these methods require isolated cells.[25]

Hence, viral and chemical delivery systems, which are also sometimes referred to as viral or chemical vectors, are preferably used for transfection experiments. Both possess innate advantages and disadvantages. Viral vectors, for example, are more potent in terms of transfection efficacy, but although they have been made safer by deleting some areas of their genomes to derange their replication, they retain their marked immunogenicity that activates the inflammatory system leading to the degeneration of treated tissue. The continued toxin production and possible insertional mutagenesis of the host genome are additional problems hampering their applicability.[26-28] Chemical vectors, such as cationic polymers, on the other hand, are a versatile platform for the design of

carrier systems, where the properties of the vector can be tuned to match the demands of the system. This approach relies on the formation of complexes due to electrostatic interactions between the negatively charged nucleic acid and polycationic nanomeric particles. If the complex is formed between a polynucleotide and a polymer, which was designed as a delivery agent for gene therapy, it is often referred to as a polyplex. Complexes between chemical delivery agents and polynucleotides, in comparison to viral vectors, offer longer shelf life as well as improved biocompatibility, due to their reduced toxicity and antigenicity, but are usually less efficient transfecting agents.[29] The versatility of these cationic scaffolds, however, offers numerous opportunities to overcome this limitation. For example the covalent modification with cell-targeting ligands, such as antibodies, small chemical compounds, peptides or carbohydrates has been shown to enhance the uptake by a large margin.[30]

1.2 Gene silencing via RNA interference

RNA interference (RNAi) is a cellular mechanism, which allows the degradation of specific messenger RNA molecules (mRNA), thereby decreasing the synthesis of the encoded protein.[31] It was discovered by chance through the injection of double stranded RNA (dsRNA) into living cells of *C. elegans*, which prohibited the translation of complementary mRNA sequences.[32] Since then, RNAi has been further elucidated as a method to regulate gene expression, making it a valuable tool for biomedical research and the treatment of genetic disorders.[33]

1.2.1 Mechanism of RNA interferance

The translation of genes is regulated *via* RNAi in most organisms. Nevertheless, differences in its effectiveness exist. Mammals, for example, possess a less responsive RNAi apparatus in comparison to organisms with short lifespans, such as C. elegans, a free-living transparent nematode.[34] However, the underlying mechanism, an intracellular multistep process, is similar (Figure 1.2).[35] Initially, transcribed or introduced dsRNA is cleaved by the endoribonuclease Dicer into shorter chains with a length of approximately 20 to 25 base pairs. These fragments with a typical two-base overhang on the 3' end are called small interfering RNA (siRNA).[36] The size of the siRNA, which is generated in this fashion, depends on the distance between the RNA molecule and the polynucleotide interacting PAZ domain of the Dicer enzyme. Following this initial step of RNAi, the RNA induced silencing complex (RISC) is formed. Here, a siRNA molecule

enters the preformed multi-protein cluster of the RISC, where it is not only bound, but also unwound by a RNA helicase into single strands. One of the strands is further degraded into oligonucleotides and discarded (passenger strand), while the other siRNA strand (guide strand) is retained.[37] The guide strand is then utilized as a selective sensor for a complementary mRNA sequence, which is then bound and degraded by the RISC.[38] The selective degradation of mRNA and the resulting decrease in the expression of the target protein, which is coded on a certain gene, is often referred to as "gene silencing".

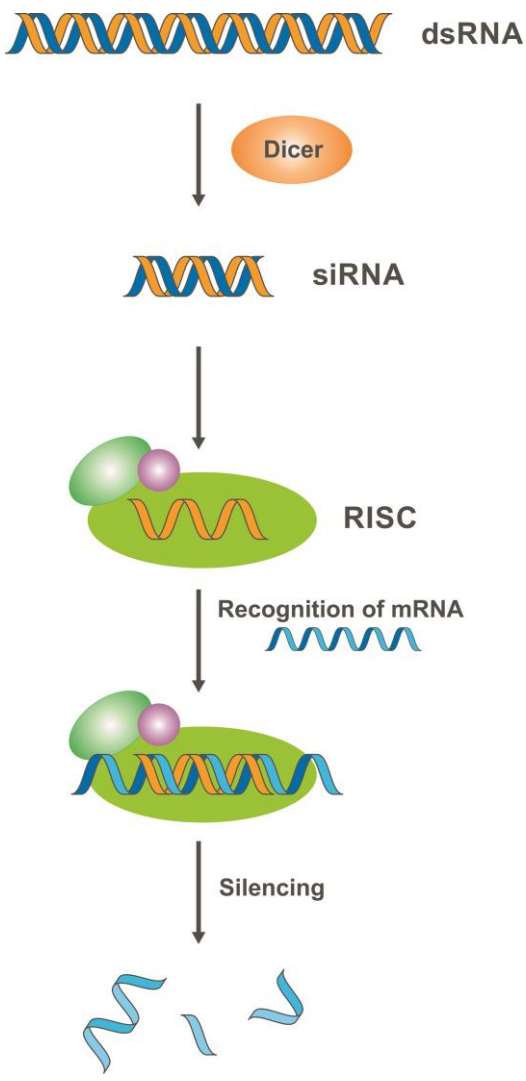

Figure 1.2. Mechanism of the RNA interference

The discovery of RNAi encouraged the frequent use of dsRNAs in research to silence specific genes.[39] However, it was shown that long dsRNA molecules induce not only the RNAi pathway. They also stimulate the production of type 1 interferon (IFN) and,

as a consequence, the expression of IFN-related genes, which regulate the immune system.[40] To avoid the risks posed by dsRNA, small interfering RNA (siRNA) is commonly utilized as its replacement.[41] Since the much shorter siRNA, which is a double stranded RNA molecule with a length of only 21 to 27 base pairs equaling a molecular weight of about 13.5 kDa, enters the RNAi pathway unhindered at a later stage of RNAi by skipping the degradation step by the endoribonuclease Dicer. Hence, adverse side effects associated with dsRNA can be avoided.[42] Another advantage of this approach is that naturally occurring siRNA sequences allow a more consistent and predictable activation of the RNAi pathway. Nevertheless, utilizing siRNA for therapeutic purposes offers a variety of challenges that need to be met. siRNA is highly prone to degradation by ubiquitous nucleases, which leads to short half-life times. Its sensitivity towards hydrolysis is much higher than that of DNA due to its rod-like character, short length, and the additional hydrodyl group of its backbone compound ribose.[43] An additional problem of siRNA is its inability to cross cellular membranes without the use of delivery systems. This characteristic is retained from dsRNA and DNA due to its polyanionic nature, although siRNA molecules possess substantially shorter base pair sequences.[44, 45]

Hence, to tap the full therapeutic potential of siRNA as tools for the silencing a desired protein by pre-translational destruction of the respective mRNA, efficient delivery systems are required.[46, 47] Although many attempts for a safe and efficient delivery of the siRNA have been made, a convincing carrier system, which fulfills all requirements of siRNA delivery, remains to be found.[48] These requirements include: a) water solubility, b) strong affinity towards siRNA to ensure complexation, c) protection against enzymatic degradation, d) ability to bypass plasma membranes, and e) biocompatibility. To promote efficient gene silencing, carrier systems should f) be also equipped with the ability to target specific cells, g) possess a lysosome- or endosome escape mechanism, and h) be able to not only efficiently bind siRNA, but also release it in the cytosol.

1.3 Polymers for polynucleotide delivery

Following the introduction of the concept of gene delivery in 1963 and the first human gene therapy trials in 1989, research was hampered due to the observed adverse side effects of virus-based delivery agents.[49] Since then, cationic polymers, such as poly(dimethylaminoethyl methacrylate) (PDMAEMA)[50-52], poly(L-lysine) (PLL)[53-55], chitosan[56-58] and polyethylenimine (PEI)[59-61] (Figure 1.3) became popular in the de-

sign of polynucleotide delivery agents, since their properties can be tailored to address the issues of this challenging application.

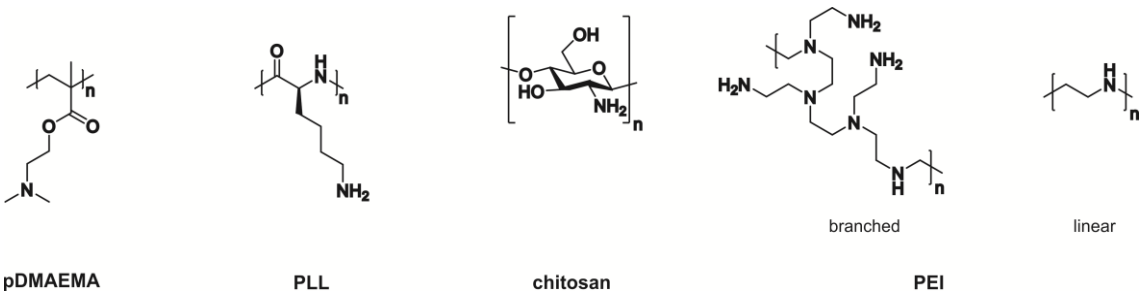

Figure 1.3. Polymers commonly applied in the delivery of polynucleotides

The idea of using cationic polymers for that purpose was first introduced by Wu and Wu in 1987.[62] They utilized PLL to transport plasmid DNA into living cells. Several years later, in 1995, Behr *et al.* unveiled the utility of PEI as a transfection agent.[63] Prompted by the initial success, a variety of linear and branched cationic polymers were researched. However, PLL and PEI remain the most widely studied cationic polymers. Correlations between the length of the polymers and the transfection efficacy as well as the toxicity have been found.[64-66] In addition, modification strategies have been developed to overcome the encountered challenges, such as the aggregation with serum proteins, which are caused by non-specific polymer-protein interactions. They can be avoided by covalently functionalizing the polyplexes with, e.g., polyethylene glycol (PEG) chains, which is often referred to as PEGylation.[67] This strategy, however, was shown to affect the gene delivery efficacy of cationic polymers by decreasing their ability to bypass cellular membranes, by reducing the proton sponge effect, which impacted endosomal escape as well as the release of the cargo.[68] Another challenge are the poor transition properties across plasma membranes, which can be addressed by utilizing targeting vectors and by attaching receptor binding motifs.[69, 70] In spite of the advances in the design of such carrier systems, the development of successful nonviral delivery agents for *in vivo* applications is still in its adolescence and more efforts are needed. Nevertheless, the success of recent clinical studies bolstered optimism in this field of research and ratified the efforts of the last 30 years.[71-73]

Polymeric carriers, which bear positive charges for the reversible formation of polyplexes with negatively charged nucleic acids, are a versatile platform for gene delivery,

where the properties of the vector can be tuned to match the demands of the system.[64] Strong binding, i.e. strong electrostatic interactions between the polynucleotide and a polymer, and stable complexes can be promoted by using varying polymer architectures, which, in the present case, relates to different ways to arrange monomers with the ability to bear cationic charges. High local cationic charge densities can be achieved in, for example, block copolymers[74-76], stars[77] or comb-shaped structures[78]. Using statistical or even alternating copolymers, on the other hand, facilitates a more even distribution. Block copolymers are particularly efficient in forming non-immunogenic polyplexes. Here, the cationic block will interact electrostatically with the polyanion enabling the formation of a complex, whereas the second block will form a hydrophilic outer layer. This characteristic core-shell structure endows the polyplex with a high colloidal stability and reduced interaction with blood components, which are the major advantages of a micellar DNA delivery system for in vivo application.[79]

1.4 Reversible addition-fragmentation chain transfer polymerization (RAFT)

Polymethacrylamides and polymethacrylates, such as pDMAEMA, are of similar importance as PLL or PEI in the search for the ideal gene delivery agent, but their utility was initially hindered by the drawbacks of the free radical polymerization, which was mainly employed for their synthesis.[80, 81] Polymers usually face challenges in pharmaceutical applications, because they are synthesized with an inherently heterogeneous weight distribution. This shortcoming is further emphasized, if the polymerization method does not provide sufficient control. However, using living polymerization techniques, where the kinetics for chain growth termination are negligible and the initiation rate is much larger than the rate of chain propagation, has, for the longest time, been the orthodox choice to obtain precise polymer structures. Similarly, it has been chosen to utilize reversible addition-fragmentation chain transfer polymerization (RAFT) as the polymerization technique for all polymers this thesis.

Anionic-, cationic- and the ring-opening metathesis polymerization have been shown to provide excellent control, however, they require demanding reaction conditions and offer only a limited monomer selection due to their intolerance of functional groups, such as hydroxyls or amines. Protective groups can be employed to widen the amount of available monomers, but the concomitant deprotection step can lead to unwanted side reactions.[82] Controlled radical polymerization (CRP) techniques, on the other hand,

provide an attractive alternative for the synthesis of functional polymethacrylamides and polymethacrylates.[83-86] The CRPs have branched into three fundamental techniques: atom transfer radical polymerization (ATRP), nitroxide-mediated polymerization (NMP) and RAFT. Among these techniques RAFT, which is a reversible deactivation radical polymerization, is recognized for its versatility, because of its capability to provide living characteristics to the radical propagation of a large variety of unprotected vinyl-based monomers under mild conditions.[87] It is not affected by charges or by functional groups such as primary amines[88-92], thiols[93, 94], hydroxy-groups[95-97] or even activated esters[98-102]. Other advantages of RAFT include its compatibility with a wide variety of reaction conditions, since it can be applied for bulk-, suspension-, emulsion-, mini-emulsion polymerizations due to its high tolerance for both organic as well as aqueous media.[103] An additional benefit of utilizing RAFT polymerizations for the synthesis of medically applied polymers is avoiding the use of transition metals, which limits the applicability of ATRP. Hence, RAFT is among the best choices to synthesize DNA/RNA carriers with precise architectures, predetermined structopendant or -terminal functionalities, and narrow molecular weight distributions. These numerous advantages of the RAFT polymerization make it a potent technique for the design of gene delivery and –silencing agents, which lead to a significant increase of RAFT-synthesized polymers for therapeutic applications.[104-108] Although predominantly linear copolymer structures (statistical or block copolymers) remain the focus for DNA and siRNA delivery applications, other polymer architectures have been tested as well. For example, Konkolewicz *et al.*[109] and Tao *et al.*[110] were the first to report the utility of hyperbranched RAFT-synthesized polymers as delivery agents for DNA. Core-shell nanoparticles carrying siRNA cargo were prepared by Siegwart et al.[111] Nuhn et al. synthesized covalently stabilized cationic nanohydrogel particles, which were shown to possess favorable properties as a delivery system for gene silencing.[112]

1.4.1.1 The process of the RAFT polymerization

RAFT was first introduced as a controlled radical polymerization technique in 1998.[113] Since then, its versatility elicited intensive research elucidating specific applications and features. These include, for example, descriptive properties, such as the kinetics and the mechanism of RAFT[114, 115] or the control of the molecular weight distribution[116], but also application focused information have been gained in regard to RAFT polymerization in aqueous[117] or heterogeneous[118] media and the synthesis of differently struc-

tured or functionalized polymers[119-123]. The crucial equilibria of the RAFT polymerization are shown in Figure 1.4. While radical generation, propagation and termination occur in the same manner as for conventional free radical polymerization, reversible chain deactivation gives this technique its qualities of a living polymerization. Initially the RAFT pre-equilibrium, which is tantamount to the activation of the RAFT agent, is established. Here, the generated radical (**1**) can add to the chain transfer agent (**2**), thereby forming the intermediate radical **4**, which can decompose into the new RAFT agent **9** and the radical **7**. This fragmentation is favored, if the R group of the chain transfer agent is a better free radical leaving group than the initially generated radical **1**. The R group derived radical will then initiate polymer propagation by forming the adduct **8** with a monomer molecule. The described sequence of reactions is referred to as the RAFT pre-equilibrium, in which common RAFT agents are activated and oligomeric RAFT agents are formed. This pathway is most likely to take place due to the inherently high chain transfer constants of most RAFT agents, however, it is also possible for the radical **1** to initiate chain growth by forming the adduct **3** with a monomer molecule. In this case, the high chain transfer constants will also favor the addition of **3** to the RAFT agent **2**, thereby forming the intermediate radical **5**, which in turn will yield the chain initiating radical **7**. Although compound **6** is capable in acting as a chain transfer agent, a polymer chain with a terminal functionality differing from R will have been generated. It is possible to eliminate this problem fully by using identical R- and I radicals.

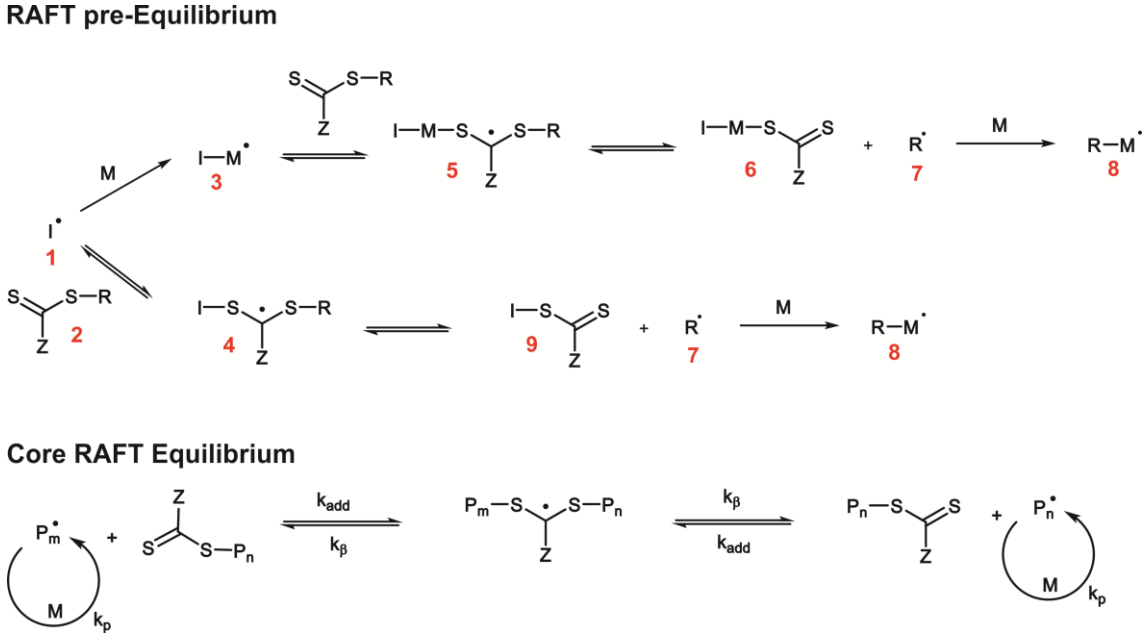

Figure 1.4. Mechanism of the reversible addition-fragmentation chain transfer (RAFT)

Once the pre-equilibrium has been established, the polymerization enters the core RAFT equilibrium, in which propagation takes place. Here, the degenerative chain transfer between active and dormant polymers chains occurs, which is supported by macromolecular chain transfer agents as the mediator with a radical intermediate species. In this radical driven process it is not possible to fully suppress conventional termination reactions. Nevertheless, the rapid equilibrium between the active and dormant polymer species ensures linear increase of the molecular weight with monomer conversion and thereby narrow molecular weight distributions. The resulting polymers possess terminal thiocarbonylthio groups making them macromolecular chain transfer agents. These moieties can be removed or transformed into another functional groups based on the requirements of the desired application and multiple methods have been devised to achieve this goal (Figure 1.5).[124-126] These end group modification strategies are vital in the design of RAFT polymer based gene delivery agents, which are intended for systemic administration, because the toxicity of these carriers is dependent not only on the transfected cell line and the polymer pendent groups, but also on the used CTA type during polymerization.[127, 128] Dithioesters, for example, readily interact with nucleophilic groups of proteins in living tissue, thereby causing acute toxicity.

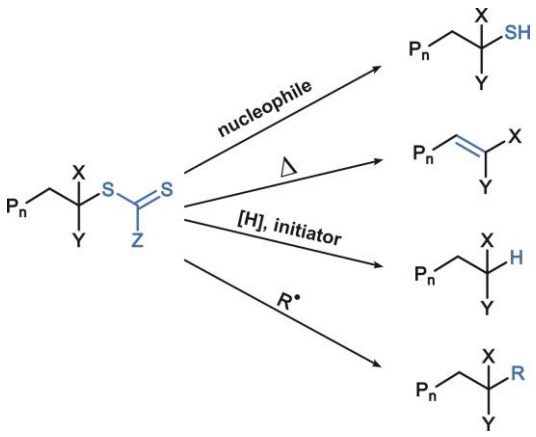

Figure 1.5. Possibilities for end group functionalization, where X as well as Y are functional groups of the respective monomer and [H] represents a hydrogen atom donor

1.4.1.2 RAFT chain transfer agents

The presence of a chain transfer agent (CTA), which are also known as RAFT agents, in the reaction mixture is the key factor to establish control, since it enables the reversible deactivation of the majority of the propagating radicals. Hence, retaining the terminal CTA functionalities during the polymerization process is a prerequisite to ensure the living character of RAFT. The general structure of CTAs is shown in Figure 1.6.

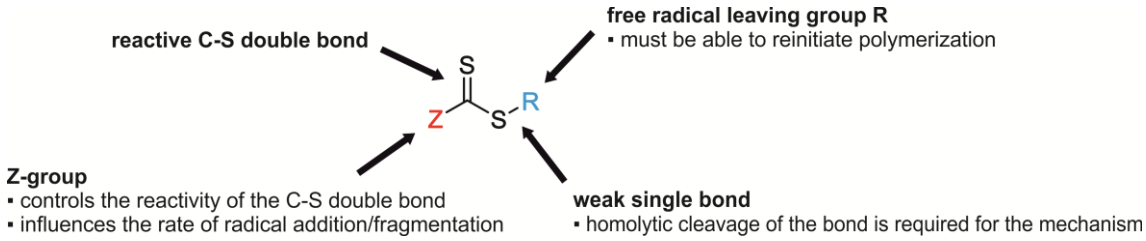

Figure 1.6. General structure and the function of the molecular components of a chain transfer agent

Their effectiveness as a RAFT agent is determined by the substituents R and Z, which can be chosen based on developed guidelines to suit the reactivity of the monomers and the reaction conditions.[125, 129, 130] The commonly employed classes of RAFT agents are dithiobezoates[131], trithiocarbonates[132], xanthates[133], and dithiocarbamates[134] (Figure 1.7).

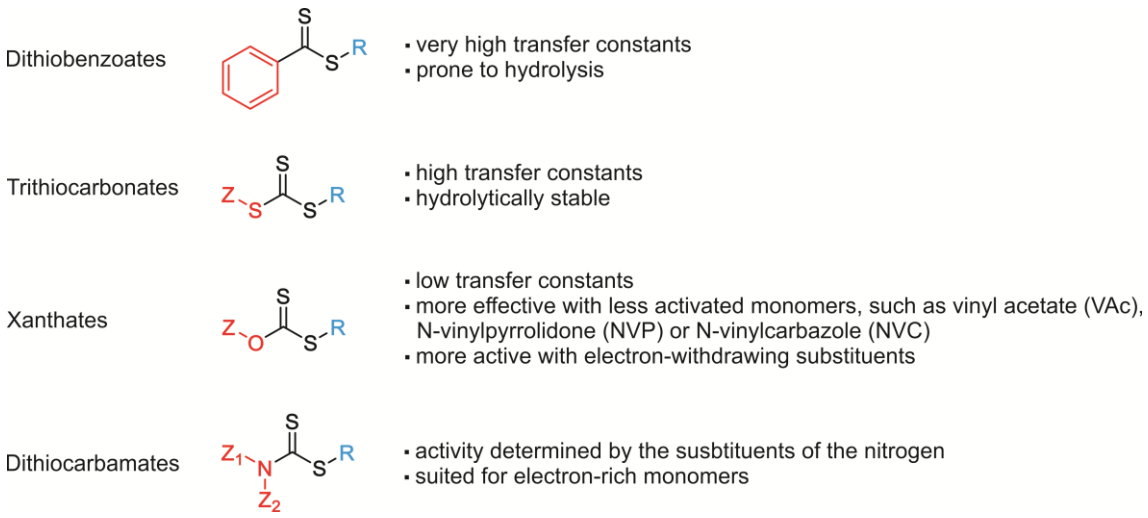

Figure 1.7. Classes of chain transfer agents

1.4.1.3 Theoretical molar mass

In an ideal RAFT polymerization polymer chains are initiated by the R group of the CTA and favorable experimental conditions are facilitated by the commonly applied initial RAFT polymerization stochiometries, where 2 to 10 equivalents of the RAFT agent are employed for each equivalent of the primary radical. Hence, while the total number of radicals is dictated by the amount of primary radicals, due to the RAFT equilibrium, the total number of polymer chains is controlled by the concentration of the CTA. A single primary radical can activate multiple RAFT agent molecules due to the reversibility of the radical addition/fragmentations steps. Based on this theoretical background, it is possible to state that the molar mass of RAFT polymers is controlled by the concentration$^{\text{monomer}}$/concentration$^{\text{RAFT agent}}$ ratio instead of the conventional concentration$^{\text{monomer}}$/concentration$^{\text{free radical initiating species}}$ ratio. Since ideal conditions cannot be guaranteed, a small fraction of the polymer chains will be initiated by primary radicals, but their number is negligible in the overall process. The number average molar mass ($M_{n,theory}$) can be therefore estimated by using equation 1.[117]

$$M_{n,theory} = \frac{[monomer]_0 \cdot M_{monomer} \cdot \rho}{[CTA]_0 + 2f[I]_0(1-e^{-k_d t})} + M_{CTA} \quad (1)$$

Here, $[monomer]_0$ represents the initial monomer concentration, $M_{monomer}$ is the molecular weight of the used monomer, ρ is the fractional conversion, M_{CTA} is the molecular weight of the RAFT agent, $[CTA]_0$ is the concentration of the chain transfer agent at the start of the polymerization and the second term in the denominator factors in the

efficacy, the starting concentration and the decomposition rate of the initiator. Since the radical initiation does not impact the RAFT polymerization to a significant degree, the equation can be further simplified.

$$M_{n,theory} = \frac{[monomer]_0 \cdot M_{monomer} \cdot \rho}{[CTA]_0} + M_{CTA} \quad (2)$$

If appropriate reaction conditions (temperature/time) were chosen, near complete conversion of the monomer can be achieved and the equation can be reduced to:

$$M_{n,theory} = \frac{[monomer]_0 \cdot M_{monomer}}{[CTA]_0} + M_{CTA} \quad (3)$$

1.4.1.4 Limitations

The RAFT polymerization technique exhibits limitations that need to be considered when planning the synthesis and the design of the desired polymers. For example, some of the aspects of the reaction mechanism, such as the reactivity and lifetime of the intermediate radical species, have been called into question due to experimental observations of inhibited polymerizations or rate retardation, if certain monomer/CTA combinations are employed.[135-137] These phenomena are usually explained by referring to either the possible coupling reactions of the intermediate radical species (Figure 1.4), their slow fragmentation in case of an aromatic phenyl moiety as the Z group of the CTA, which strongly stabilizes the radical due to delocalization[138-140], or as a combination of these two.[114, 141] However, using CTAs that facilitate weakly stabilized radical intermediates is not an option, because the RAFT polymerization requires the strong thermodynamic driving force of a stable intermediate radical for the addition reaction. Hence, the tradeoff between increased rate retardation and the required addition rates of the RAFT agent to the propagating radicals, which are essential for a high degree of control of the polymerization, must be considered.

Another limitation of RAFT is the susceptibility of certain chain transfer agents (especially dithioesters) to nucleophilic attacks.[142] Although this property can be exploited for post-polymerization modifications (Figure 1.5), it makes polymerizations under homogeneous conditions in aqueous media difficult, since it leads to the loss of chain end functionality and thereby impacts polymerization control by increasing the polydispersity. In such cases the detected molar mass of the polymers is substantially higher than the predicted value by equation 3. Nevertheless, RAFT has been classified as an excellent technique for the synthesis of hydrophilic polymers[103, 143], because solution strate-

gies can be implemented. It was shown that the rate of degradation of dithioesters can be suppressed by using hydrolytically stable chain transfer agents, by a low reaction temperature as well as a buffered aqueous medium with a pH that is lower than 7.[144] Thomas *et al.* and Baussard *et al.* not only confirmed these findings, but also showed that the hydrolysis of dithioesters follows pseudo first-order kinetics (equation 4), since this reaction can be considered zero-order with respect to the large excess of water molecules. The kinetics of this reaction were also shown to be affected by the molecular weight as well as the R/Z substituents of the CTAs.[145, 146]

$$-\frac{d[CTA]}{dt} = k_{hyd}[CTA] \tag{4}$$

The susceptibility of the C=S bond to nucleophilic attacks makes the use of monomers bearing primary or secondary amines difficult as well. In these cases, it is paramount to use acidic buffers as the medium of the aqueous RAFT polymerization, thereby protonating the amino groups and reducing the probability of a nucleophilic attack.[145] This approach, however, can minimize, but does not fully suppress hydro- and aminolysis. The decreasing concentration of the CTA can be expressed by equation 5.

$$-\frac{d[CTA]}{dt} = k_{hyd}[CTA] + k_a[CTA][Amine] \tag{5}$$

Here k_a is the second order rate constant, as indicated by Levesque *et al.*[147], [CTA] and [Amine] represent the concentrations of the chain transfer agent and the amino group bearing monomer respectively. The integrated form of equation 5 describes the time dependent concentration of CTA:

$$[CTA] = [CTA]_0 \cdot e^{-(k_{hyd}+k_a[Amine])t} \tag{6}$$

During the RAFT pre-Equilibrium (Figure 1.4) the CTA of low molecular weight is converted to a macroCTA. Hence, this timeframe can be viewed as an induction period t_{ind}, in which the CTA is especially susceptible for hydro- and aminolysis, since predominantly low molecular weight CTAs are present in the system.[148, 149] During t_{ind} $[CTA]_0$ is reduced to $[CTA]_{ind}$. Although k_{hyd} and k_a decrease sharply once the chain length exceeds 9 monomers, only miniscule changes of the degradation constants at longer polymer chains ($k_{hyd,\ macro}$ and $k_{a,\ macro}$).[149] Hence, $k_{hyd,\ macro}$ and $k_{a,\ macro}$ have to be used to estimate further degradation of the CTA functional group during the propagation, which follows the induction period:

$$[CTA] = [CTA]_{ind} \cdot e^{-(k_{hyd,macro}+k_{a,macro}[Amine])(t-t_{ind})} \tag{7}$$

These considerations are essential when calculating the theoretical molar weight ($M_{n,theory}$, equation 2) of a polymer prepared using aqueous RAFT polymerization conditions, where hydrolysis and aminolysis of the CTA cannot be suppressed. Since all of the polymers of this thesis were prepared by utilizing RAFT polymerization conditions, these consideration need to be kept in mind by the reader when appreciating the results of Chapters 3 to 6. In particular, synthetic challenges arose when polymerizing monomers bearing primary amino groups although RAFT typically provides living characteristics to the radical propagation of a large variety of unprotected vinyl-based monomers under mild conditions.

In the next chapter, I will describe the motivation underlying the present thesis.

1.5 References

[1] E. L. Tatum, *Perspect Biol Med* **1966**, *10*, 19.

[2] P. A. Futreal, L. Coin, M. Marshall, T. Down, T. Hubbard, R. Wooster, N. Rahman, M. R. Stratton, *Nat. Rev. Cancer* **2004**, *4*, 177.

[3] G. Vassalli, B. R. Winkelmann, *Eur Heart J* **2004**, *25*, 451.

[4] V. Yechoor, L. Chan, *Gene Ther.* **2005**, *12*, 101.

[5] E. Cevher, A. D. Sezer, E. S. e. Çağlar, "Gene Delivery Systems: Recent Progress in Viral and Non-Viral Therapy", in *Recent Advances in Novel Drug Carrier Systems*, A.D. Sezer, Ed., InTech, Rijeka, 2012, p. Ch. 16.

[6] F. Griffith, *J Hyg (Lond)* **1928**, *27*, 113.

[7] O. T. Avery, C. M. MacLeod, M. McCarty, *J. Exp. Med.* **1944**, *79*, 137.

[8] N. D. Zinder, J. Lederberg, *J. Bacteriol.* **1952**, *64*, 679.

[9] T. M. Powledge, *Genome Biology* **2003**, *4*, spotlight.

[10] J. D. Watson, F. H. C. Crick, *Nature (London, U. K.)* **1953**, *171*, 737.

[11] S. A. Rosenberg, P. Aebersold, K. Cornetta, A. Kasid, R. A. Morgan, R. Moen, E. M. Karson, M. T. Lotze, J. C. Yang, a. et, *N. Engl. J. Med.* **1990**, *323*, 570.

[12] W. F. Anderson, R. M. Blaese, K. Culver, *Hum Gene Ther* **1990**, *1*, 331.

[13] D. M. Nguyen, F. R. Spitz, N. Yen, R. J. Cristiano, J. A. Roth, *J. Thorac. Cardiovasc. Surg.* **1996**, *112*, 1372.

[14] L. E. Kun, A. Gajjar, M. Muhlbauer, R. L. Heideman, R. Sanford, M. Brenner, A. Walter, J. Langston, J. Jenkins, a. et, *Hum. Gene Ther.* **1995**, *6*, 1231.

[15] D. M. Mahvi, P. M. Sondel, N. S. Yang, M. R. Albertini, J. H. Schiller, J. Hank, J. Heiner, J. Gan, W. Swain, R. Logrono, *Hum. Gene Ther.* **1997**, *8*, 875.

[16] J. Deshane, G. P. Siegal, M. Wang, M. Wright, R. P. Bucy, R. D. Alvarez, D. T. Curiel, *Gynecol. Oncol.* **1997**, *64*, 378.

[17] G. Romano, C. Pacilio, A. Giordano, *Stem Cells (Miamisburg, Ohio)* **1999**, *17*, 191.

[18] M. Elsabahy, A. Nazarali, M. Foldvari, *Curr. Drug Delivery* **2011**, *8*, 235.

[19] C. H. Jones, C.-K. Chen, A. Ravikrishnan, S. Rane, B. A. Pfeifer, *Mol. Pharmaceutics* **2013**, *10*, 4082.

[20] T. Imanaka, S. Aiba, *Ann. N. Y. Acad. Sci.* **1981**, *369*, 1.

[21] X. Gao, K.-S. Kim, D. Liu, *AAPS J.* **2007**, *9*, E92.

[22] S. Mansouri, P. Lavigne, K. Corsi, M. Benderdour, E. Beaumont, J. C. Fernandes, *Eur. J. Pharm. Biopharm.* **2004**, *57*, 1.

[23] N. Nayerossadat, T. Maedeh, P. Abas Ali, *Adv. Biomed. Res.* **2012**, *1*, 1.

[24] L. Liu, C. Johnson, S. Fujimura, F. Teque, J. A. Levy, *Journal of Immunological Methods* **2011**, *372*, 22.

[25] M. S. Al-Dosari, X. Gao, *The AAPS Journal* **2009**, *11*, 671.

[26] R. Gardlik, R. Palffy, J. Hodosy, J. Lukacs, J. Turna, P. Celec, *Med. Sci. Monit.* **2005**, *11*, RA110.

[27] M. Marsh, A. Helenius, *Cell (Cambridge, MA, U. S.)* **2006**, *124*, 729.

[28] E. M. Campbell, T. J. Hope, *Gene Ther.* **2005**, *12*, 1353.

[29] S. D. Li, L. Huang, *Gene Ther.* **2006**, *13*, 1313.

[30] O. Veiseh, F. M. Kievit, J. W. Gunn, B. D. Ratner, M. Zhang, *Biomaterials* **2008**, *30*, 649.

[31] A. Aigner, *Appl. Microbiol. Biotechnol.* **2007**, *76*, 9.

[32] Y. Dorsett, T. Tuschl, *Nat. Rev. Drug Discovery* **2004**, *3*, 318.

[33] M. A. Behlke, *Mol. Ther.* **2006**, *13*, 644.

[34] A. Fire, S. Xu, M. K. Montgomery, S. A. Kostas, S. E. Driver, C. C. Mello, *Nature (London)* **1998**, *391*, 806.

[35] R. E. Collins, X. Cheng, *FEBS Lett.* **2005**, *579*, 5841.

[36] E. Bernstein, A. A. Caudy, S. M. Hammond, G. J. Hannon, *Nature (London)* **2001**, *409*, 363.

[37] C. Matranga, Y. Tomari, C. Shin, D. P. Bartel, P. D. Zamore, *Cell (Cambridge, MA, U. S.)* **2005**, *123*, 607.

[38] J. Martinez, A. Patkaniowska, H. Urlaub, R. Luhrmann, T. Tuschl, *Cell (Cambridge, MA, U. S.)* **2002**, *110*, 563.

[39] N. J. Caplen, J. Fleenor, A. Fire, R. A. Morgan, *Gene* **2000**, *252*, 95.

[40] A. J. Karpala, T. J. Doran, A. G. D. Bean, *Immunol. Cell Biol.* **2005**, *83*, 211.

[41] S. M. Elbashir, J. Harborth, W. Lendeckel, A. Yalcin, K. Weber, T. Tuschl, *Nature (London, U. K.)* **2001**, *411*, 494.

[42] S. M. Elbashir, W. Lendeckel, T. Tuschl, *Genes Dev.* **2001**, *15*, 188.

[43] M. Banan, N. Puri, *Curr. Pharm. Biotechnol.* **2004**, *5*, 441.

[44] M. Sioud, *Expert Opin. Drug Delivery* **2005**, *2*, 639.

[45] T. Abe, K. Goda, K. Futami, Y. Furuichi, *Nucleic Acids Res.* **2009**, *37*, e56/1.

[46] D. J. Gary, N. Puri, Y.-Y. Won, *J. Controlled Release* **2007**, *121*, 64.

[47] R. C. C. Ryther, A. S. Flynt, J. A. Phillips, J. G. Patton, *Gene Ther.* **2005**, *12*, 5.

[48] W. J. Kim, S. W. Kim, *Pharm. Res.* **2009**, *26*, 657.

[49] M. Ahmed, R. Narain, *Progress in Polymer Science* **2013**, *38*, 767.

[50] T. Jiang, J. Chang, C. Wang, Z. Ding, J. Chen, J. Zhang, E.-T. Kang, *Biomacromolecules* **2007**, *8*, 1951.

[51] L. Veron, A. Ganee, C. Ladaviere, T. Delair, *Macromol. Biosci.* **2006**, *6*, 540.

[52] Y.-Z. You, D. S. Manickam, Q.-H. Zhou, D. Oupicky, *J. Controlled Release* **2007**, *122*, 217.

[53] C. Aral, J. Akbuga, *J. Pharm. Pharm. Sci.* **2003**, *6*, 321.

[54] Y. Guo, Y. Sun, J. Gu, Y. Xu, *Anal. Biochem.* **2007**, *363*, 204.

[55] T. Kawano, T. Okuda, H. Aoyagi, T. Niidome, *J. Controlled Release* **2004**, *99*, 329.

[56] M. O. Andersen, K. A. Howard, S. R. Paludan, F. Besenbacher, J. Kjems, *Biomaterials* **2007**, *29*, 506.

[57] W. Weecharangsan, P. Opanasopit, T. Ngawhirunpat, A. Apirakaramwong, T. Rojanarata, U. Ruktanonchai, R. J. Lee, *Int. J. Pharm.* **2008**, *348*, 161.

[58] K. A. Howard, U. L. Rahbek, X. Liu, C. K. Damgaard, S. Z. Glud, M. O. Andersen, M. B. Hovgaard, A. Schmitz, J. R. Nyengaard, F. Besenbacher, J. Kjems, *Mol. Ther.* **2006**, *14*, 476.

[59] S. Werth, B. Urban-Klein, L. Dai, S. Hoebel, M. Grzelinski, U. Bakowsky, F. Czubayko, A. Aigner, *J. Controlled Release* **2006**, *112*, 257.

[60] M. S. Shim, Y. J. Kwon, *Biomacromolecules* **2008**, *9*, 444.

[61] B. Urban-Klein, S. Werth, S. Abuharbeid, F. Czubayko, A. Aigner, *Gene Ther.* **2005**, *12*, 461.

[62] G. Y. Wu, C. H. Wu, *J. Biol. Chem.* **1987**, *262*, 4429.

[63] O. Boussif, F. Lezoualc'h, M. A. Zanta, M. D. Mergny, D. Scherman, B. Demeneix, J.-P. Behr, *Proc. Natl. Acad. Sci. U. S. A.* **1995**, *92*, 7297.

[64] M. X. Tang, F. C. Szoka, *Gene Ther.* **1997**, *4*, 823.

[65] M. A. Wolfert, L. W. Seymour, *Gene Ther.* **1996**, *3*, 269.

[66] D. L. McKenzie, W. T. Collard, K. G. Rice, *J. Pept. Res.* **1999**, *54*, 311.

[67] M. A. Mintzer, E. E. Simanek, *Chem. Rev. (Washington, DC, U. S.)* **2009**, *109*, 259.

[68] F. J. Xu, W. T. Yang, *Prog. Polym. Sci.* **2011**, *36*, 1099.

[69] M. E. Martin, K. G. Rice, *AAPS J.* **2007**, *9*, E18.

[70] R. Kircheis, A. Kichler, G. Wallner, M. Kursa, T. Felzmann, M. Buchberger, E. Wagner, *Gene Ther.* **1997**, *4*, 409.

[71] A. M. Maguire, F. Simonelli, E. A. Pierce, E. N. Pugh, Jr., F. Mingozzi, J. Bennicelli, S. Banfi, K. A. Marshall, F. Testa, E. M. Surace, S. Rossi, A. Lyubarsky, V. R. Arruda, B. Konkle, E. Stone, J. Sun, J. Jacobs, L. Dell'Osso, R. Hertle, J.-x. Ma, T. M. Redmond, X. Zhu, B. Hauk, O. Zelenaia, K. S. Shindelr, M. G. Maguire, J. F. Wright, N. J. Volpe, J. W. McDonnell, A. Auricchio, K. A. High, J. Bennett, *N. Engl. J. Med.* **2008**, *358*, 2240.

[72] N. Cartier, P. Aubourg, *Brain Pathol* **2010**, *20*, 857.

[73] P. A. LeWitt, A. R. Rezai, M. A. Leehey, S. G. Ojemann, A. W. Flaherty, E. N. Eskandar, S. K. Kostyk, K. Thomas, A. Sarkar, M. S. Siddiqui, S. B. Tatter, J. M. Schwalb, K. L. Poston, J. M. Henderson, R. M. Kurlan, I. H. Richard, L. Van Meter, C. V. Sapan, M. J. During, M. G. Kaplitt, A. Feigin, *Lancet Neurol.* **2011**, *10*, 309.

[74] R. Kalinova, J. A. Doumanov, K. Mladenova, D. Janevska, M. Georgieva, G. Miloshev, T. Topouzova-Hristova, I. Dimitrov, *ChemistrySelect* **2017**, *2*, 12006.

[75] P. Singhsa, D. Diaz-Dussan, H. Manuspiya, R. Narain, *Biomacromolecules* **2018**, *19*, 209.

[76] T.-I. Kim, H. J. Seo, J. S. Choi, H.-S. Jang, J. Baek, K. Kim, J.-S. Park, *Biomacromolecules* **2004**, *5*, 2487.

[77] F. J. Xu, Z. X. Zhang, Y. Ping, J. Li, E. T. Kang, K. G. Neoh, *Biomacromolecules* **2009**, *10*, 285.

[78] F. J. Xu, Y. Ping, J. Ma, G. P. Tang, W. T. Yang, J. Li, E. T. Kang, K. G. Neoh, *Bioconjugate Chem.* **2009**, *20*, 1449.

[79] Y. Kakizawa, K. Kataoka, *Adv. Drug Delivery Rev.* **2002**, *54*, 203.

[80] J.-Y. Cherng, P. van de Wetering, H. Talsma, D. J. A. Crommelin, W. E. Hennink, *Pharm. Res.* **1996**, *13*, 1038.

[81] P. Van de Wetering, E. E. Moret, N. M. E. Schuurmans-Nieuwenbroek, M. J. Van Steenbergen, W. E. Hennink, *Bioconjugate Chem.* **1999**, *10*, 589.

[82] M. A. Gauthier, M. I. Gibson, H.-A. Klok, *Angew. Chem., Int. Ed.* **2009**, *48*, 48.

[83] J. Nicolas, G. Mantovani, D. M. Haddleton, *Macromol. Rapid Commun.* **2007**, *28*, 1083.

[84] M. Li, P. De, S. R. Gondi, B. S. Sumerlin, *Macromol. Rapid Commun.* **2008**, *29*, 1172.

[85] A. J. Convertine, D. S. W. Benoit, C. L. Duvall, A. S. Hoffman, P. S. Stayton, *J. Controlled Release* **2009**, *133*, 221.

[86] P. De, M. Li, S. R. Gondi, B. S. Sumerlin, *J. Am. Chem. Soc.* **2008**, *130*, 11288.

[87] G. Moad, E. Rizzardo, S. H. Thang, *Australian Journal of Chemistry* **2005**, *58*, 379.

[88] A. W. York, Y. Zhang, A. C. Holley, Y. Guo, F. Huang, C. L. McCormick, *Biomacromolecules* **2009**, *10*, 936.

[89] Y. Li, B. S. Lokitz, C. L. McCormick, *Angew. Chem., Int. Ed.* **2006**, *45*, 5792.

[90] L. He, E. S. Read, S. P. Armes, D. J. Adams, *Macromolecules (Washington, DC, U. S.)* **2007**, *40*, 4429.

[91] Z. Deng, H. Bouchekif, K. Babooram, A. Housni, N. Choytun, R. Narain, *J. Polym. Sci., Part A: Polym. Chem.* **2008**, *46*, 4984.

[92] A. H. Alidedeoglu, A. W. York, C. L. McCormick, S. E. Morgan, *J. Polym. Sci., Part A: Polym. Chem.* **2009**, *47*, 5405.

[93] Z. Jia, L. Wong, T. P. Davis, V. Bulmus, *Biomacromolecules* **2008**, *9*, 3106.

[94] L. Wong, C. Boyer, Z. Jia, H. M. Zareie, T. P. Davis, V. Bulmus, *Biomacromolecules* **2008**, *9*, 1934.

[95] A. W. York, F. Huang, C. L. McCormick, *Biomacromolecules* **2010**, *11*, 505.

[96] Z. Ozdemir, M. Topuzogullari, I. A. Isoglu, S. Dincer, *Polym. Bull. (Heidelberg, Ger.)* **2013**, *70*, 2857.

[97] A. Kelsch, S. Tomcin, K. Rausch, M. Barz, V. Mailaender, M. Schmidt, K. Landfester, R. Zentel, *Biomacromolecules* **2012**, *13*, 4179.

[98] M. J. Yanjarappa, K. V. Gujraty, A. Joshi, A. Saraph, R. S. Kane, *Biomacromolecules* **2006**, *7*, 1665.

[99] A. Favier, F. D'Agosto, M.-T. Charreyre, C. Pichot, *Polymer* **2004**, *45*, 7821.

[100] J. J. Vosloo, M. P. Tonge, C. M. Fellows, F. D'Agosto, R. D. Sanderson, R. G. Gilbert, *Macromolecules* **2004**, *37*, 2371.

[101] M. Eberhardt, P. Theato, *Macromol. Rapid Commun.* **2005**, *26*, 1488.

[102] Y. Li, B. S. Lokitz, C. L. McCormick, *Macromolecules* **2006**, *39*, 81.

[103] C. L. McCormick, A. B. Lowe, *Acc. Chem. Res.* **2004**, *37*, 312.

[104] A. W. York, S. E. Kirkland, C. L. McCormick, *Adv. Drug Delivery Rev.* **2008**, *60*, 1018.

[105] M. Ahmed, R. Narain, *Prog. Polym. Sci.* **2013**, *38*, 767.

[106] V. Bulmus, *Polym. Chem.* **2011**, *2*, 1463.

[107] C. Boyer, J. Liu, V. Bulmus, T. P. Davis, *Aust. J. Chem.* **2009**, *62*, 830.

[108] D. Smith, A. C. Holley, C. L. McCormick, *Polym. Chem.* **2011**, *2*, 1428.

[109] D. Konkolewicz, A. Gray-Weale, S. Perrier, *J. Am. Chem. Soc.* **2009**, *131*, 18075.

[110] L. Tao, J. Liu, B. H. Tan, T. P. Davis, *Macromolecules (Washington, DC, U. S.)* **2009**, *42*, 4960.

[111] D. J. Siegwart, K. A. Whitehead, L. Nuhn, G. Sahay, H. Cheng, S. Jiang, M. Ma, A. Lytton-Jean, A. Vegas, P. Fenton, C. G. Levins, K. T. Love, H. Lee, C. Cortez, S. P. Collins, Y. F. Li, J. Jang, W. Querbes, C. Zurenko, T. Novobrantseva, R. Langer, D. G. Anderson, *Proc. Natl. Acad. Sci. U. S. A.* **2011**, *108*, 12996.

[112] L. Nuhn, M. Hirsch, B. Krieg, K. Koynov, K. Fischer, M. Schmidt, M. Helm, R. Zentel, *ACS Nano* **2012**, *6*, 2198.

[113] J. Chiefari, Y. K. Chong, F. Ercole, J. Krstina, J. Jeffery, T. P. T. Le, R. T. A. Mayadunne, G. F. Meijs, C. L. Moad, G. Moad, E. Rizzardo, S. H. Thang, *Macromolecules* **1998**, *31*, 5559.

[114] C. Barner-Kowollik, M. Buback, B. Charleux, M. L. Coote, M. Drache, T. Fukuda, A. Goto, B. Klumperman, A. B. Lowe, J. B. McLeary, G. Moad, M. J. Monteiro, R. D. Sanderson, M. P. Tonge, P. Vana, *J. Polym. Sci., Part A: Polym. Chem.* **2006**, *44*, 5809.

[115] C. Barner-Kowollik, Editor, "*Handbook of RAFT Polymerization*", Wiley-VCH Verlag GmbH & Co. KGaA, 2008, p. 543 pp.

[116] M. J. Monteiro, *J. Polym. Sci., Part A: Polym. Chem.* **2005**, *43*, 3189.

[117] A. B. Lowe, C. L. McCormick, *Prog. Polym. Sci.* **2007**, *32*, 283.

[118] F. J. Schork, Y. Luo, W. Smulders, J. P. Russum, A. Butte, K. Fontenot, *Adv. Polym. Sci.* **2005**, *175*, 129.

[119] M. H. Stenzel, C. Barner-Kowollik, T. P. Davis, *J. Polym. Sci., Part A: Polym. Chem.* **2006**, *44*, 2363.

[120] C. L. McCormick, S. E. Kirkland, A. W. York, *Polym. Rev. (Philadelphia, PA, U. S.)* **2006**, *46*, 421.

[121] C. Barner-Kowollik, T. P. Davis, M. H. Stenzel, *Aust. J. Chem.* **2006**, *59*, 719.

[122] G. Moad, Y. K. Chong, A. Postma, E. Rizzardo, S. H. Thang, *Polymer* **2005**, *46*, 8458.

[123] S. Pearson, N. Allen, M. H. Stenzel, *J. Polym. Sci., Part A: Polym. Chem.* **2009**, *47*, 1706.

[124] Y. K. Chong, G. Moad, E. Rizzardo, S. Thang, *Macromolecules (Washington, DC, U. S.)* **2007**, *40*, 4446.

[125] G. Moad, E. Rizzardo, S. H. Thang, *Aust. J. Chem.* **2005**, *58*, 379.

[126] H. Willcock, r. K. O'Reilly, *Polym. Chem.* **2010**, *1*, 149.

[127] C.-W. Chang, E. Bays, L. Tao, S. N. S. Alconcel, H. D. Maynard, *Chem. Commun. (Cambridge, U. K.)* **2009**, 3580.

[128] J. Hentschel, K. Bleek, O. Ernst, J.-F. Lutz, H. G. Boerner, *Macromolecules (Washington, DC, U. S.)* **2008**, *41*, 1073.

[129] G. Moad, E. Rizzardo, S. H. Thang, *Polymer* **2008**, *49*, 1079.

[130] A. Favier, M.-T. Charreyre, *Macromol. Rapid Commun.* **2006**, *27*, 653.

[131] Y. K. Chong, J. Krstina, T. P. T. Le, G. Moad, A. Postma, E. Rizzardo, S. H. Thang, *Macromolecules* **2003**, *36*, 2256.

[132] R. T. A. Mayadunne, E. Rizzardo, J. Chiefari, J. Krstina, G. Moad, A. Postma, S. H. Thang, *Macromolecules* **2000**, *33*, 243.

[133] S. Perrier, P. Takolpuckdee, *J. Polym. Sci., Part A: Polym. Chem.* **2005**, *43*, 5347.

[134] R. T. A. Mayadunne, E. Rizzardo, J. Chiefari, Y. K. Chong, G. Moad, S. H. Thang, *Macromolecules* **1999**, *32*, 6977.

[135] A. R. Wang, S. Zhu, *J. Polym. Sci., Part A: Polym. Chem.* **2003**, *41*, 1553.

[136] C. Barner-Kowollik, T. P. Davis, J. P. A. Heuts, M. H. Stenzel, P. Vana, M. Whittaker, *J. Polym. Sci., Part A: Polym. Chem.* **2003**, *41*, 365.

[137] S. Perrier, C. Barner-Kowollik, J. F. Quinn, P. Vana, T. P. Davis, *Macromolecules* **2002**, *35*, 8300.

[138] C. Barner-Kowollik, P. Vana, J. F. Quinn, T. P. Davis, *J. Polym. Sci., Part A: Polym. Chem.* **2002**, *40*, 1058.

[139] C. Barner-Kowollik, J. F. Quinn, T. L. U. Nguyen, J. P. A. Heuts, T. P. Davis, *Macromolecules* **2001**, *34*, 7849.

[140] M. J. Monteiro, R. Bussels, S. Beuermann, M. Buback, *Australian Journal of Chemistry* **2002**, *55*, 433.

[141] Y. Kwak, A. Goto, Y. Tsujii, Y. Murata, K. Komatsu, T. Fukuda, *Macromolecules* **2002**, *35*, 3026.

[142] M. Deletre, G. Levesque, *Macromolecules* **1990**, *23*, 4733.

[143] A. B. Lowe, C. L. McCormick, *Aust. J. Chem.* **2002**, *55*, 367.

[144] G. Levesque, P. Arsene, V. Fanneau-Bellenger, T.-N. Pham, *Biomacromolecules* **2000**, *1*, 400.

[145] D. B. Thomas, A. J. Convertine, R. D. Hester, A. B. Lowe, C. L. McCormick, *Macromolecules* **2004**, *37*, 1735.

[146] J.-F. Baussard, J.-L. Habib-Jiwan, A. Laschewsky, M. Mertoglu, J. Storsberg, *Polymer* **2004**, *45*, 3615.

[147] A. S. A. S. Shawali, S. S. Biechler, S. S. Biechler, *J. Am. Chem. Soc.* **1967**, *89*, 3020.

[148] M. H. Stenzel, L. Cummins, G. E. Roberts, T. P. Davis, P. Vana, C. Barner-Kowollik, *Macromol. Chem. Phys.* **2003**, *204*, 1160.

[149] D. B. Thomas, A. J. Convertine, L. J. Myrick, C. W. Scales, A. E. Smith, A. B. Lowe, Y. A. Vasilieva, N. Ayres, C. L. McCormick, *Macromolecules* **2004**, *37*, 8941.

2 Motivation and objectives

Gene therapy and gene silencing possess a high potential as a treatment approach for most acquired and inherited genetic disorders. However, their utilization for medical applications requires the development of suitable delivery agents, since neither siRNA-, nor DNA molecules can enter cells unaided through passive diffusion. Such carriers must be able to:

1. complex the polynucleotides
2. be water-soluble and non-toxic
3. protect the cargo against nucleases *via* dense packing or shielding
4. hide from the immune system by avoiding interactions with serum proteins
5. deliver the payload to the tissue of interest
6. transport the polynucleotides across the plasma membrane
7. release the cargo inside the cytosol

However, finding a delivery agent, which can satisfy all of the requirements on this straightforward list, is a challenging task, which requires a close collaboration between chemists and biochemists. Viral vectors with an artificially deranged replication have been tested as carrier system, but pronounced adverse effects have been observed in patients due to the inherent immunogenicity of viruses, which causes the degeneration of the affected tissue by the inflammatory system. Furthermore, they also require genetic retargeting to not only be specific to their natural target cells. Nonviral vectors, such as the cationic polymers, offer more safety for patients, since their properties can be tailored to ensure biocompatibility and biodegradability. The most common sources of the cationic charges, which were used up until now, are either basic primary- or inherently charged quaternary amino groups and polymers, such as pDMAEMA, PEI and chitosan shaped this field of study. However, polymers, which use guanidinium groups to bind and deliver polynucleotides into cells, have shown the potential to outperform polymer structures that rely on amino groups for the same purpose. The design of such guanidinium group-based scaffolds lead to a renaissance of such carrier systems due to their ability to mimic cell penetrating peptides with arginine rich peptide sequences and to remain cationically charged over a wide pH range, thereby exhibiting not only excellent binding of polynucleotides, but also the facility for the transduction across plasma membranes. The first reported example for a guanidinium-based delivery system was the homopolymer poly(guanidinopropyl methacrylate) (pGuaMa), which has been de-

veloped by Funhoff *et al.* It possessed extraordinary complexation properties due to its strong affinity towards DNA. However, the polyplexes between pGuaMa and plasmid DNA aggregated with negatively charged serum proteins, which impeded transfection. The length and charge density of pGuaMa, which had a SEC-determined molar weight of 180 kDa, were identified as the leading cause for this observation. The aggregation of cationic polymers or -polyplexes with serum proteins led not only to reduced transfection efficacy, but also increased toxicity and stimulated an immune response. This initial design was further improved in the year 2008. Tew and coworkers utilized the ring-opening metathesis polymerization technique to synthesize guaidinium group-bearing oxanorbornene-based polymers with the ability to bypass cellular membranes. In the same year norbornene-based structures were prepared by Kiessling and coworkers. These studies were further preceded by the works of Wylie and coworkers, Goodman and coworkers and Chung and coworkers, who were working on oligocarbamates, functionalized dendrimers and carbohydrates respectively.

The scope of application for guanidinium group-bearing continues to increase, but aside from increasing structural variety, no studies have been performed with the aim to understand the observed effects. In particular, the cationic charge density of the chosen delivery agents requires fine tuning for the most efficient tradeoff between strong affinity towards siRNA and toxicity. To solve this problem of siRNA delivery systems, which also affects their transfection properties, a different approach to this topic was chosen. Instead of simply development of a novel system that entails a new set of advantages and disadvantages, the influence of the polymer architecture was investigated. In this regard statistical, gradient and diblock copolymers as well as cationic homopolymers have been studied, wherein not only the block-length, but also the source of the cationic charges has been varied.

Commonly applied nonviral vectors utilize amino groups as cationic moieties to bind nucleic acids. However, guanidinium groups are more advantageous to establish electrostatic interactions with anions, because they remain protonated over a wide pH range. This fact is reflected in the high pKa value of their protonated counterpart of 12.48. However, this group recognizes and binds the phosphate anions of polynucleotides not only through ion pairing, but also by forming multiple hydrogen bonds. The design of such scaffolds is further enhanced due to their ability to mimic cell penetrating peptides with arginine rich peptide sequences. In order to obtain a detailed understanding of the value this functional moiety has for the design of siRNA/DNA carrier systems, an in-

depth study of the relationship between the guanidinium group bearing monomer's distribution inside the polymer chain (diblock copolymer, statistical copolymer, gradient copolymer, homopolymer) and the effects on binding affinity, toxicity, internalization into cells as well as the transport efficacy of cargo molecules across cellular boundaries is required.

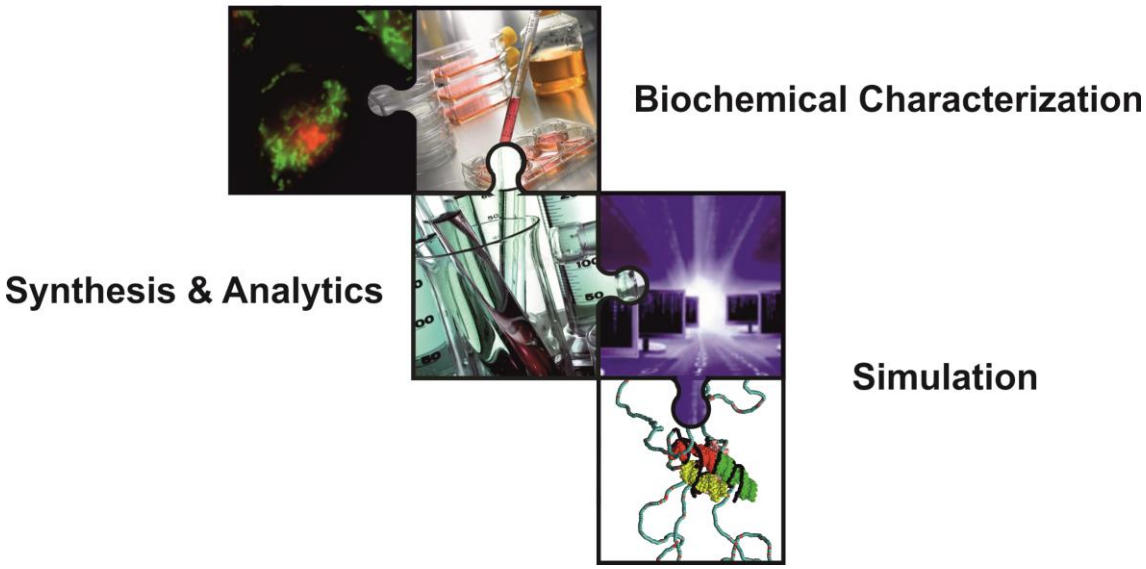

The next chapters of the present thesis are structured as follows:

Chapter 3 describes the synthesis of a library of diblock copolymers with uniform molar mass and narrow dispersities, but varying block lengths and monomer composition. The effects of these alterations on binding affinity towards siRNA, polyplex size, toxicity, internalization into cells as well as knock-down properties. It is expected that altering block size, monomer composition and structure would affect the viability of the respective polymer as a siRNA delivery agent. Four questions are at the forefront of interest:

1. Do the primary amino groups of APMA or the guanidinium groups of GPMA have precedence for the application in polynucleotide delivery?

In order to find an answer to the first question, the twelve diblock copolymers were divided into two groups, where group *I* relied on an APMA block for the complexation of siRNA and group *II* used a GPMA block for the same purpose. Since each polymer of group *I* had its structural counterpart in group *II*, a meaningful conclusion was drawn by an intergroup comparison.

2. Do long or short cationic blocks achieve the best tradeoff between siRNA-binding, plasma membrane transduction and toxicity?

Answering the second question required further division of the groups into the subgroups *Ia* and *Ib* as well as *IIa* and *IIb*. The subgroups were created based on the length of the APMA or GPMA homopolymer blocks. The subgroups *Ia* and *IIa* encompass diblock copolymers with a long cationic block, whereas the subgroups *Ib* and *IIb* contain those with a short APMA or GPMA block respectively. It is possible to find hints as to how the length of the cationic block influences the functionality of a siRNA delivery agent by comparing the subgroup *Ia* with *Ib* and *IIa* with *IIb*.

3. To which degree does the first block, which possesses a low cationic charge density, participate during polyplex formation? Or does it offer other merits for siRNA delivery in consideration of its length and composition?

The third question, which is aimed at the function of the blocks with high HPMA content, makes an intragroup comparison of the block copolymers within the individual subgroups necessary.

4. Given a certain overall chain length of a diblock copolymer (e.g. 200 monomers long), how long does a cationic block need to be to facilitate efficient complexation of siRNA or more specifically, what $\text{length}^{\text{binding block}}/\text{length}^{\text{non-biding block}}$ ratio is required?

The last question was answered by complementing the experimental results with a computational study employing a coarse-grained model of the system at the molecular level to study the interactions between polymer chains and small interfering RNA.

Chapter 4 aimed to further improve the design of nonviral vectors for gene silencing discussed in Chapter 3 by covalently attaching triphenylphosphonium cations. This modification strategy was intended to reduce toxicity and facilitate the internalization of polyplexes even into the hard to transfect $CD8^+$ T cells without affecting the size or the binding properties of the formed polyplexes. Particular interest was placed on resolving the issue of the poor intracellular release of polynucleotides, which was observed in connection with the use of guanidinium groups.

In Chapter 5 cationic statistical and gradient copolymers at varying monomer ratios and compositions, but uniform molar masses, were synthesized to study the effects of the distribution of cationic charges (statistical vs. gradient) and the origin of cationic charg-

es (primary amines vs. gunidinium groups) on key parameters of pDNA delivery. The gradual increase of cationic charge densities along the linear polymer chain, which has never been studied for gene delivery agents, leads to a segments with predominantly statistical character and also block-like segments at the termini. Hence, it was expected to observe differences with respect to the established types of charge distribution.

Chapter 6 deals with the topic of using copolymers composed of hydrophilic and hydrophobic monomers as mimics for the cell penetrating peptide CADY, which is an effective delivery system for siRNA achieving efficient transfection and knock-down in different cell lines. Taking inspiration from the CADY peptide and utilizing hydrophobic and cationic monomers as starting materials in a batch copolymerization would circumvent the need for post-polymerization modification, which was described in Chapter 4. Since uncharged, cationic and lipophilic monomers, i.e. those possessing different solubilization profiles, were used as building blocks, an extensive trial-and-error approach was necessary to find ideal conditions allowing control over a terpolymers' molar mass and the monomer composition. Nevertheless, the potential of the thusly obtained terpolymers is extraordinary.

Chapter 7 departs from the topic of gene delivery. It is dedicated to demonstrate that the findings of this thesis can be applied in other fields of study as well. In particular, it has been repeatedly observed that guanidinium group bearing polymers quench fluorescent dyes. Hence, an ulta-sensitive detection method for malathion has been developed by utilizing guanidinium group-bearing homopolymers as an intermediary component between detection and data validation.

Chapter 8 summarizes the previous chapters and outlines design ideas for novel gene delivery agents on the basis of the results of this thesis.

Finally, Chapter 9 gives a detailed overview of the used methods.

3 The role of polymer architecture in siRNA delivery

In order to improve this promising design idea of using guanidinium group bearing polymers as siRNA carrier systems, a library of twelve different diblock copolymer structures was synthesized using the monomers N-(2-hydroxypropyl)methacrylamide (HPMA), N-(3-aminopropyl)methacrylamide (APMA) and 3-guanidinopropyl methacrylamide (GPMA). The RAFT polymerization technique, which not only tolerates all employed functional groups and solvents, but also and facilitates narrow dispersities (Đ < 1.12), was used to make alterations in block size, composition and structure, while keeping the final molecular weight constant at 30 kDa. This upper limit of the molar mass was chosen to improve biocompatibility, since HPMA-based copolymers are not biodegradable, but with a molecular weight below 50 kDa they have access to renal clearance as well as other routes of elimination from the blood stream.[1] Thereby, the risk of long time toxicity in *in vivo* studies can be avoided. The synthesized block copolymers are expected to behave in a similar fashion, since HPMA is the main component of the backbone. Diblock copolymers were chosen as the scaffolds structure due to their ability to form micellar polyplexes with polynucleotides, which have been repeatedly shown to exhibit sufficient serum stability without losing the ability to transfect cells.[2] This approach allowed the systematic investigation on the effect these alterations have on the suitability of the respective structures for siRNA delivery.

The diblock copolymers were screened regarding their binding properties *via* the electrophoretic mobility shift assay (EMSA) and their affinity towards siRNA was further quantified by microscale thermophoresis (MST). In addition, the size and shape of the formed polymer/siRNA complexes was determined by means of dynamic light scattering (DLS) and cryogenic transmission electron microscopy (cryo-TEM). Fluorescence correlation spectroscopy (FCS) was used to determine the loading efficacy in regard to the complex-bound amount of siRNA molecules.

The investigation on the utility of these diblock copolymer structures as siRNA delivery agents was completed by a bio-characterization. Here, the internalization of the corresponding polyplexes as well as their knock-down properties and toxicity were studied *in vitro*.

Complementary to this experimental investigation a computational study employing molecular simulations as well as an analytical description of systemic properties was performed in cooperation with Maziar Heidari (Prof. Dr. Raffaello Potestio and Prof.

Dr. Kurt Kremer, Max Planck Institute for Polymer Research), who developed a coarse-grained model of the system at the molecular level in a top-down approach using experimental results as a template. The combined insights from the experiments and the theoretical investigation resulted in a wealth of information about the properties of cationic diblock copolymers employed as RNA delivery agents, in particular regarding the molecular and mechanistic details of the interaction.

3.1 Preparation of the diblock copolymers

The library of diblock copolymers was synthesized via aqueous RAFT polymerization (aRAFT) in a two-step approach, where the required monomer and CTA concentrations were calculated by using the guidelines described in section 1.4. 4-Cyanopentanoic acid dithiobenzoate (CTP) was chosen as the RAFT agent, since it belongs to the dithiobenzoate class of chain transfer agents, which have the highest transfer constants and therefore offer the highest degree of polymerization control.

Shortly prior to the aRAFT polymerization, CTP was synthesized by following the procedure described by Thang *et al.*.[3] This synthetic strategy uses an excess of the common RAFT initiator 4,4'-azobis (4-cyanovaleric acid) (ACVA), which undergoes a radical reaction with di(thiobenzoyl)disulfide in dry ethylacetate at 80 °C (Figure 3.1).

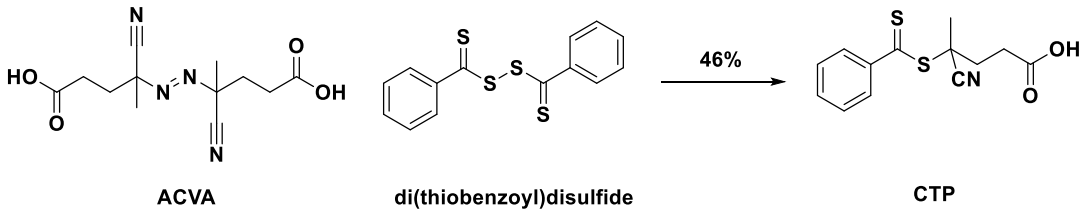

Figure 3.1. Synthesis of 4-cyano-4-((phenylcarbonothioyl)thio)pentanoic acid

3-Guanidinopropyl methacrylamide (GPMA), the other required starting compound, was synthesized by following the procedure described by Treat *et al.* (Figure 3.2).[4] This synthetic approach utilizes de-acidified N-(3-aminopropyl)methacrylamide (APMA), which attacks the guadinylation reagent 2-ethyl-2-thiopseudourea hydrobromide nucleophilically, thereby forming the desired product by releasing the side product ethanethiol.

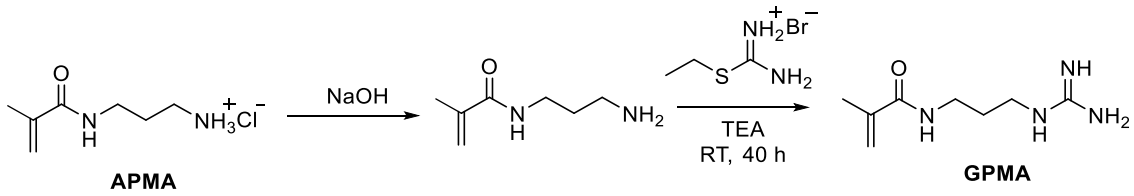

Figure 3.2. Synthesis of 3-guanidinopropyl methacrylamide

The macromolecular chain transfer agents (MacroCTAs) PHPMA as well as copolymers between HPMA and statistically incorporated APMA or GPMA (10 mol%) were prepared via aRAFT in acetate buffer at 70 °C by using CTP as the chain transfer agent and ACVA as the radical initiator. The successful synthesis of the MacroCTAs at low dispersities (Đ < 1.14) and only marginal deviations from the theoretical polymer size was confirmed by means of size exclusion chromatography (SEC) with hexafluoroisopropanol (HFIP) as the eluent (Table 3.1). In two cases the experimentally determined molecular weight exceeds the theoretical value. This can be attributed to the aminolysis or hydrolysis of the dithioester during the polymerization. It is a limitation of the RAFT polymerization, which was discussed in detail in section 1.4.[5-7]

Table 3.1 Theoretical and experimental molecular weight (M_n), dispersity (Đ) and the monomer composition of the MacroCTAs

MacroCTA	$M_{n_{theo}}$ [a] [g·mol^{-1}]	$M_{n_{exp}}$ [b] [g·mol^{-1}]	Đ [b]	composition (theor.)	composition (exp.)[c]
PHPMA$_{147}$	21000	21500	1.076	-	-
PHPMA$_{199}$	28000	28000	1.096	-	-
(HPMA$_{126}$-*s*-APMA$_{14}$)	21000	21000	1.070	9:1	9:1
(HPMA$_{180}$-*s*-APMA$_{20}$)	28000	29000	1.147	9:1	9:1
(HPMA$_{157}$-*s*-GPMA$_{13}$)	21000	25000	1.107	9:1	12:1
(HPMA$_{180}$-*s*-GPMA$_{12}$)	28000	27000	1.078	9:1	15:1

[a] Theoretical molecular weight was calculated using the Formula $M_{n,th} = ([M]_0/[CTA]_0) \cdot M_{w,monomer} \cdot \rho + M_{w,CTA}$ while the conversion ρ was taken from the kinetic studies done by Treat et al.[4]; [b] determined by HFIP SEC; [c] monomer composition of HPMA:APMA or HPMA:GPMA as determined by ^{1}H-NMR

In addition, ^{1}H-NMR (spectra in section 9.7.3.1) disclosed the average monomer composition of these polymer structures. Here, the intensities to the methylene proton reso-

nances of HPMA (3.92 ppm) as well as the methylene resonances of APMA or GPMA (3.08-3.21 ppm) were used to calculate the monomer ratios, which were in good agreement with the theoretical values (Table 3.1). The total number of monomers per polymer chain was estimated by utilizing the following exemplary calculation, which takes the molecular weight and the monomer composition into account:

$$\frac{M_n(Polymer)}{(9 \cdot M(HPMA) + 1 \cdot M(APMA)} = \frac{29000\ ^g/_{mol}}{1467.37\ ^g/_{mol}} \approx 20 \qquad (3.1)$$

The structure of this MacroCTA can therefore be expressed as $HPMA_{180}$-s-$APMA_{20}$.

In a subsequent step, the MacroCTAs were extended by cationic homopolymer blocks, which were comprised of either GPMA or APMA (Figure 3.4 – 3.6). Lastly, the terminal thiocarbonyl end group of the RAFT polymers was removed *via* the procedure described by Perrier *et al.* using azo-bis-(isobutyronitril) (AIBN) as the source of radicals.[8] This approach allowed the introduction of a nitrile, which provides an additional point for possible modification strategies. The first blocks (MacroCTAs) were synthesized with a desired size of either 21 or 29 kDa, while the addition of the second block was intended to increase the molar mass uniformly to 30 kDa. The final molar mass of the polymers was limited to this value to ensure the viability of these delivery agents in *in vitro* as well as *in vivo* experiments, since HPMA-based copolymers with a molecular weight of 25-50 kDa exhibit longer half-life times in the bloodstream, while still ensuring renal clearance.[9, 10] The controlled polymerization approach *via* aRAFT enabled the successful synthesis of the designed polymer structures at low dispersities ($Đ < 1.12$) and only marginal deviations from the theoretical polymer size (Table 3.2), which was confirmed by means of SEC with HFIP as the eluent. The SEC chromatogram in Figure 3.3 shows exemplary the terminal chain elongation of a MacroCTA with APMA and GPMA blocks. The removal of the thiocarbonylthio functionality was monitored using SEC as well, since this procedure not only changed the color of the polymer (from pink to colorless), but also drastically reduced its UV-vis absorbance at 310 nm. In order to estimate the number of monomer units (APMA or GPMA), which were attached as the second block, calculations based on the SEC results were performed. The following equation shows an exemplary calculation for polymer **7**:

$$\frac{M_n(\text{block copolymer}) - M_n(\text{MacroCTA})}{M(GPMA)} = \frac{31000\ ^g/_{mol} - 29000\ ^g/_{mol}}{184{,}24\ ^g/_{mol}} \approx 11 \qquad (3.2)$$

The measured ^{1}H-NMR spectra of the diblock copolymers could not be used for this purpose, due to peak-broadening. The formation of aggregates results in diminished

peak intensity and worsened resolution. It was not possible to fully circumvent this problem by utilizing salt additives or by varying the pH.

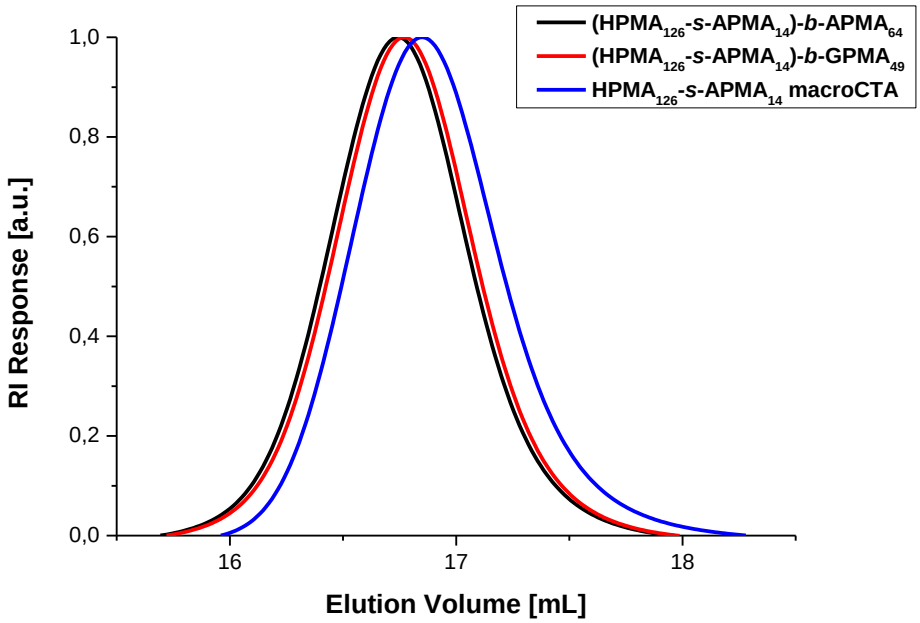

Figure 3.3. HFIP-SEC demonstrating exemplary the terminal chain elongation of (HPMA-s-APMA) macroCTA with GPMA or APMA. (blue)$HPMA_{126}$-s-$APMA_{14}$ macroCTA, (black) ($HPMA_{126}$-s-$APMA_{14}$)-b-$APMA_{64}$, and (red) ($HPMA_{126}$-s-$APMA_{14}$)-b-$GPMA_{49}$

Table 3.2. Synthesized polymer structures

polymer	monomer composition[a]	$M_{n_{exp}}$ [b] [g·mol^{-1}]	Đ [b]
1	(HPMA$_{180}$-s-APMA$_{20}$)-b-APMA$_{14}$	31500	1.109
2	(HPMA$_{126}$-s-APMA$_{14}$)-b-APMA$_{64}$	32500	1.103
3	HPMA$_{147}$-b-APMA$_{45}$	29000	1.079
4	HPMA$_{199}$-b-APMA$_{10}$	30000	1.117
5	(HPMA$_{157}$-s-GPMA$_{13}$)-b-APMA$_{28}$	30000	1.065
6	(HPMA$_{180}$-s-GPMA$_{12}$)-b-APMA$_{22}$	31000	1.097
7	(HPMA$_{180}$-s-APMA$_{20}$)-b-GPMA$_{11}$	31000	1.097
8	(HPMA$_{126}$-s-APMA$_{14}$)-b-GPMA$_{49}$	30000	1.076
9	HPMA$_{150}$-b-GPMA$_{58}$	32500	1.070
10	HPMA$_{196}$-b-GPMA$_{16}$	31000	1.059
11	(HPMA$_{157}$-s-GPMA$_{13}$)-b-GPMA$_{27}$	29500	1.057
12	(HPMA$_{180}$-s-GPMA$_{12}$)-b-GPMA$_{22}$	31000	1.072

[a)] Calculations are founded on the results of the HFIP-SEC and ^{1}H-NMR; [b)] Determined by HFIP-SEC

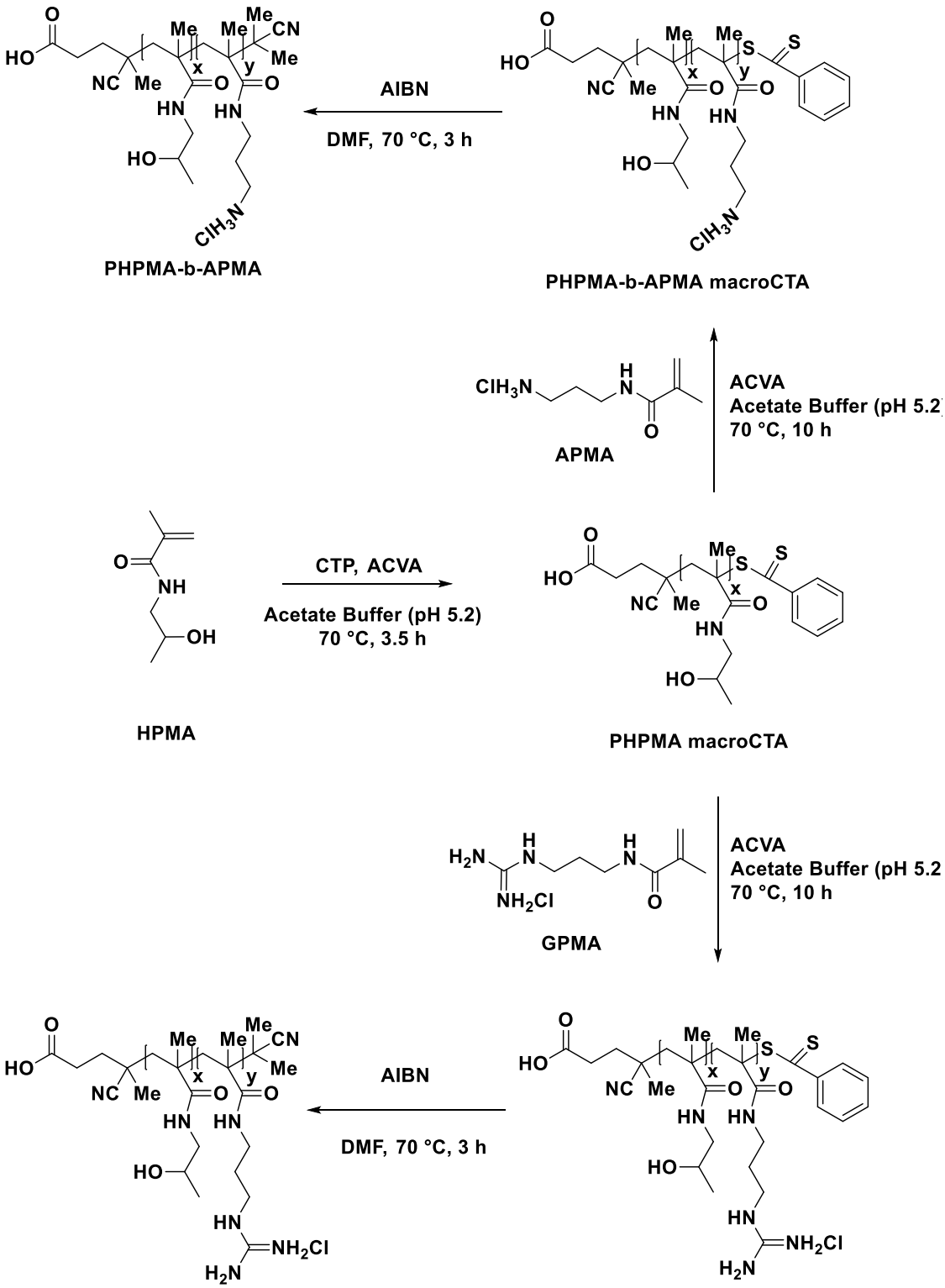

Figure 3.4. Synthesis pathway for HPMA-b-APMA and HPMA-b-APMA

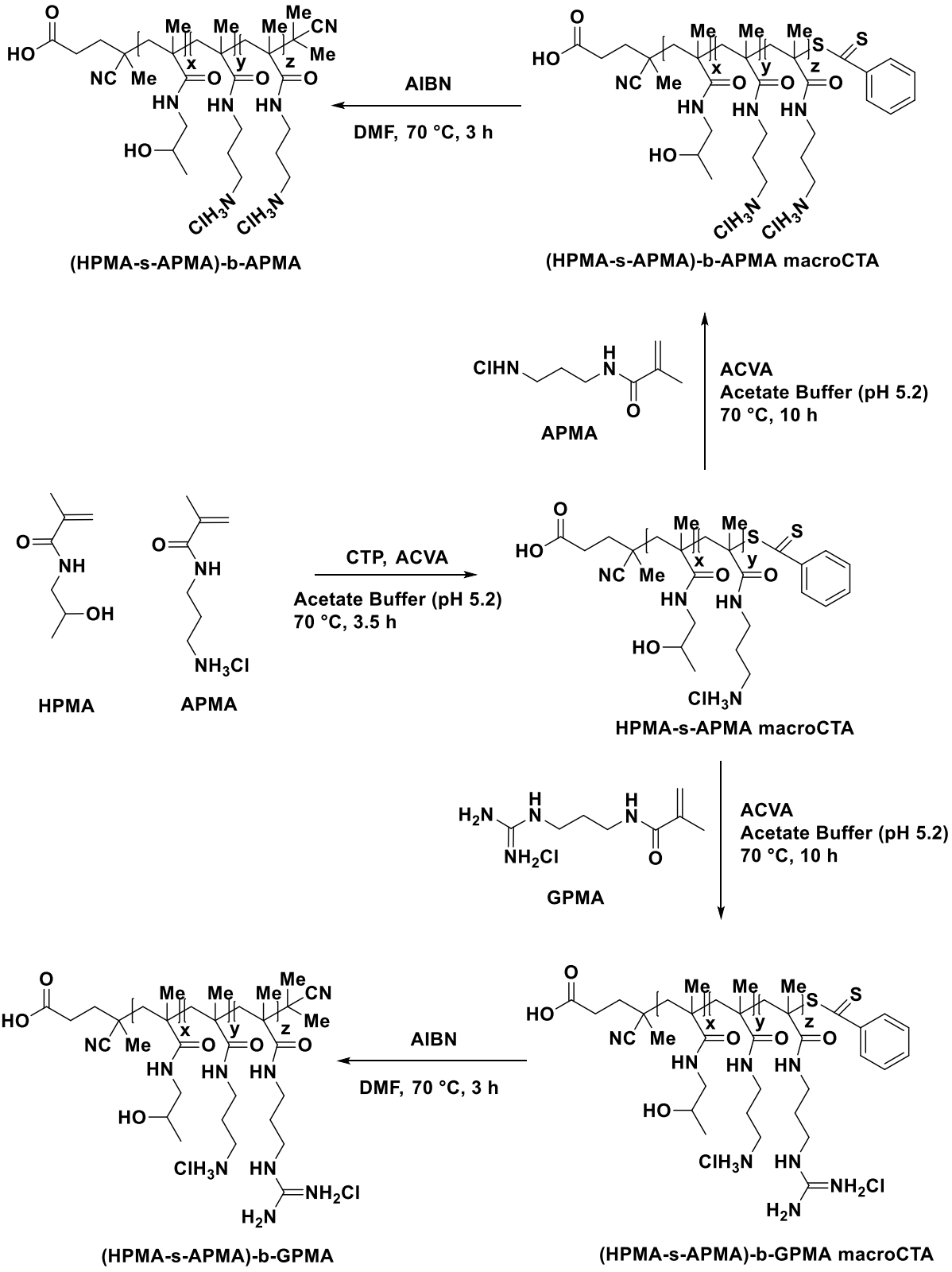

Figure 3.5. Synthesis pathway for (HPMA-s-APMA)-b-GPMA and (HPMA-s-APMA)-b-APMA

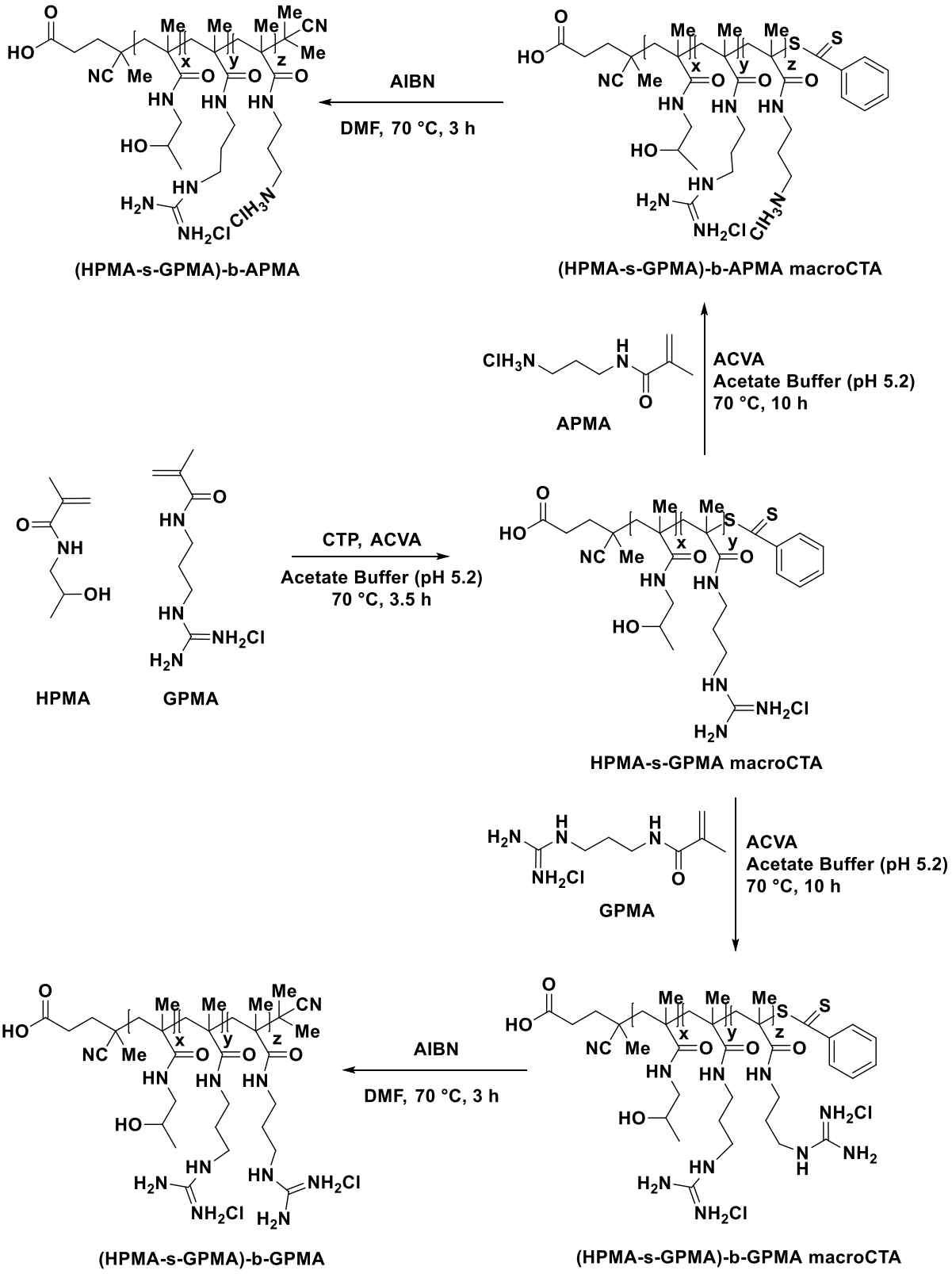

Figure 3.6. Synthesis pathway for (HPMA-s-GPMA)-b-APMA and (HPMA-s-GPMA)-b-GPMA

3.2 Complexation of siRNA

With the exception of dynamic light scattering, all binding studies were performed by utilizing FRET-labeled siRNA with Alexa555 on the 3'-end of the sense and Atto647N at the 5'-end of the antisense strand. This fluorescently labeled polynucleotide was incubated with the respective polymer structures in phosphate-buffered saline at different $mass^{polymer}/mass^{siRNA}$ ratios and the complex formation was then studied. The diblock copolymers were screened regarding their ability to complex siRNA. In particular, their binding properties was investigated *via* the electrophoretic mobility shift assay (EMSA) and their affinity towards siRNA was further quantified by microscale thermophoresis (MST), which helped determine dissociation constants. In addition, the size of the formed polymer/siRNA complexes was studied by means of dynamic light scattering (DLS), fluorescence correlation spectroscopy (FCS) and cryogenic transmission electron microscopy (cryo-TEM) for selected samples. FCS also helped to determine the loading efficacy in regard to the complex-bound amount of siRNA molecules.

3.2.1 Introduction of the methods

3.2.1.1 Electrophoretic Mobility Shift Assay (EMSA)

The electrophoretic mobility shift assay, which is an affinity electrophoresis technique commonly applied for the characterization of protein-DNA or protein-RNA interactions[11-13], can be applied to examine the complexes formed between cationic polymers and siRNA molecules. These polyplexes are also known as interpolyelectrolyte complexes (IPECs). In principle, the EMSA works by separating such complexes electrophoretically in a given gel (agarose or polyacrylamide). Here, the external charge, the size and, to a minor extent, the shape of the investigated polyplexes determine the direction and the distance of travel. The formation of complexes between cationic polymers and polynucleotides entails not only the compensation of negative charges, but also an increase in size. Hence, in case of a binding event, the well-defined band corresponding to unbound DNA or RNA will gradually fade, whereas the band corresponding to the formed polyplex will appear as separate, up-shifted band. However, if the overall charge of the polyplex is positive and its size does not exceed the mesh of the gel, it is possible to observe movement to the anode. If their size becomes too big to enter the network of the gel no movement will be observed. The same holds true in case the overall charge of the respective polyplex is neutral and are therefore unaffected by the electric field.[14]

The EMSA is a method only employed to investigate, whether the polymer of interest is able complex siRNA and if so, to determine the necessary $mass^{siRNA}/mass^{polymer}$ ratio for complete complexation. The evaluation of the results is based on said ratio. If less polymer molecules are required to achieve complexation (the lower the $mass^{siRNA}/mass^{polymer}$ ratio is), the higher the polymer's binding efficacy.

It is difficult to make a statement regarding the size of a complex based on the band shift, even if commercial DNA/RNA marker were employed, since the retention of polyplexes depends on parameters that are not relevant in a homologous series of nucleic acids of different length. Hence, to ensure comparability, a lane loaded only with free siRNA or DNA is used as a marker for the shift and intensity of the uncomplexed polynucleotide. The visualization of the bands is usually done via ethidium bromide or fluorescently labeled RNA/DNA are employed.[15]

3.2.1.2 Microscale thermophoresis (MST)

Microscale Thermophoresis (MST) is a comparatively new method for measuring binding affinity. It was recently commercialized by Nano Temper Technologies in Munich in light of the disadvantages of the preceding techniques (isothermal titration calorimetry (ITC), affinity capillary electrophoresis, fluorescence based ELISA assay), which are either expensive, time- or substance demanding.[16] MST allows precise measurement of binding constants (picomolar region) while requiring only small amounts of time and substance.[17] Measurements are usually performed in a volume of less than 1 µL, which is why glass capillaries are sufficient to hold the sample solution. The MST device itself is comparable to a fluorescence microscope with the exception that the detection is done not only by a photomultiplier but also by a CCD camera.[18, 19] Indicative by the name, thermophoresis, where the directed movement of molecules is correlated to a temperature gradient, is the main principle upon which this measuring technique is based.[20] Since MST is an optical method, where detection relies on fluorescence, samples are required to be either intrinsically fluorescent or labeled with fluorescent markers.[21]

The MST process can be described as follows: An infrared laser is utilized to induce a precise rise in temperature (1 to 6 K) by focusing on the glass capillary containing the sample solution for a time frame of 30 seconds at constant laser power.[22, 23] This procedure provides a temperature gradient inside the capillary, which in turn induces the desired thermophoretic motion of the molecules (Figure 3.7, 2). Continues irradiation

with the IR-laser for a time frame of 30 seconds leads to a plateau in detected fluorescence, marking the equilibrium state (Figure 3.7, 3). At this point the diffusion caused by temperature gradient compensates the mass diffusion.[22] Removing the heat source allows backward diffusion of the fluorescent molecules following the concentration gradient (Figure 3.7, 4).[19] The measured values of fluorescence intensity are correlated to the concentration of the non-fluorescent binding partner. Finally, the Hill method fit provides the dissociation constant, which helps quantify the binding strength.

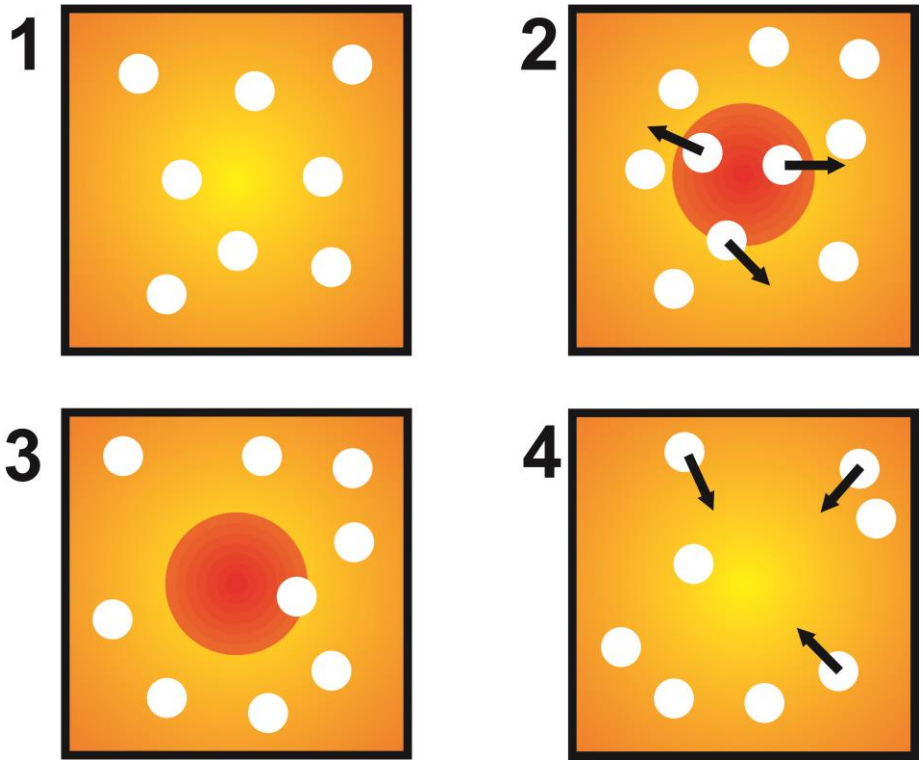

Figure 3.7. Schematic representation of the molecular events in a MST experiment: (1) distribution of molecules due to Brownian molecular motion (2) switched on infrared laser induces positive thermophoresis (3) steady-state (4) switched off infrared laser allows backward diffusion following the concentration gradient

Two types of thermophoretic movements can be differentiated. Positive thermophoresis decreases fluorescence, whereas negative thermophoresis is a phenomenon, by which particles migrate from low to high temperatures, thereby increasing the detected fluorescence signal. Such changes in fluorescence intensity can be directly correlated to the properties of the investigated molecule, such as its size, charge and its hydrodynamic volume.[24-26] All of these properties are affected in case of a binding event between a

cationic polymer and an anionic polynucleotide, since charge compensation and changes in size as well as shape take place. Hence, MST is a viable technique to determine the binding affinity of polymers towards siRNA or DNA.

3.2.1.3 Fluorescence correlation spectroscopy (FCS)

Fluorescence correlation spectroscopy (FCS) is a high-resolution analysis method, which synergistically combined with confocal microscopy illumination for single-molecule detection in the 1990s.[27] It facilitates the investigation of dynamic properties of fluorescent molecules possess in different solutions, if low concentrations are employed. This method primarily relies on detecting the continuously occurring fluctuations of fluorescence intensity $\delta I(t)$, which are induced by the diffusion of fluorescent species through the observation volume at ambient temperature. Figure 3.8 shows a typical setup in a FCS experiment. It is comprised of a high numerical aperture objective (NA), which is necessary to focus and direct a laser beam into the sample solution of a chamber. The fluorescence of the molecules in the observation volume is collected using the same objective, redirected by a dichroic mirror, filtered and finally focused by a tube lens onto a confocal aperture before it can be detected. The detection is usually done by either single photon counting avalanche photo diodes (APDs) or by utilizing photomultiplier tubes (PMTs). The recorded time-dependent fluctuations of the fluorescent intensity $\delta I(t)$ are then evaluated by using the autocorrelation function 3.3.

$$G(\tau) = 1 + \frac{<\delta I(t)\cdot\delta I(t+\tau)>}{<I(t)>^2} \tag{3.3}$$

As has been shown theoretically for an ensemble of m different types of freely diffusing identical fluorescence species, $G(\tau)$ has the following analytical form[28]:

$$G(\tau) = 1 + \frac{1}{N}\left[1 + \frac{f_T}{1-f_T}e^{-t/\tau_T}\right]\sum_{i=1}^{m}\frac{F_i}{\left[1+\frac{\tau}{\tau_{Di}}\right]\sqrt{1+\frac{\tau}{S^2\tau_{Di}}}} \tag{3.4}$$

Here, N is the average number of diffusing fluorescence species in the observation volume, f_T and τ_T are the fraction and the decay time of the triplet state, $S = z_0/r_0$ is the structure parameter with z_0 and r_0 representing the axial and radial dimensions of the confocal volume. As the structure parameter depends strongly on the specific characteristics of the optical setup a calibration using a dye with a known diffusion coefficient as a reference is required. F_i is the fraction of the i-th species and τ_{Di} is their diffusion time through the observation volume that is related to their diffusion coefficient, D_i, through:

$$D_i = \frac{r_0^2}{4\tau_{D_i}} \tag{3.5}$$

The hydrodynamic radius R_h can be calculated (assuming spherical particles) using the Stokes-Einstein relation:

$$R_h = \frac{k_B T}{6\pi\eta D_i} \tag{3.6}$$

Here, k_B is the Boltzmann constant, T is the temperature, and η is the viscosity of the solution. When only one type of fluorescent species are present (m = 1), the fluorescent brightness can be estimated as the ratio of the average fluorescent intensity and the average number of species in the confocal volume. This approach allows the calculation of the loading capacity (average number of siRNA molecules per polyplex):

$$\frac{<I(t)>}{N} \tag{3.7}$$

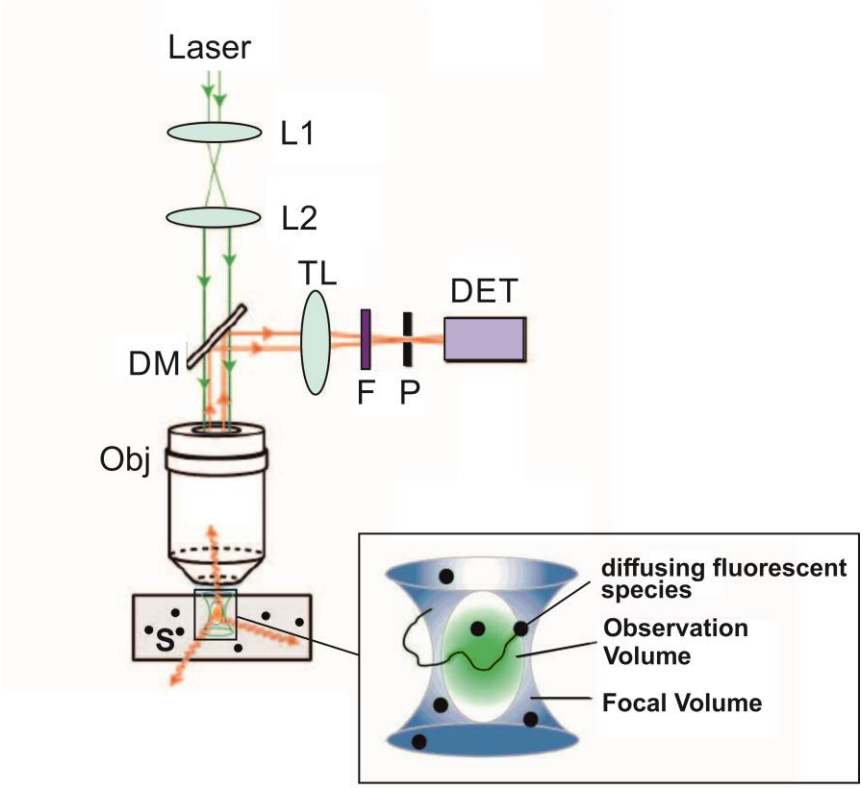

Figure 3.8. FCS septip (schematic representation): A laser beam is expanded by a telescope (L1 and L2) and focused by a high-NA objective lens (Obj) on a fluorescent sample (S) creating a focal volume within which sample particles (•) are illuminated. The same objective lens collects the epifluorescence. The beam is then guided by a dichroic mirror (DM) into a tube lens for focusing. Passing the filter (F) and the confocal aperture (P) the beam arrives at the detector (DET).

3.2.2 Polyplex formation

Among the twelve polymer structures only polymers **1**, **4** and **10** were not able to complex siRNA (Figure 3.9 and Table 3.3). The poor affinity of these three polymers even at the highest $mass^{polymer}/mass^{siRNA}$ ratio indicates the challenge of complexation. Although modification or functionalization strategies could remedy this flaw, these polymers, were deemed unsuited as carriers for siRNA, since they did not fulfill the most important requirement, namely the complexation.

EMSA experiments (Figure 3.9) showed that only one of the three structures belonging to group *Ib* was able to form complexes with siRNA, namely polymer **6**. Its affinity towards siRNA was, however, only observed *via* EMSA. Dynamic light scattering and microscale thermophoresis did not confirm these results. Due to the first observation that all block copolymer structures with a short APMA cationic block failed to pass the initial screening, it can be derived that a long cationic block with a $length^{binding\ block}/length^{non\text{-}biding\ block}$ ratio lower than 1:8.7 (lowest observed ratio, calculated based on the HFIP-SEC results) is unsuited for the design of siRNA delivery agents, if primary amino groups are used as the source of the cationic charges.

Additional insights were gained by evaluating the EMSA results. For example, the polymer group *II* showed that binding can be improved not only by elongating the cationic block, which increases the cationic charge density, but also by utilizing the guanidinium group as a source of cationic charges. The comparison of the groups *IIa* and *IIb* reaffirmed that an increased cationic charge density due to a longer cationic block improves binding. The only polymer structure in group *II* unable to form complexes with siRNA, namely polymer **10**, belongs to the subgroup *IIb*. In addition, polymer **12**, which belongs to the subgroup *IIb* as well, does not bind siRNA effectively. It forms a heterogenic mixture of polyplex sizes, which was observed not only *via* EMSA (no distinct bands), but also by means of DLS, where multiple large species were detected and data evaluation had to be abandoned. Based on these findings, one can conclude that long cationic blocks are required to ensure efficient complexation of siRNA.

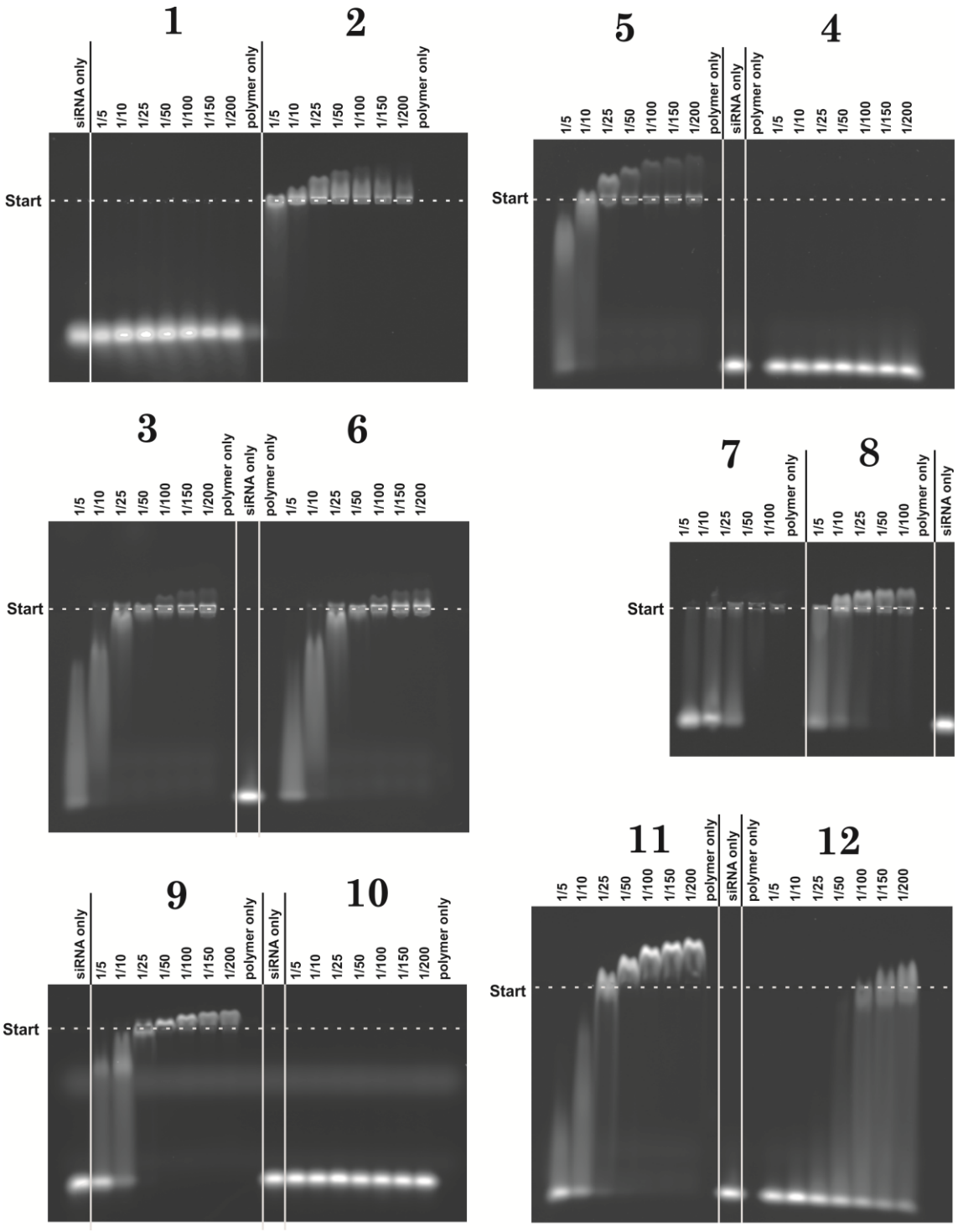

Figure 3.9. Electrophoretic mobility shift assay for polymers 1 to 12 to determine the required mass^{siRNA}/mass^{polymer} ratio for complete complexation

Although polymer structures with long cationic chains did not differ significantly in terms of the mass^{polymer}/mass^{siRNA} ratio, which is required to achieve complete complexation (Table 3.3), polymers with short APMA (subgroup *Ib*) or GPMA blocks (subgroup *IIb*) were shown to behave differently. While none of the polymers in subgroup

Ib were able to complex siRNA, two of the three polymers with a short GPMA block were able to form stable complexes under the same conditions. Here, statistic incorporation of GPMA or APMA monomers into the non-binding block (≈ 10 mol%) was enough to achieve the formation of polyplexes between siRNA and the polymers **7** and **12**. Utilizing the same strategy for polymers with a short APMA block (polymers **1** and **6**) did not suffice to compensate for the poor binding properties. The role of these added cationic charges, which could be that of a direct binding site for the siRNA or that of a binding promoter, was further investigated by simulating the formation of the complexes (section 3.5). We can expect that the non-binding block, which consists mainly of uncharged HPMA monomers, puts an entropic strain on the electrostatic interaction between the siRNA molecule and the cationic polymer, which must be compensated by means of binding strength. This can be achieved by either increasing the length of the cationic block or by incorporating an increased amount of cationic charges into the HPMA block.

To further quantify the binding affinity, microscale thermophoresis (MST) was utilized. It allowed the qualitative evaluation of the binding strength of the polymers, since dissociation constants for the interaction between FRET-labeled siRNA and each polymer structure (plotted graphs in section 8.7.1.1; K_d values in Table 3.3) were obtained. This analytical method evaluates the binding affinity by detecting the binding event induced changes of the thermal diffusion coefficient of a fluorescently labeled molecule.[24-26] Here, similar to previous studies, where cationic diblock copolymers were employed[29], quenching of the FRET signal was observed. This phenomenon can be partly explained with self-quenching and an inner filter effect of the locally concentrated fluorophores, but it is expected that the main reason lies with the properties of the various polymer structures. With the exception of polymer **9**, all polymer structures that were able to complex siRNA lead to quenching. However, to determine the dissociation constant by means of thermophoresis the fluorescence signal is required to independent to the used concentrations of the binding partner. Hence, except for polymer **9**, the binding strength of the polymer structures was calculated by using the Hill-method fit on the results of the fluorescence mode of the MST, which follows the binding-induced changes of the fluorescence intensity. In these cases, the utilized approach is comparable to measuring a binding curve based on a fluorimetric titration.

Table 3.3. The hydrodynamic radius (R_h) of the polymers as well as the hydrodynamic radius of the respective polyplexes, the dissociation constant (K_d) of the polyplexes and the required $mass^{polymer}/mass^{siRNA}$ for complete complexation (color code: subgroup *Ia*, *Ib*, *IIa*, *IIb*, where (green) corresponds to guanidinium group bearing polymers and (orange) to polymers with primary amino groups, i.e. polymers groups I and II)

polymer	$R_{h\ (polymer)}{}^{a}$ *[nm]*	$R_{h\ (polyplex)}{}^{b}$ *[nm]*	$mass^{polymer}/mass^{siRNA}$ *ratio*[c]	$K_d{}^{d}$ *[nM]*
1	4.6	free polymer	no complexation	no affinity
2	5.1	79.7	5	134 ± 3.0
3	6.9	25.0	25	60.9 ± 3.2
4	7.8	free polymer	no complexation	no affinity
5	4.3	52.0	25	15.1 ± 0.2
6	5.2	free polymer	25	no affinity
7	5.1	83.6	50	14.9 ± 0.4
8	6.3	49.6	50	43.8 ± 5.6
9	5.8	110.0	25	49.2 ± 1.2
10	7.4	free polymer	no complexation	no affinity
11	4.7	32.7	25	31.6 ± 0.7
12	3.7	heterogeneous	100[e]	68.0 ± 3.5

[a)]determined by DLS in aqueous 0.15 M sodium chloride solutions after filtering at 0.2 µm cut-off; [b)]determined *via* DLS in aqueous 0.15 M sodium chloride solutions, where unlabeled siRNA was added to the filtered polymer solutions to form the polyplexes in the cuvette; [c)]values for complete complexation were determined *via* EMSA; [d)]determined by MST using the Hill-Method for fitting the results; [e)]complete complexation is not achieved even at the highest used concentration, but a very heterogenous complex composition can be observed

All polymers that did not achieve complex formation during the EMSA showed no affinity towards siRNA during the MST measurement of the dissociation constants. Meaningful comparison of the binding strength according to differences of the lowest $mass^{siRNA}/mass^{polymer}$ ratio, at which siRNA complexation was achieved, was not possi-

ble, since this approach allows only a crude approach. In addition, almost all polymers required $mass^{polymer}/mass^{siRNA}$ ratios of 25 or 50 to achieve complete complexation of the siRNA molecules. Calculating the K_d values *via* MST, on the other hand, made it possible to rank the architectures according to their affinity towards siRNA excluding the four samples that did not bind siRNA (polymers **1**, **4**, **6**, **10**):

7 (14.9 ± 0.4 nM) > **5 (**15.1 ± 0.2 nM) > **11 (**31.6 ± 0.7 nM) > **8** (43.8 ± 5.6 nM) > **9 (**49.2 ± 1.2 nM) > **3** (60.9 ± 3.2 nM) > **12 (**68.0 ± 3.5 nM) > **2** (134 ± 3.0 nM)

The majority of the polymers showed significantly stronger binding affinity towards siRNA in comparison to modified cyclodextrin ($K_a = 1.6 \cdot 10^4 M^{-1}, i.e. K_d = 62{,}5\ \mu M$) or cationic lipids, such as 1,3-dimyristoylamidopropane-2-[bis(2-dimethylaminoethane)] ($K_a = 10^5 M^{-1}, i.e. K_d = 10\ \mu M$).[30, 31] Polymer **7** and polymer **5** were even shown to bind siRNA only seven times less effectively than the naturally occurring siRNA-binding protein translin (K_d = 1.9 ± 0.5 nM).[32] This comparison is intended to only provide an indication regarding the ranking of these polymers within the known siRNA binding substances. It was not the aim of this chapter or this thesis to develop a siRNA delivery agent with the highest possible binding strength. In fact, such comparisons to literature-known carrier systems do not provide additional insight for the connection between the structure of a carrier system and its properties. As soon as more than one variable (e.g. the backbone structure or the length of the cationic polymer) differ, it is no longer possible to accurately state, whether the observed difference in binding strength would be based on the first, or the second or even a combination of both. Other properties of delivery agents, such as polyplex size, internalization into cells or knock-down efficacy are affected analogously. Since this thesis aims to unveil such connections, it must be heavily relied upon comparison of polymers with a similar structure, i.e. those that were synthesized by me.

Based on the MST and EMSA results several general statements concerning the relationship between a polymers structure and the measured binding strength can be made:

(1) The elongation of the cationic block improves the binding strength.

Comparing the subgroups a (short cationic block) and b (long cationic block) in each respective group of polymers distinctly favors subgroup b. Not were all polymers belonging to subgroup b able to for polyplexes with siRNA, but also their dissociation constants were substantially lower.

(2) The HPMA block plays a role during polyplex formation and the incorporation of protonatable monomers within said block affects the binding strength.

Using a diblock copolymer with an uncharged HPMA homopolymer block and a long GPMA or APMA block (polymers **3** and **9**) as comparative examples, the binding affinity can be enhanced by incorporating GPMA monomers into the non-binding HPMA block (polymers **5** and **11**). Utilizing APMA monomers for the same purpose leads to only minor improvements of the K_d value (polymer **8**) and can even have an adverse effect (polymer **2**). This observation supports the hypothesis that the guanidinium groups of GPMA monomers offer more utility in the design of siRNA delivery agents.

(3) The source of the cationic charges matters. Guanidinium groups provide stronger binding.

Intergroup comparison of the K_d values of the polymers belonging to group *I* and *II* (polymers across from each other in Figure 3.10) supports this observation:

$K_{d\ \text{polymer}\ \mathbf{1}}$ = none	<	$K_{d\ \text{polymer}\ \mathbf{7}}$ = 14 nM
$K_{d\ \text{polymer}\ \mathbf{2}}$ = 134 nM	<	$K_{d\ \text{polymer}\ \mathbf{8}}$ = 43 nM
$K_{d\ \text{polymer}\ \mathbf{3}}$ = 60 nM	<	$K_{d\ \text{polymer}\ \mathbf{9}}$ = 49 nM
$K_{d\ \text{polymer}\ \mathbf{4}}$ = none	=	$K_{d\ \text{polymer}\ \mathbf{10}}$ = none
$K_{d\ \text{polymer}\ \mathbf{5}}$ = 15 nM	>	$K_{d\ \text{polymer}\ \mathbf{11}}$ = 31 nM
$K_{d\ \text{polymer}\ \mathbf{6}}$ = none	<	$K_{d\ \text{polymer}\ \mathbf{10}}$ = 68 nM

Only the polymer pair of **5** and **11** did not follow this trend. It is expected that this phenomenon is not the result of a strong electrostatic interaction alone, but the consequence of a steric phenomenon. siRNA molecules are much smaller than DNA, which makes them behave like rigid rods and affects their binding to cationic polymers.[33, 34] siRNA is not only less multivalent than DNA, when interacting with the cationic carriers due to the fewer binding sites per molecule, but it also condenses very little making it less capable in adapting conformations that are ideal for high affinity binding. To overcome this challenge polymers with a high charge density have been suggested in literature.[35] However, it appears that the ability of guanidinium groups to not only form electrostatic interactions, but also multiple hydrogen bonds at a single interaction site allows for efficient binding and circumvents the need for high charge densities.

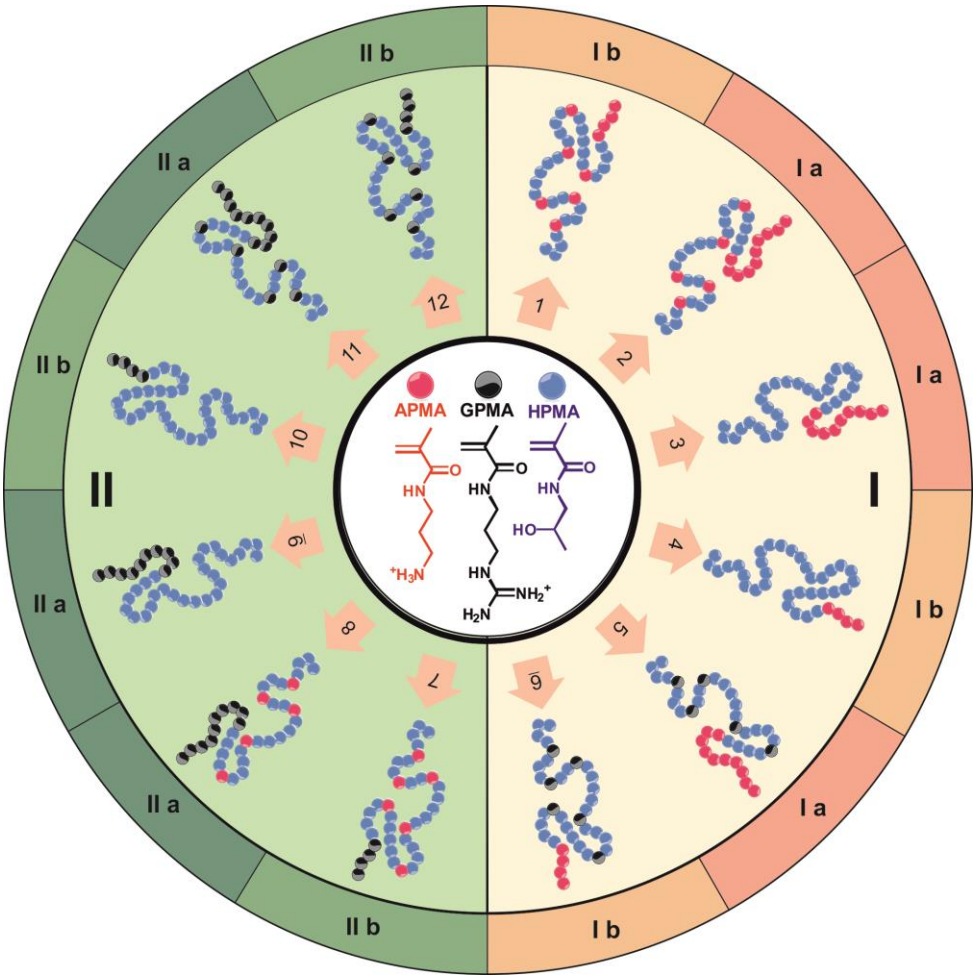

Figure 3.10. Schematic representation and classification of the polymer structures, which have been allocated the numbers 1 to 12 (Table 3.1). Group I (orange) are equipped with an APMA block for the complexation of siRNA. Group II (green) rely on a GPMA block for the same purpose. The polymers are further divided into subgroups Ia, Ib, IIa and IIb based on the length of the APMA or GPMA blocks, where "a" is corresponds to copolymers with long cationic blocks and "b" to those with a short one. Color code of the monomer-representing beads: HPMA (blue), APMA (red) and GPMA (black).

(4) A threshold length$^{\text{binding block}}$/length$^{\text{non-biding block}}$ ratio exists, which is required for the formation of polyplexes.

Considering the fact that throughout the study diblock copolymers of similar overall length at different block ratios were used and small binding blocks (in most cases) did not provide sufficiently strong electrostatic (or other) interactions between the respective polymer and siRNA molecules, but long binding blocks did, it is indicated that a threshold regarding the necessary (minimal) size of the cationic block must exists. Find-

ing the ideal block ratio between the binding and non-binding block for optimal binding properties is a daunting task, if tackled by a purely synthetic approach. This statement is especially true, if other sizes of the carrier system (40 kDa, 50 kDa, etc.) need to be considered. Utilizing simulations (section 3.4) is the more prudent approach to find the ideal length$^{\text{binding block}}$/length$^{\text{non-biding block}}$ ratio of cationic diblock copolymer siRNA carrier systems impartial to their overall size.

Following the binding studies *via* EMSA and MST, the packing efficacy of the twelve polymers was investigated by means of DLS (plotted graphs in section 9.7.2.1; R_h values in Table 3.3). Polymer aggregates, which affect the results, were removed by filtering the polymer samples prior to the complexation step and by using an aqueous solution of sodium chloride (0.15 M), where the formation of new aggregates was suppressed. This approach allowed the study of the hydrodynamic radius of free polymer chains and that of the respective polyplexes. While the twelve polymers were of similar length (~30 kDa, HFIP-SEC determined), variations of the hydrodynamic radius of the free polymer chains have been observed. The polymers can be arranged based on their solubilization size before they were incubated with siRNA:

12 (3.7 nm) < **5** (4.3 nm) < **1** (4.6 nm) < **11** (4.7 nm) < **7** (5.1 nm) = **2** (5.1 nm) < **6** (5.2 nm) < **9** (5.8 nm) < **8** (6.3 nm) < **3** (6.9 nm) < **10** (7.4 nm) < **4** (7.8 nm)

It was expected that an increased cationic charge density would lead to a higher bending stiffness of the monomers along the polymer chain, due to charge-repulsion, and thereby to larger hydrodynamic radii.[36] Nevertheless, it was not possible to correlate both parameters for either group *I*, or group *II*. Polymers **4** and **10**, for example, had the lowest charge density, but they formed the biggest structures in aqueous solution. The solubilization properties of the HPMA comonomers, which have a water-solubility of only 13 wt% at 25 °C, are expected to have impacted the detected hydrodynamic radii to a higher degree than the bending stiffness.[37-39]

With the exception of the polymers **1**, **4**, **6** and **10**, all diblock copolymers formed DLS-detectable polyplexes with siRNA, which further supports the findings of the EMSA and MST experiments. Among the polymers, which are able to form polyplexes with siRNA, polymer **12** represents a special case. Here, a heterogenic polyplex mixture with more than three large species was observed. Due to this, it was not possible to calculate the hydrodynamic radius of its respective polyplexes. The remaining seven polymers can be ordered according to the size of their respective polyplexes with siRNA:

9 (110 nm) > **7** (84 nm) > **2** (80 nm) > **5** (52 nm) > **8** (50 nm) > **11** (33 nm) > **3** (25 nm)

The rigid rod-like character of siRNA molecules makes condensation by the polymeric carrier difficult.[34] Hence, it was not expected to observe similar effects as those described for DNA.[40, 41] For example, it was not possible to correlate the measured polyplex size to either the binding efficacy, the charge density, the source of the cationic charges (GPMA or APMA) or even the hydrodynamic radius of the polymer structures. The difficulty of finding such a correlation strongly relates to the fact that siRNA molecules are less capable in adapting bent conformations than DNA allowing only three types of interactions with linear cationic polymers: (i) a longitudinal arrangement, (ii) a transversal arrangement, where a cationic polymer bridges two or more siRNA molecules and (iii) an enveloping arrangement, where the cationic polymer chain winds around the siRNA molecule by following the phosphodiester backbone of the sense- or the antisense strands. Which of these interactions is predominant, can be influenced by the structure of the polymer and also by the chosen conditions, such as the salt concentration, during the binding event.[42, 43] For example, in case of a diblock copolymer, the binding block must be sufficiently short to impede bridging of multiple siRNA molecules, if complexes consisting of predominantly a single siRNA molecule and multiple polymer chains are desired. In this case, the non-binding blocks protruding from the complex's center are responsible for the detected hydrodynamic radius. On the other hand, if polyplexes with multiple siRNA molecules per complex are intended, diblock copolymers with long binding blocks should be utilized. The multitude of parameters influencing the polyplex size, which includes the concentration of the binding partners as well as the used $mass^{polymer}/mass^{siRNA}$ ratio during the complexation, makes a straightforward correlation difficult.[44]

To determine whether the shape of the polyplexes affected the DLS results, cryogenic transmission electron microscopy (cryo-TEM) was employed. In particular, the unexpectedly large size of polymer **9**-based polyplexes appeared upon initial review as too large if compared to its counterpart (polymer **3**), especially considering its lower dissociation constants, which should have led to better condensation of siRNA. The cryo-TEM experiments were performed in collaboration with Philip Biel (Prof. Dr. Felix H. Schacher, Institute of Organic Chemistry and Macromolecular Chemistry, Friedrich Schiller University).

All diblock copolymers were expected to form core-corona structures with a polyplex core and a neutral shell comprising the non-binding HPMA containing blocks. Such spherical structures were confirmed for polyplexes between polymer **3** and siRNA. Here, a heterogeneous distribution of the detected diameters was observed (Figure 3.11). Averaging 60 complexes, a mean diameter of 60 nm was calculated, which is in good agreement with the DLS results. Nevertheless, it is plain to see that the sizes of these polyplexes are heterogeneous, which cannot ensure reliable treatment of a disease in patients. Even if polymer **3** were to induce exceptional knock-down, it would be still lacking in terms of applicability.

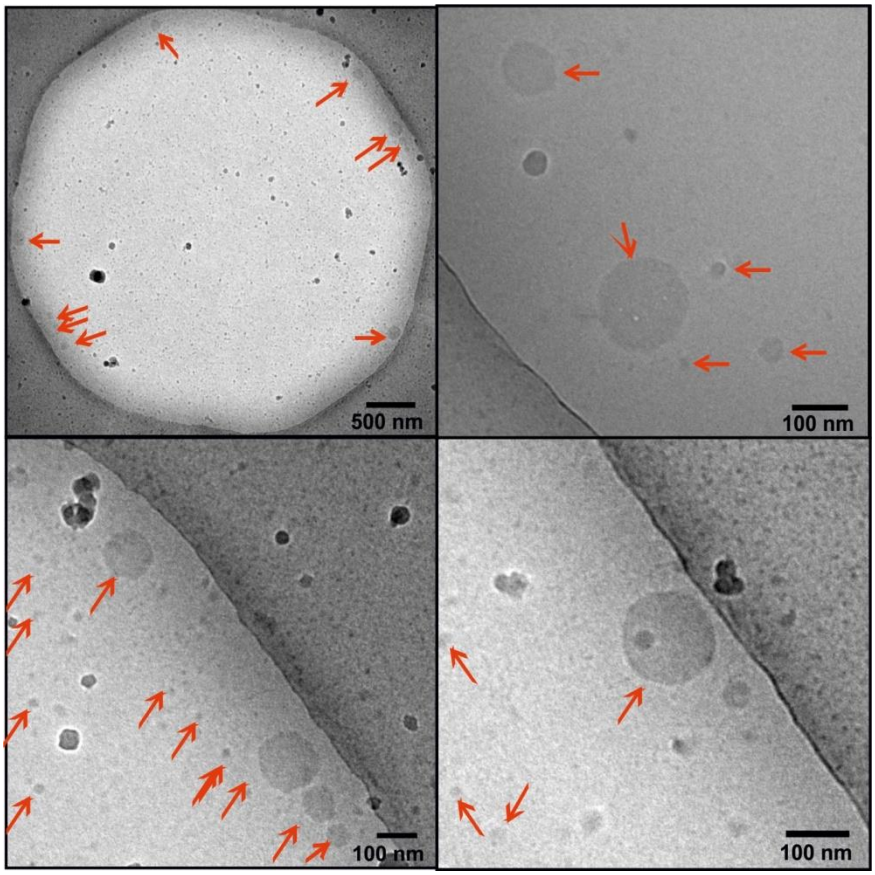

Figure 3.11 Cryo-TEM-micrographs of a vitrified aqueous suspension of polymer 3/siRNA polyplexes in PBS-buffer; red arrows mark aggregates.

The size of the less heterogeneously distributed but also spherical polymer **8**-based polyplexes was determined to be 26 nm *via* cryo-TEM (averaging 41 complexes, Figure 3.12). This value equals approximately half of the value measured *via* DLS (Table 3.3), hhowever this disparity was expected. cryo-TEM experiments typically provide lower

values than DLS measurements due to the different weighing of the occurring large species during the calculation of the radius. As previously outlined, a large species will suppress the signal of a small one in DLS measurements.

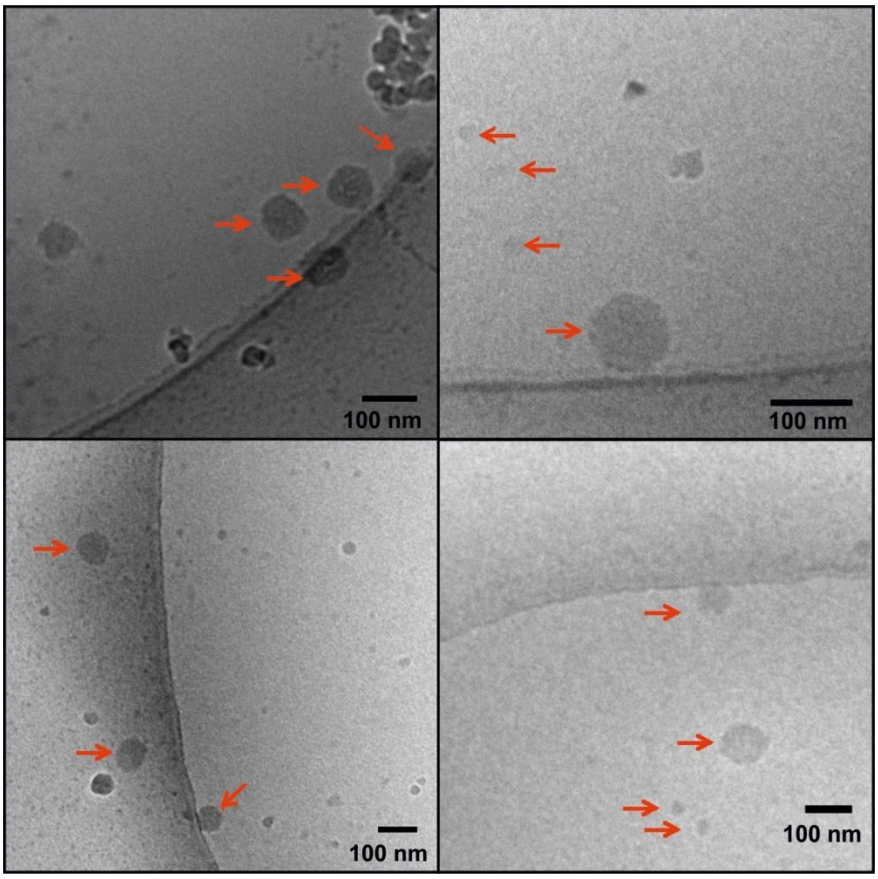

Figure 3.12 Cryo-TEM-micrographs of a vitrified aqueous suspension of polymer 8/siRNA polyplexes in PBS-buffer; red arrows mark aggregates.

Polymer **9** facilitated the formation of the largest (DLS-observed) polyplexes of this study, however, cryo-TEM revealed them to be worm-like structures with an average width of 7.3 nm and lengths up to and exceeding 100 nm (Figure 3.13). Since these worms scatter light differently than spherical particles, it is clear why the DLS results were misleading. Wormlike micelles possess advantages over their spherical counterparts, including increased tumor accumulation *via* the enhanced penetration and retention effect, and improved cellular uptake efficiency.[45] A statement regarding a connection between the structure of polymer **9** and the formation of worm-like structures cannot be made.

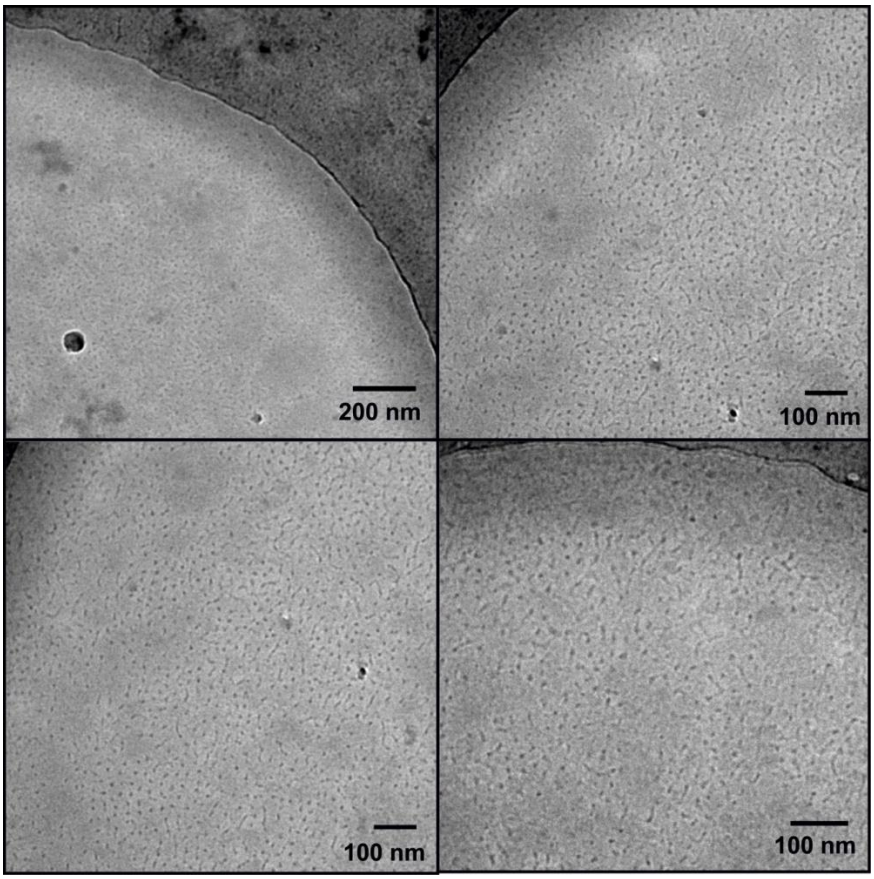

Figure 3.13 Cryo-TEM-micrographs of a vitrified aqueous suspension of polymer 9/siRNA polyplexes in PBS-buffer.

Fluorescence correlation spectroscopy (FCS) experiments, which were performed in collaboration with Dr. Kaloian Koynov and Andreas Best (group of Prof. Dr. Hans-Jürgen Butt, Max Planck Insititute for Polymer Research), provided further insights on the interdependence of the size of a complex and the amount of complex-bound siRNA molecules (Figure 3.14). This investigation was performed only for the polymers **7** and **8**. They have the highest structural similarities to the simulated copolymers **7+** and **8**, for whom a computational investigation of the same properties was performed (section 3.4). This approach ensures comparability between the experimental study and the simulation. Uncomplexed siRNA molecules were shown to possess a hydrodynamic radius of 2.8 nm. Adding polymer **7** or 8 to the solution at the $weight^{polymer}/weight^{siRNA}$ ratio of 100:1 resulted in a distinct shift of the measured FCS autocorrelation function to longer decay times (Figure 3.14), which indicates the formation of larger fluorescent species. The collected FCS data also gives insights into the packing of siRNA molecules. In case of polymer **8,** an average hydrodynamic radius of 45 nm was calculated and the number of siRNA molecules per complex was estimated to 12. However, the

used calculation approach to determine the loading capacity (equation 3.7) relies on the average molecular brightness, which forces a bias towards large complexes. In addition, the fluorescent brightness of polymer **8**-based polyplexes was heterogeneously distributed (time trace, Figure 3.14). Hence, the calculated number of siRNA molecules per complex is overestimated and the real number is expected to be lower. The FCS data of polymer **7**-based complexes, on the other hand, was best quantified by fitting the curve with a 3-components-fit, where one component is fixed to free siRNA. These results indicate that polymer **7** facilitates the formation of two types of complexes: predominantly small polyplexes (R_h = 6 nm) with one siRNA molecule per complex and a minor population (~5%) of larger complexes (R_h > 35 nm) that contain multiple siRNA molecules. Packing efficacy of polynucleotides is an issue, which is also addressed in nature, where histone, a highly basic protein, is used to achieve DNA condensation.[46, 47] However, siRNA molecules, which lack the ability to adopt different conformations due to its rigid rod-like character, are an exception. Nevertheless, Cheng *et al.* were able to demonstrate that a copolymer comprised of a PEG chain and a GPMA block forms spherical polyplexes with oligonucleotides.[48] This observation indicates that higher packing orders with internal symmetry can be achieved. Similar results are expected for the block copolymers of this study.

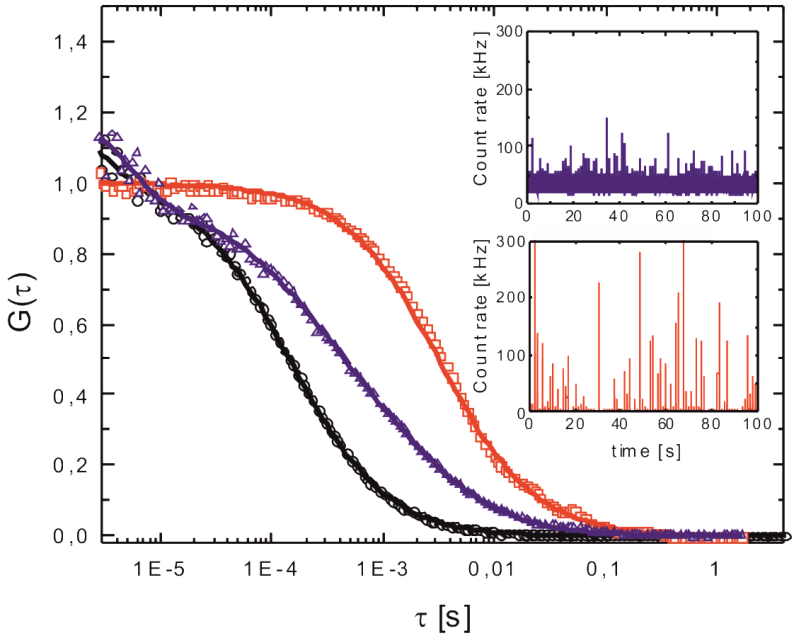

Figure 3.14. Normalized FCS autocorrelation curves of (black) fluorescently labeled siRNA alone, (red) polyplexes between siRNA and polymer 8 ((HPMA$_{126}$-s-APMA$_{14}$)-b-GPMA$_{49}$) or (blue) polyplexes between siRNA and polymer 7 ((HPMA$_{180}$-*s*-APMA$_{20}$)-*b*-GPMA$_{11}$). The solid lines represent the autocorrelation fits with equation 3.4. The inlay shows the plot of the time trace for each complex.

FCS was also used in order to investigate the stability of the siRNA/polymer **8** polyplexes at different degrees of dilution and in the presence sodium dodecyl sulfate (SDS), which is commonly used as a denaturing agent, since it disrupts non-covalent bonds. If such polyplexes were to be found not stable in solution, it is not possible to use them for medication purposes, since they will be strongly diluted in the body of a patient (concentration gradient: vial > blood stream > interstitium > cells). Here, diluting the polyplex solution by a factor exceeding 100 was not performed. In order to compensate for the fewer number of fluorescent molecules traveling through the observation volume and obtain sufficient data points for the autocorrelation, the measurement period had to be increased drastically. In this context, it was found that the estimated measuring time for a 1:1000 dilution of 24 hours would place an undue burden on the apparatus.

The results of the investigation are depicted in Figure 3.15. The formed polyplexes remained stable regardless of the degree of dilution. According to the time traces, dilution

only impacted the event count of detected fluorescent species. Neither did the amount of free siRNA molecules increase. Nor was the hydrodynamic radius of the polyplexes (R_h = 45 nm) affected by dilution. This observation indicates that the formed polyplexes are not affected by a constant equilibrium of detaching and reattaching polymer or siRNA molecules. Otherwise, their size would have decreased over time and the event count would have regenerated itself over time.

In contrast to dilution, the use of SDS, fully abolished all interactions between the polymer and siRNA molecules. This effect is made visible not only by the time trace, but also by the calculated hydrodynamic radius of 3.4 nm (Figure 3.15, D), which corresponds to free siRNA. This investigation has shown the formed polyplexes to be sufficiently stable for *in vivo* experiments

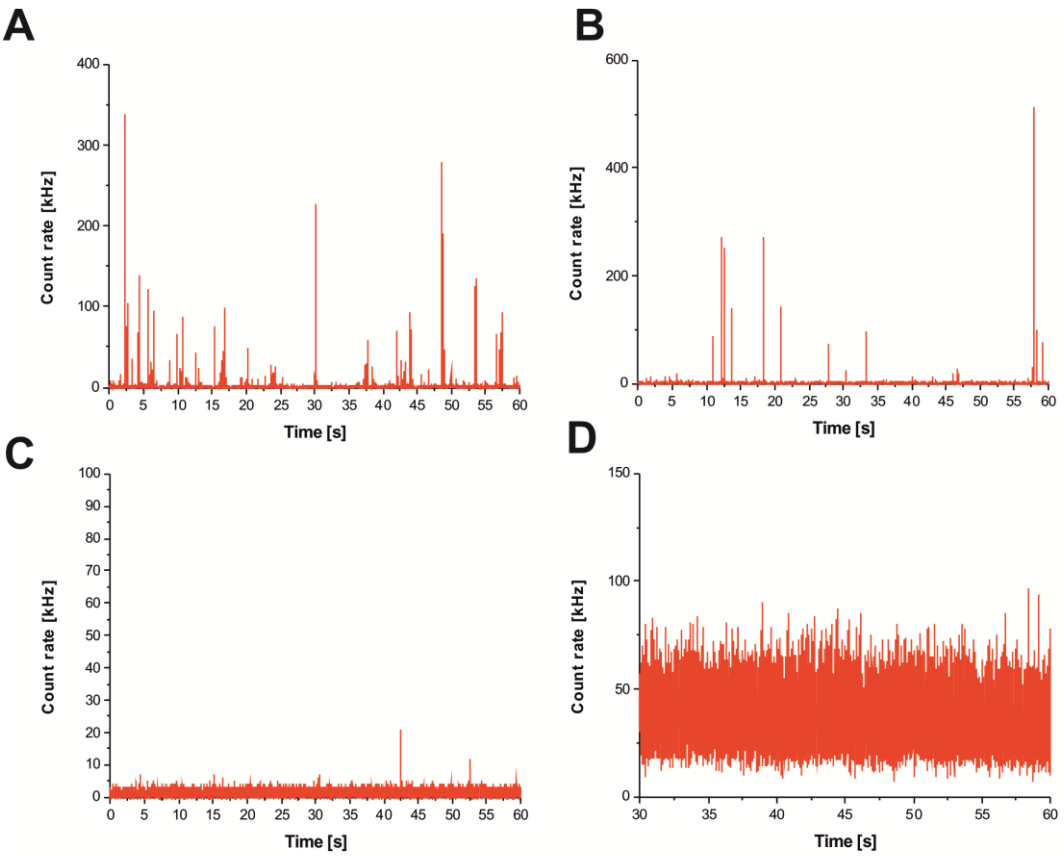

Figure 3.15. FCS time trace plot of the polyplexbes between siRNA and polymer 8 ((HPMA$_{126}$-s-APMA$_{14}$)-b-GPMA$_{49}$). (A) no dilution, (B) dilution of 1:10, (C) dilution of 1:100, (D) addition of 10 µL of a 20 w% solution of sodium dodecyl sulfate (SDS)

3.3 Biochemical characterization

3.3.1 Cytotoxicity

The investigation of the binding properties has revealed that polymers belonging to the subgroups *Ia* and *IIa* complex siRNA than their counterparts with a short cationic block (subgroups *Ib* and *IIb*). An increased cationic charge density of polymeric siRNA delivery agents due to high mol% content of the monomers with the ability to bear cationic charges is not only known to improve internalization into cells, but also to promote cytotoxicity.[49, 50] To investigate, whether the elongation of the cationic block caused a similar effect, a viability study using the CellTiterGlo® assay was performed (Table 3.4). Here, the polymers **7** and **8** were chosen as representatives, because polymer **7** was the only one of the six polymer structures belonging to the subgroups *Ib* and *IIb*, which formed stable polyplexes with siRNA. The architecture of polymer **8** is closely related to that of of polymer **7**, but it has a five times longer GPMA block for siRNA complexation, which increases its overall charge (63 protonatable monomers instead of 31) to double the value of polymer **7**. Hence, it was expected to observe higher toxicity for polymer **8**. These literature-based estimations were confirmed. Comparing the IC_{50} values, which were obtained via CellTiterGlo® assays, polymer **8** was 1.5 to 2.8 times more toxic than polymer **7**. Nevertheless, neither of the two structures impacted cell viability to the same extent as PEI-[51], PLL-[52] or PDMAEMA-based[53], which are more commonly utilized as delivery agents for polynucleotides.[54]

Table 3.4. Calculated IC_{50} values for the tested block copolymers 7 ($HPMA_{180}$-*s*-$APMA_{20}$)-*b*-$GPMA_{11}$) and 8 (($HPMA_{126}$-*s*-$APMA_{14}$)-*b*-$GPMA_{49}$)

cell line	7	8
MCF7	52.35 µM	31.01 µM
Kelly wt	17.06 µM	6.05 µM
HeLa	47.46 µM	32.42 µM
C2C12	11.07 µM	3.78 µM
HEK293	67.44 µM	39.88 µM

3.3.2 Internalization into cells

The internalization efficacy into cells can be measured by both the total amount of internalized polyplexes and the minimal incubation time required for said polyplexes to be observable inside either the organelles or the cytosol of cells. In the present study cLSM imaging is utilized, which is less suitable than flow cytometry to quantify the total amount of polyplex-containing cells. Hence, the internalization rate was used to measure the ability of the polymers to bypass cellular membranes.

Here, Polymer **8** and polymer **7** were investigated in regard to their ability to transport siRNA across cellular barriers. This property has a similar significance for the applicability of siRNA delivery agents as their ability to form polyplexes. Inability to transport cargo across cellular barriers instantly invalidates the implemented design choices. To investigate, whether the length of the binding block influences internalization efficacy, fluorescence-based confocal laser scanning microscopy was employed and the uptake of the complexes formed between ATTO488-labelled siRNA and the polymers **7** or **8** into HEK293 cells was monitored by taking a layer image every 10 min for the duration of 15 h. The commercially obtained ATTO488-labelled siRNA did not show traces of free dye molecules in HPLC experiments. Hence, it can be excluded that observed uptake was attributed to the internalization of free ATTO488. In addition, siRNA molecules are unable to cross the plasma membrane unaided.

Figures 3.16 and 3.17 show that both polymers were able to mediate internalization of siRNA after only 30 minutes and the accumulation of the labeled complexes in intracellular compartments indicates endocytosis as the predominant route of uptake. Only few other polymer architectures are known to deliver their cargo as quickly.[55] In case of polymer **7**, which forms much larger complexes with siRNA (R_h (polymer **7** + siRNA) = 83.6 nm) than polymer **8** (R_h (polymer **8** + siRNA) = 49.6 nm), it was surprising to observe such a quick uptake. After an initial burst of uptake, polymer **7**-based polyplexes were continuously expelled from the cells. They were also never detected in the cytosol, which indicates that only poor results will be achieved during a knock-down study. Polymer **8**-based polyplexes, on the other hand, accumulated inside the HEK293 cells and even entered the cytosol after 2 h of incubation, allowing a distinction between the cytosol and the unstained nuclei. In addition, neither of the two polymer/siRNA complexes adsorbed to the outer cell membrane. This trait is advantageous, since the accumulation of cationic macromolecules at the plasma membrane has been shown to promote membrane defects that are associated with strong cytotoxicity.[56] Furthermore, the

results of the toxicity study were confirmed during microscopy, since neither polymer **7**-, nor polymer **8**-based polyplexes induced morphological changes of the cells. During all cLSM experiments a final concentration of 2.5 µM was used for the polymers, which is well below the IC_{50} values for HEK293 cells.

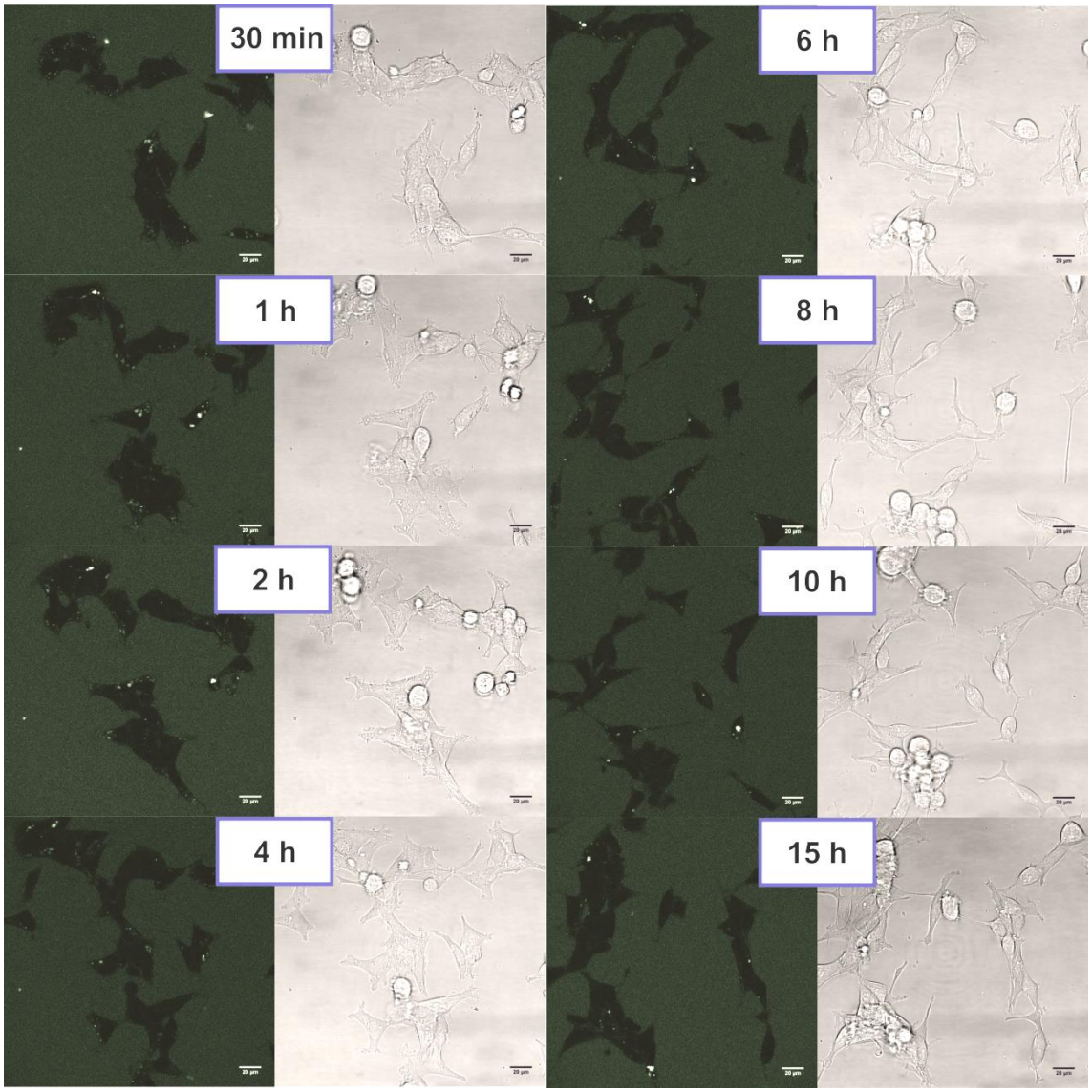

Figure 3.16. Confocal laser scanning fluorescence microscopy images (SP5, Leica) of living HEK293 cells, which were incubated with complexes between ATTO488-labelled siRNA and the diblock copolymer 8 ($(HPMA_{126}$-s-$APMA_{14})$-b-$GPMA_{49}$). Layer images were taken every 10 minutes for the duration of 15 hours, while keeping the imaging conditions constant. The scale bar represents 20 µm.

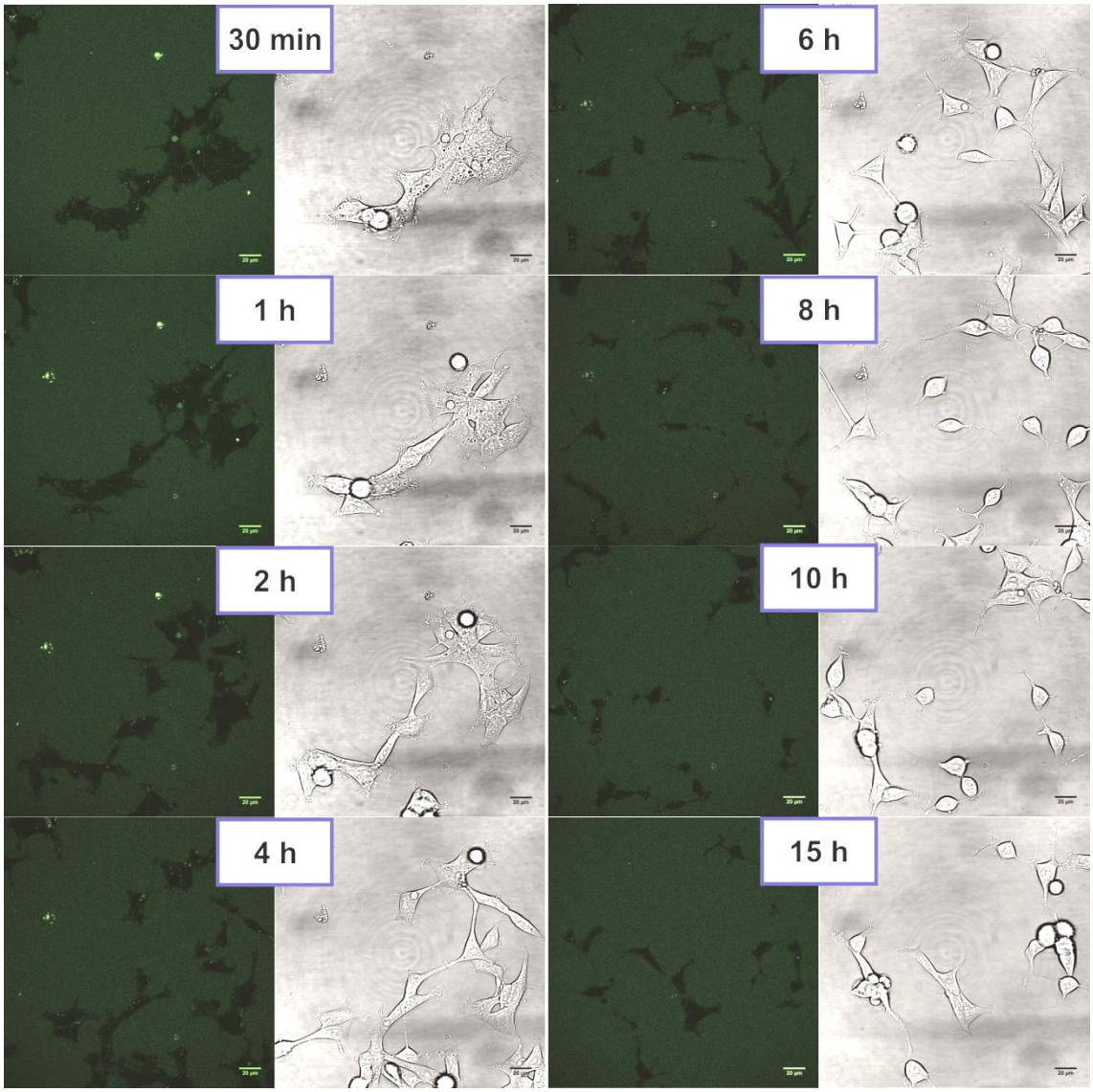

Figure 3.17. Confocal laser scanning fluorescence microscopy images (SP5, Leica) of living HEK293 cells, which were incubated with complexes between ATTO488-labelled siRNA and the diblock copolymer 7 ($(HPMA_{180}$-*s*-$APMA_{20})$-*b*-$GPMA_{11}$). Layer images were taken every 10 minutes for the duration of 15 hours, while keeping the imaging conditions constant. The scale bar represents 20 µm.

3.3.3 **Knock-down efficacy**

During the cLSM experiments it was shown that polymer 8-based polyplexes not only accumulated inside the HEK293 cells, but also entered the cytosol after 2 h of incubation. However, this observation alone is not sufficient proof for efficient delivery, since a stained cytosol is not tantamount to the release of the siRNA molecules, which is the crucial step of inducing RNAi. To elucidate this issue, a knock-down study was performed, using siRNA against the Kif2a protein in murine IMCD3 cells. Prof. Dr. Wolfrum (Institute of Molecular Physiology, Johannes Gutenberg-University of Mainz) kindly provided me with access to his laboratories. In order to validate the other trends, which were observed during the complexation studies, all polymer structures with the ability to form stable complexes with siRNA were tested as well. Polymers lacking the ability to complex siRNA molecules, such as the polymer **1**, **4**, **6** and **10**, did not fulfill the first requirement of siRNA delivery agents and were therefore excluded from further investigation.

Knock-down tests were performed using the starvation-inducing medium Opti-MEM to improve the internalization. In each case, polyplexes loaded with non-targeting siRNA (pool) were used as the reference instead of uncomplexed siRNA, to improve comparability. This approach eliminated the falsifying effect of toxic or cell-stimulating compounds, since the RNA sequence and its functionality was the only variable during the quantification. The commercially available transfection reagent LTX RNAiMAX (LTX), which is a Lipofectamine optimized to most effectively deliver siRNA into adherent cells, was used as the positive control. Uncomplexed siRNA (medium), i.e. a solution containing only siRNA, wherein the medium is used as the solvent, was used as the negative control.

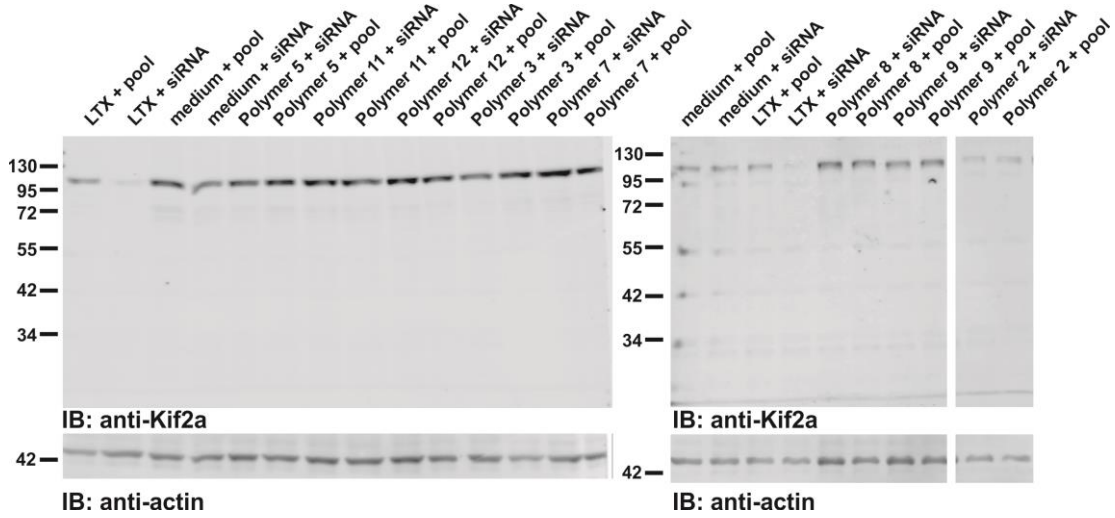

Figure 3.18. Western blot analysis of the Kif2a knock-down with actin as the loading control.

Figure 3.18 provides an example for a western blot. Multiple western blots were used as the basis to calculate the mean knock-down efficacies, which are shown in Figure 3.19. Successful knock-down, as shown by the western blot, leads to the disappearance of the Kif2a band, i.e. sinking value of the detected band intensity, and, in order to avoid errors due to incorrect loading of the gels (non-uniform protein concentrations of the samples), the intensity of each band was not used as is, but a relative value to the actin control is calculated. The thusly calculated value was then compared to the analogously treated value of the comparative "pool" sample. Thereby (formula in section 9.3.3), the knock-down efficacy was calculated. Here, a value of 100% equals complete abolition of the intracellular synthesis of the Kif2a protein in IMCD3 cells. This means that at a given knock-down efficacy of 45%, the Kif2a protein was successfully down-regulated by 45%, if compared to the efficacy of the same delivery system, wherein a non-functional siRNA pool was used as the cargo.

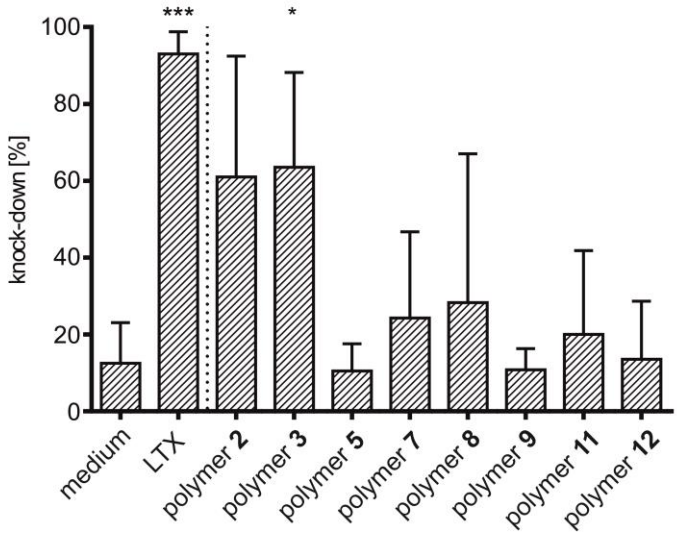

Figure 3.19. The evaluated knock-down efficacy of the western blot-investigated polymer samples and controls (mean with SD) in [%]: (medium) free siRNA molecules, (LTX) LTX RNAiMAX, (2) (HPMA$_{126}$-*s*-APMA$_{14}$)-*b*-APMA$_{64}$, (3) HPMA$_{147}$-*b*-APMA$_{45}$, (5) (HPMA$_{157}$-*s*-GPMA$_{13}$)-*b*-APMA$_{28}$, (6) (HPMA$_{180}$-*s*-GPMA$_{12}$)-*b*-APMA$_{22}$, (7) (HPMA$_{180}$-*s*-APMA$_{20}$)-*b*-GPMA$_{11}$, (8) (HPMA$_{126}$-*s*-APMA$_{14}$)-*b*-GPMA$_{49}$, (9) HPMA$_{150}$-*b*-GPMA$_{58}$, (11) (HPMA$_{157}$-*s*-GPMA$_{13}$)-*b*-GPMA$_{27}$, and (12) (HPMA$_{180}$-*s*-GPMA$_{12}$)-*b*-GPMA$_{22}$. Here, a value of 100% represents a complete abolition of the intracellular synthesis of the Kif2a protein in IMCD3 cells after 72 h of incubation. In all transfection experiments siRNA was employed in final concentrations of 50 nM.

LTX achieved high levels of knock-down reliably (93%), but although it outperformed the polymer-based delivery systems, the applicability of lipofectamine in *in vivo* experiments is limited due to high toxicity, thereby underlining once more the importance of finding solutions to the current limitations in siRNA delivery.[57] Among the polymer structures belonging to group *II* only one polymer was excluded from the knock-down study, whereas half of the polymers belonging to group *I* had to be removed from testing due to their poor binding properties. Nevertheless, polymers **2** and **3**, which rely on an APMA block for the complexation of siRNA, facilitated the highest knock-down efficacies among the tested polymers by achieving values of 61% and 63% on average respectively. The diblock copolymer **5**, on the other hand, possessing not only a long APMA block, but also a HPMA block with statistically incorporated GPMA monomers, did not induce knock-down of Kif2a under the conditions section described in section 9.3.3. It achieved a knock-down efficacy of only 11%, which is comparable to that of the negative control (12%), where free siRNA was utilized. The polyplexes formed be-

tween siRNA and the polymers of group *II*, which rely on a GPMA block for binding purposes, lead to a limited down-regulation of Kif2a (polymer **7** ⇒ 24%, polymer **8** ⇒ 28%, polymer **9** ⇒ 11%, polymer **11** ⇒ 20% and polymer **12** ⇒ 14%).

The knock-down efficacy could be correlated to the interplay between the architecture-influenced affinity of a polymer towards siRNA and the respective polyplex size. Polymers favoring large structures, such as polymer **9** for example, are disadvantaged at entering cells making its binding properties inconsequential.[58] However, the affinity towards siRNA and thereby its release becomes crucial once the size of the complex is reduced. Polymer **3** performed best in terms of knock-down efficacy (63%), which can be attributed to the small hydrodynamic radius of its polyplexes (25 nm) and the binding strength of this block copolymer was determined to be comparatively mediocre. Polymer **11** formed similarly sized complexes with siRNA, however, its binding strength was measured to be higher by a factor of two, which appears to have strongly impeded knock-down (20%). Poor release of the complexed siRNA due to a higher affinity explains also the knock-down performance of polymer **8**. cLSM experiments demonstrated not only quick internalization of the polymer **8**/siRNA polyplexes into cells, i.e. detectable amounts of said polyplexes were observed in the cytosol after only 30 minutes, but they were also observed to accumulate in the cytosol, the locus of effect of the RNAi pathway.[59] This observation explains why polymer **8** was able to reduce the production of the Kif2a protein by up to 73% in individual cases. Hence, it is expected that poor release of siRNA was the leading cause for the low knock-down value (28%). Polymer **5**, which facilitated the formation of polyplexes with siRNA that were of similar size as those formed between polymer **8** and siRNA, bound the polynucleotide stronger by a factor of three, which, in turn, fully arrested the down-regulation of Kif2a.

Overall, due to the investigation of the interdependency between the sources of the cationic charge (amino groups of APMA or guanidinium groups of GPMA), the length of the cationic block and by extension the binding affinity of the copolymers towards polynucleotides and the size of the polyplexes with the polymers' ability to induce knock-down, it became clear that GPMA-based compolymers performed poorer than their APMA-counterparts. It is expected that the ability of the guanidinium group to establish not only electrostatic interactions, but also multiple hydrogen bonds with its binding partner, thereby facilitating not only exceptionally strong binding, but also poor release, was the leading cause for this observation.[60] APMA-based polymers, on the other

hand, have inherently weaker binding properties. While strong binding impedes the release of siRNA, using weak binders as siRNA delivery agents, such as polymer **2**, to achieve high knock-down efficacies is also not a valid alternative, if one aims for *in vivo* experiments. Loosely bound siRNA is prone to degradation by ubiquitous RNases and will not reach the targeted cell.[29]

Following the experimental study of the formed polyplexes a simulation was performed to gain additional insights into (i) the threshold length of a cationic block required for efficient complexation of siRNA molecules, (ii) the amount of bound siRNA molecules in correlation to the length of the cationic block and (iii) the structure of the formed polyplexes in solution. Although the simulation of the complexes' packing order can only be a rough estimation, studying this property and comparing the findings with the cryo-TEM results provides the opportunity to validate the data gained from the simulation.

3.4 Simulations

The experimental study has shown that the block composition and, in particular, the length of the cationic block, which needs to exceed a threshold ($length^{binding\ block}/length^{non\text{-}biding\ block}$ ratio of 1:8.7), play an important role in the formation of polyplexes. Although knowledge with respect to the formation of these polyplexes has been gained, only marginal characterization of their internal structure is possible. Utilizing for example cryo-TEM, it was only possible to obtain data with respect to the shape and size of a complex as a whole, but knowledge regarding the dependency of the siRNA loading capacity or packing order within a polyplex would further improve the design of future carrier systems.

The computational approach of simulating the formation of such complexes is highly suited to elucidate this issue. Hence, a computational model of the system was developed at the molecular level and employed to simulate the complexation of single as well as multiple RNA molecules. This work was performed in collaboration with Maziar Heidari and Prof. Dr. Raffaello Potestio (group of Prof. Dr. Kurt Kremer, Max Planck Institute for Polymer Research). I was placed in the role of a consultant in the development phase of the model and also gave input regarding the relevant data evaluation.

Before the present work, several other authors tackled the topic of polyplex formation between a polymer and a polynucleotide by means of computer simulations. To this

end, they employed models of varying levels of detail, which ranged from coarse-grained ones[61, 62] to the more refined representations at an all-atom level[63-69]. Their work, which helped to pioneer this field of study, was aimed at a characterization of the binding process between polymers and DNA fragments or RNA molecules. The interaction of these species was studied in detail to identify the role of the positive and negative charges during a binding event as well as to elucidate the mechanism of polyplex formation.[68, 69] For that purpose, the focus was placed on the interaction between one or a few polynucleotides with a similarly small number of polyelectrolytes. Here, in contrast to the single molecule approach, the polyplex formation process was studied by using conditions that are close to the experimental setup.

3.4.1 Simulated complexation

In order to facilitate the required large-scale simulations, a top-down approach was employed, where the cationic block copolymers are simulated by a coarse-grained model, whereas the RNA molecules are viewed as rigid objects at the atomistic level, which possess a limited number of binding sites (21 base pairs, structure 255D of the protein data bank[70]).

Due to the short contour length of the RNA in comparison to its persistence length ($l_p \cong 100$ base pairs[71]), it was assumed that the RNA can be aptly modeled as a rigid body for the present purpose, which coincides with its previous description as a rigid rod-like structure.[72] In case of the polymers, a semi-flexible bead-and-spring model was chosen, where the GPMA and APMA units hold a single positive charge.

The binding properties of the complexes between siRNA and the block copolymers containing varying amounts of APMA and GPMA were already known (section 3.3). In order to adjust the hydrogen bond strength of the copolymer blocks with RNA accordingly, a top-down coarse-graining procedure was carried out by setting up complexation simulations with “simple” diblock copolymers (polymers **3**, **4**, **9** and **10**) of the same size containing either a short or long HPMA-block and a second block of respectively varying length consisting of either GPMA or APMA. Thereby, binding strength parameters were allocated to APMA or GPMA repeat units respectively. Based on these results, it attempted to anticipate the experimental results of polymers **7** and **8**.

Initially, it has been studied, whether the above-described model can replicate the ability of polymers **8** and **7** to electrostatically interact with and complex siRNA. Simulat-

ing the exact structure of polymer **7** did not lead to stable complexes although they have been observed experimentally. Their formation has been observed during the simulation, too, but entropic forces made these polyplexes only temporary. Hence, a replacement, namely the block copolymer ($HPMA_{166}$-*s*-$APMA_{20}$)-*b*-$GPMA_{25}$ (polymer **7+**) has been studied. Polymer **7+** corresponds to polymer **7**, wherein the length of the cationic GPMA block was increased from 11 to 25 units. Based on the FCS-data of polymer **7**-based complexes, which required a 3-components-fit ((i) predominantly small polyplexes (R_h = 6 nm) with one siRNA molecule per complex, (ii) a minor population (~5%) of larger complexes (R_h > 35 nm) that contain multiple siRNA molecules and (iii) free siRNA), stability of said polyplexes might be an issue due to the heterogeneity of the complex mixture. The DLS data of polymer 7 also show the formation of large (R_h = 83.6 nm) and most probably ill-defined polyplexes. The lack of stability might be the reason for this behavior. In addition, it was not possible to observe polymer **7**-based polyplexes *via* cryo-TEM. Lacking explicit confirmation due to ambivalent results, the difference must be viewed as the first sign that the simulation, due to its inherent limitations, cannot exactly replicate experimental results. The study was continued nonetheless, because observed trends might be transferable even if they are not in full accord. Please note that the simulation can only be an approximation.

The simulated complexation of siRNA was studied by using either 8 or 16 RNA molecules within a cubic simulation box. In these setups, the number density of the polymers was set by the experimentally relevant number density of $1.56 \times 10^5 (1/\mu m^3)$ (Figure 3.20).

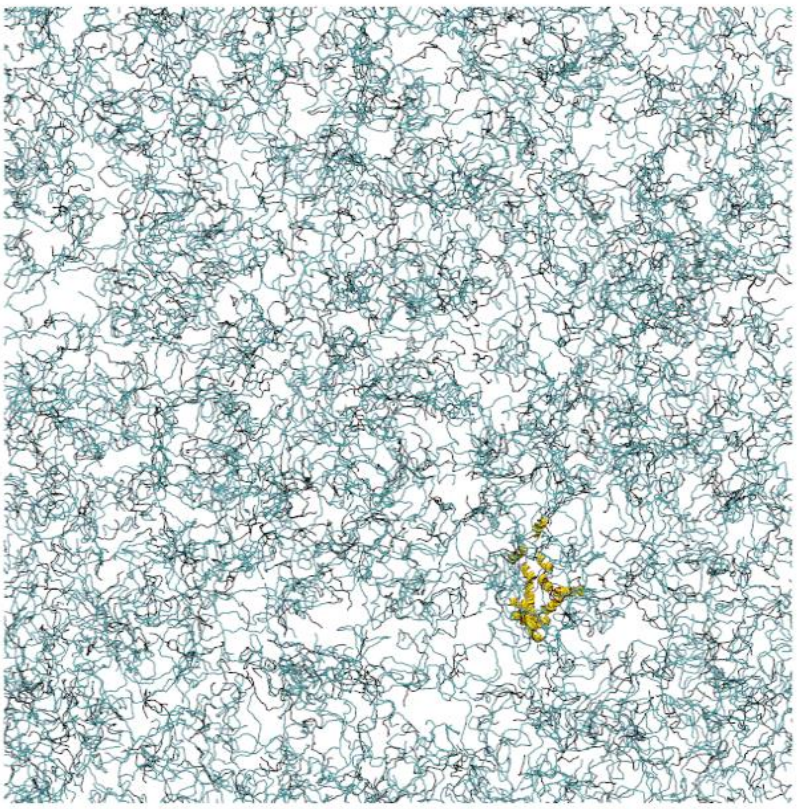

Figure 3.20. Illustration of the initial configuration of the simulation box containing copolymers (shown in black, blue and red) and RNA molecules (shown in yellow). At the initial configuration, the RNA molecules, while randomly aligned, are located close to each other similar to the intial experimental setup of injecting siRNA molecules into a polymer solution.

While randomly aligned, the RNAs are initially placed next to one another. This concentrated arrangement of RNAs mimics the experimental setup, in which a siRNA stock solution was injected into a solution containing the respective polymers. In each case six simulation runs were performed for prolonged durations of time and complex formation was observed. For data evaluation clusters were defined as structures containing either a single or multiple RNA molecules interacting electrostatically with polymer molecules. Snapshots of the two described systems are illustrated in Figure 3.21. Here, one can observe that the majority of the polymers chains, not depending on the polymer structure, interconnect siRNA molecules to form complexes. This observation can support the idea that each complex is made up by substructures consisting of one siRNA molecule and two polymer molecules as building blocks during cluster formation.

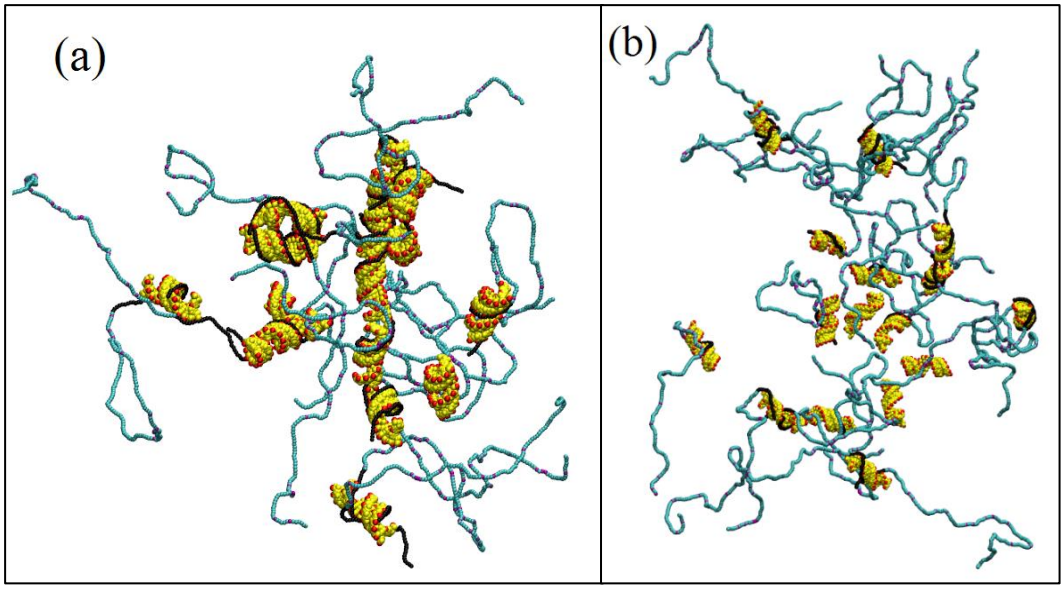

Figure 3.21. Snapshots of formed clusters between siRNA molecules and either (a) polymer 8 or (b) polymer 7+. In both cases a total of 16 siRNA molecules were present in the simulation box. The RNA molecules are shown in yellow color and its binding sites are marked in red. The color scheme of the coarse-grain model of the block copolymers is as follows: blue (HPMA), pink (APMA) and black (GPMA). For the sake of improved visibility only RNA-attached copolymers are illustrated.

Having shown that complexation takes place, it has been studied, whether the above-described model can reproduce the experimentally determined length$^{\text{binding block}}$/length$^{\text{non-biding block}}$ threshold ratio of 1:8.7 as well as the shape of the polyplexes, by investigating the complexation properties of a replica of polymer **8** as well as the block copolymer (HPMA$_{166}$-*s*-APMA$_{20}$)-*b*-GPMA$_{25}$ (polymer **7+**).

3.4.2 Minimal length of the cationic block to achieve complexation

The minimal length of a cationic block in a diblock copolymer structure, which still provides sufficient binding affinity for efficient complexation of siRNA, was studied using a model of a polymer chain in good solvent conditions. This number of repeat units can be estimated by calculating the free energy difference of the RNA-copolymer system before and after the complexation. This estimation relies on a two-state model, in which the primary state is represented by detached polymers and RNA molecules, and the secondary state is defined by polymers adhering to the siRNA. The free energy difference between these two states is:

$$\Delta F = \Delta E - T\Delta S \tag{3.8}$$

Here, ΔE is the adhesion energy difference after the copolymer has bound to the RNA molecule. The entropy of a chain with a length of N can be approximated with the entropy of a simple, fully flexible model polymer with excluded volume. In addition, it must be considered that there is a difference between the total number of cationic monomers (N_f) with the ability to interact with siRNA and the effective number, which is able to form electrostatic bonds (N_e). Considering the short-ranged character of the interaction, the finite distance between the RNA binding sites, and also the binding conformation, the effective number of monomers interacting with RNA must be less than the total number of monomers able to form an electrostatic interaction ($N_e < N_f$). Figure 3.22 shows the fraction of N_e/N_f obtained from the simulations of diblock copolymers with short and long GPMA blocks (polymers **9** and **10**) in correlation to the interacting energy ϵ.

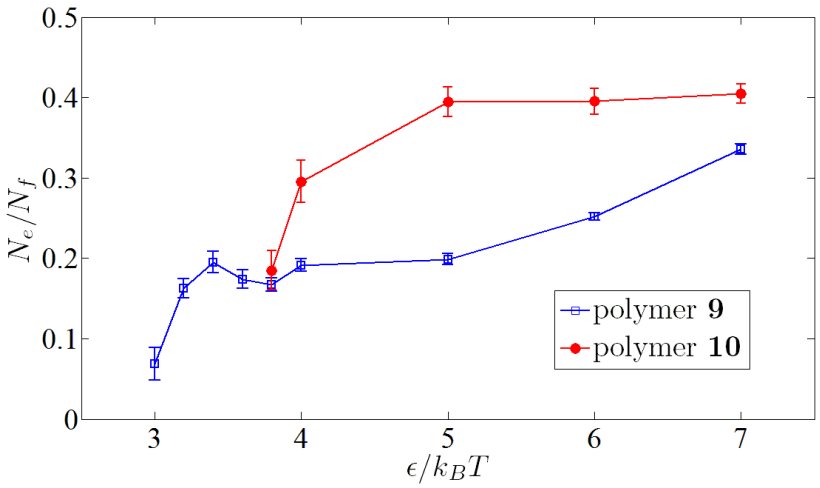

Figure 3.22 The normalized effective number of GPMA monomers interacting with RNA binding sites shown as a function of the interaction strength.

In these simulations, the effective number of interacting monomers was calculated by normalizing the interaction energy between the GPMA blocks of the diblock copolymers and the siRNA molecules to the number of attached block copolymers and the theoretically possible corresponding strength of interaction with respect to the total amount of available GPMA units. For polymer **9**, after which the simulation has been partially modeled, it was found that N_e/N_f was 0.2. Out of 58 GPMA units, which constitute the cationic block of polymer **9**, only approximately 12 monomers were effectively interacting with the RNA molecule.

Furthermore, it was observed that the number of block copolymers attaching to siRNA varies from 1 or 2 in the low ϵ regime to 3 or 4 in the high ϵ regime. It was also seen that for both polymers **9** and **10**, the ratio N_e/N_f grows with increasing ϵ and falls within the range 0.10 to 0.4 for the range of $\epsilon = 3\ to\ 7\ k_BT$. At $\epsilon = 3.4k_BT$ polymer **9** formed complexes with the siRNA. Polymer **10**, on the other hand, was not able to complex siRNA at the same interacting energy due to a positive free energy. This constitutes the lowest value of the interacting energy, where polymer **9** formed complexes, but polymer **10** did not. To approacimate the simulation to the experimental results in our top-down approach, ϵ was fixed to the said value for all simulated GPMA building blocks. This approach, however, caused the problems regarding polymer **7** outlined above, which had a short cationic block of only 11 GPMA units (even less than polymer **10**), but was in reality able to complex siRNA. Here, it needs to be considered that according to the simulation model complexation of a siRNA molecule using a short cationic block of only 16 or 11 GPMA units (polymer **10** or **7**) is possible in theory. However, rapid decomposition of the complexes occurs due to entropy. To avoid this issue, the lowest number of GPMA units, which is required for a sufficiently low free energy difference was calculated. For a polymer chain of 205 monomers, as has been the case for the experimentally investigated block copolymers, a cationic block length of 25 was found to be necessary. This correlated to a length$^{\text{binding block}}$/length$^{\text{non-biding block}}$ of 1:7.5. These findings support the presivously described results of the the experimental binding study, where a length$^{\text{binding block}}$/length$^{\text{non-biding block}}$ ratio of 1:8.7 was observed. Not only was the existance of a threshold length of the cationic block ensuring efficient complexation confirmed, but also the calculated ratios deviate only marginally. As described above, it was decided to evaluate the relevancy of the simulation based on its ability to reporduce or predict experimental data. If the threshold length would not have been identified previously, it would have been indeed possible to apply the results of the simulation in this regard. It has therefore passed the first hurdle. The next step relates to the shape of the polyplexes. Polymer 8 was shown to form spherical as well as near uniform complexes. In the next section, it will be revealed, whether the simulation was able to reporduce these results, too.

3.4.3 Charge distribution

The charge distribution of the simulated complexes was calculated by using the following equation:

$$g_q^{\mp}(r) = \sum_i \delta(q_i - q^{\mp})\delta(r - |\vec{r}_{CM} - \vec{r}_i|) \quad (3.9)$$

Here, i runs over all positive or negative charged components of the complex and $\vec{r}_{CM}$ is the position of the complex's center of mass. The results of the calculated charge distribution are depicted in Figure 3.23.

The cationic charges of the block copolymers and the negative charges of the siRNA molecules were almost fully co-localized. It is possible to differentiate a core (0 – 20 nm) and a shell region (starting from 20 nm). The negative charges of the core region are either compensated or overcompensated, but, in case of the shell region, it is possible to observe uncompensated positive charges, which fade with increasing distance from the center of mass. In addition, the normalized distribution of the complex charge becomes sharper as the number of the siRNA molecules in the complex increases, which indicates efficient packing of the cargo. Considering also the polymer **8**-based polyplexes depicted in Figure 3.21(a), wherein siRNA are amassed inside the core and the neutral blocks constitute a shell, spherical complexes are to be expected.

These results, in particular the formation of nano-sized spherical core-shell polyplexes, not only coincide with the cryo-TEM results, but were also expected of cationic diblock copolymers as outlined in section 1.3. During cryo-TEM, polymer **8**, which is equipped with a long GPMA block formed spherical aggregates featuring a radius of 26 nm on average (Figure 3.12). The intergroup comparison using polymer **3** and **9** as references (Figure 3.11 and 3.13), revealed that a long cationic block bearing guanidinium groups (polymer **9**) can also promote the formation of micelles (diameter of 9.4 nm), which in turn form worm-like structures (width of 7.3 nm), presumably *via* fusion-fission processes. Replacing the guanidinium groups with primary amines (polymer **3**) led to spherical polyplexes with an average radius of 30 nm. Although the simulation did not predict the possibility of worm-like structures, it has, nonetheless, been shown to possess the ability to predict experimental results to some degree. Not only was the threshold length of a cationic block required for efficient complexation of siRNA molecules confirmed, but also the shape of the polymer **8**-based polyplexes was reproduced.

The next steps relate to a property, which could be only superficially investigated in an experimental setup, namely, the relationship between the amount of bound siRNA molecules and the length of the cationic block. In addition, the question with respect to the packing order of the siRNA molecules has been raised.

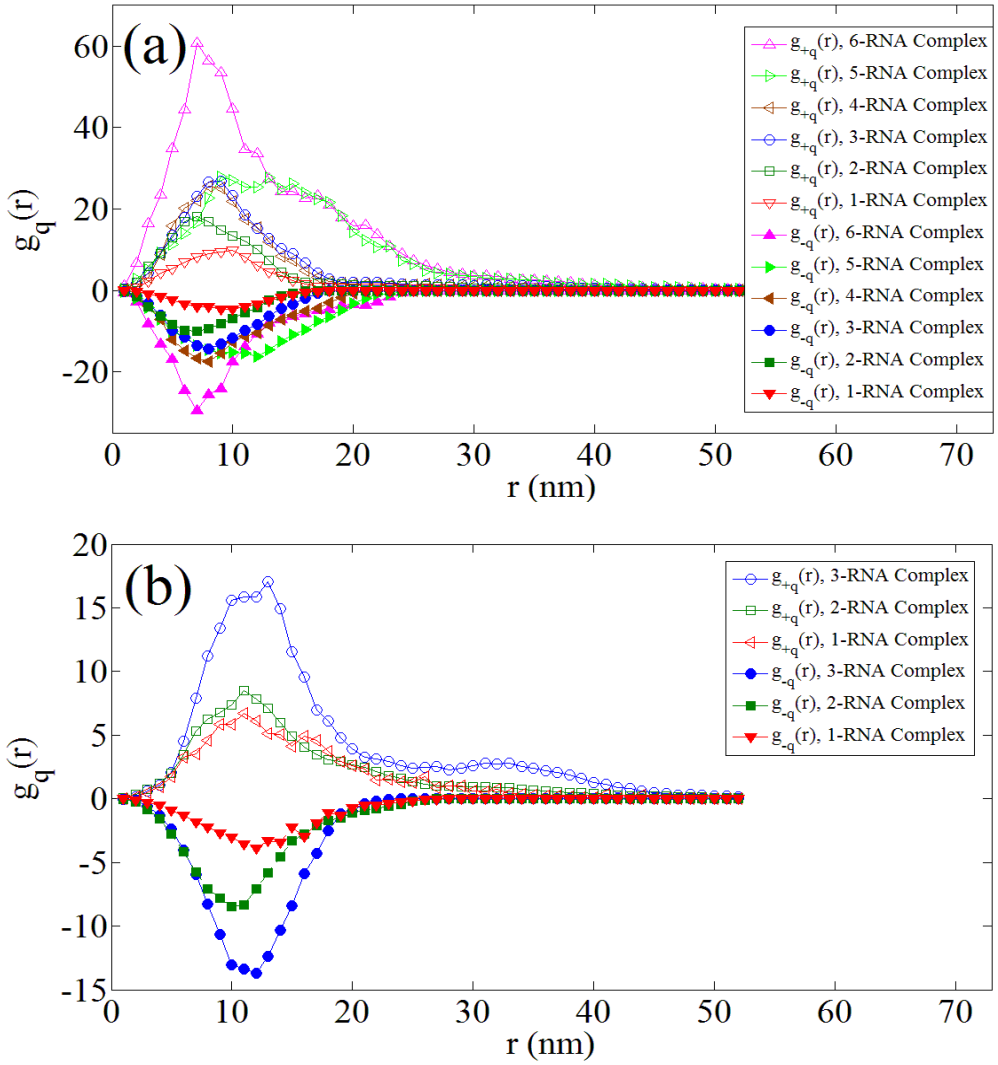

Figure 3.23. Positive (open symbols) and negative (filled symbols) charge distribution $g_q(r)$ as a function of the radial distance originating from a complex's center of mass. The plots are devided by used block copolymers: panel (a) polymer 8 and panel (b) polymer 7+ and further differentiated by the number of siRNA molecules per complex.

3.4.4 Loading capacity

The loading capacity is the threshold number of siRNA molecules below which stable encapsulation by the polymer is expected. To investigate this parameter the number of observed complexes in correlation to their respective number of siRNA molecules was visualized (Figure 3.24, a). While in all observed complexes the number of the siRNA molecules was limited to an upper limit of 6 molecules, the polydispersity of the clusters with respect to the number of cluster-bound RNA molecules was higher for the co-

polymer system with a long GPMA block. The simulation showed good agreement with data obtained during fluorescence correlation spectroscopy experiments (section 3.2.2). FCS experiments were performed for polymers **7** and **8**, which have the highest structural comparability to the simulated copolymers **7+** and **8**. In case of polymer **8,** an average value of 12 siRNA molecules per complex was observed, however, the actual number is lower, because, as previously stated, the calculation approach enforces a bias towards large complexes. The FCS data of polymer **7**-based complexes, on the other hand, showed that polymer **7** favors the formation of single siRNA complexes. The different behavior of the two polymers was well estimated by the simulation. Polymer **8** and its simulated analogue formed large complexes by bridging many siRNA molecules, while polymer **7** and its simulated counterpart predominantly formed small polyplexes, which contained only few siRNA molecules. In addition, in case of the polymer with a short GPMA block, complexes are distributed much more homogeneously. Concerning the average number of adhered polymers in relation to the total amount of siRNA molecules within each cluster, it can be said that the ratio (6 : 5) appears to stay the same for all observed cluster-sizes without a clear dependency on the polymer structure (Figure 3.24, b). While this ratio does not change for either structure even at growing cluster size, the simulated polymer **8** an additional utility. Figure 3.25, which depicts the number of siRNA molecules joint by a single polymer chain in correlation to the total number of siRNA molecules per complex, shows clearly that long cationic blocks can bridge up to 5 siRNA molecules. In contrast, polymer **7+** bridged only up to 2 siRNA molecules. This observation can be taken as a clue that block copolymer structures such as polymer **8**, possessing a comparatively long block for siRNA interaction, are following a different mode of cluster formation. These observations support the previously described interaction types between siRNA and linear cationic polymers (longitudinal, transversal and enveloping). We also confirmed that the polymer architecture determines which interaction type is predominant.

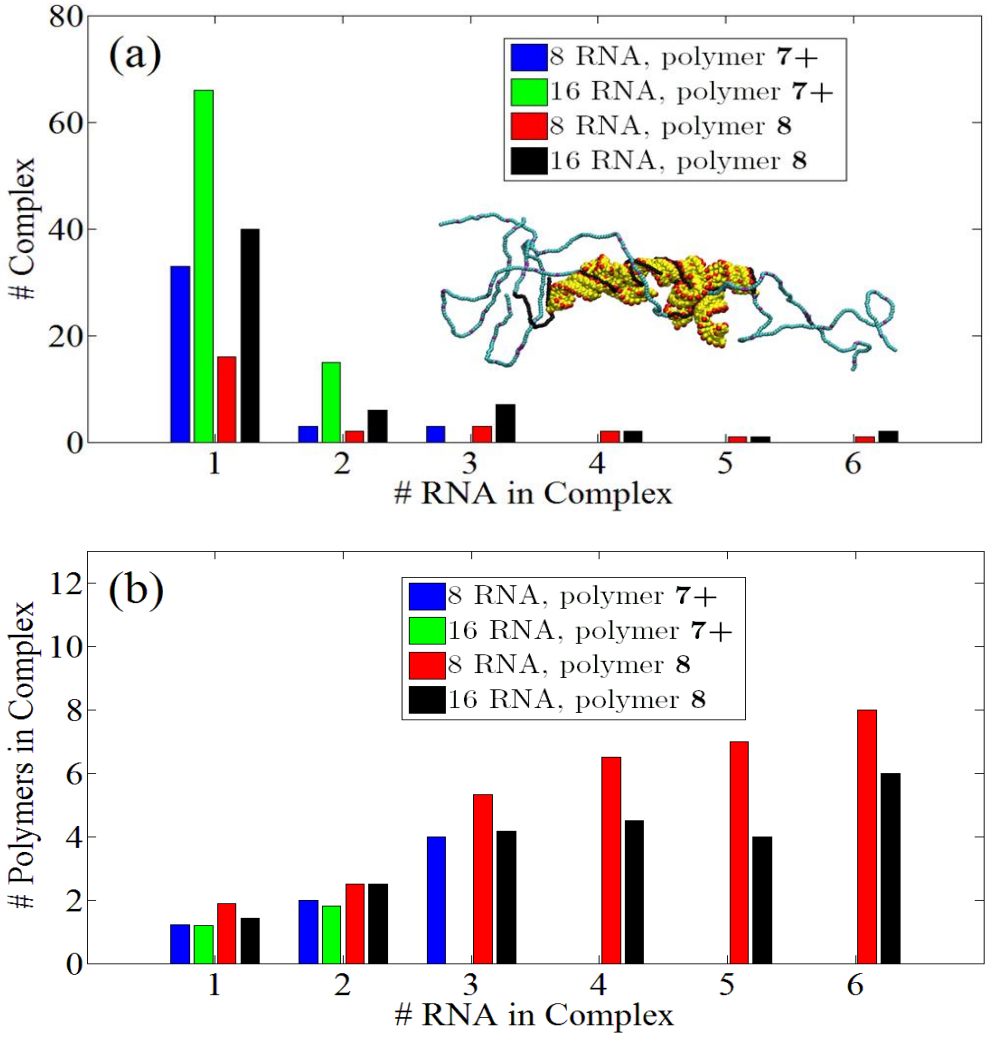

Figure 3.24. (a) Distribution of the complex size with respect to the number of RNA molecules inside a respective cluster for both systems containing either short (blue and green bars, polymer 7+) or long (red and black, polymer 8) GPMA blocks. Inset illustrates a single cluster composed of six siRNA molecules and six block copolymers. (b) Correlation between the number of polymers and the number of siRNA molecules inside a respective cluster depending on on the polymer structure and the amount of siRNA molecules inside a simulation box

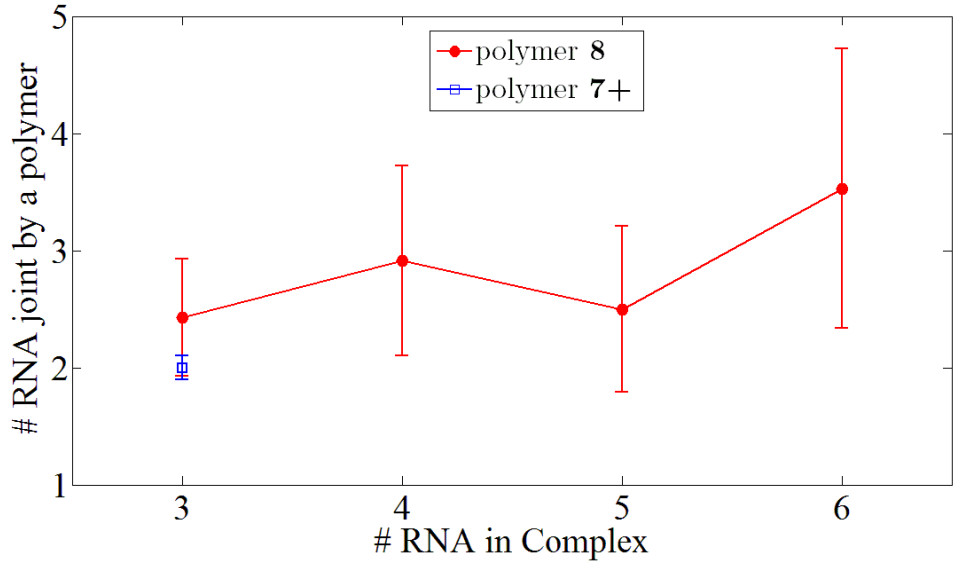

Figure 3.25. Number of siRNA molecules joint by a single polymer chain in correlation to the total number of siRNA molecules per complex. The results are differentiated in regard to the investigated polymer structure: (red) polymer 8 and (blue) polymer 7+

3.4.5 Packing order parameter

To further study the inner structure of the clusters and to understand if the proximity of the siRNA molecules, which is enforced by the polymers, affects the degree of order, the degree of mutual alignment of siRNA molecules in a complex was investigated. It was hypothesized that a high packing order would correlate to denser and therefore smaller polyplexes. In order to objectively quantify this property, the order parameter S (equation 3.10) was utilized. It is usually employed for liquid crystals.[73]

$$S = \frac{\langle \frac{1}{N_c} \sum_{i=1}^{N_c} (3\cos^2 \theta_i - 1) \rangle}{2} \tag{3.10}$$

For the i^{th} siRNA molecule inside a complex composed of N_c RNAs, θ_i is the angle between the unit vector defined along its longitudinal axis $\vec{t}_i^{RNA}$ and the complex director $\vec{T}^{cmp}$, which is obtained by summation over all directions of the RNA unit vector inside a respective complex ($\vec{T}^{cmp} = \sum_{i=1}^{N_c} \vec{t}_i^{RNA}$) and the time averaging is shown with bracket $\langle \cdots \rangle$.

For a completely randomly oriented structure, the order parameter becomes zero, while it equals 1 for a perfectly aligned structure. For the purpose of better evaluation of the

collected results, control simulations were run, in which only steric interactions between the siRNA molecules and the block copolymers were possible (no binding). In this control the order parameters were calculated by grouping neighboring siRNA molecules.

The calculated order parameters of the complexes are reported in Figure 3.26. This evaluation provides several levels of information:

i) The degree of ordering between siRNA molecules does not depend on the type of polymer involved in the complex, that is, the order parameter S is practically the same for either structure at the points of comparison (for 2 and 3 RNA molecules in the polyplex).

ii) The parameter S is, within the statistical error, independent of the number of involved nucleic acid molecules.

iii) In absence of the polymers, the RNA molecules would attain a lower degree of mutual orientation (randomly oriented).

iv) Complex formation increases the order parameter, if only 2 to 3 siRNA molecules are complexed and drops to a plateau once 4 and more polynucleotides are complexed.

The consequence that one can draw from these observations is that the polymer-mediated binding of two siRNA molecules introduces a mechanical coupling, which results in a mildly increased orientational correlation. This coupling, however, is not additive with the number of complexed RNA molecules. For more than two molecules the degree of ordering remains the one that can be observed in a group of neighboring, but randomly oriented molecules only subject to the constraints imposed by excluded volume. In particular, this last property supports the viability of a mesoscopic modeling of the complexes as spherically symmetric objects.

Due to the results of sections 3.4.2 and 3.4.3, it is possible to apply these findings to the real case. The importance of the size as well as the shape of nanoparticles for their ability to penetrate plasma membranes is well documented in the works of Dasgupta *et al.*[74], Chithrani *et al.*[75] or He *et al.*[76] However, according to the simulation results, there is no apparent influence of the polymers structure on the ordering inside the polyplex. The only observed differences stem from the polymers' ability to complex a more or fewer polynucleotides (loading capacity). Hence, the packing order parameter should not be considered in the design of future siRNA delivery agents. Although the final ver-

dict in this regard has been negative, it represents an important conclusion, which drives home the difference between DNA and siRNA: The rigid rod-like character of siRNA molecules makes condensation by the polymeric carrier more difficult. These molecules are not able to adopt bent conformations, thereby allowing only three types of interactions with linear cationic polymers: (1) a longitudinal arrangement, (2) a transversal arrangement, where a cationic polymer bridges two or more siRNA molecules and (3) an enveloping arrangement, where the cationic polymer coils around the siRNA molecule. Although (1) and (2) would theoretically allow ordered packing, this was not the case.

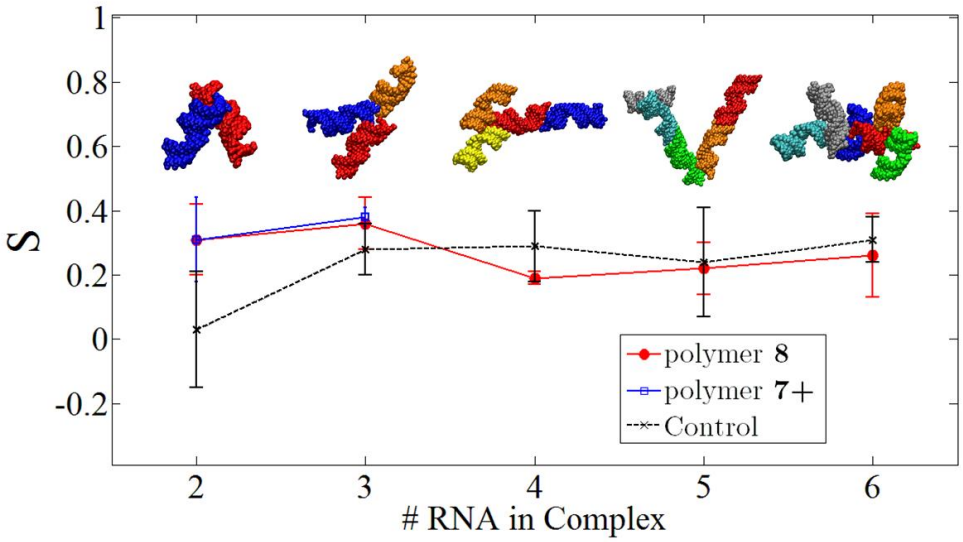

Figure 3.26. The calculated orientational order parameters for the siRNA molecules inside different complexes in correlation to the number of siRNA molecules per complex are shown for the clusters formed between siRNA and either (red) polymer 8 or (blue) polymer 7+. The illustrated complex structures, inset in the figure, belong to the control simulations, whose order parameters are shown in black.

In the experimental section twelve different polymer block copolymers were synthesized by using a controlled polymerization approach. The block length as well as the source of the cationic charges has been varied while keeping the length of the linear polymer chain constant. Low polydispersities (PDI < 1.12) and only marginal deviations from the desired polymer size ensured comparability.

Among these structures only polymers **1**, **4**, **6** and **10** were not able to form stable complexes with siRNA, which was attributed to an unfavorable length$^{\text{binding block}}$/length$^{\text{non-}}$

$^{\text{biding block}}$ ratio (lower than the threshold ratio of 1:8.7). EMSA and MST analysis showed that changing the length of the cationic block and the source of the cationic charges (primary amines or gunidinium groups), modulates the binding affinity. The length of the cationic block also had an impact on the polymers' knock-down efficacy. In addition, differences with respect to the source of the cationic charges were not only relevant with respect to binding, but also knock-down. In fact, GPMA-based compolymers performed less efficiently than their APMA-counterparts due to their higher affinity towards siRNA. Their ability to form not only electrostatic interactions, but also multiple hydrogen bonds leads to strong binding, which in turn reduced the release of the siRNA molecules.

Numerical simulations of same-sized block copolymers confirmed these above-described observations and a $\text{length}^{\text{binding block}}/\text{length}^{\text{non-biding block}}$ threshold ratio of 1:7.5 was calculated as necessary to support the stability of the complex. Specifically, the simulation showed that a shorter guanidinium block - and correspondingly a longer non-binding segment - impedes bridging of multiple siRNA molecules and favors the formation of single siRNA/single polymer chain complexes. Such structures were shown to be unexpectedly large due to the non-binding blocks protruding from the complex's center. Using long binding blocks, on the other hand, lead to polyplexes with multiple bridged siRNA molecules without strongly increasing the overall size.

Detailed insights into the structural organization of the complexes and their polymer sequence-dependent architecture were obtained by investigating the size and order of the complexes. The rigid rod-like character of siRNA molecules makes condensation by the polymeric carrier more difficult. It was therefore expected to observe no correlation between the measured polyplex size to either the binding efficacy, the charge density, the source of the cationic charges (GPMA or APMA monomers) or even the hydrodynamic radius of the polymer structures. However, it was shown that the length of the cationic block strongly impacts the size of the resulting polyplex. Nevertheless, investigating the order parameter *via* simulation showed that the reduction in size was not caused by an increased symmetry/order of the packed siRNA. In fact, the ordering inside polyplexes was observed to be rather random than ordered. This observation can be explained by the inability of siRNA molecules to adopt bent conformations, thereby allowing only three types of interactions with linear cationic polymers: (1) a longitudinal arrangement, (2) a transversal arrangement and (3) an enveloping arrangement. Alt-

hough efficient packing is at least theoretically possible, it seems to be improbably due to entropy.

The biochemical characterization has revealed a flaw of the carrier design, which needs to be addressed. Polymer **8**-based complexes, for example, were shown to possess the ability to bypass cellular membranes even if carrying a payload (siRNA), but the knock-down study revealed only a reduced efficacy in down-regulating gene expression. In particular, they were less effective than their APMA counterparts to release their cargo and induce knock-down. In spite of this flaw, the present data represents a valuable starting point for the structure-effect trend-based design of improved nonviral polynucleotide delivery vectors and, consequently, for their systematic usage in safer and more effective gene regulation therapies. Hence, it was decided not to avoid the above-described problems by researching a completely different polymer design, but to face them using post-polymerization modification. Here, the diblock copolymer **8**, which has shown the best results of the guanidinium group bearing copolymers was chosen as the candidate. The implementation of the strategy and the improvements gained will be described in the next chapter.

3.5 References

[1] L. W. Seymour, R. Duncan, J. Strohalm, J. Kopecek, *J. Biomed. Mater. Res.* **1987**, *21*, 1341.

[2] O. Samsonova, C. Pfeiffer, M. Hellmund, O. M. Merkel, T. Kissel, *Polymers (Basel, Switz.)* **2011**, *3*, 693.

[3] S. H. Thang, Y. K. Chong, R. T. A. Mayadunne, G. Moad, E. Rizzardo, *Tetrahedron Lett.* **1999**, *40*, 2435.

[4] N. J. Treat, D. Smith, C. Teng, J. D. Flores, B. A. Abel, A. W. York, F. Huang, C. L. McCormick, *ACS Macro Lett.* **2012**, *1*, 100.

[5] C. W. Scales, F. Huang, N. Li, Y. A. Vasilieva, J. Ray, A. J. Convertine, C. L. McCormick, *Macromolecules* **2006**, *39*, 6871.

[6] C. W. Scales, Y. A. Vasilieva, A. J. Convertine, A. B. Lowe, C. L. McCormick, *Biomacromolecules* **2005**, *6*, 1846.

[7] D. B. Thomas, A. J. Convertine, L. J. Myrick, C. W. Scales, A. E. Smith, A. B. Lowe, Y. A. Vasilieva, N. Ayres, C. L. McCormick, *Macromolecules* **2004**, *37*, 8941.

[8] S. Perrier, P. Takolpuckdee, C. A. Mars, *Macromolecules* **2005**, *38*, 2033.

[9] Y. Matsumura, H. Maeda, *Cancer Research* **1986**, *46*, 6387.

[10] M. Hemmelmann, K. Mohr, K. Fischer, R. Zentel, M. Schmidt, *Molecular Pharmaceutics* **2013**, *10*, 3769.

[11] M. Fried, D. M. Crothers, *Nucleic Acids Res.* **1981**, *9*, 6505.

[12] M. M. Garner, A. Revzin, *Nucleic Acids Res.* **1981**, *9*, 3047.

[13] W. Hendrickson, *BioTechniques* **1985**, *3*, 198.

[14] A. Varshavsky, *Methods Enzymol.* **1987**, *151*, 551.

[15] M. M. Garner, A. Revzin, *Trends Biochem. Sci. (Pers. Ed.)* **1986**, *11*, 395.

[16] http://www.nanotemper-technologies.com/home/?no_cache=1, 27.11.2013, 15:00.

[17] M. Jerabek-Willemsen, S. Duhr, P. Baaske, *BIOspektrum* **2012**, *18*, 30.

[18] P. Baaske, C. J. Wienken, P. Reineck, S. Duhr, D. Braun, *Angew. Chem., Int. Ed.* **2010**, *49*, 2238.

[19] P. Reineck, C. J. Wienken, D. Braun, *Electrophoresis* **2010**, *31*, 279.

[20] S. Duhr, D. Braun, *Proc. Natl. Acad. Sci. U. S. A.* **2006**, *103*, 19678.

[21] S. A. I. Seidel, C. J. Wienken, S. Geissler, M. Jerabek-Willemsen, S. Duhr, A. Reiter, D. Trauner, D. Braun, P. Baaske, *Angew. Chem., Int. Ed.* **2012**, *51*, 10656.

[22] S. A. I. Seidel, P. M. Dijkman, W. A. Lea, d. B. G. van, M. Jerabek-Willemsen, A. Lazic, J. S. Joseph, P. Srinivasan, P. Baaske, A. Simeonov, I. Katritch, F. A. Melo, J. E. Ladbury, G. Schreiber, A. Watts, D. Braun, S. Duhr, *Methods (Amsterdam, Neth.)* **2013**, *59*, 301.

[23] C. J. Wienken, P. Baaske, U. Rothbauer, D. Braun, S. Duhr, *Nat. Commun.* **2010**, *1*, Wien1/1.

[24] M. Jerabek-Willemsen, C. J. Wienken, D. Braun, P. Baaske, S. Duhr, *Assay Drug Dev. Technol.* **2011**, *9*, 342.

[25] S. A. I. Seidel, P. M. Dijkman, W. A. Lea, d. B. G. van, M. Jerabek-Willemsen, A. Lazic, J. S. Joseph, P. Srinivasan, P. Baaske, A. Simeonov, I. Katritch, F. A. Melo, J. E. Ladbury, G. Schreiber, A. Watts, D. Braun, S. Duhr, *Methods* **2013**, *59*, 301.

[26] K. Zillner, M. Jerabek-Willemsen, S. Duhr, D. Braun, G. Laengst, P. Baaske, *Methods Mol. Biol.* **2012**, *815*, 241.

[27] H. Qian, E. L. Elson, *Appl. Opt.* **1991**, *30*, 1185.

[28] R. Rigler, E. S. Elson, "*Fluorescence Correlation Spectroscopy: Theory and Applications. [In: Springer Ser. Chem. Phys., 2001; 65]"*, 2001, p. 487 pp.

[29] B. Krieg, M. Hirsch, E. Scholz, L. Nuhn, I. Tabujew, H. Bauer, S. Decker, A. Khobta, M. Schmidt, W. Tremel, R. Zentel, K. Peneva, K. Koynov, A. J. Mason, M. Helm, *Pharm. Res.* **2015**, *32*, 1957.

[30] M. Spelios, M. Kearns, M. Savva, *Biochemistry* **2010**, *49*, 5753.

[31] S. Menuel, S. Fontanay, I. Clarot, R. E. Duval, L. Diez, A. Marsura, *Bioconjugate Chem.* **2008**, *19*, 2357.

[32] S. Sahu, F. Philip, S. Scarlata, *The Journal of Biological Chemistry* **2014**, *289*, 5134.

[33] P. J. Hagerman, *Annu. Rev. Biophys. Biomol. Struct.* **1997**, *26*, 139.

[34] A.-L. Bolcato-Bellemin, M.-E. Bonnet, G. Creusat, P. Erbacher, J.-P. Behr, *Proc. Natl. Acad. Sci. U. S. A.* **2007**, *104*, 16050.

[35] A. E. Smith, A. Sizovs, G. Grandinetti, L. Xue, T. M. Reineke, *Biomacromolecules* **2011**, *12*, 3015.

[36] Y. Deng, Z. Yan, *Curr. Top. Colloid Interface Sci.* **2001**, *4*, 183.

[37] A. M. I. Ali, P. Pareek, L. Sewell, A. Schmid, S. Fujii, S. P. Armes, I. M. Shirley, *Soft Matter* **2007**, *3*, 1003.

[38] J. Madsen, S. P. Armes, K. Bertal, S. MacNeil, A. L. Lewis, *Biomacromolecules* **2009**, *10*, 1875.

[39] M. Save, J. V. M. Weaver, S. P. Armes, P. McKenna, *Macromolecules* **2002**, *35*, 1152.

[40] V. A. Bloomfield, *Biopolymers* **1998**, *44*, 269.

[41] S. C. De Smedt, J. Demeester, W. E. Hennink, *Pharm. Res.* **2000**, *17*, 113.

[42] X. Liu, K. A. Howard, M. Dong, M. O. Andersen, U. L. Rahbek, M. G. Johnsen, O. C. Hansen, F. Besenbacher, J. Kjems, *Biomaterials* **2006**, *28*, 1280.

[43] X.-C. Shen, J. Zhou, X. Liu, J. Wu, F. Qu, Z.-L. Zhang, D.-W. Pang, G. Quelever, C.-C. Zhang, L. Peng, *Org. Biomol. Chem.* **2007**, *5*, 3674.

[44] D. J. Gary, J. B. Min, Y. Kim, K. Park, Y.-Y. Won, *Macromolecular bioscience* **2013**, *13*, 1059.

[45] P. Zhao, L. Liu, X. Feng, C. Wang, X. Shuai, Y. Chen, *Macromol. Rapid Commun.* **2012**, *33*, 1351.

[46] E. Bartova, J. Krejci, A. Harnicarova, G. Galiova, S. Kozubek, *J. Histochem. Cytochem.* **2008**, *56*, 711.

[47] K. Kunath, H. A. von, D. Fischer, H. Petersen, U. Bickel, K. Voigt, T. Kissel, *J. Controlled Release* **2003**, *89*, 113.

[48] Q. Cheng, Y. Huang, H. Zheng, T. Wei, S. Zheng, S. Huo, X. Wang, Q. Du, X. Zhang, H.-Y. Zhang, X.-J. Liang, C. Wang, R. Tang, Z. Liang, *Biomaterials* **2013**, *34*, 3120.

[49] M. Hellmund, K. Achazi, F. Neumann, B. N. S. Thota, N. Ma, R. Haag, *Biomater. Sci.* **2015**, *3*, 1459.

[50] Z. Rezvani Amin, M. Rahimizadeh, H. Eshghi, A. Dehshahri, M. Ramezani, *Iranian Journal of Basic Medical Sciences* **2013**, *16*, 150.

[51] K. Kunath, A. von Harpe, D. Fischer, H. Petersen, U. Bickel, K. Voigt, T. Kissel, *J. Controlled Release* **2003**, *89*, 113.

[52] M. Mannisto, S. Vanderkerken, V. Toncheva, M. Elomaa, M. Ruponen, E. Schacht, A. Urtti, *J. Controlled Release* **2002**, *83*, 169.

[53] F. J. Verbaan, G. W. Bos, C. Oussoren, M. C. Woodle, W. E. Hennink, G. Storm, *J. Drug Delivery Sci. Technol.* **2004**, *14*, 105.

[54] H. Lv, S. Zhang, B. Wang, S. Cui, J. Yan, *J. Controlled Release* **2006**, *114*, 100.

[55] M. A. Mintzer, E. E. Simanek, *Chem. Rev. (Washington, DC, U. S.)* **2009**, *109*, 259.

[56] E. Fröhlich, *International Journal of Nanomedicine* **2012**, *7*, 5577.

[57] J. Suhorutsenko, N. Oskolkov, P. Arukuusk, K. Kurrikoff, E. Eriste, D.-M. Copolovici, U. Langel, *Bioconjugate Chem.* **2011**, *22*, 2255.

[58] C. He, Y. Hu, L. Yin, C. Tang, C. Yin, *Biomaterials* **2010**, *31*, 3657.

[59] G. J. Hannon, *Nature (London, U. K.)* **2002**, *418*, 244.

[60] D. M. Perreault, L. A. Cabell, E. V. Anslyn, *Bioorgan Med Chem* **1997**, *5*, 1209.

[61] J. Ziebarth, Y. Wang, *Biophys. J.* **2009**, *97*, 1971.

[62] J. Ziebarth, Y. Wang, *J. Phys. Chem. B* **2010**, *114*, 6225.

[63] C.-B. Sun, T. Tang, H. Uludag, *Biomacromolecules* **2011**, *12*, 3698.

[64] D. Ouyang, H. Zhang, H. S. Parekh, S. C. Smith, *Biophys. Chem.* **2011**, *158*, 126.

[65] H. S. Antila, M. Sammalkorpi, *J. Phys. Chem. B* **2014**, *118*, 3226.

[66] D. Meneksedag-Erol, T. Tang, H. Uludag, *Biomaterials* **2014**, *35*, 7068.

[67] D. Meneksedag-Erol, T. Tang, H. Uludag, *J. Phys. Chem. B* **2015**, *119*, 5475.

[68] D. A. Kondinskaia, A. Y. Kostritskii, A. M. Nesterenko, A. Y. Antipina, A. A. Gurtovenko, *J. Phys. Chem. B* **2016**, *120*, 6546.

[69] M. Serucnik, C. Podlipnik, B. Hribar-Lee, *J. Phys. Chem. B* **2018**, Ahead of Print.

[70] S. R. Holbrook, C. Cheong, I. Tinoco, Jr., S. H. Kim, *Nature (London)* **1991**, *353*, 579.

[71] P. Kebbekus, D. E. Draper, P. Hagerman, *Biochemistry* **1995**, *34*, 4354.

[72] K. Hayashi, H. Chaya, S. Fukushima, S. Watanabe, H. Takemoto, K. Osada, N. Nishiyama, K. Miyata, K. Kataoka, *Macromol. Rapid Commun.* **2016**, *37*, 486.

[73] M. Kleman, O. D. Laverntovich, **2003**, 76.

[74] S. Dasgupta, T. Auth, G. Gompper, *Nano Letters* **2014**, *14*, 687.

[75] B. D. Chithrani, A. A. Ghazani, W. C. W. Chan, *Nano Letters* **2006**, *6*, 662.

[76] Y. He, K. Park, *Molecular Pharmaceutics* **2016**, *13*, 2164.

4 Modification strategy achieving siRNA transport into $CD8^+$ T cells

Bioengineering immune cells via gene therapy offers treatment opportunities for currently fatal viral infections as well as a new approach to combat cancer. $CD8^+$ T-cells belong to this category of cells. They are a vital part of the immune system and their operability is crucial during the treatment of noteworthy illnesses, such as the human and simian immunodeficiency virus infection, since they control the retrovirus replication through both non-cytotoxic and conventional cytotoxic mechanisms.[1-3] $CD8^+$ T-cells are also able to recognize tumor associated antigens, thereby facilitating anti-tumor effects.[4, 5] This ability can the enhanced by regulating the expression of suppressing proteins with the RNA interference (RNAi) pathway using extrinsic small interfering RNA (siRNA). Therefore, these cells possess the potential to be a universal mediator in the treatment of tumors and viral infects. The successful introduction of foreign nucleic acids into these nonadhesive fully differentiated primary human cells, however, is a major challenge, since they do not possess a pronounced metabolic apparatus and therefore neither a noteworthy endosomal uptake. Physical methods such as electroporation, sonoporation, gene gun and microinjection are the most commonly employed approaches to transfect primary cell lines, but they lead to poor results due to reduced cellular viability and inconsistent transfection efficacy.[6] They also offer limited opportunity for *in vivo* application, since these methods require isolated cells.[7] The commonly applied delivery agents, such as Lipofectamine or other strongly cationic structures, are also not applicable, since $CD8^+$ T cells are highly sensitive to positive charge-induced cytotoxicity. These polymer vectors, however, require a positive net-charge for two reasons: Firstly, it is needed for the formation and stabilization of the polyplexes between the negatively charged RNA and the polymer. Secondly, a positive net charge is advantageous for internalization into cells. Due to this background no polymer based siRNA delivery system has been reported to be applicable for $CD8^+$ T-cells so far. Investigating the polymer library of Chapter 4, polymer **8** was shown to exhibit excellent siRNA-complexation properties, comparatively low cytotoxicity, fast uptake into cells and the ability to induce knock-down. This polymer relies on the the guanidinium group for the complexation of siRNA, which allows efficient binding even at low positive charge densities.[8] Hence, polymer **8** is expected to show a reduced charge-related cytotoxicity towards $CD8^+$ T cells. This chapter is aimed to improve the design of this polymeric siRNA carrier system in a way, which would allow efficient internalization of polyplex-

es into CD8$^+$ T cells without affecting their viability and thereby removing the current limitations in the field. The issue of uptake efficacy can be addressed by equipping the delivery agent with uptake-promoting moieties like the lipid-soluble triphenylphosphonium (TPP) cation.[9, 10] The conjugation of these moieties facilitates increased accumulation in cells and mitochondria.[11] They have been also shown to enable targeting of pathogenic mitochondria due to structural differences between physiological and pathogenic cells, such as the negativity of the membrane potential of the respective mitochondria.[12, 13] The ability of TPP to bypass not only one but two plasma membranes, if bound to fluorescent dyes[14], drugs[15] or antioxidants[16], makes it a prime candidate as a modification moiety in the design of polymeric siRNA carrier systems. Nevertheless, polymer-bound triphenylphosphonium cations have up until now only been used in solid supported synthesis of carbon-carbon bonds, due to their reduced solubility in water.[17]

Triphenylphosphonium (TPP) cation-modified diblock copolymer structures, which employ a terminal 3-guanidinopropyl methacrylamide block for the complexation of siRNA were prepared. The impact of this modification strategy on the polymers' viability as a siRNA delivery agent was then analyzed. Electrophoretic mobility shift assay (EMSA), microscale thermophoresis (MST), dynamic light scattering (DLS) as well as fluorescence correlation spectroscopy (FCS) were used to investigate a possible effect on the complex formation properties. Following this physicochemical characterization an extensive internalization study on differentiated CD8$^+$ T-cells was performed.

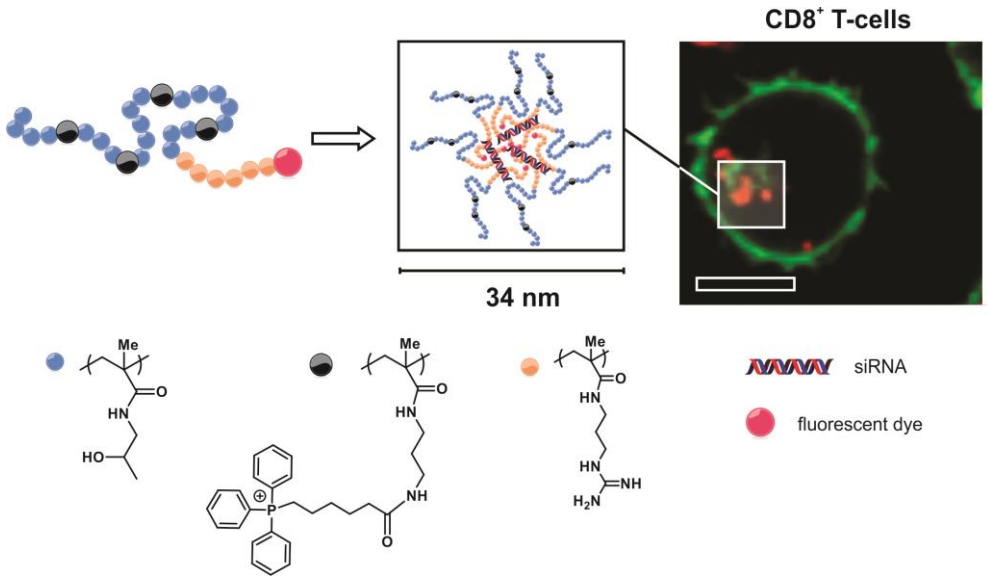

Figure 4.1. TPP-modified diblock copolymer delivering siRNA into CD8$^+$ T cells

4.1 Preparation of the modified diblock copolymer

Initially, a compound bearing not only the triphenylphosphonium group, but also a carboxyl functionality was synthesized. It allows conjugation to the primary amino groups of the APMA units of the block copolymer. In order to circumvent any steric problems that might arise from the conjugation step, the flexible carbon chain of 6-bromocaproic acid was chosen as a spacer. 6-Bromocaproic acid and triphenylphosphin readily underwent a substitution at elevated temperature and formed the desired compound (Figure 4.2)

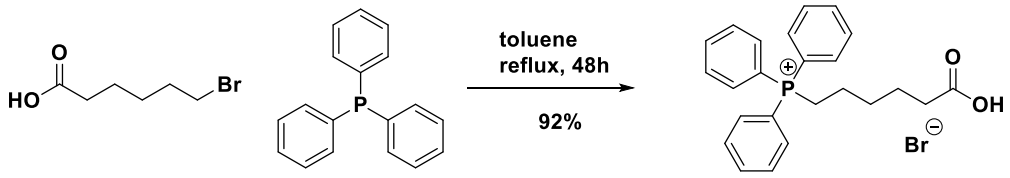

Figure 4.2. Synthesis of (5-carboxypentyl)triphenylphosphonium bromide

The synthesis of polymer **8** ($(HPMA_{126}\text{-s-}APMA_{14})\text{-b-}GPMA_{49}$), which was employed as the precursor molecule for the modification strategy using triphenylphosphonium moieties, has been described in section 3.1. In this case, however, the terminal thiocarbonylthio functionality of the (HPMA-*s*-APMA)-*b*-GPMA block copolymer was cleaved to a free thiol group via aminolysis. This controlled polymerization technique of aRAFT facilitated the synthesis of precise polymer structures. Here, not only the length of the blocks and the dispersity of the polymers were of importance, but also the composition of the statistical copolymer HPMA-s-APMA, which corresponds to the first block. The incorporation of APMA monomers provides pendant primary amino groups for conjugation. Using ^{1}H-NMR spectroscopy a HPMA:APMA ratio of 9:1 was found. These functional groups were quantitatively functionalized with triphenylphosphonium moieties (TPP) by utilizing N,N,N',N'-tetramethyl-O-(N-succinimidyl)uronium tetrafluoroborate (TSTU). The procedure is depicted in Figure 4.3.

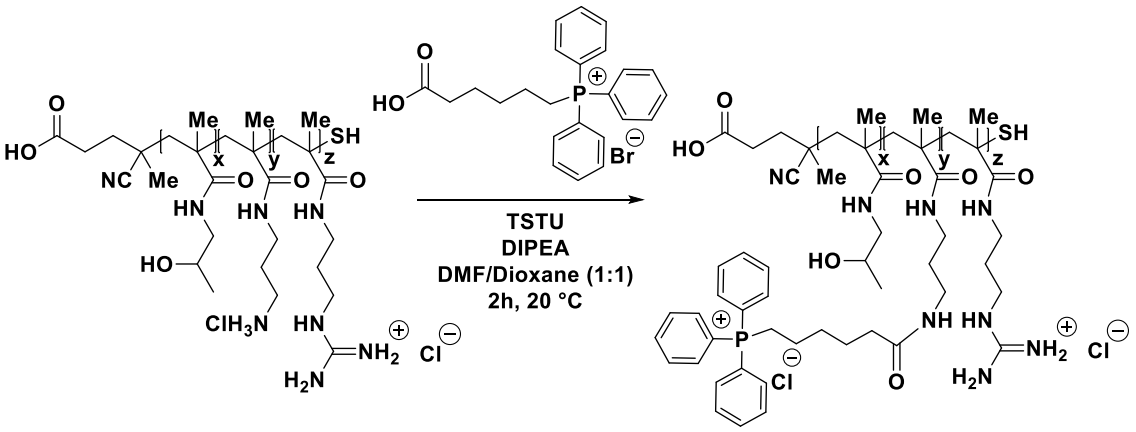

Figure 4.3. Preparation of the (HPMA$_{126}$-*s*-APMA$_{14}$)-*b*-GPMA$_{49}$-TPP conjugate (TDBC)

^{31}P-NMR spectroscopy confirmed that the phosphor atoms of the attached triphenylphosphonium moieties remained in the oxidative state of phosphonium cations during this reaction (section 9.7.3.2). Storing the compound in DPBS solution for the duration of a month did not lead to oxidation either.

Some biochemical experiments, such as cLSM or flow cytometry, require the molecule of interest to be fluorescently labeled. Hence, the TPP-modified diblock copolymer (TDBC) as well as its precursor molecule (polymer **8**) were conjugated to a perylene dye, namely (N-(2,6-diisopropylphenyl)-N'-(4-aminoethyl)-1,5,7,12-tetraphenoxyperylene-3.4:9,10-tetracarboxy diimide). I synthesized said dye by following the procedure described by Peneva *et al.*[18] (Figure 4.4).

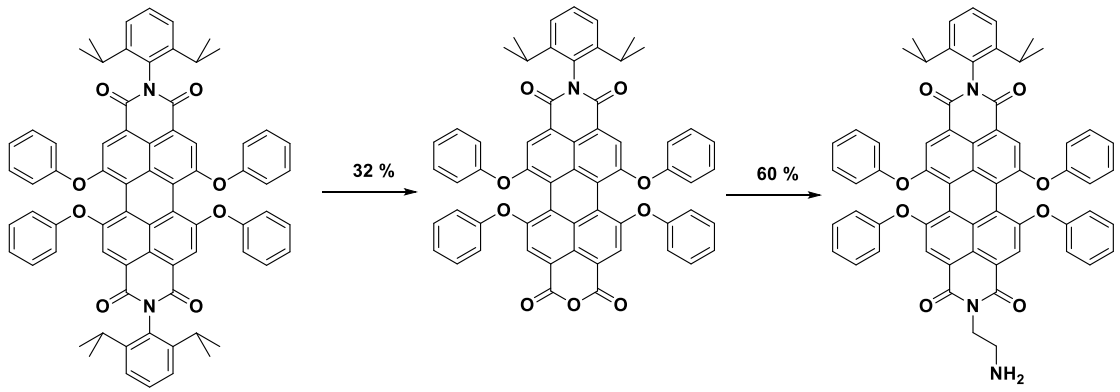

Figure 4.4. Synthesis of the water-soluble perylene

The conjugation between the polymer chains and the perylene dye was performed by using N-γ-maleimidobutyryl-oxysuccinimide ester (GMBS) as a linker (Figure 4.5). It allowed quantitative as well as selective labeling.

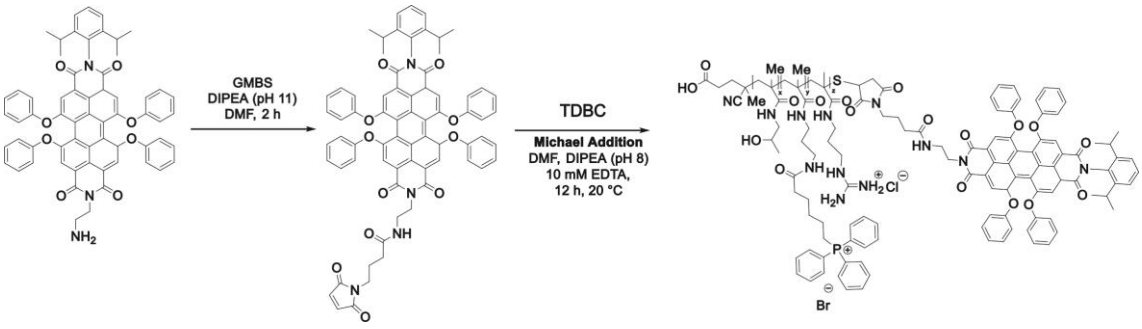

Figure 4.5. Labeling of the ($HPMA_{126}$-*s*-$APMA_{14}$)-*b*-$GPMA_{49}$-TPP conjugate

Here, the terminal thiol group of the polymers, made accessible via aminolysis of the thiocarbonylthio moiety of the macromolecular chain transfer agent, was used for a site selective functionalization. Its removal from polymer **8** was confirmed by monitoring the UV signal at 310 nm before and after removal. Initially, in order to avoid implementing a hydrophobic terminus, the water-soluble perylene was used for labeling. However, the strong electrostatic interaction between the sulfonyl and the guanidinium groups made purification by conventional means impossible. Free dye was observed during SDS-PAGE gels even after repeated use of ion exchange columns. Since this opportunity was barred, it was decided to employ the hydrophobic monofunctional perylene as the label. Incidentally, this choice simplified the workup, because the unreacted dye, in contrast to the polymer attached species, was insoluble in water. The different stages of modification have been monitored by means of SEC with HFIP as the eluent (Table 4.1). The SEC chromatogram (Figure 4.6) visualizes the shift to shorter elution times as well as the narrow molecular weight distributions.

Table 4.1. Molecular weight (M_n in [g/mol]) and Polydispersity (Đ) of the copolymer $HPMA_{126}$-*s*-$APMA_{14}$, the block copolymer ($HPMA_{126}$-*s*-$APMA_{14}$)-b-$GPMA_{49}$ (polymer 8), the perylene labeled ($HPMA_{126}$-*s*-$APMA_{14}$)-b-$GPMA_{49}$ and the TPP-modified ($HPMA_{126}$-$_s$-$APMA_{14}$)-b-$GPMA_{49}$ as well as its perylene labeled form

sample	$M_{n_{theo}}$ [a]	$M_{n_{exp}}$ [b]	Đ
$HPMA_{126}$-s-$APMA_{14}$	21000	21000	1.07
($HPMA_{126}$-s-$APMA_{14}$)-b-$GPMA_{49}$	29700	30000	1.08
($HPMA_{126}$-s-$APMA_{14}$)-b-$GPMA_{49}$ (labeled)	31100	33000	1.11
($HPMA_{126}$-s-$APMA_{14}$)-b-$GPMA_{49}$-TPP conjugate	36000	35500	1.13
($HPMA_{1826}$-s-$APMA_{14}$)-b-$GPMA_{49}$-TPP conjugate (labeled)	36600	40000	1.12

[a] The theoretical molecular weight of the conjugates was calculated by considering the possible molecular weight of the respective polymer structure after quantitative conjugation with either TPP or the perylene dye. The theoretical molecular weight of the unmodified polymers was calculated by using the formula $M_{n,th} = ([M]_0/[CTA]_0) \cdot M_{w,monomer} \cdot \rho + M_{w,CTA}$, while the conversion ρ was taken from the kinetic studies done by Treat et al.[19] and the results of York et al.[20]; [b] determined by HFIP SEC;

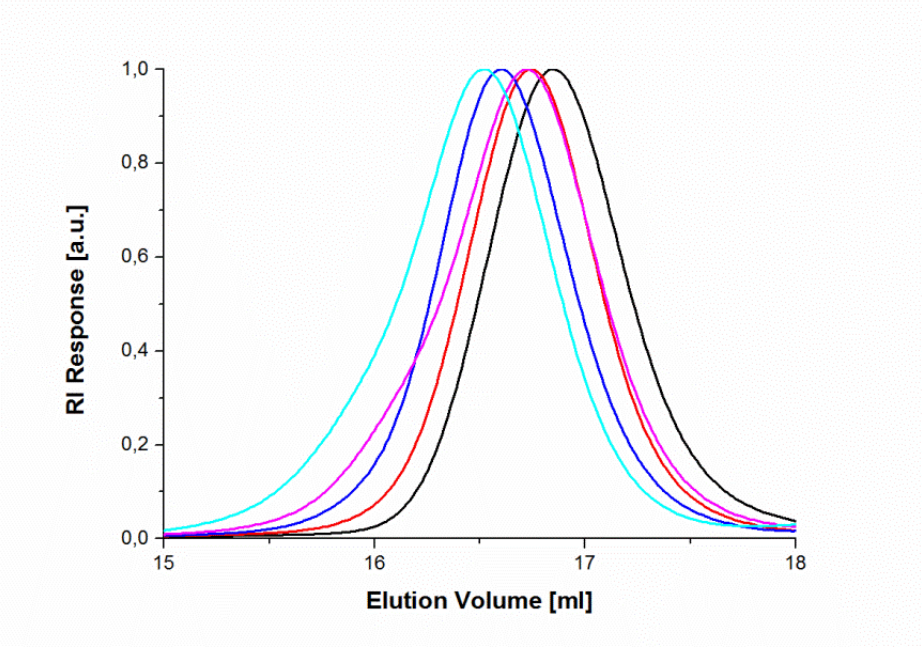

Figure 4.4.6. HFIP-SEC demonstrating the chain elongation in the process of polymer-modification. $HPMA_{126}$-*s*-$APMA_{14}$ macroCTA (black), ($HPMA_{126}$-*s*-$APMA_{14}$)-b-$GPMA_{49}$ (red), ($HPMA_{126}$-*s*-$APMA_{14}$)-b-$GPMA_{49}$-TPP conjugate (blue) and perylene dye labelled ($HPMA_{126}$-*s*-$APMA_{14}$)-b-$GPMA_{49}$ (magenta) or ($HPMA_{126}$-*s*-$APMA_{14}$)-b-$GPMA_{49}$-TPP conjugate (cyan)

4.2 Complexation of siRNA

In analogy to the procedure of Chapter 3, complex formation, the basic requirement for siRNA delivery agents, was investigated *via* electrophoretic mobility shift assay (EMSA), microscale thermophoresis (MST), dynamic light scattering (DLS) and fluorescence correlation spectroscopy (FCS). These methods were introduced in section 3.3.1.

EMSA was used to study the required $mass^{siRNA}/mass^{polymer}$ ratio for complete complexation (Figure 4.7). The copolymer structure, which lacks guanidinium groups bearing monomers ($HPMA_{126}$-*s*-$APMA_{14}$, precursor to polymer **8**) does not lead to the formation of complexes even at very high siRNA to polymer ratios (Figure 4.7, A). Polymer **8**, on the other hand, due to the addition of a GPMA block, is able to effectively complex the polyanionic siRNA (Figure 4.7, B). The band corresponding to free siRNA starts disappearing at a $mass^{siRNA}/mass^{polymer}$ ratio of 1:10, almost completely vanishes at 1:25 and it is fully gone at the ratio of 1:50 (N/P ratios of 18, 45 and 90 respectively). In addition, an upward shift of the fluorescent bands was observed. This behavior indicates not only that the formed polyplexes are small enough to bypass the network of the agarose gel, but also that they possess a positive net charge. The addition of TPP moieties did not diminish the binding affinity towards siRNA, since there is no difference between polymer **8** and TDBC in terms of the required $mass^{siRNA}/mass^{polymer}$ ratio for complete or partial complexation. This observation underlines the fact that neither the statistically incorporated APMA, nor TPP moieties play a significant role during the binding event. However, TDBC demonstrated an even stronger shift of the fluorescent band towards the cathode (Figure 4.7, C), which indicates either a smaller size, a higher positive net charge of the polyplexes or a combination of both. In addition, TDBC did not quench the fluorescence of the labelled siRNA to the same degree as the unmodified block copolymer, which is advantageous for microscopy experiments.

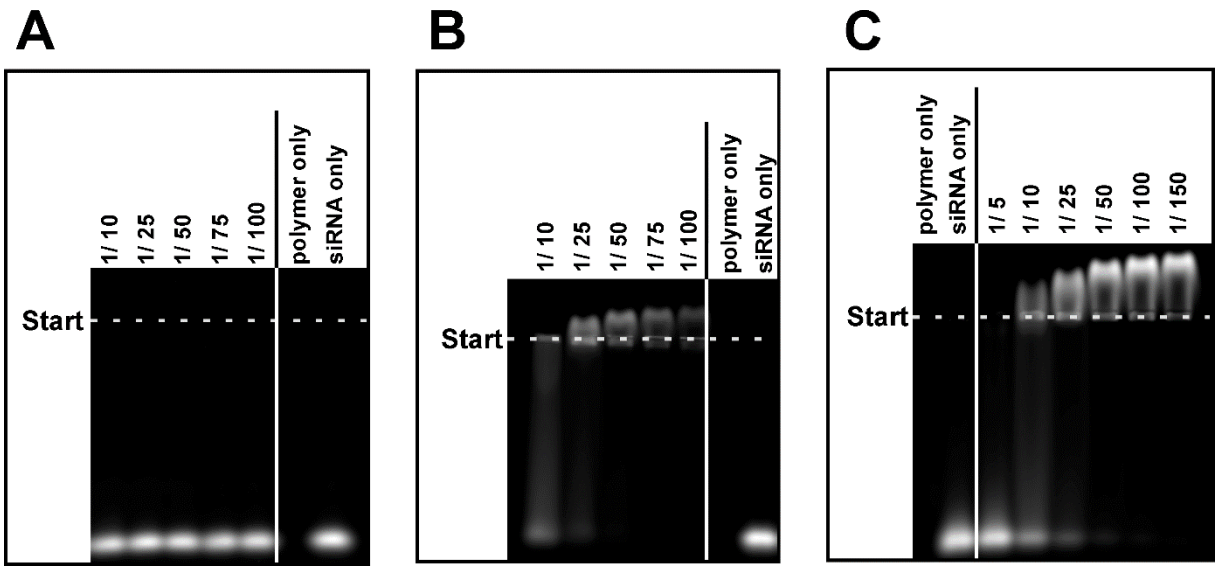

Figure 4.7. Electrophoretic Mobility Shift Assay to determine the mass^{siRNA}/mass^{polymer} ratio necessary for complete complexation: (A) HPMA$_{126}$-*s*-APMA$_{14}$, (B) (HPMA$_{126}$-*s*-APMA$_{14}$)-*b*-GPMA$_{49}$ and (C) TDBC

The binding affinity was further quantified using MST, a method by which dissociation constants can be calculated based on changes of the thermal diffusion coefficient.[21] In this experiment ATTO488 labeled siRNA was used as the fluorescent component with the static concentration, whereas unlabeled TDBC or polymer **8** were used as a complexation partner in varying mass^{polymer}/mass^{siRNA} ratios, providing the basis for the calculation of the dissociation constant via the Hill-method fit (Figure 4.8). This analytical method confirmed the findings of the EMSA, since strong binding of TDBC to siRNA was detected (K_d(TDBC) = 29.1 ± 2.0 nM). The binding affinity of the unmodified polymer **8** was shown to be only marginally weaker (K_d((polymer **8**) = 43.8 ± 5.6 nM), which further supports the previous statement about the role of TPP and APMA pendant primary amino groups. The binding strength of either of these two polymer structures towards siRNA, however, is several orders of magnitude higher than that of equally sized nucleotide delivery agents, like modified cyclodextrin or cationic lipids.[22, 23] Although a direct comparison is difficult due to the large number of distinguishing features not shared by these structures, such as different backbone structures, the sources of the cationic charges or even the utilized charge densities, few studies include measurements of the binding strength.

As will be shown in the upcoming paragraphs TDBC forms significantly smaller polyplexes than both of the cited delivery agents and it stands to reason that it is more suited to transfect $CD8^+$ T-cells.

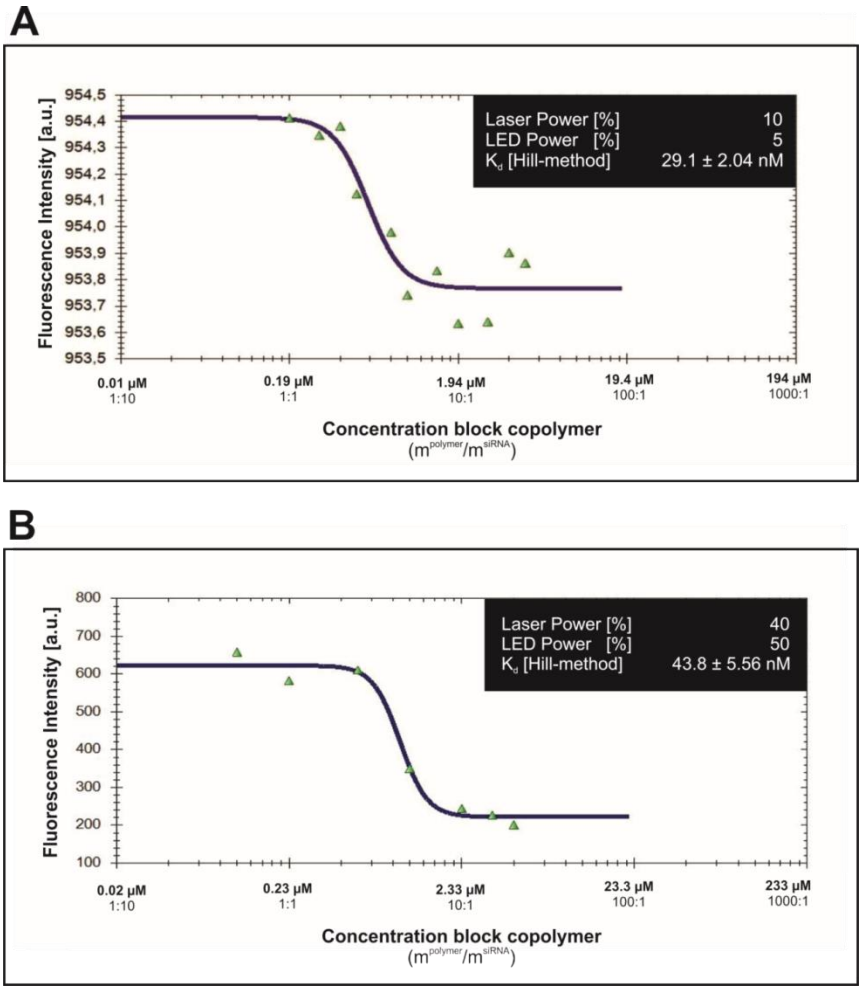

Figure 4.8. Fluorescence mode-evaluated MST results (Hill method fit - ratio of polymer/siRNA (1:10) - (50:1)): (A) TDBC and (B) polymer 8

The effect of the TPP-modification on the size of the formed polymer/siRNA polyplexes was studied. For that purpose multi-angle dependent DLS as well as FCS were employed. In initial experiments to study the hydrodynamic radius of polymers not interacting electrostatically with siRNA molecules, the signal of the aggregates they formed upon dissolving in MilliQ water near fully suppressed the signal of free polymers. In order to study the hydrodynamic radius of free polymers and to be able to calculate the size of the above-mentioned polyplexes (not falsified by aggregates, which were of similar size), it was necessary to suppress aggregate formation of the polymers. For that

purpose, the TDBC and polymer **8** were dissolved in aqueous solution of sodium chloride and filtered. The filter with a cut-off of 0.2 µm removed formed aggregates due to shear forces and the salt solution inhibited their rearrangement for the duration of the measurement. Hence, it was possible to study the hydrodynamic radius of the free polymer chains (Figure 4.9). TDBC (R_h(TDBC)$_{DLS}$ = 10.2 nm) was shown to be bigger than polymer 8 (R_h(polymer **8**)$_{DLS}$ = 6.3 nm) by a factor of 2. In addition it was observed that TDBC interacted with the filters, thereby making the characterization of TDBC-based complexes via DLS difficult. Polymer **8**, the precursor polymer of TDBC, did not interact with the filters and it was possible to evaluate the size of its polyplexes *via* DLS. It formed polyplexes with siRNA with a hydrodynamic radius of R_h(polymer **8** + siRNA)$_{DLS}$ = 49.6 nm.

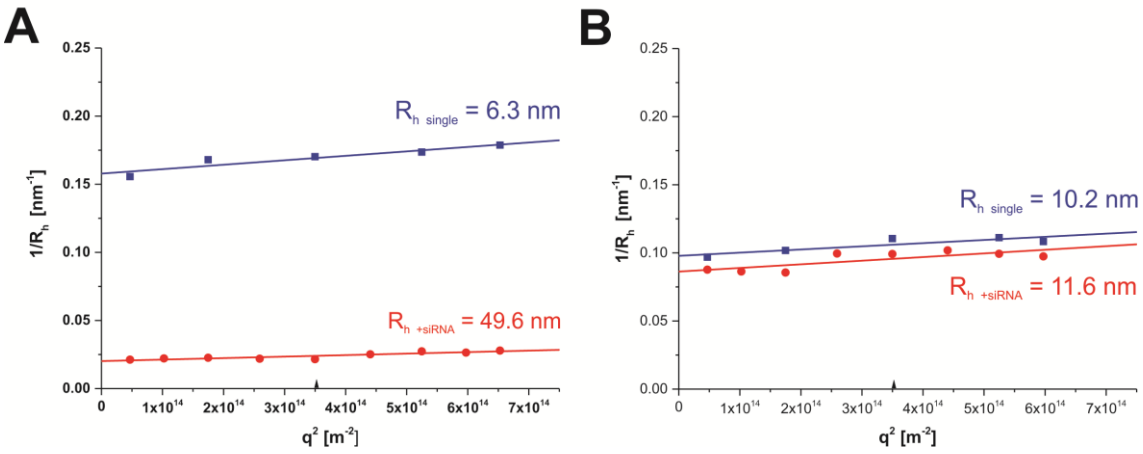

Figure 4.9. Plotted Dynamic Light Scattering results for the determination of the hydrodynamic radii ($R_{h\ single}$) of (A) polymer 8, (B) TDBC and the hydrodynamic radii of the polyplexes ($R_{h\ +siRNA}$)

The polyplexes of TDBC could not be studied *via* DLS, because unfiltered solutions does not allow appropriate differentiation between polymer aggregates and complexes. Filtration, on the other hand, removes large quantities of the polymer from the solution, thereby leaving a low polymer concentration, which does not facilitate complexation (Figure 4.9, B). To circumvent this problem, FCS was employed. This analytical method does not require filtration of the sample to provide meaningful results on the polymer/siRNA polyplexes formation. The FCS-determined hydrodynamic radius of the ATTO488-labeled siRNA was 2.0 ± 0.2 nm and the addition of TDBC at a weight^{siRNA}/weight^{polymer} ratio of 1:100 caused the formation of complexes with an average hy-

drodynamic radius of 17.1 ± 1.3 nm (Figure 4.10). Thus, the polymer structure has been shown to form stable, exceptionally small complexes with siRNA. TDBC and polymer **8** differ only in one aspect: the modification with TPP-moieties. Hence, the increased size of TDBC in the unbound state and the decreased size of siRNA/TDBC polyplexes can be directly attributed to the presence of triphenylphosphonium functional groups.

Their sizes are substantially smaller than the lipoplexes formed between the cationic lipid 1,3-dimyristoylamidopropane-2-[bis(2-dimethylaminoethane)] carbamate and siRNA (diameter of 634 nm).[24] Nevertheless, said lipoplexes were shown to induce knock-down in the human prostate carcinoma cell line PC-3 even in the presence of serum. Hence, it is anticipated that TDBC could facilitate efficient knock-down in immortalized adherent cell lines as well, but the $CD8^+$ T-cells, which are cultivated in suspension, are a different matter altogether. Due to the absence of literature known polymeric transfection agents for these cells, it is difficult to formulate a hypothesis in this regard.

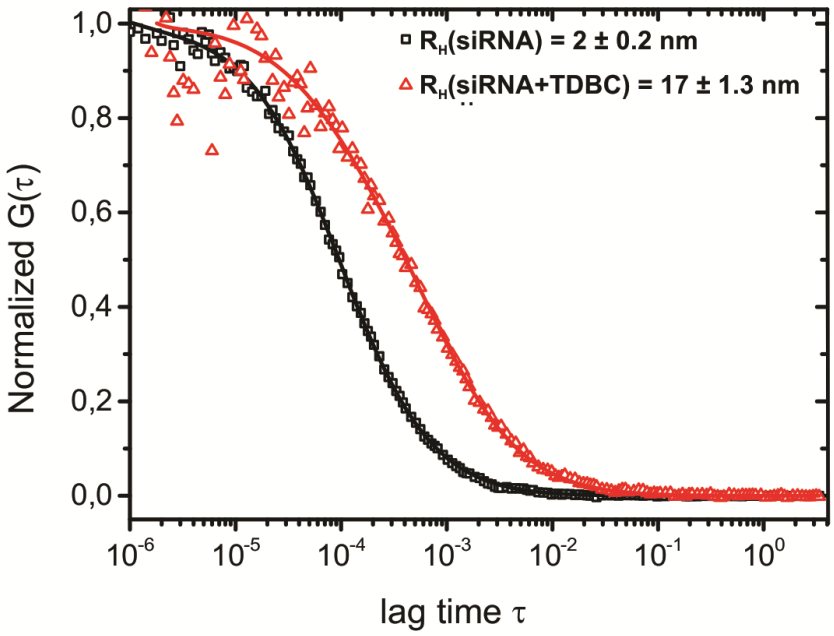

Figure 4.10. Fluorescence correlation spectroscopy autocorrelation curve of (black squares) the fluorescently labeled siRNA before and (red triangles) after complexation with TDBC

4.3 Cytotoxicity

The cytotoxicity of TDBC was studied for $CD8^+$ T-cells in cooperation with Dr. Marleen Willig (group of Prof. Dr. Katharina Landfester, Max Planck Institute for Polymer Research).

The T-cells were incubated for 72 hours in concentrations ranging from 75 µg/ml to 800 µg/ml and staining with 7-AAD as well as Annexin V allowed the identification of apoptotic and necrotic cells (Figure 4.11).

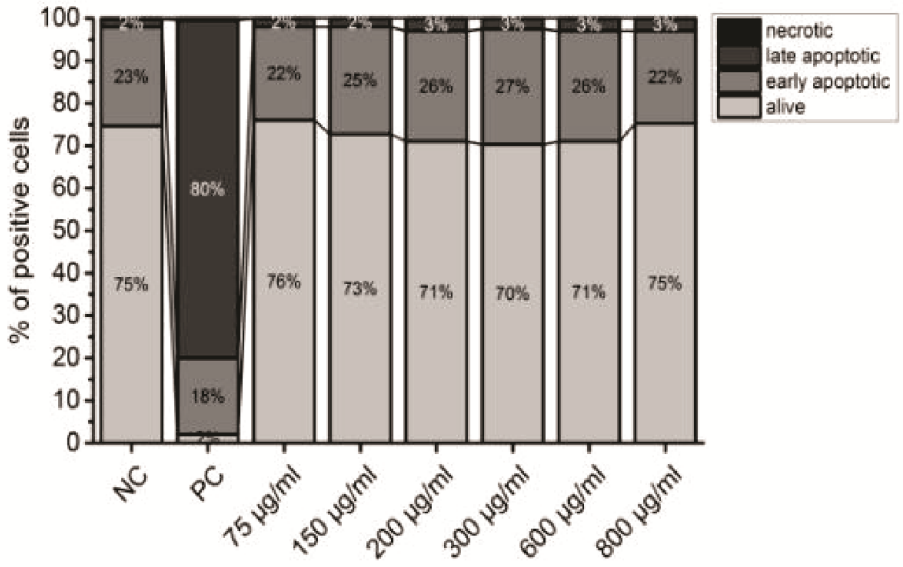

Figure 4.11. Flow cytometry analyzed cytotoxicity of TDBC towards CD8+ T-cells by using the 7-AAD/Annexin V staining protocol after 72 h of incubation. Untreated cells were used as the negative control (NC), whereas a medium containing 5% DMSO was employed as the positive control (PC)

According to DIN ISO 10993-5:2009, TDBC can be regarded as non-toxic towards $CD8^+$ T-cells, since even at the highest tested concentration (800 $\mu g \cdot ml^{-1}$) viability does not decrease below the value of 70%. The 7-AAD/Annexin V staining showed that 70 to 75% of the cells remained alive and only 20-25% of the cells were early apoptotic, while 2% were late apoptotic, which coincides with the negative control. Besides the primary T-cells other cell-lines were used to investigate the toxicity of TDBC including HeLa [cervical cancer cells, human], MCF-7 [breast cancer cells, human], C2C12 [myoblast cells, murine], and HEK293 cells [embryonic kidney cells, human] using the pro-

tocol of the CellTiterGlo® Assay. The used concentration range (3.6 – 720 µg·ml^{-1}) did not induce toxicity in the tested cell-lines and since the viability of the cells did not drop below 70% it was not possible to calculate IC_{50} values. Since TDBC is not toxic to $CD8^+$ T-cells, the uptake studies should not be affected by apoptotic and necrotic cells, which internalize external particles easily, since they lack membrane integrity. The modification strategy of introducing TPP moieties, in spite of increasing the cationic charge density due to the addition to permanent positive charges, effectively reduced the cytotoxicity of the block copolymer structure of the precursor polymer. Polymer **8**, contrary to TDBC, was shown to be toxic to all the tested cell lines (section 3.4.1). This discovery is remarkable for all polymer structures that were not viable as siRNA delivery agents due to their strong cytotoxicity.[25, 26] A possible explanation for this observation could be that the introduction of TPP-moieties effectively improves the internalization into cells, thereby diminishing the accumulation of cationic polymer molecules on the plasma membrane, which would otherwise induce the perforation and lysis of a cell.

4.4 Uptake into cells

The uptake of TDBC-based complexes was studied in detail for $CD8^+$ T-cells via cLSM and flow cytometry in cooperation with Dr. Marleen Willig (group of Prof. Dr. Katharina Landfester and Prof. Dr. Mailänder, Max Planck Institute for Polymer Research). Flow cytometry is a laser-based analytical technique, which is commonly employed in biotechnology. It is used for cell counting, cell sorting and for the detection of biomarkers. In this study, fluorescence-activated cell sorting (FACS) was employed, which is a specialized type of flow cytometry. The concept of this technique can be described as follows: Subsequent to the staining experiment the cells are injected into a flow cytometer. Here, the cell suspension is directed to a rapidly flowing stream of liquid, which passes through a narrow corridor. The flow rate and a vibrating mechanism destroy the cohesion between the cells and facilitate a large separation between the cells relative to their diameter. This procedure facilitates the measurement of the fluorescent character of individual cells in the detection unit.

At first the concentration-dependency of the uptake was investigated. Here, the incubation time was kept constant (3 h), while alterations to the used complex concentration were made. Quantification of the flow cytometry results was done by using the median fluorescence intensity (MFI) of the perylene label of the modified polymer structure

(Figure 4.12). The polyplexes formed between siRNA and TDBC were internalized in a concentration-dependent manner.

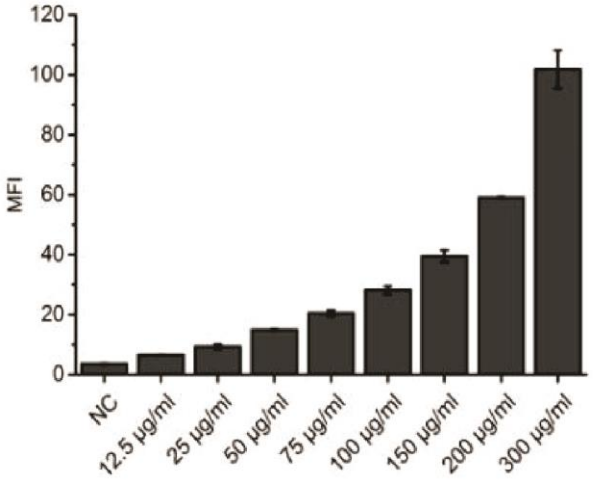

Figure 4.12. Flow cytometry quantified uptake *via* mean fluorescence intensity (MFI, n = 2) of polyplexes between siRNA and TDBC into $CD8^+$ T-cells in correlation to the used concentration

The excellent internalization was also confirmed via cLSM imaging (Figure 4.13). In addition, it was possible to clarify that TDBC entered the $CD8^+$ T cells and did not accumulate on the membrane.

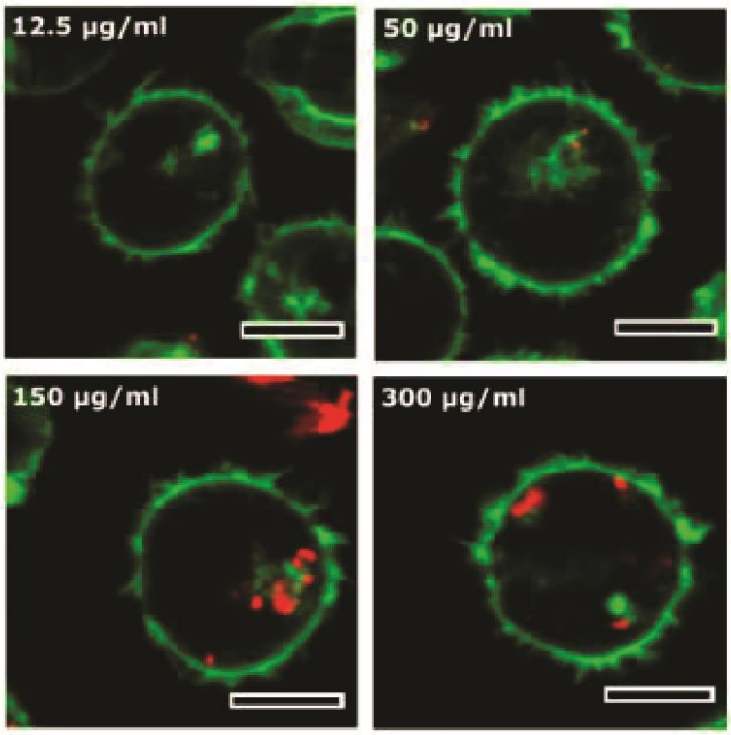

Figure 4.13. cLSM imaging of the concentration-dependent uptake of the polyplexes formed between TDBC and siRNA (pseudocolor: red) into $CD8^+$ T-cells. Co-staining with CellMask™ Green (pseudocolor: green). Scale bar equals 5 µm

The internalization of TDBC/siRNA complexes into CD8+ T-cells was followed by using labeled polymer molecules. However, this procedure allows the possibility of falsely positive results, since there is no clear distinction between free polymer and polyplexes. To avoid such an error, internalization studies *via* cLSM were performed, where both binding partners were fluorescently labeled (Figure 4.14). Co-localization inside the cells was confirmed (highlighted with **). At the given incubation conditions, where an excess of the polymer was used ($mass^{siRNA}/mass^{polymer}$ ratio of 1:100), uncomplexed TDBC expectedly entered the cells as well (highlighted with *).

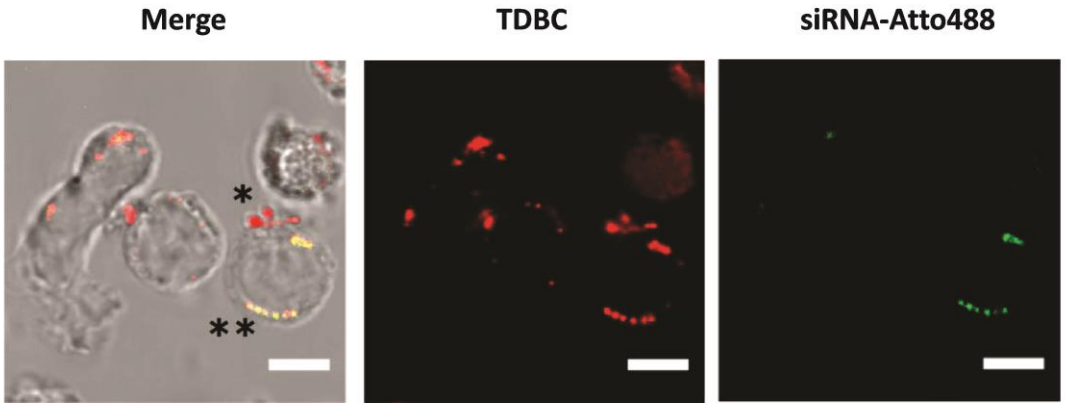

Figure 4.14. cLSM-analyzed uptake into CD8$^+$ T-cells of polyplexes consisting of perylen dye-labeled TDBC (pseudocolor: red) and ATTO488-labeled siRNA (pseudocolor: green) after 24 h of incubation; *uptake of free TDBC, **co-localization of fluorescently-labeled siRNA and TDBC. Scale bar equals 5 µm.

To determine whether the efficient internalization of TDBC is linked to the modification with TPP, its and its precursor polymers uptake into CD8$^+$ T cells was studied *via* flow cytometry (Figure 4.15) and *via* cLSM (Figure 4.16) in their uncomplexed form.

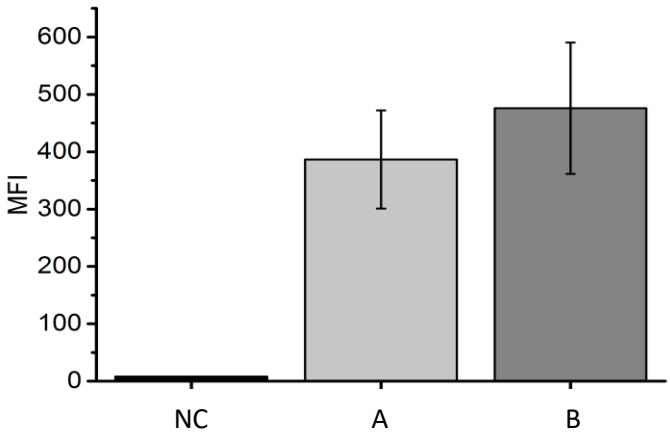

Figure 4.15. Flow cytometry quantified uptake of uncomplexed block copolymers after 3 h of incubation with CD8$^+$ T-cells. (NC) negative control, (A) Polymer 8 and (B) TDBC

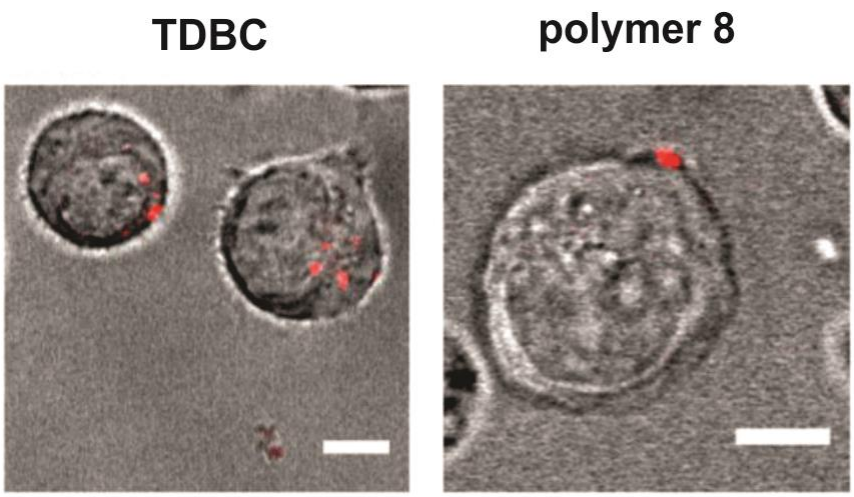

Figure 4.16. cLSM live cell imaging of the uptake into CD8$^+$ T-cells for the perylene labeled polymer 8 and TDBC (pseudocolor: red); Incubation for 3 h. Scale bar equals 5 µm.

TDBC was found not only in cell-organelles close to the nucleus, but also in the cytosol (Figure 4.16). Polymer **8**, on the other hand, accumulates at the cell membrane. This differentiation would not have been possible if only the quantification via flow cytometry was used (Figure 4.15), since this method does not distinguish between fluorescence signals coming from the outside or inside of a cell, thereby showing no significant difference in uptake between TDBC and polymer **8**. Here, cLSM provided us with proof that polymer **8** was able to enter CD8$^+$ T-cells only after being subjected to the modification strategy. These results confirm the hypothesis that TPP-moieties effectively improve the internalization into cells by diminishing the accumulation of cationic polymer molecules on the plasma membrane, which in turn reduces toxicity.

The addition of TPP-moieties has been shown in literature to introduce mitotropic properties.[27-29] To determine, whether the amount of these polymer-bound groups was sufficient to enable localization of the polyplexes to mitochondria, co-staining with MitoTracker® Green FM was performed (Figure 4.17). However, the utilized content (< 10%) appears to be too low for this task, since the free TDBC showed only marginal co-localization with the MitoTracker. To investigate at which TPP content the mitotropic properties will take effects, statistical HPMA-*s*-APMA copolymers with different mol% of APMA (10, 20, 40, 60, and 75) were synthesized and subjected to this chapter's modification strategy. However, the results of the co-localization experiments with MitoTracker® Green FM have not yet been received. Hence, it is not possible to make a

meaningful statement regarding the TPP content, which is required to stimulate the accumulation of a modified polymer in mitochondria or on mitochondrial membranes.

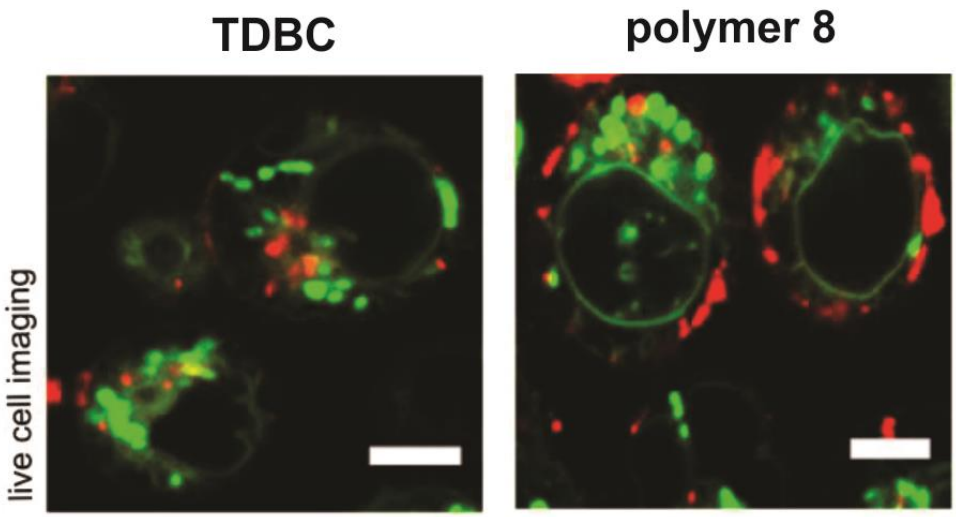

Figure 4.17. cLSM live cell imaging of the uptake into $CD8^+$ T-cells for the perylene labeled polymer 8 and TDBC (pseudocolor: red); Incubation for 30 min and co-staining of the cells with MitoTracker® Green FM (pseudocolor: green). Scale bar equals 5 µm.

The excellent internalization of TDBC-based complexes into $CD8^+$ T cells, which was observed by both cLSM as well as flow cytometry, might be affected by anionic proteins in the serum. Cationic polyplexes have been shown to for large aggregates with anionic proteins, if the positive ζ-potential high enough.[30] Similar behavior is to be expected for the cationic diblock copolymer structure TDBC, since TDBC-based polyplexes readily moved towards the cathode during the EMSA experiments, thereby confirming a positive net charge. To estimate the impact of protein-polyplex interactions on the internalization rate into $CD8^+$ T-cells, the uptake was not only correlated to the protein content in the medium (2, 10, and 100% of fetal bovine serum (FBS)), but also to the incubation time (30 min, 1 h, 3 h, 6 h, 18 h, and 24 h). Internalization was quantified via flow cytometry using the fluorescent label of TDBC for detection (Figure 4.18).

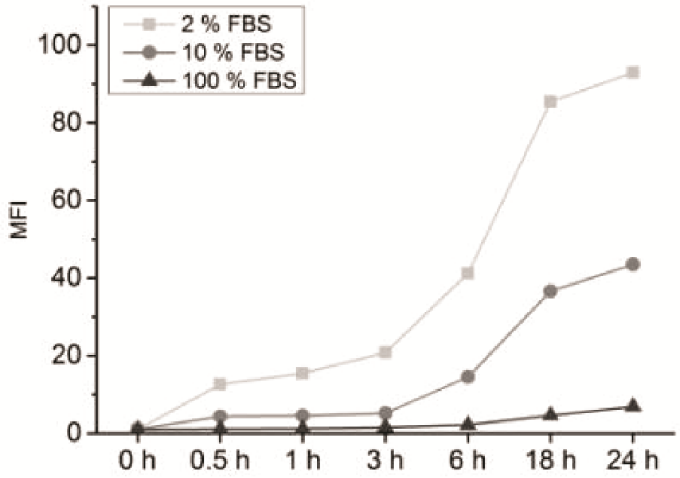

Figure 4.18. Flow cytometry quantified internalization (MFI, n = 2) of polyplexes between siRNA and fluorescently labeled TDBC into $CD8^+$ T-cells in correlation to the incubation time and FBS-content of the medium.

TDBC entered $CD8^+$ T-cells after incubation times of only 30 min. However, 6-18 hours were required to reach its full potential. The internalization of TDBC at 2% FBS is roughly two times higher in comparison to 10% FBS containing medium and comparing 10% with 100% FBS content the uptake is increased by a factor of five after 6 hours of incubation. Thus it was possible to confirm a strong dependency of the uptake of TDBC-based polyplexes on the protein content of the medium.

In order to study whether TDBCs ability to transport siRNA across plasma membranes to other cell lines as well, fluorescence-based confocal laser scanning microscopy was employed to study the uptake into HEK293 cells. Here, similar to the procedure described in Chapter 3, the uptake of the complexes was monitored by taking a layer image every 10 min. The duration was set to 15 hours in case of the polyplexes (Figure 4.20) and the internalization of free TDBC was followed for 1 hour (Figure 4.19).

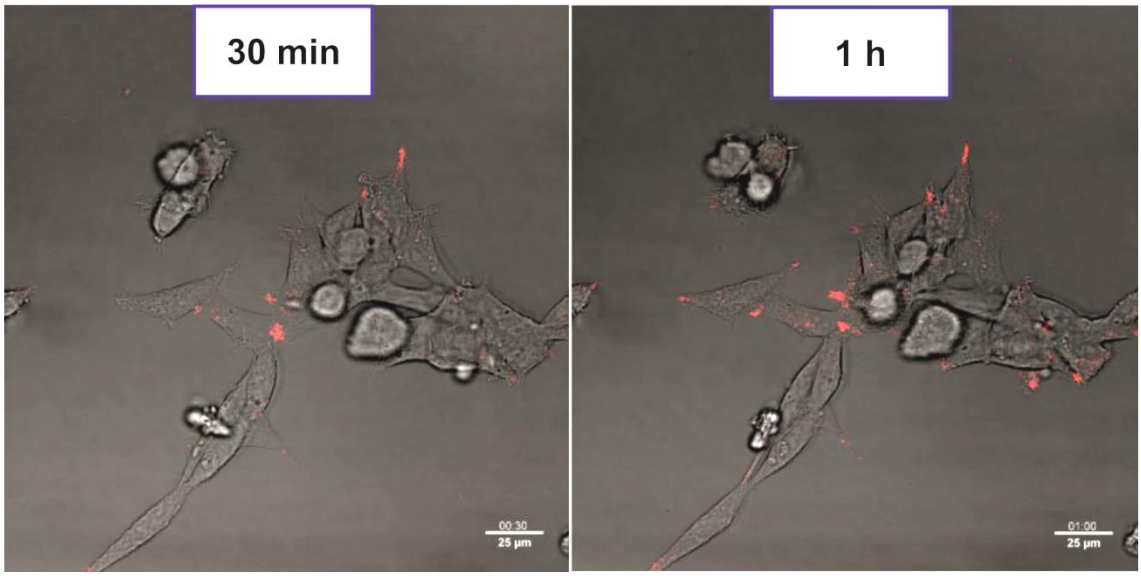

Figure 4.19. Confocal laser scanning fluorescence microscopy (layer) images (SP5, Leica) of living HEK293 cells, which were incubated with perylene-labeled TDBC. Layer images were taken while keeping the imaging conditions constant. The scale bar represents 25 µm.

As depicted in Figure 4.19, the TPP-modified block copolymer once again demonstrated excellent internalization into cells in its uncomplexed form. After an incubation time of 30 minutes large quantities were detected inside the cells. The fact that the cells have only few red spots is misleading because this type of experiments, where internalization is continuously observed, washing of the cells prior to taking the pictures is not possible. Hence, it was necessary to down-regulate the gain. In truth, confocal microscopy confirmed the polymer in the cytosol after only 10 minutes of incubation. The ability to bypass the plasma membrane so quickly indicates that TDBC does rely on endosomal uptake alone. Direct plasma membrane translocation, which is usually associated with much smaller molecules, is a possibility. The hydrophobic nature of the perylene label excludes the possibility of falsely positive results due to free dye molecules. These would have precipitated and would not be visible in the layer images.

The internalization study over time for the TDBC/siRNA polyplexes (Figure 4.20) confirmed that complexes between siRNA and the TPP-modified polymer are taken up exceptionally fast. In these experiments siRNA was chosen to carry the fluorescent label, in order to minimize falsely positive results due to the excess of polymer molecules during polyplex formation. After only 30 min noteworthy amounts of the complexes can be found inside the cells, which exceeds the uptake results of polymer **8**-based polyplexes

(section 3.4.2) by far. Here, it was even possible to reduce the gain to a point where no background fluorescence can be observed. The cytosol was an exception, since it had roughly the same fluorescence as the cell medium containing the polyplexes solution. The presence of the polyplexes in the cytosol indicates that the knock-down experiments should be fruitful, unless the release of the cargo is hampered. An intriguing observation was also that the extensions of the cells were heavily stained. Such extensions of cells are stabilized by microtubule, which are used for intracellular transport of vesicles or organelles. In consequence, it can be assumed that the uptake of these polyplexes is not solely reliant on direct transduction, but also endocytosis. These results confirmed, that TDBC can be utilized to deliver siRNA not only inside suspension cells (CD8+ T cells), but also into adherent cell lines (HEK293). In addition, since no morphological changes of the cells were observed during cLSM, the lack of toxicity of TDBC (at the given concentration) towards HEK293 cells could be confirmed.

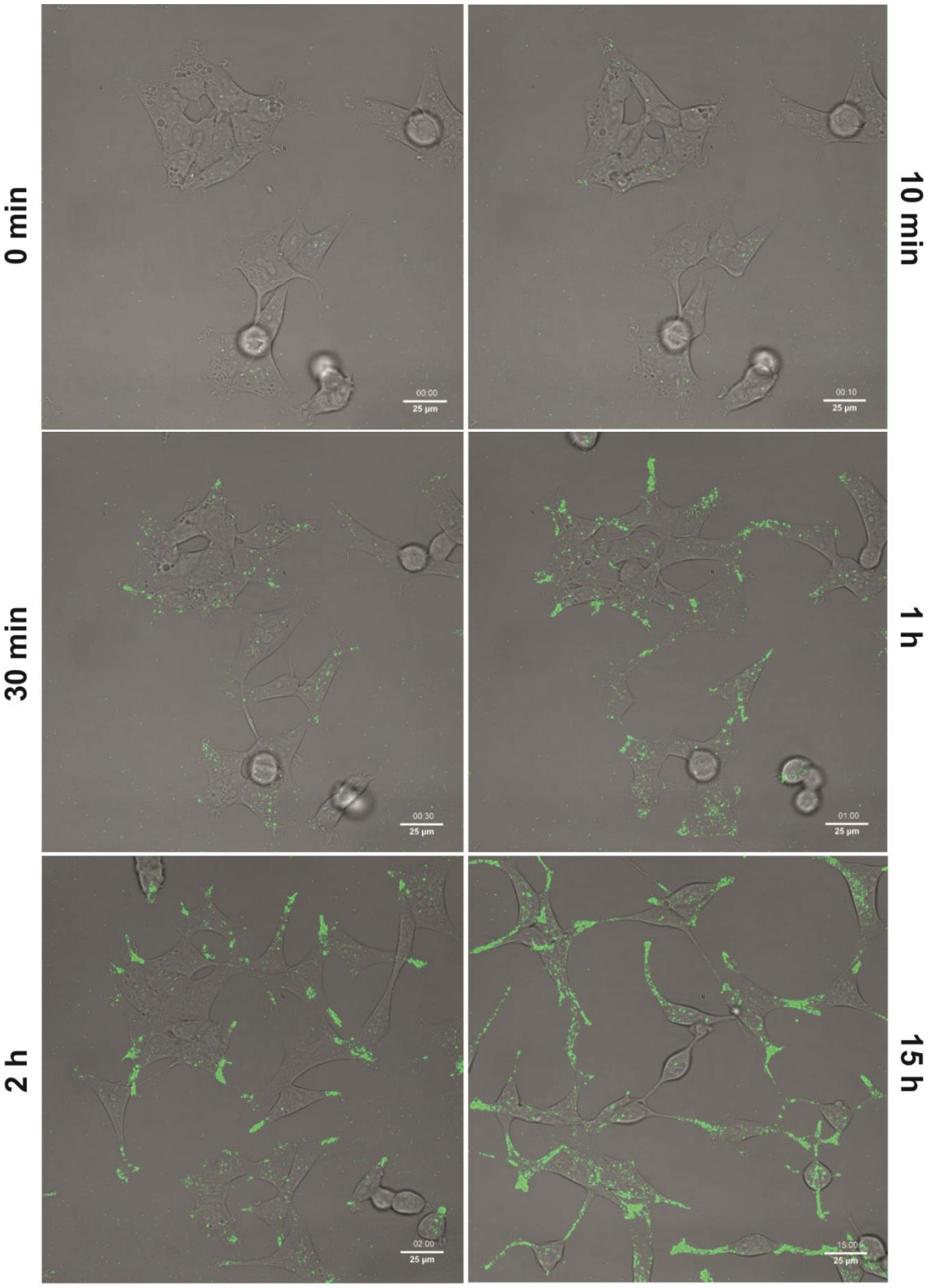

Figure 4.20. Confocal laser scanning fluorescence microscopy images (SP5, Leica) of living HEK293 cells, which were incubated with complexes between ATTO488-labelled siRNA and TDBC. Layer images were taken every 10 minutes for the duration of 15 hours, while keeping the imaging conditions constant. The scale bar represents 25 µm.

In order to confirm that the uptake of TDBC-based polyplexes also relies on endocytosis, co-staining with antibodies against the early endosome protein Rab5 has been performed for $CD8^+$ T cells and evaluated *via* cLSM (Figure 4.21).

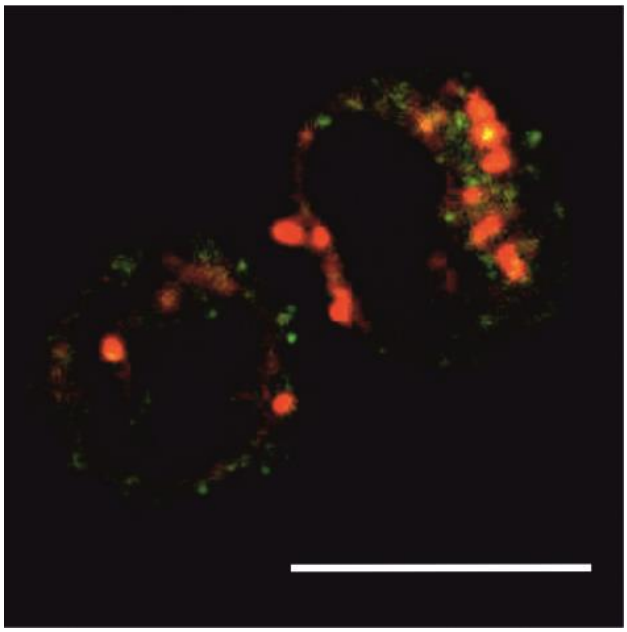

Figure 4.21. cLSM live cell imaging of the uptake into $CD8^+$ T-cells for polyplexes based on the perylene labeled TDBC (pseudocolor: red); Incubation for 3 h and co-staining of the cells with antibodies against the early endosome protein Rab5 (pseudocolor: green). Scale bar equals 10 µm.

Partial co-localization with the early endosome specific Rab5 antibodies has been observed, while a large amount of the polyplexes was detected in different cell compartments. In addition, in spite of the short incubation time, elevated concentrations of the complexes were observed in the cytosol. Hence, both direct transcytosis and endocytosis appear to be viable internalization pathways for TDBC-based polyplexes. In order to fully confirm this hypothesis, however, an in-depth uptake study is required, where internalization pathways are made exclusive alternatingly.

4.5 Knock-down

In order to investigate the knock-down efficacy of TDBC, a series of knock down experiments was performed in cooperation with Dr. Marleen Willig (group of Prof. Dr. Katharina Landfester and Prof. Dr. Mailänder, Max Planck Institute for Polymer Research). Here, $CD8^+$ T cells were initially stimulated with 4-beta-phorbol-12-myristate 13-acetate (PMA) to induce the production of protein tumor necrosis factor alpha (TNF-α). These cells were then treated with polymer **8**- or TDBC-based polyplexes containing siRNA against TNF-α for 24 hours. Here, concentrations of 100 nM were employed in respect to the loaded siRNA and the concentration of TNF-α was measured to quantify the knock-down efficacy (Figure 4.22). Untransfected cells (Figure 4.22, A) were used as a reference, where PMA-stimulated $CD8^+$ T cells provided the highest possible value of the TNF-α concentration and unstimulated cells gave the cells' intrinsic baseline.

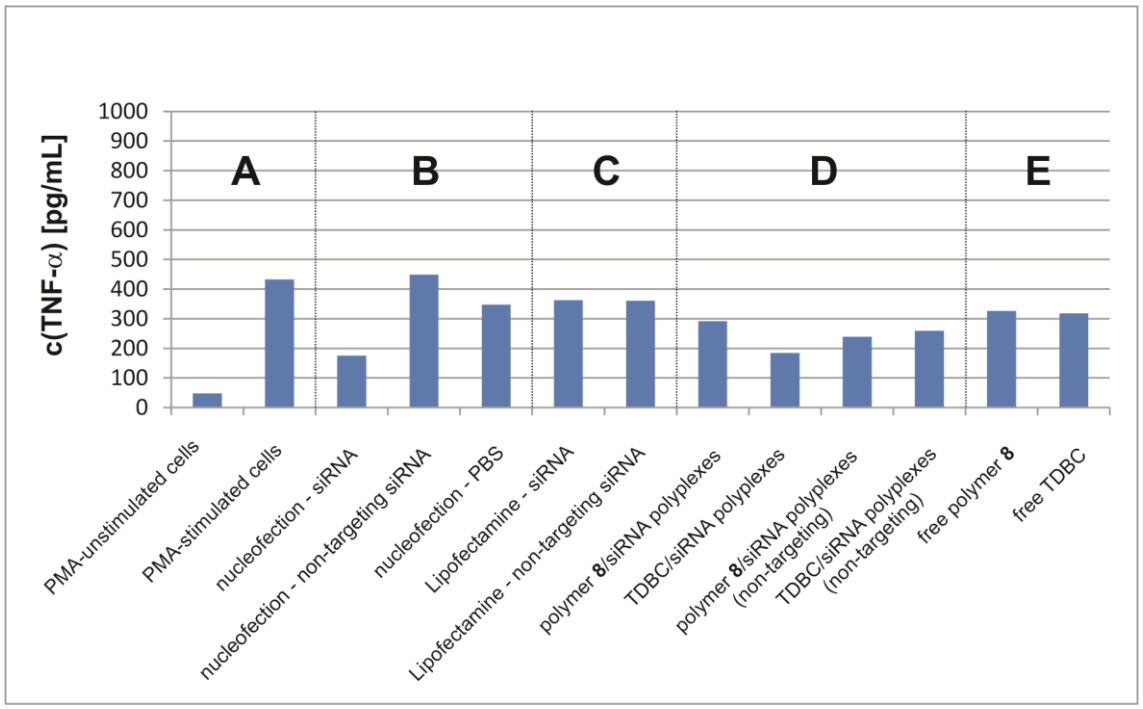

Figure 4.22. The knock-down efficacy due to the detected concentration of TNF-α after 24 hours of incubation. In all transfection experiments siRNA was employed in final concentrations of 100 nM. (A) untransfected cells, which provide reference values for maximal or minimal concentration of TNF-α, (B) transfection *via* nucleofection, (C) transfection by using Lipofectamine, (D) polymer 8 as well as TDBC-related knock-down results, (E) effects of the uncomplexed polymer molecules

Nucleofection (Figure 4.22, B), which does not rely on a delivery agent to transport siRNA into cells, since it is an electroporation-based transfection method (section 1.1), demonstrated that the used siRNA was functional (on-target siRNA induced knock-down; non-targeting siRNA did not facilitate knock-down). The sensitivity of these cells to external stimulants is indicated by the c(TNF-α) value obtained for nucleofection with PBS. Near identical results were recorded for uncomplexed TDBC and polymer **8** (Figure 4.22, E). Irrespective of the used siRNA, Lipofectamine was not able to induce knock-down as well (Figure 4.22, C). TDBC-based complexes on the other hand lead to reduced c(TNF-α) concentrations. Using the PMA-stimulated cells of Figure 4.22 A as a reference, a knock-down of 55% was achieved. Factoring in the polymers intrinsic anabolism-arresting properties, a knock-down of 24% (polyplexes with non-targeting siRNA as a reference, Figure 4.22, D) to 49% (free polymer as a reference, Figure 4.22,) was induced. In case of polymer **8**, which was shown to be unable to transport siRNA across the plasma membrane of $CD8^+$ T cells, expectedly no knock-down was observed. Although it induced 20% knock-down, if compared to the untransfected PMA-stimulated cells, only miniscule differences of the measured concentration of TNF-α to the values obtained for free polymer and polyplexes with non-targeting siRNA were observed. These results suggest that the modification strategy not only improve the internalization into cells, but also positively affect knock-down. Especially intriguing is TDBCs ability to induce knock-down in $CD8^+$ T cells, since no other polymeric siRNA delivery agent could achieve similar results. These results must be taken with a grain of salt, however, because they could not be replicated due to irregular behavior of the cells during nucleofection as well as problems with the used siRNA, which Dr. Willig could not resolve. Nevertheless, this knock-down study is a useful reference point. In order to affirm the knock-down properties of TDBC a knock-down study was performed by me, using siRNA against the Kif2a protein in murine IMCD3 cells (Figure 4.23). Prof. Dr. Wolfrum (nstitute of Molecular Physiology, Johannes Gutenberg-University of Mainz) kindly provided me with access to his facilities. Here, identical conditions were used as those described in section 3.4.3, thereby ensuring comparability of the results between polymer **8** and TDBC. Figure 4.23 A provides an example for a western blot. Multiple western blots were used as the basis to calculate the mean knock-down efficacies of polymer **8** and TDBC, which are shown in Figure 4.23 B. Here, a value of 100% equals a complete abolition of the intracellular synthesis of the Kif2a protein in IMCD3 cells.

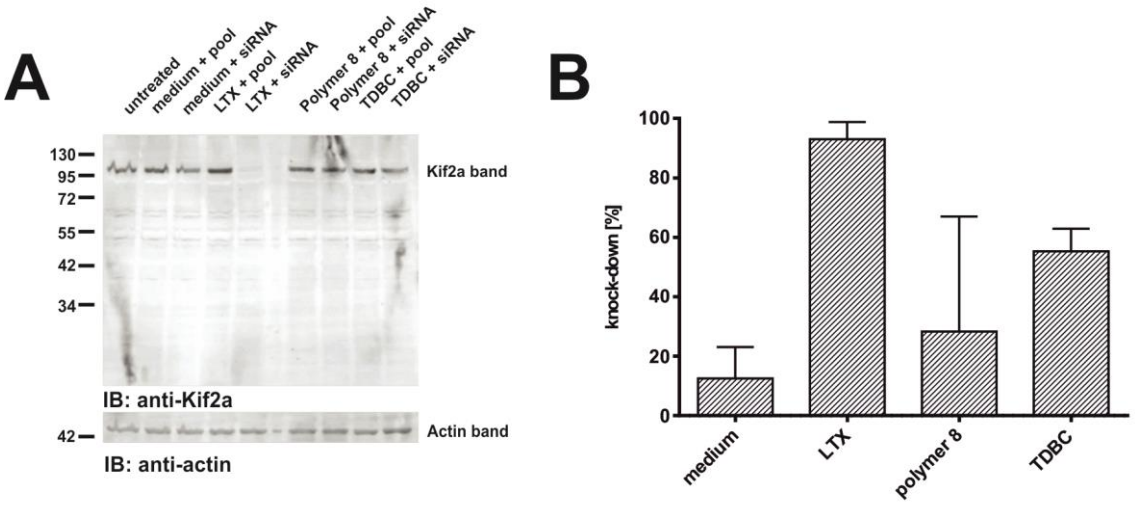

Figure 4.23. (A) Western blot analysis of the Kif2a knock-down with actin as the loading control; (B) The evaluated knock-down efficacy of the western blot-investigated samples and controls (mean with SD) in [%]: (medium) free siRNA molecules, (LTX) LTX RNAiMAX, (polymer 8) polymer 8-based polyplexes, (TDBC) TDBC-based polyplexes. Here, a value of 100% represents a complete abolition of the intracellular synthesis of the Kif2a protein in IMCD3 cells after 72 h of incubation. In all transfection experiments siRNA was employed in final concentrations of 50 nM.

The commercially available transfection reagent LTX RNAiMAX (LTX) once again achieved high levels of knock-down reliably (93%). The results of polymer **8** were discussed in section 3.4.3. It was able to reduce the production of the Kif2a protein by up to 73% in individual cases, however, due to poor release of siRNA, an average knock-down efficacy of only 28% was achieved. TDBC, on the other hand, achieved high knock-down of Kif2a reliably (55%). Its excellent results were partially expected due TDBCs ability to transport siRNA into the cytosol of cells, which is much more pronounced than that of polymer **8**. In addition, near identical down-regulation of TNF-α was achieved in the knock-down study with $CD8^+$ T cells as the organism of interest. The modification strategy of functionalizing a cationic block copolymer with triphenylphosphonium groups was thereby also shown to positively affect knock-down.

Summarizing, it was demonstrated that triphenylphosphonium-modified diblock copolymers are able to deliver siRNA into $CD8^+$ T-cells which in turn successfully induced knock-down. Hence, in particular when comparing these results to those of the precursor polymer, it was proven that the chosen approach for carrier system-modification is

indeed a viable strategy for improving siRNA delivery agents. Said improvement was observed on several levels:

(1) The functionalization of cationic diblock copolymers with the uptake-promoting triphenylphosphonium groups resulted in the formation of exceptionally small polyplexes.

(2) Due to the small size of the polyplexes the plasma membrane of $CD8^+$ T-cells was bypassed, thereby allowing quick delivery of the cargo into the cytosol (only 10 to 30 minutes) even at low concentrations.

(3) As a result efficient and reliable knock-down was induced.

(4) All of the above-described effects were achieved without increasing cytotoxicity. Neither the uncomplexed modified carrier, nor the formed polyplexes were shown to be more toxic than the precursor polymer **8**.

TDBC is currently the only polymeric carrier system which is able to deliver siRNA into $CD8^+$ T-cells. These cells, which have become a treatment tool for currently fatal diseases, were inaccessible for gene silencing by polymeric siRNA carrier systems. Nevertheless, the results of this study remove these limitations and pave the way for bioengineering *via* gene therapy. Hence, it is vital to investigate the *in vivo* applicability this carrier system.

Chapters 3 was dedicated to study the structural influence of guanidinium group-bearing polymers on their ability to complex siRNA, transfect cells and induce knock-down of functional proteins in non-immortalized cell cultures. It was then found that diblock copolymers with a sufficiently long cationic block ($length^{binding\ block}/length^{non\text{-}biding\ block}$ ratio of 1:8.7 (experimental) or 1:7.5 (simulated)) displayed many of the above mentioned advantages such as low cytotoxicity, efficient complexation as well as condensation of nucleotides in nano-sized polyplexes (R_h(complex) = 25 - 134 nm), and quick internalization into cells. By utilizing the modification strategy described in the present chapter it was possible to improve all of them. However, herein the issue of siRNA release was overcome by drastically improving the internalization rate, thereby facilitating high concentrations of the polyplexes in the cytosol and reliable knock-down. To address the poor release and realize efficient transfection, another strategy than the post-polymerization functionalization was envisioned. Said strategy is described in the following chapter.

4.6 References

[1] R. A. Koup, D. D. Ho, *Nature* **1994**, *370*, 416.

[2] J. D. Lifson, J. L. Rossio, M. Piatak, Jr., T. Parks, L. Li, R. Kiser, V. Coalter, B. Fisher, B. M. Flynn, S. Czajak, V. M. Hirsch, K. A. Reimann, J. E. Schmitz, J. Ghrayeb, N. Bischofberger, M. A. Nowak, R. C. Desrosiers, D. Wodarz, *J. Virol.* **2001**, *75*, 10187.

[3] C. M. Walker, A. L. Erickson, F. C. Hsueh, J. A. Levy, *J. Virol.* **1991**, *65*, 5921.

[4] M. J. Brunda, L. Luistro, R. R. Warrier, R. B. Wright, B. R. Hubbard, M. Murphy, S. F. Wolf, M. K. Gately, *J. Exp. Med.* **1993**, *178*, 1223.

[5] R. A. Morgan, M. E. Dudley, J. R. Wunderlich, M. S. Hughes, J. C. Yang, R. M. Sherry, R. E. Royal, S. L. Topalian, U. S. Kammula, N. P. Restifo, Z. Zheng, A. Nahvi, C. R. de Vries, L. J. Rogers-Freezer, S. A. Mavroukakis, S. A. Rosenberg, *Science (Washington, DC, U. S.)* **2006**, *314*, 126.

[6] L. Liu, C. Johnson, S. Fujimura, F. Teque, J. A. Levy, *Journal of Immunological Methods* **2011**, *372*, 22.

[7] M. S. Al-Dosari, X. Gao, *The AAPS Journal* **2009**, *11*, 671.

[8] I. Tabujew, C. Freidel, B. Krieg, M. Helm, K. Koynov, K. Muellen, K. Peneva, *Macromol. Rapid Commun.* **2014**, *35*, 1191.

[9] D. Y. Cho, H. Cho, K. Kwon, M. Yu, E. Lee, K. M. Huh, D. H. Lee, H. C. Kang, *Adv. Funct. Mater.* **2015**, *25*, 5479.

[10] E. Mendez, R. Manian, J.-h. Moon, "Cellular toxicity and uptake behavior of triphenyl phosphonium-containing conjugated polymer nanoparticles", American Chemical Society, 2015PMSE.

[11] R. A. J. Smith, R. C. Hartley, M. P. Murphy, *Antioxid. Redox Signaling* **2011**, *15*, 3021.

[12] J. S. Modica-Napolitano, M. Kulawiec, K. K. Singh, *Curr. Mol. Med.* **2007**, *7*, 121.

[13] C. Frezza, E. Gottlieb, *Semin. Cancer Biol.* **2009**, *19*, 4.

[14] S. Kaloyanova, Y. Zagranyarski, S. Ritz, M. Hanulova, K. Koynov, A. Vonderheit, K. Muellen, K. Peneva, *J. Am. Chem. Soc.* **2016**, *138*, 2881.

[15] S. S. Malhi, A. Budhiraja, S. Arora, K. R. Chaudhari, K. Nepali, R. Kumar, H. Sohi, R. S. R. Murthy, *Int. J. Pharm. (Amsterdam, Neth.)* **2012**, *432*, 63.

[16] V. J. Adlam, J. C. Harrison, C. M. Porteous, A. M. James, R. A. J. Smith, M. P. Murphy, I. A. Sammut, *FASEB J.* **2005**, *19*, 1088.

[17] C. Ornelas-Megiatto, P. R. Wich, J. M. J. Frechet, *J. Am. Chem. Soc.* **2012**, *134*, 1902.

[18] K. Peneva, G. Mihov, F. Nolde, S. Rocha, J.-i. Hotta, K. Braeckmans, J. Hofkens, H. Uji-i, A. Herrmann, K. Muellen, *Angew. Chem., Int. Ed.* **2008**, *47*, 3372.

[19] N. J. Treat, D. Smith, C. Teng, J. D. Flores, B. A. Abel, A. W. York, F. Huang, C. L. McCormick, *ACS Macro Lett.* **2012**, *1*, 100.

[20] A. W. York, F. Huang, C. L. McCormick, *Biomacromolecules* **2010**, *11*, 505.

[21] M. Jerabek-Willemsen, C. J. Wienken, D. Braun, P. Baaske, S. Duhr, *Assay Drug Dev. Technol.* **2011**, *9*, 342.

[22] M. Spelios, M. Kearns, M. Savva, *Biochemistry* **2010**, *49*, 5753.

[23] S. Menuel, S. Fontanay, I. Clarot, R. E. Duval, L. Diez, A. Marsura, *Bioconjugate Chem.* **2008**, *19*, 2357.

[24] M. Spelios, M. Kearns, M. Savva, *Biochemistry* **2010**, *49*, 5753.

[25] D. J. Gary, N. Puri, Y.-Y. Won, *J. Controlled Release* **2007**, *121*, 64.

[26] S. Zhang, B. Zhao, H. Jiang, B. Wang, B. Ma, *J. Controlled Release* **2007**, *123*, 1.

[27] R. A. J. Smith, C. M. Porteous, C. V. Coulter, M. P. Murphy, *Eur. J. Biochem.* **1999**, *263*, 709.

[28] B. Zhang, H. Jiang, *Zhongguo Yaoke Daxue Xuebao* **2015**, *46*, 659.

[29] CN105833289A (2016), Shanghai Jiao Tong University, Peop. Rep. China . invs.: D. Cui, C. Yue, Y. Yang;

[30] L. Nuhn, S. Gietzen, K. Mohr, K. Fischer, K. Toh, K. Miyata, Y. Matsumoto, K. Kataoka, M. Schmidt, R. Zentel, *Biomacromolecules* **2014**, *15*, 1526.

5 Potential of cationic gradient and statistical copolymers for gene delivery

Cationic gradient copolymers, whose monomer composition and thereby the cationic charge density changes continuously along the chain, possess distinctly different properties in comparison to block- or statistical copolymers with analogous monomer compositions. The gradual increase of cationic charge densities along the linear polymer chain leads to a segments with predominantly statistical character and also block-like segments at the termini. Other regions, that can neither be described as statistical or block-like in-between the other section types, are expected to be present also. Gradient copolymers thereby allow the formation of a not yet seen cationic charge density, which might constitute a viable alternative in polymer-based carrier design.

The potential of gradient copolymers for gene delivery or -silencing has not yet been fathomed and there are no literature documented studies on cationic gradient copolymers. Up until now, the research of gradient copolymers was heavily focused on material science-oriented applications. They were utilized, for example, as pressure sensitive adhesives[1], blend compatibilizers[2], amphiphiles[3], as the backbone of hydrophobic polymer brushes[4, 5] and as a corona for aluminium oxide particles to improve compatibility with organic solvents[6]. These studies capitalized on the thermal and mechanical properties of gradient copolymers including glass transition temperature[7], morphology[8, 9], surface activity[10] as well as their behavior in solution[11] or micellization[12].[13] Medical applications require not only functionally efficient, but also water-soluble and well defined polymers, which can only be achieved *via* controlled polymerization techniques. Hence, it was decided to utilize the already established aRAFT polymerization. RAFT initiation kinetics exceed the propagation speed and the reactive chain ends remain active for the duration of the polymerization. Since all chains propagate concertedly, the resulting polymers are near uniform and variations in monomer concentration, which are caused by the respective monomer reactivity, are directly linked to the composition of the copolymers.[14] The statistical (batch) copolymerization of multiple monomers has been extensively researched in literature to predict polymer composition and characteristics.[15] For example, choosing monomers, such as styrene and n-butyl acrylate or poly(ethylene glycol) methylether methacrylate and (2,2-dimethyl-1,3-dioxolane)methyl acrylamide, with significantly different reactivity ratios, it is possible to promote the spontaneous formation of a gradient of the monomer-

composition along the chain.[16-18] However, the forced gradient (semi-batch) copolymerization (Figure 5.1), where the second monomer is continuously added to the reaction mixture containing the first monomer, is more advantageous for the preparation of gradient copolymers, since this approach is less reliant on the reactivity of the chosen monomers.[19] This strategy broadens the range of possible monomers, since it facilitated the synthesis of gradient copolymers from even styrene and acrylonitrile, which usually copolymerize in an alternating fashion.[20]

In order to study the capabilities of gradient copolymers in gene delivery a library of 14 gradient copolymers was synthesized *via* the semi-batch RAFT polymerization. In order to carry out a comprehensive study 14 statistical copolymers with an identical monomer composition were prepared by using the batch copolymerization. In both cases, the content of the cationic monomer was varied with values ranging from 5 to 90%, while the molar mass of the copolymers is kept at 12 kDa to ensure comparability. This study also includes the comparison of the two sources of cationic charges, which were addressed in the discussion of the block copolymers (Chapter 3), namely: N-(3-aminopropyl)methacrylamide hydrochloride (APMA), which relies on its primary amino group to bind pDNA, and N-(3-guanidinopropyl)methacrylamide (GPMA), which uses a guanidinium group for the same purpose. N-(2-hydroxypropyl)methacrylamide (HPMA), which is one of the most extensively studied monomers in gene and drug delivery[21], was chosen as the inert "spacer-monomer". In the previous studies, it did not contribute to the binding of polynucleotides, while supporting the polymers' solubility in aqueous media.[22] The batch copolymerization of APMA, GPMA and HPMA provides predominantly statistical copolymers.[23-27]

Following the physico-chemical characterization by means of size-exclusion chromatography, NMR spectroscopy and analytical ultracentrifugation, which was used in combination with viscosity- and density measurements to determine the molar masses of the polymer samples, the suitability of these copolymers for gene delivery was evaluated. Here, electrophoretic mobility shift assays and fluorophore exclusion assays were used to investigate the binding affinity and the polymers' DNA condensation properties respectively, which are the principal requirements for a DNA carrier system. Luciferase expression in CHO-K1 cells was used as a marker to quantify transfection efficacy of the formed polymer/pDNA polyplexes at different N/P ratios and the in vitro toxicity was studied as well.

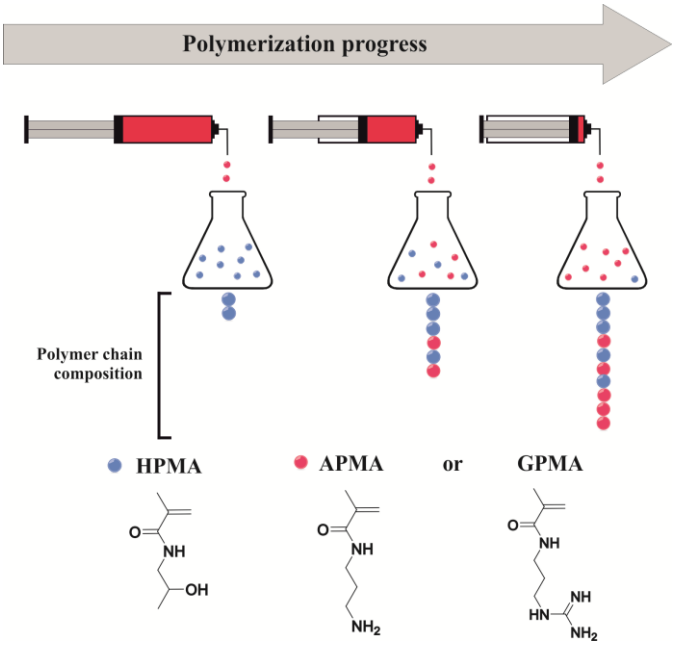

Figure 5.1. Schematic illustration of synthetic approach for gradient copolymers via semi-batch copolymerization

5.1 Preparation of the copolymers

The library of copolymers was synthesized via aqueous RAFT polymerization (aRAFT) in a one-step approach, where the required monomer and CTA concentrations were calculated by using the guidelines described in section 1.4.

Initially, conditions analogous to those used in section 3.1 were tested. However, at higher content of the aminolytically active monomers (> 10 mol%) only poor control over the polymerization was observed, where the dispersity was higher than 1.3 and the theoretical molar mass was exceeded by a factor of 2. The cause for this observation was rapid aminolysis of the thiocarbonyl thio functional group of the chain transfer agent, which is essential for continuation of the RAFT polymerization. The effects of using monomers with nucleophilic groups on the molar mass were discussed in section 1.4. This estimation was further underlined by the fact that the solution and the polymers lost their colour, which is attributed to the terminal dithioester group of the MacroCTAs. To solve this issue different reaction conditions were tested, which included lowering the monomer concentration to 0.5 M (from 1M), increasing the buffering strength of the acetate buffer to 1M (from 100 mM), used different solvents as polymerization media, and combinations thereof. However, the only strategy, which effectively

alleviated the problems in polymerization control, was the utilization of the hydrolytically stable 4-((((2-carboxyethyl)thio)carbonothioyl)thio)-4-cyanopentanoic acid as the chain transfer agent (Figure 5.2). This RAFT agent required longer reaction times of 5 hours (from 3.5 h) at slightly increased temperature (80 instead of 75 °C) to achieve the theoretical molar masses experimentally.

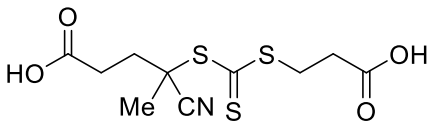

Figure 5.2. 4-((((2-carboxyethyl)thio)carbonothioyl)thio)-4-cyanopentanoic acid

The desired statistic and gradient copolymers consisting of either HPMA and APMA or HPMA and GPMA were then successfully synthesized via aRAFT (Figure 5.3 and 5.4).

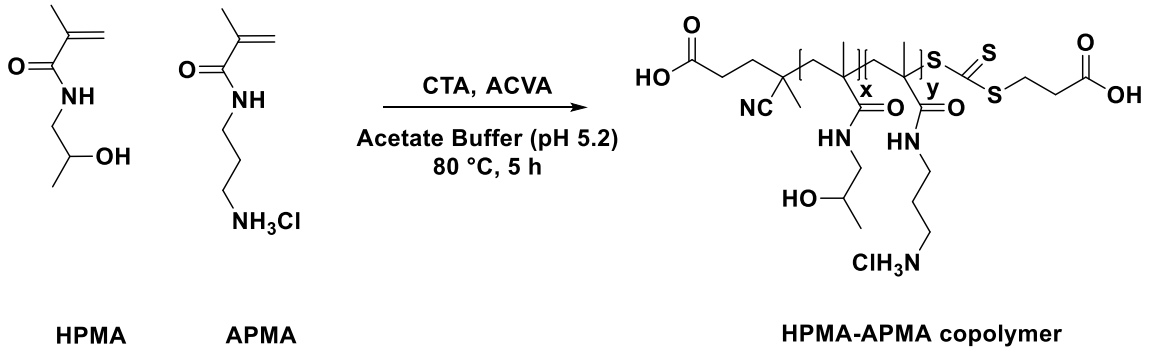

Figure 5.3. Synthesis of HPMA-APMA copolymers

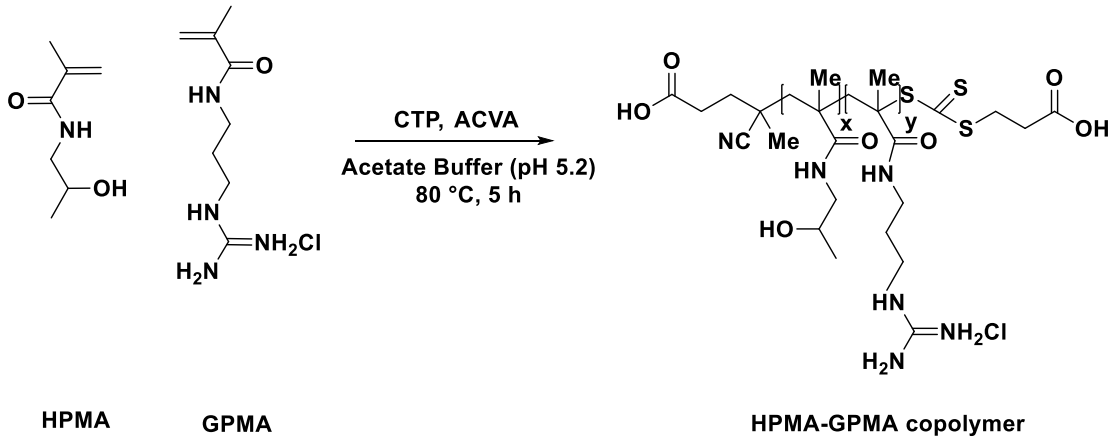

Figure 5.4. Synthesis of HPMA-GPMA copolymers

While 4-((((2-carboxyethyl)thio)carbonothioyl)thio)-4-cyanopentanoic acid was employed as the CTA instead of 4-cyanopentanoic acid dithiobenzoate, 4,4'-azobis(4-cyanopentanoic acid) was retained as the radical initiator. The theoretical molar mass ($M_{n,\ theo}$) was kept constant at 12 kDa for all polymer samples. The monomer composition, on the other hand, was changed by influencing monomer stoichiometry during the polymerization step. Thereby, for each source of cationic charges, be it primary amines (APMA) or guanidinium groups (GPMA), a polymer spectrum of increasing charge densities was prepared.

In contrast to statistical copolymers, which were prepared in a batch copolymerization, gradient copolymers made the use of a forced gradient copolymerization method, the semi-batch copolymerization, necessary. Here, buffered solutions of the cationic monomers (1 M) were continuously added into the polymerization mixture via a syringe pump at varying monomer addition rates (Table 5.1). This approach, in combination with using a living polymerization technique, allows precise synthesis of gradient polymers with less dependence on the reactivity ratios of the used monomers.[28] The semi-batch copolymerization method enables even the preparation of gradient copolymers with varying sequence distributions.[19] This level of precision is necessary for the intended use of these polymers as a component in drug formulations.

Table 5.1. Monomer addition rates in [mmol/h] of APMA and GPMA throughout the semi-batch copolymerization

Gradient copolymer with x mol% APMA/GPMA	monomer addition rate [mmol/h]
5%	0.097
10%	0.150
20%	0.276
40%	0.653
50%	0.954
60%	1.407
75%	2.764
90%	8.193

It has been shown in literature that gradient copolymers are also formed spontaneously during batch copolymerization.[29] In these cases, the utilized monomers are consumed unequally due to a huge difference in reactivity. The different rates are based on steric

and electronic properties of the reactants. Hence, the copolymer composition will drift with conversion. In a living polymerization, such as RAFT, where all chains grow concertedly, the composition drift will be captured within the chain structure, since reactivity ratios are unaffected by the RAFT process. This spontaneous (batch) gradient copolymerization approach does not affect the statistical copolymerization of the chosen monomers, however, since the physico-chemical properties of the utilized monomers, especially the solubility in the polymerization medium, do not differ significantly. Similarly, this was the reason why the semi-batch copolymerization was required to prepare gradient copolymers.

The synthesized polymers were obtained in low dispersities ($Đ_{median}$ = 1.08), which were determined by size-exclusion chromatography with either water or dimethylacetamide (DMAc) as the eluent (Table 5.2, Đ). Determination of the molar mass, on the other hand, was challenging due to the cationic nature of the copolymers (Table 5.2, M_n). Statistical and gradient polymers with an APMA content exceeding 20 mol% were no longer soluble in DMAc and thereby not measureable. In case of the GPMA-containing copolymers, the solubility in DMAc was reduced at high GPMA-contents (≥ 20 mol%) as well, however, it was still possible to perform size-exclusion chromatography to obtain an estimation of molar mass against reference standards. The molar mass that was determined by means of SEC_{DMAc} not only exceeded the theoretical value by a factor of up to 2.4, but also showed an inversely proportional correlation to the co-monomer content, since it steadily decreased at increasing APMA/GPMA ratios. Using RAFT polymerization, which is usually efficient in molar mass control, it was not expected that the differences in elution time for the SEC were caused by decreased chain lengths of the polymers. To observe, whether other SEC systems are affected by the cationic nature of the copolymers as well, SEC_{water} was employed. Here, only atypical standards were available (PVP). Although it was not expected that the SEC_{water}-determined molar masses were accurate, in several cases the SEC_{water}-determined molar mass coincided with the theoretical value. Nevertheless, this characterization approach was not applied to reliably determine the molar mass of the polymers, but to observe, whether a correlation to the co-monomer content can be established for the DMAc-insoluble samples as well. SEC_{water} showed that the estimated molar mass of the polymers is influenced by the content of the cationic monomer. However, the observed trend was not in agreement with the results of SEC_{DMAc}. In case of increasing APMA-ratios, the SEC_{water}-estimated molar mass rose from 5.3 kDa (5 mol% of APMA) to 11 kDa (90 mol% of APMA). In

addition, the GPMA-containing copolymers did not exhibit the inverse proportionality between co-monomer content and calculated molar mass that they showed during analysis with SEC_{DMAc}. Instead, the SEC_{water}-determined molar mass increased with rising GPMA content. Nevertheless, GPMA-ratios exceeding 40 mol% once again caused an inverse effect and the detected molar mass became smaller. These observations for APMA- and GPMA-based copolymers were made for both, statistical and gradient, copolymers alike. Hence, the cationic charge density and the thereby affected hydrodynamic volume is expected to cause the deviations in the SEC-determined molar mass, not the distribution of the cationic charges along the linear polymer chain.

For an accurate and representative comparison of the synthesized polymers regarding their physicochemical properties and their ability to bind polynucleotides it is necessary to show, beyond any doubt, that all synthesized polymers are of the same molar mass and that the SEC-determined values of M_n are merely the results of the inherent positive charge density of the polymers. To achieve this goal, the hydrodynamic properties of the polymers were determined by employing viscometry, densitometry and sedimentation velocity experiments using an analytical ultracentrifuge. These measurements were performed in cooperation with Ceren Cokca (Institute of Organic Chemistry and Macromolecular Chemistry, Friedrich Schiller University Jena) and PD Dr. Ivo Nischang (Institute of Pharmacy, Friedrich Schiller University Jena). Analytical ultracentrifugation (AUC) can provide absolute values of the molar mass of the analyzed samples.[30] The equation, which is used to calculate the molar mass, can be derived as follows.

A dissolved particle with the mass *m*, which is subjected to centrifugation, is affected by three forces (Figure 5.5): the sedimenting (or gravitational) force F_s, the buoyant force F_b, and the frictional force F_f. F_f and F_b act in the opposite direction to sedimentation.

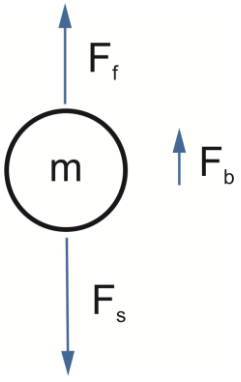

Figure 5.5. The forces acting on a solute particle in a gravitational field

The sedementing force is proportional to the mass of the particle and the applied acceleration, which, in a spinning rotor, equals the product of the radius of the orbit (*r*) and the angular velocity (ω) squared. It can be expressed as:

$$F_s = m\omega^2 r = \frac{M}{N}\omega^2 r \tag{5.1}$$

Here, *M* is the molar weight of the particle and *N* is the Avogadro constant. Since centrifugation does not take place in vacuum, but in a solvent with its own density ($\rho_{solvent}$), which is similarly affected by the centrifugal force, buoyancy and friction become an issue. If the density of the particle exceeds that of the solvent, the particle sediments at the velocity *u* while displacing solvent molecules. The increasing radial distance of the particle from the center of rotation in turn raises its velocity. Simultaneously, the particle's movement is further hampered, because it is moving through a viscous fluid and experiences a frictional drag due to the interaction with the solvent molecules, which is proportional to its velocity. The boyant force can be expressed as:

$$F_b = -m_0\omega^2 r \tag{5.2}$$

Here, m_0 is the mass of the fluid, which was displaced by the particle. It can be described by taking the density of the solvent as well as the volume that each gram of the particle occupies in solution (partial specific volume *v*) into consideration:

$$m_0 = mv\rho_{solvent} = \frac{M}{N}v\rho_{solvent} \tag{5.3}$$

The frictional force can be expressed as:

$$F_f = -fu \tag{5.5}$$

The frictional coefficient (*f*) understandably depends in the shape and size of the particle, since compact, smooth, and spherical particles incur less resistance, when they passing through the solution. It is proportional to the radius, r, of a spherical particle.

$$f = 6\pi\eta r \tag{5.6}$$

During centrifugation a very short time period occurs, where the three forces compensate each other and the particle does not move up or down:

$$F_s - F_b - F_f = \frac{M}{N}\omega^2 r(1 - v\rho_{solvent}) - fu = 0 \tag{5.7}$$

Rearranging the particle-related parameters on one side and those affected by the experimental conditions on the other, we obtain:

$$\frac{M(1-v\rho_{solvent})}{Nf} = \frac{u}{\omega^2 r} \equiv s \tag{5.8}$$

The sedimentation coefficient (s) is proportional to the buoyant effective molar weight of the particle and it is inversely proportional to the frictional coefficient. Hence, molecules with different shapes, sizes, or molecular weights will move at different velocities in a given centrifugal field. s is often given in Svedberg units (S, defined as 10^{-13} s). To calculate the molecular weight (equation in section 9.2.7) without having to consider possible particle-particle interactions during their movement, the limiting (ideal) sedimentation coefficient (s^0) must be utilized. It was obtained by measuring the sedimentation coefficient at different concentrations of each polymer and extrapolating the fited values to the zero concentration (Figure 5.7). This approach allows the calculation of the absolute molar mass and thereby solves the previously described problem of having SEC-incompatible samples.

The preparation of the copolymers for the hydrodynamic characterization required the utilization of PBS as the solvent, to compensate for charge effects imposed by the varying content of the basic monomers. The results of this study are presented in tables and, for better visualization of the trends, as graphs. Hence, the results of the viscosity and density measurements are shown in Table 5.3 and in Figure 5.6. The equation $\frac{\eta_r - 1}{c} = [\eta] + k_H[\eta]^2 c$ was used to determine the intrinsic viscosities, $[\boldsymbol{\eta}]$, and the Huggins constant, $\boldsymbol{k_H}$. It was observed for both monomer arrangement types (statistical and gradient) that with increasing content of either APMA or GPMA, an overall increase of the intrinsic viscosity ($[\eta]$) and a decrease of the apparent Huggins constant (k_H) occurred (Table 5.3). It can be therefore stated that the incorporation of positively charged monomers improved the polymers' solubility in the PBS buffer. In spite of the polymers better solubilization properties at high GPMA/APMA contents, their density, which is inversely proportional to their partial specific volume, increased. The higher density in turn lead to a shift of the sedimentation coefficient distributions of the respective polymer populations (Figure 5.8), however, the calculated molar masses, according to the equation $M_{s,f} = 9\pi\sqrt{2}N_a([s](f/f_{sph})_0)^{3/2}\sqrt{\bar{v}}$, remained invariant (Table 5.2). This shift was less pronounced for gradient copolymers with GPMA. This characterization approach showed the real molar masses of the polymer structures to be located in an area in between the values of the two SEC methods. The employed hydrodynamic methods also confirmed that the fluctuations of the SECs were likely based on the polymers' chemical composition and did not reflect the actual molar mass. Thereby, the successful syn-

thesis of the gradient as well as statistical copolymers at low dispersities and near uniform molar mass, which coincides with the theoretical value, was confirmed. Further, the monomer composition of gradient and statistical copolymers was investigated *via* ^{1}H-NMR. When establishing the polymerization conditions, it was observed that, in spite of high conversion, the experimentally determined amount of incorporated APMA or GPMA monomers was lower than the desired value. This setback was corrected by using higher amounts of the cationic monomers (Table 5.3, co-monomer content). The molar mass values determined *via* the analytical ultracentrifuge were then used to calculate the monomer composition of the respective polymer chains by taking the NMR-estimated monomer content into account. This approach reveals the maximum possible amount of positive charges and the number of electrophoretically inert HPMA monomers per polymer chain (Table 5.3, Monomers). Taking also our knowledge about the distribution of these cationic charges along the linear polymer chains into consideration, a more meaningful conclusion can be drawn from the biochemical characterizations.

Table 5.2. Molar mass ([g/mol]) and dispersity (Đ) for each polymer prepared *via* RAFT polymerization

Polymer	$M_{n,\,theo}$ [a]	SEC_{DMAc}		SEC_{water}		$M_{s,\,f}$ [b]
		M_n	Đ	M_n	Đ	
$HPMA_{95\%}$-s-$APMA_{5\%}$	12100	28500	1.08	5300	1.18	11500
$HPMA_{90\%}$-s-$APMA_{10\%}$	12096	28000	1.09	6000	1.18	12300
$HPMA_{80\%}$-s-$APMA_{20\%}$	12095	28000	1.05	7000	1.18	11700
$HPMA_{60\%}$-s-$APMA_{40\%}$	12115	-	-	7800	1.18	11600
$HPMA_{50\%}$-s-$APMA_{50\%}$	12134	-	-	8500	1.18	10900
$HPMA_{40\%}$-s-$APMA_{60\%}$	12158	-	-	8000	1.17	10500
$HPMA_{25\%}$-s-$APMA_{75\%}$	12203	-	-	9000	1.17	11200
$HPMA_{10\%}$-s-$APMA_{90\%}$	12258	-	-	11000	1.05	10700
$HPMA_{95\%}$-g-$APMA_{5\%}$	11907	25000	1.10	6100	1.06	11400
$HPMA_{90\%}$-g-$APMA_{10\%}$	11843	25500	1.08	7300	1.04	12100
$HPMA_{80\%}$-g-$APMA_{20\%}$	11767	22000	1.11	8000	1.06	12400
$HPMA_{60\%}$-g-$APMA_{40\%}$	11760	-	-	8300	1.19	9700
$HPMA_{50\%}$-g-$APMA_{50\%}$	11805	-	-	8100	1.08	9400
$HPMA_{40\%}$-g-$APMA_{60\%}$	11874	-	-	8000	1.21	9800
$HPMA_{25\%}$-g-$APMA_{75\%}$	12010	-	-	8500	1.30	10000
$HPMA_{10\%}$-g-$APMA_{90\%}$	12176	-	-	11000	1.05	10400
$HPMA_{95\%}$-s-$GPMA_{5\%}$	11762	24000	1.09	4500	1.07	10600
$HPMA_{90\%}$-s-$GPMA_{10\%}$	11759	26000	1.06	5500	1.06	9600
$HPMA_{80\%}$-s-$GPMA_{20\%}$	11759	24000	1.11	6500	1.04	10200
$HPMA_{60\%}$-s-$GPMA_{40\%}$	11782	23000	1.07	6750	1.04	11300
$HPMA_{50\%}$-s-$GPMA_{50\%}$	11804	20500	1.07	6400	1.04	11300
$HPMA_{25\%}$-s-$GPMA_{75\%}$	11884	14500	1.05	5000	1.04	11400
$HPMA_{95\%}$-g-$GPMA_{5\%}$	11541	24500	1.09	5000	1.05	10100
$HPMA_{90\%}$-g-$GPMA_{10\%}$	11468	23500	1.09	5200	1.05	9500
$HPMA_{80\%}$-g-$GPMA_{20\%}$	11384	21000	1.10	5500	1.04	10900
$HPMA_{60\%}$-g-$GPMA_{40\%}$	11380	18000	1.09	5500	1.05	8500
$HPMA_{50\%}$-g-$GPMA_{50\%}$	11433	16000	1.08	5500	1.05	8400
$HPMA_{25\%}$-g-$GPMA_{75\%}$	11667	12000	1.05	4200	1.06	10000

[a)]The theoretical molar mass was calculated using the Formula $M_{n,th} = ([M]_0/[CTA]_0) \cdot M_{w,monomer} \cdot \rho + M_{w,CTA}$, while complete conversion was assumed; [b)]determined via sedimentation-velocity experiments with analytical ultracentrifugation;

Table 5.3. The theoretical and experimental APMA- or GPMA content in mol%, intrinsic viscosity ([η]), Huggins constants (k_H), partial specific volumes (v) and the average total value of monomer units per polymer chain for each sample

Polymer	Co-monomer content			$[\eta]$	k_H	v	Monomers	
	desired	theo[a]	exp[b]				APMA / GPMA	HPMA
$HPMA_{95\%}$-s-$APMA_{5\%}$	5	12.0	8.9	7.57	1.8	0.78	7	72
$HPMA_{90\%}$-s-$APMA_{10\%}$	10	17.1	14.2	8.6	1.8	0.81	12	71
$HPMA_{80\%}$-s-$APMA_{20\%}$	20	27.3	23.4	8.18	1.7	0.79	18	59
$HPMA_{60\%}$-s-$APMA_{40\%}$	40	46.9	44.0	7.83	1.6	0.80	32	41
$HPMA_{50\%}$-s-$APMA_{50\%}$	50	56.4	54.1	8.98	1.3	0.77	36	31
$HPMA_{40\%}$-s-$APMA_{60\%}$	60	65.5	63.2	9.41	1.1	0.75	40	23
$HPMA_{25\%}$-s-$APMA_{75\%}$	75	78.8	77.6	9.7	1.1	0.74	51	15
$HPMA_{10\%}$-s-$APMA_{90\%}$	90	91.7	87.9	9.7	1.0	0.73	54	7
$HPMA_{95\%}$-g-$APMA_{5\%}$	5	18.8	6.7	7.16	1.8	0.80	5	73
$HPMA_{90\%}$-g-$APMA_{10\%}$	10	26.4	15.1	7.73	1.4	0.80	12	69
$HPMA_{80\%}$-g-$APMA_{20\%}$	20	39.7	25.8	8.24	1.4	0.80	21	60
$HPMA_{60\%}$-g-$APMA_{40\%}$	40	60.9	41.3	7.67	1.5	0.77	25	36
$HPMA_{50\%}$-g-$APMA_{50\%}$	50	69.5	47.7	7.37	1.4	0.77	28	31
$HPMA_{40\%}$-g-$APMA_{60\%}$	60	77.0	58.0	7.96	1.3	0.76	35	25
$HPMA_{25\%}$-g-$APMA_{75\%}$	75	86.8	80.6	8.62	1.2	0.73	47	11
$HPMA_{10\%}$-g-$APMA_{90\%}$	90	95.1	89.1	-	1.1	0.74	53	6
$HPMA_{95\%}$-s-$GPMA_{5\%}$	5	12.0	5.7	8.4	1.3	0.79	4	68
$HPMA_{90\%}$-s-$GPMA_{10\%}$	10	17.1	9.9	6.51	2.5	0.78	6	57
$HPMA_{80\%}$-s-$GPMA_{20\%}$	20	27.3	18.5	10.1	0.6	0.77	12	53
$HPMA_{60\%}$-s-$GPMA_{40\%}$	40	46.9	35.1	9.2	0.9	0.79	23	43
$HPMA_{50\%}$-s-$GPMA_{50\%}$	50	56.4	40.7	8.3	1.3	0.78	26	38
$HPMA_{25\%}$-s-$GPMA_{75\%}$	75	78.8	52.8	8.74	1.2	0.78	33	29
$HPMA_{95\%}$-g-$GPMA_{5\%}$	5	18.8	5.0	8.85	1.2	0.78	3	65
$HPMA_{90\%}$-g-$GPMA_{10\%}$	10	26.4	10.5	10.0	1.07	0.78	7	56
$HPMA_{80\%}$-g-$GPMA_{20\%}$	20	39.7	14.9	8.82	1.15	0.79	10	60
$HPMA_{60\%}$-g-$GPMA_{40\%}$	40	60.9	34.4	7.2	1.61	0.77	17	33
$HPMA_{50\%}$-g-$GPMA_{50\%}$	50	69.5	41.5	7.5	1.28	0.75	20	28
$HPMA_{25\%}$-g-$GPMA_{75\%}$	75	86.8	60.8	7.0	1.39	0.73	32	21

[a)]according to the used stoichiometry; [b)]determined via ^{1}H-NMR.

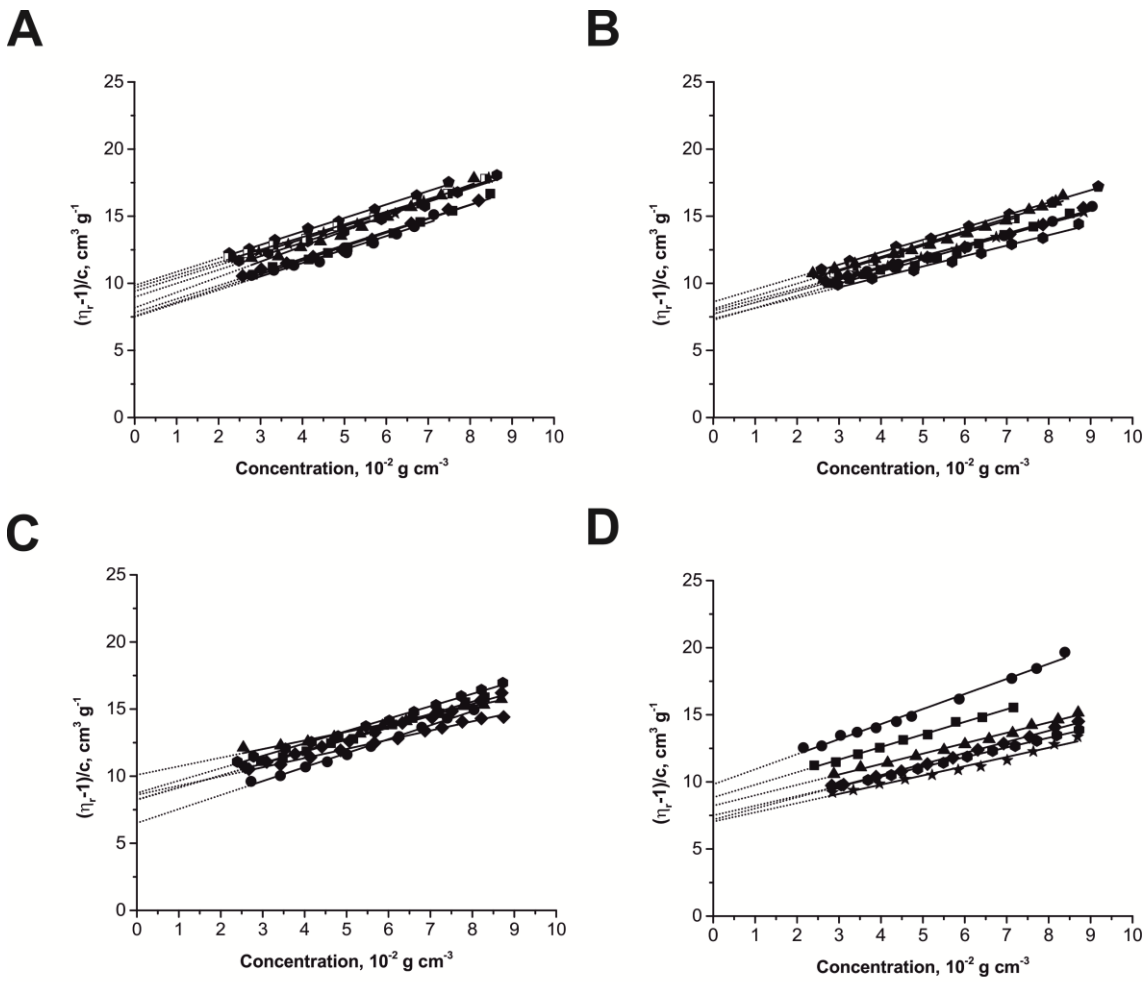

Figure 5.6. Plots to determine intrinsic viscosities, $[\eta]$, and Huggins constant, k_H, for: (A) statistical copolymers of HPMA and APMA, (B) the gradient copolymers of of HPMA and APMA, (C) the statistical copolymers of HPMA and GPMA, and (D) the gradient copolymers of HPMA and GPMA. Fits to the equation are shown as solid lines and extrapolations to determine $[\eta]$ as dotted lines. Symbol assignment for polymers: ■ $HPMA_{95\%}$-s-$APMA_{5\%}$ $HPMA_{95\%}$-g-$APMA_{5\%}$ / $HPMA_{95\%}$-s-$GPMA_{5\%}$ / $HPMA_{95\%}$-g-$GPMA_{5\%}$; ● $HPMA_{90\%}$-s-$APMA_{10\%}$ / $HPMA_{90\%}$-g-$APMA_{10\%}$ / $HPMA_{90\%}$-s-$GPMA_{10\%}$ / $HPMA_{90\%}$-g-$GPMA_{10\%}$; ▲ $HPMA_{80\%}$-s-$APMA_{20\%}$ / $HPMA_{80\%}$-g-$APMA_{20\%}$ / $HPMA_{80\%}$-s-$GPMA_{20\%}$ / $HPMA_{80\%}$-g-$GPMA_{20\%}$; ♦ $HPMA_{60\%}$-s-$APMA_{40\%}$ / $HPMA_{60\%}$-g-$APMA_{40\%}$ / $HPMA_{60\%}$-s-$GPMA_{40\%}$ / $HPMA_{60\%}$-g-$GPMA_{40\%}$; ❑$HPMA_{50\%}$-s-$APMA_{50\%}$ / $HPMA_{50\%}$-g-$APMA_{50\%}$ / $HPMA_{50\%}$-s-$GPMA_{50\%}$ / $HPMA_{50\%}$-g-$GPMA_{50\%}$; ★ $HPMA_{40\%}$-s-$APMA_{60\%}$ / $HPMA_{40\%}$-g-$APMA_{60\%}$; ⬢ $HPMA_{25\%}$-s-$APMA_{75\%}$ / $HPMA_{25\%}$-g-$APMA_{75\%}$ / $HPMA_{25\%}$-s-$GPMA_{75\%}$ / $HPMA_{25\%}$-g-$GPMA_{75\%}$; ◧ $HPMA_{10\%}$-s-$APMA_{90\%}$ / $HPMA_{10\%}$-g-$APMA_{90\%}$

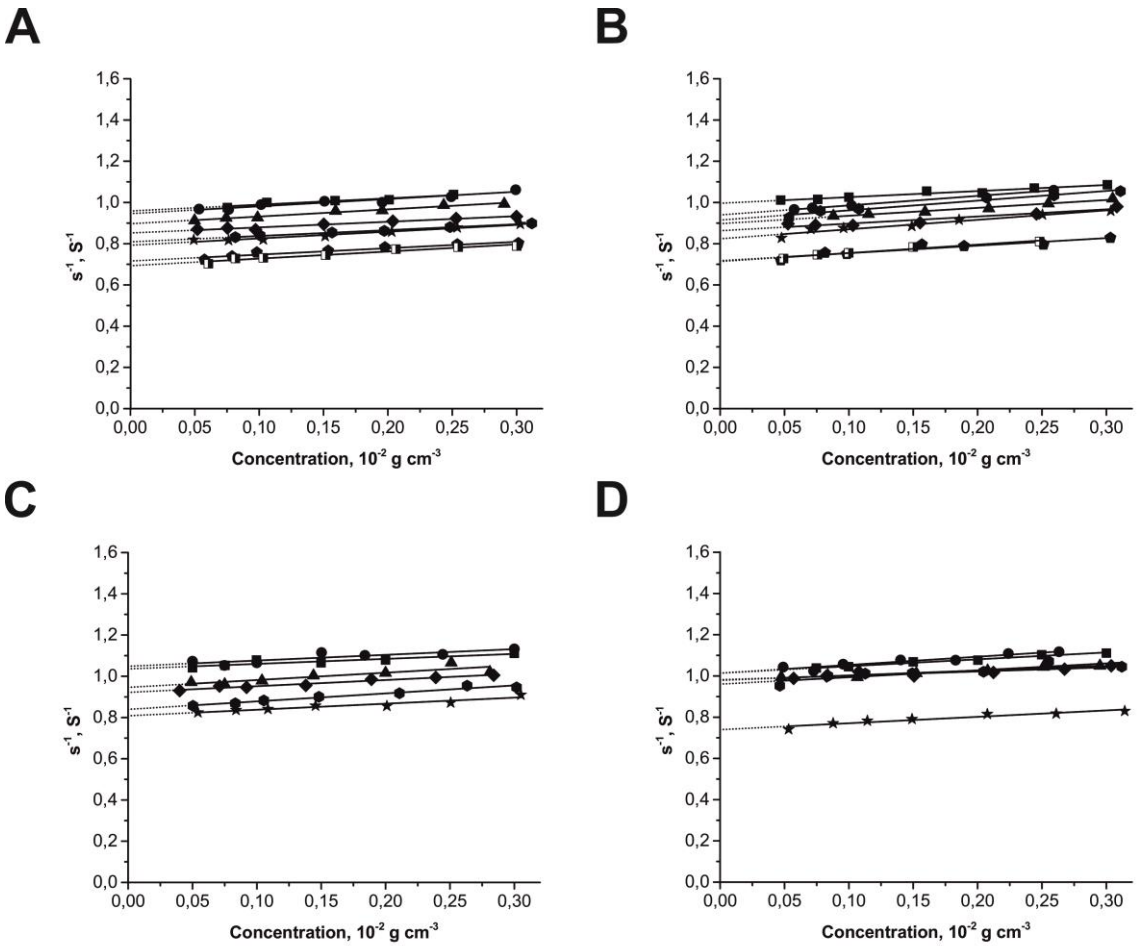

Figure 5.7. Plots of inverse sedimentation coefficients, s^{-1}, against macromolecule solution concentration with linear fits (solid lines) and extrapolations to zero concentration (dotted lines) to determine s_0 for (A) statistical copolymers of HPMA and APMA, (B) the gradient copolymers of of HPMA and APMA, (C) the statistical copolymers of HPMA and GPMA, and (D) the gradient copolymers of HPMA and GPMA. Symbol assignment for polymers: ■ $HPMA_{95\%}$-s-$APMA_{5\%}$ $HPMA_{95\%}$-g-$APMA_{5\%}$ / $HPMA_{95\%}$-s-$GPMA_{5\%}$ / $HPMA_{95\%}$-g-$GPMA_{5\%}$; ● $HPMA_{90\%}$-s-$APMA_{10\%}$ / $HPMA_{90\%}$-g-$APMA_{10\%}$ / $HPMA_{90\%}$-s-$GPMA_{10\%}$ / $HPMA_{90\%}$-g-$GPMA_{10\%}$; ▲ $HPMA_{80\%}$-s-$APMA_{20\%}$ / $HPMA_{80\%}$-g-$APMA_{20\%}$ / $HPMA_{80\%}$-s-$GPMA_{20\%}$ / $HPMA_{80\%}$-g-$GPMA_{20\%}$; ♦ $HPMA_{60\%}$-s-$APMA_{40\%}$ / $HPMA_{60\%}$-g-$APMA_{40\%}$ / $HPMA_{60\%}$-s-$GPMA_{40\%}$ / $HPMA_{60\%}$-g-$GPMA_{40\%}$; ❑$HPMA_{50\%}$-s-$APMA_{50\%}$ / $HPMA_{50\%}$-g-$APMA_{50\%}$ / $HPMA_{50\%}$-s-$GPMA_{50\%}$ / $HPMA_{50\%}$-g-$GPMA_{50\%}$; ★ $HPMA_{40\%}$-s-$APMA_{60\%}$ / $HPMA_{40\%}$-g-$APMA_{60\%}$; ⬢ $HPMA_{25\%}$-s-$APMA_{75\%}$ / $HPMA_{25\%}$-g-$APMA_{75\%}$ / $HPMA_{25\%}$-s-$GPMA_{75\%}$ / $HPMA_{25\%}$-g-$GPMA_{75\%}$; ◧ $HPMA_{10\%}$-s-$APMA_{90\%}$ / $HPMA_{10\%}$-g-$APMA_{90\%}$

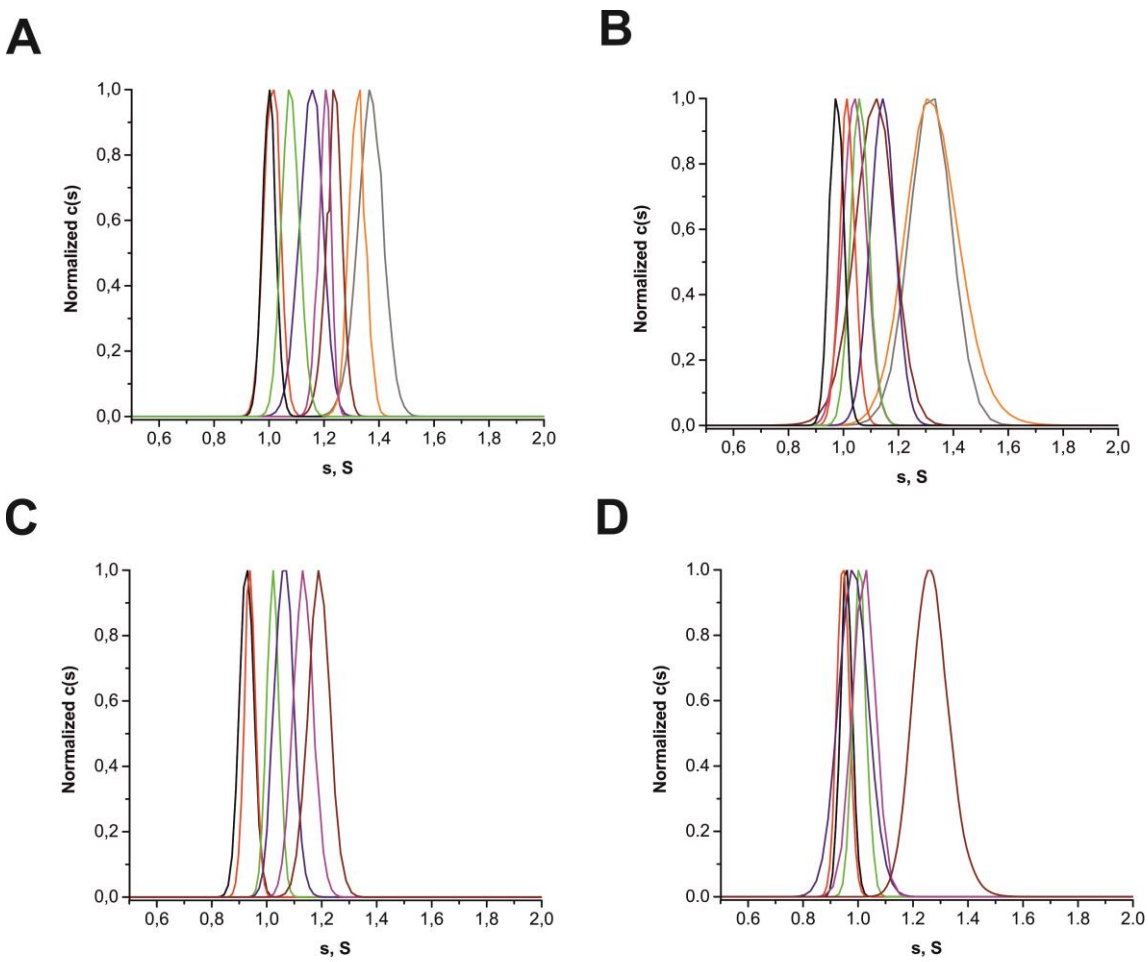

Figure 5.8. Differential distributions of sedimentation coefficients, *s*, of (A) statistical copolymers of HPMA and APMA, (B) the gradient copolymers of HPMA and APMA, (C) the statistical copolymers of HPMA and GPMA, and (D) the gradient copolymers of HPMA and GPMA. Trace color assignment: black $HPMA_{95\%}$-s-$APMA_{5\%}$ $HPMA_{95\%}$-g-$APMA_{5\%}$ / $HPMA_{95\%}$-s-$GPMA_{5\%}$ / $HPMA_{95\%}$-g-$GPMA_{5\%}$; red $HPMA_{90\%}$-s-$APMA_{10\%}$ / $HPMA_{90\%}$-g-$APMA_{10\%}$ / $HPMA_{90\%}$-s-$GPMA_{10\%}$ / $HPMA_{90\%}$-g-$GPMA_{10\%}$; green $HPMA_{80\%}$-s-$APMA_{20\%}$ / $HPMA_{80\%}$-g-$APMA_{20\%}$ / $HPMA_{80\%}$-s-$GPMA_{20\%}$ / $HPMA_{80\%}$-g-$GPMA_{20\%}$; blue $HPMA_{60\%}$-s-$APMA_{40\%}$ / $HPMA_{60\%}$-g-$APMA_{40\%}$ / $HPMA_{60\%}$-s-$GPMA_{40\%}$ / $HPMA_{60\%}$-g-$GPMA_{40\%}$; magenta $HPMA_{50\%}$-s-$APMA_{50\%}$ / $HPMA_{50\%}$-g-$APMA_{50\%}$ / $HPMA_{50\%}$-s-$GPMA_{50\%}$ / $HPMA_{50\%}$-g-$GPMA_{50\%}$; wine $HPMA_{40\%}$-s-$APMA_{60\%}$ / $HPMA_{40\%}$-g-$APMA_{60\%}$; orange $HPMA_{25\%}$-s-$APMA_{75\%}$ / $HPMA_{25\%}$-g-$APMA_{75\%}$ / $HPMA_{25\%}$-s-$GPMA_{75\%}$ / $HPMA_{25\%}$-g-$GPMA_{75\%}$; grey $HPMA_{10\%}$-s-$APMA_{90\%}$ / $HPMA_{10\%}$-g-$APMA_{90\%}$

5.2 Binding and condensation of pDNA

The biochemical characterization of the statistical and gradient copolymers was performed in cooperation with Leon Zartner (Prof. Dr. Dagmar Fischer, Institute of Pharmacy, Friedrich Schiller University Jena).

The copolymers' ability to bind pDNA was assessed by using electrophoretic mobility shift assays. The fluorophore exclusion assay, which quantifies the displacement of dye molecules by polymer chains trough competitive binding to pDNA and the inhibition of dye-DNA interactions through dense packing, on the other hand, was employed to study the degree of pDNA-condensation inside the polyplexes. These techniques rely on the formation of polyplexes from polycationic polymers and polyanionic DNA due to electrostatic attraction, which is an entropy supported process due to the release of a relatively large numbers of small counter ions.[31, 32] To follow the results of these analytical techniques, Ethidium bromide and AccuBlue™ were employed. Both dyes have very low fluorescence signals in their unbound state, whereas upon binding to double stranded nucleic acids, their fluorescence signal is enhanced considerably.[33]

The results depicted in Figure 5.9 and 5.10 allow two general statements regarding the binding efficacy of statistical and gradient copolymers.

(1) All copolymers, with the exception of the copolymers with the lowest cationic charge densities ($HPMA_{95\%}$-s-$APMA_{5\%}$, $HPMA_{95\%}$-g-$APMA_{5\%}$, $HPMA_{95\%}$-g-$GPMA_{5\%}$ and $HPMA_{95\%}$-s-$GPMA_{5\%}$), hindered the migration of pDNA towards the anode already at the N/P ratio of 1. In case of the two special cases, a smeared band migrating to the anode was detected at low N/P ratios. This behaviour is tantamount to either incomplete charge compensation of the pDNA molecules, or the formation of small polyplexes with the ability to migrate through the gel (Figure 5.9).

(2) For both types of monomer arrangement different states of complexation were detected. These states included forms of complete fluorescence quenching as well as forms with residual fluorescence that remained in the wells or migrated towards the cathode.[34] Comparing the higher residual fluorescence of $HPMA_{95\%}$-s-$APMA_{5\%}$- or $HPMA_{80\%}$-s-$APMA_{20\%}$-based polyplexes to the results of their gradient counterparts confirmed a weaker binding affinity of the statistical copolymers towards pDNA (Figure 5.9, A and B). This correlation can be made, because the staining of the EMSA gels was done with Ethidium bromide and a weak signal corresponds to inaccessible DNA molecules, which can only be explained by the formation of densly packed polyplexes.

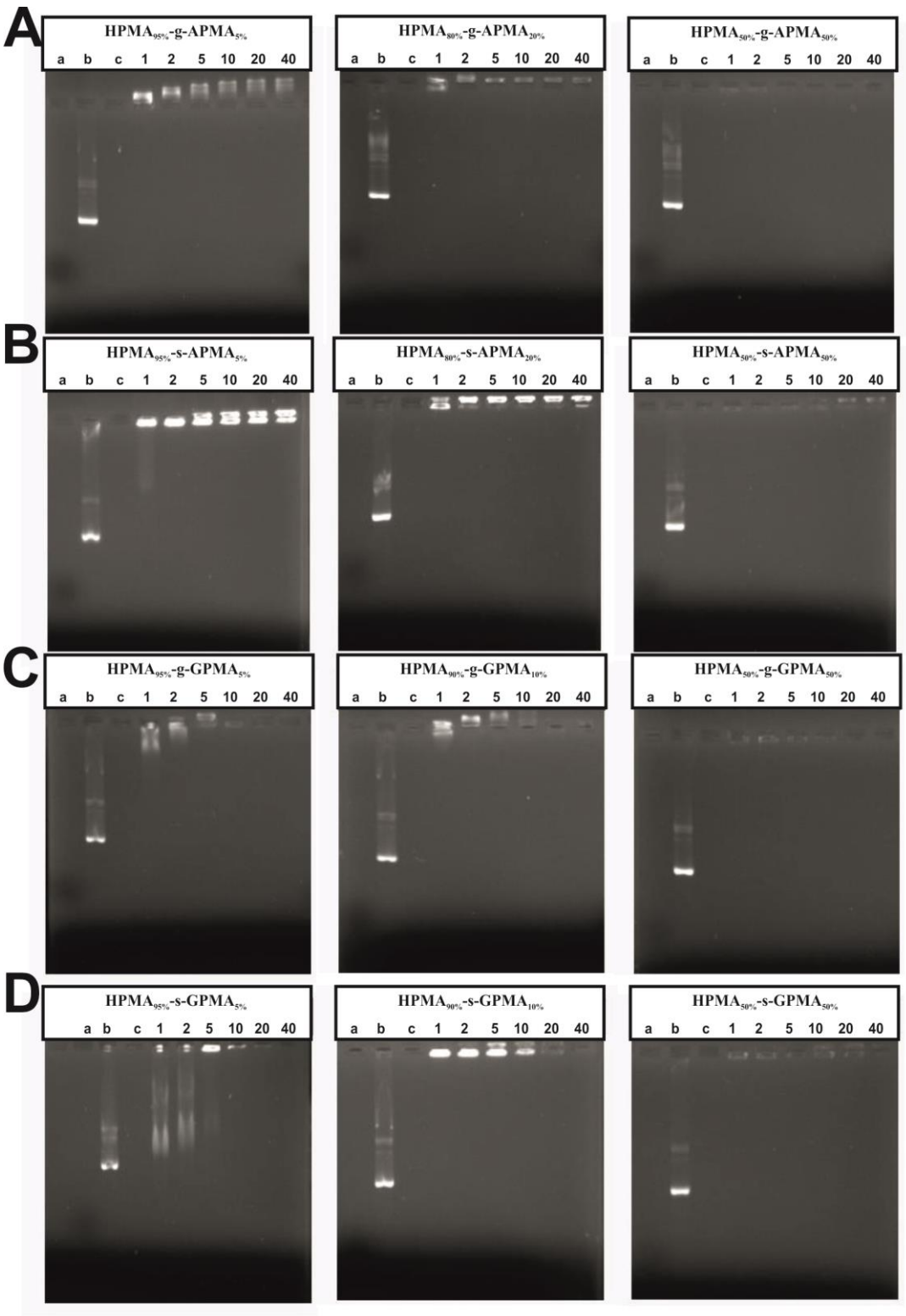

Figure 5.9. Electrophoretic mobility shift assay for (A) HPMA-g-APMA copolymers, (B) HPMA-s-APMA copolymers, (C) HPMA-g-GPMA copolymers, and (D) HPMA-s-GPMA copolymers

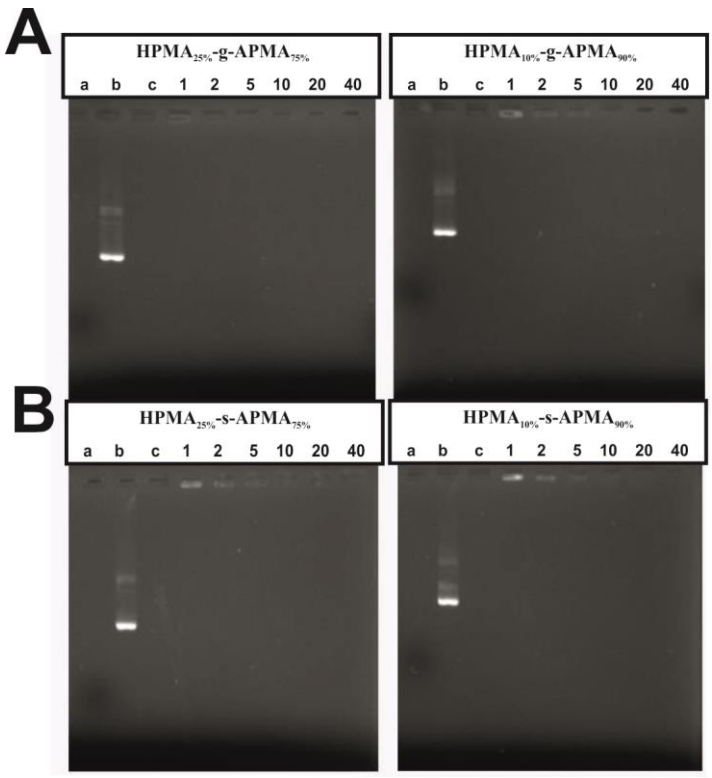

Figure 5.10. Electrophoretic mobility shift assay for HPMA-APMA copolymers with high cationic charge densities (A) gradient copolymers, (B) statistical copolymers

The investigated statistical and gradient copolymers varied only marginally in terms of their APMA content. In fact, the gradient copolymers, which performed better than their statistical counterparts, were the ones with a lower overall charge density, since only every 15th ($HPMA_{95\%}$-g-$APMA_{5\%}$) or 7th monomer ($HPMA_{80\%}$-g-$APMA_{20\%}$) was bearing a primary amino group, in contrast to every 11th ($HPMA_{95\%}$-s-$APMA_{5\%}$) or 7th monomer ($HPMA_{80\%}$-s-$APMA_{20\%}$). The observed difference in binding strength is seemingly paradox, considering that the binding affinity towards polynucleotides and the packing efficacy are usually closely associated with the cationic charge density of the respective polymeric carrier system. This observation can be explained, however, if the locally high cationic charge densities of the gradient copolymers are considered. As described before, cationic gradient copolymers are expected to be comprised of polymer chain segments with varying charge densities. Sections with predominantly statistical charge distributions, sections at the chains ends with block-like character and regions that can neither be described as statistical or block-like in-between the other section types offer different degrees of electrostatic interaction. It is possible that the increased density of APMA monomers at the terminus of the polymer acts in a similar fashion as

a cationic block, which allows the formation of micellar polyplexes with densly packed polynucleotides.[35, 36]

Increasing the APMA content and thereby the overall cationic charge density diminished the significance of highly charged block-like polymer segments (Figure 5.10). For gradient as well as statistic copolymers a virtually complete extinction of fluorescence was observed for APMA contents equal to or exceeding 50 mol%. In these cases, full condensation of the pDNA and a strong binding affinity were assumed. To prove this hypothesis fluorophore exclusion assays were performed (Figure 5.11).

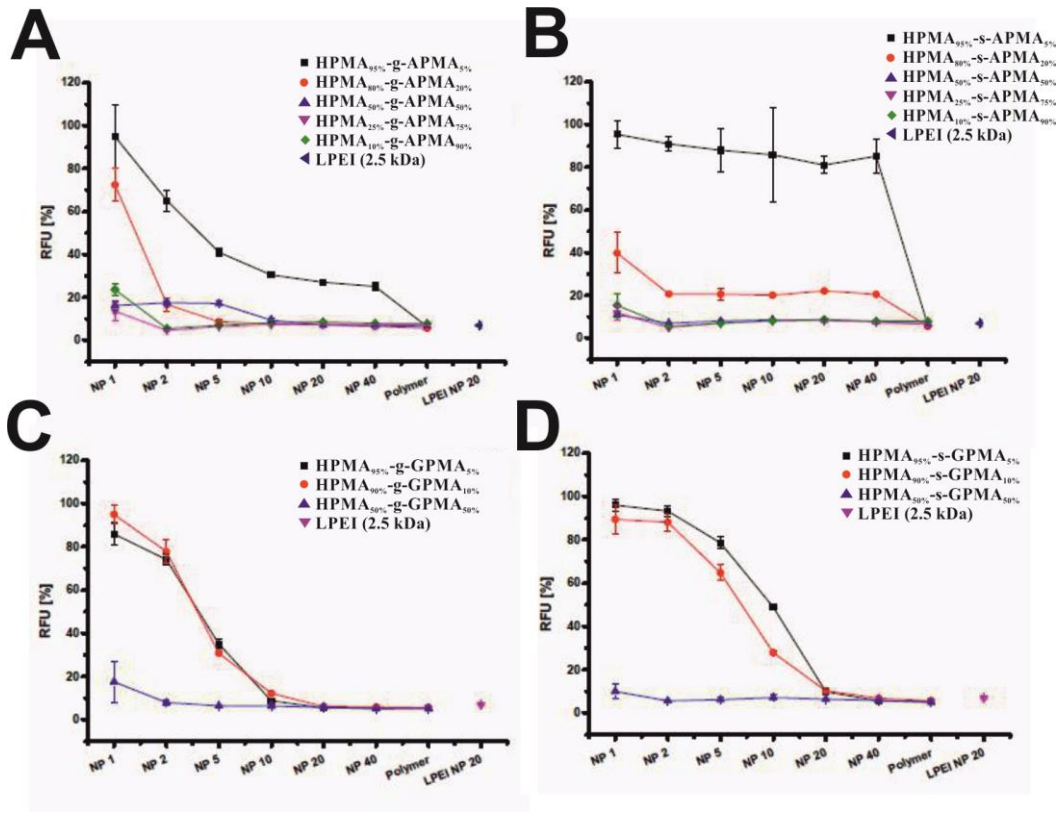

Figure 5.11. Fluorophore exclusion assay for (A) HPMA-g-APMA copolymers, (B) HPMA-s-APMA copolymers, (C) HPMA-g-GPMA copolymers, and (D) HPMA-s-GPMA copolymers

The fluorophore exclusion assay allowed a more detailed study of pDNA condensation, since AccuBlue™ is more sensitive to traces of free DNA than Ethidium bromide. Since low fluorescence values correspond to a denser packing of DNA, relative fluorescence units (RFU) can be used to quantify pDNA condensation. For both gradient and statistical copolymers an inverse proportionality of the fluorescence intensity to the cat-

ionic charge density and the used N/P ratio was observed. Hence, strongly charged polymers lead to densely packed pDNA and increasing the polymer content during polyplex formation has a beneficial effect on pDNA condensation as well. Among the APMA-based copolymers, only $HPMA_{95\%}$-g-$APMA_{5\%}$, $HPMA_{95\%}$-s-$APMA_{5\%}$ and $HPMA_{80\%}$-s-$APMA_{20\%}$ were not able to decrease fluorescence intensity to the low level of the 2.5 kDa LPEI control ($RFU_{control} \approx 6\%$, Figure 5.11). $HPMA_{80\%}$-g-$APMA_{20\%}$, in contrast to its statistical counterpart, reached the RFU value of the control. Hence, it can be stated that the condensation efficacy is not only dependent on the overall charge density, but also on the monomer arrangement. This hypothesis is further supported by comparing the packing efficacy of $HPMA_{95\%}$-g-$APMA_{5\%}$ to $HPMA_{95\%}$-s-$APMA_{5\%}$ at the N/P ratio of 40. The gradient copolymer facilitated a decrease in fluorescence intensity to a RFU value of 25%, but its statistical counterpart only led to a slight drop to about 85% RFU, which suggest that nearly all of the pDNA molecules remained accessible to AccuBlue™. The packing efficacy of the gradient copolymer with the lowest cationic charge density ($HPMA_{95\%}$-g-$APMA_{5\%}$) was matched by a statistical HPMA-APMA copolymer only upon increasing the APMA content by 400% ($HPMA_{80\%}$-s-$APMA_{20\%}$). In addition, the RFU levels of $HPMA_{95\%}$-s-$APMA_{5\%}$ and $HPMA_{80\%}$-s-$APMA_{20\%}$ formed a plateau at the high N/P ratios. $HPMA_{95\%}$-g-$APMA_{5\%}$ and $HPMA_{80\%}$-g-$APMA_{20\%}$, on the other hand, facilitated a steady decrease in fluorescence intensity, if more polymer molecules were available during polyplex formation (Figure 5.11). Hence, HPMA-APMA gradient copolymers were more effective in densely packing pDNA. However, these differences were only observed for polymers with low APMA contents. Incorporating 50 mol% or more APMA monomers into either polymer structure lead to efficient condensation of pDNA at all tested N/P ratios. Hence, increasing the cationic charge density can be utilized as a strategy to compensate for the disadvantages of a statistical charge distribution in terms of polynucleotide complexation. However, strongly charged polymers are known to induce adverse side effects, such as cytotoxicity.[37]

Analogous to the APMA derivatives, binding experiments between GPMA-based copolymers and pDNA were performed via gel electrophoresis as well as fluorophore exclusion assay (Figure 5.9, C and D; Figure 5.11, C and D). Similarly to the results of the APMA-based copolymers, polymers with a high cationic charge density, such as $HPMA_{50\%}$-g-$GPMA_{50\%}$ or $HPMA_{50\%}$-s-$GPMA_{50\%}$, inhibited the interaction between pDNA and ethidium bromide or AccuBlue™, thereby inducing near complete loss of

fluorescence at all tested N/P ratios. Copolymers with a lower GPMA content, on the other hand, facilitated the previously described stages of DNA complexation and -condensation. While these observations are similar to the correlations between the binding affinity and the utilized N/P ratio as well as the cationic charge density of the APMA derivatives, additional insights into the structure-function relationship have been gained. This comparison elucidated the importance of the origin of cationic charges. Even low amounts of pendant guanidinium groups, such as 1 in 18 ($HPMA_{95\%}$-s-$GPMA_{5\%}$) or 1 in 23 monomers ($HPMA_{95\%}$-g-$GPMA_{5\%}$), were sufficient to fully condense pDNA, thereby extinguishing fluorescence intensity during gel electrophoresis as well as achieving RFU values of the control during the fluorophore exclusion assay. Although high N/P ratios (20) were required in these cases, this feat could not be repeated by using primary amines as the source of cationic charges. HPMA-APMA copolymers with low cationic charge densities ($HPMA_{95\%}$-g-$APMA_{5\%}$ and $HPMA_{95\%}$-s-$APMA_{5\%}$) exhibited residual fluorescence at all N/P ratios during both gel electrophoresis and fluorophore exclusion assay. The basicity of the functional groups is expected to be at least partially responsible for the observed variations in binding affinity. While the guanidinium group of the GPMA monomers is strongly basic with a pK_a of about 13, primary amines of APMA exhibit a lower pk_a of about 10,6.[38, 39] The higher basicity of guanidinium groups makes them more prone to protonation at physiological pH. This property promotes higher charge densities in GPMA-based copolymers than in their APMA-based counterparts. In addition, the guanidinium group has the ability to establish hydrogen bonds with DNA in higher quantity and with better geometry than primary amines.[40, 41] This strong affinity of guanidinium group towards polynucleotides made the differences between the statistical and gradient organization of monomers less apparent. Nevertheless, delicate distinctions were observed for copolymers with GPMA contents equal to or below 10 mol%. For example, the statistical copolymers $HPMA_{95\%}$-s-$GPMA_{5\%}$ and $HPMA_{90\%}$-s-$GPMA_{10\%}$ facilitated efficient condensation of pDNA, which is made visible by the steady decrease of the RFU value (Figure 5.11). Both polymers were able to shield the polynucleotide molecules from the interaction with AccuBlue™ at the N/P ratio of 20. In case of their gradient counterparts, however, an even stronger binding affinity was observed. $HPMA_{95\%}$-g-$GPMA_{5\%}$ and $HPMA_{90\%}$-g-$GPMA_{10\%}$, following a steeper decrease in fluorescence intensity, reached the RFU value of the control at the N/P ratio of 10. The hypothesis that a gradient organization of the cationic charges facilitates superior binding properties is further supported by the

fact that these copolymers had similar overall charge densities. In case of the gradient copolymers, 1 in 22 ($HPMA_{95\%}$-g-$GPMA_{5\%}$) or 1 in 8 monomers ($HPMA_{90\%}$-g-$GPMA_{10\%}$) were bearing a guanidinium group. The statistical copolymers, had a similar composition, since 1 in 17 ($HPMA_{95\%}$-s-$GPMA_{5\%}$) or 1 in 9 monomers ($HPMA_{90\%}$-s-$GPMA_{10\%}$) was a GPMA.

5.3 Transfection efficacy based on luciferase expression in CHO-K1 cells

After testing the affinity of each polymer structure toward DNA, the initial obstacle for a gene delivery agent, a bioluminescence assay was conducted to determine the polymers' ability not only to condense pDNA, but also to deliver its plasmid payload into cells while conserving its integrity and functionality. The successful delivery of DNA into the nucleus or pDNA into the cytosol is a challenging task for gene delivery agents. Polyplexes, which are suspended in cell culture medium, have to suffer attacks from polyanionic serum proteins, which can displace DNA from the complexes or form a protein corona, thereby making the polyplexes visible to the immune system. Such an environment also contains nucleases, which degrade DNA to non-effective fragments.[42] Having accomplished protection of the cargo, the polyplexes have to cross the plasma membrane and once they are inside the cell, sufficient amounts of the still functional pDNA must be released into the cytosol. Inducing the expression of luciferase by transfecting CHO-K1 cells with polyplexes containing functional pDNA, is a facile way to study the capability of the copolymers to become gene delivery agents.

Polyplexes formed with APMA copolymers demonstrated potential to deliver pDNA into the nucleus depending on the APMA content of the copolymer and the used N/P ratio (Figure 5.12, A). Since the copolymers with an APMA content of lower than 75 mol% were not able to induce luciferase expression (data not shown), the pair of $HPMA_{10\%}$-g-$APMA_{90\%}$ and $HPMA_{10\%}$-s-$APMA_{90\%}$ were chosen as a representative for APMA structures. Both of these copolymers showed the best results at an N/P ratio of 5. However, the statistic derivative induced a significantly higher luciferase expression than the gradient copolymer. Using higher N/P ratios also affected the viability of the cells, which can be followed by the decreasing protein concentration, since fewer living cells remained. This cytotoxic stress may have interfered with luciferase expression. Similar to the APMA-based copolymers, HPMA-GPMA derivatives showed potential in delivering pDNA into the nucleus (Figure 5.12, B). Their ability to do so was also

affected by the charge density of the polymer and the utilized N/P ratio. GPMA-based polymers achieved reasonable luciferase expression at much lower co-monomer contents than APMA-based structures (50 mol%). However, using much lower or higher charge densities hampered transfection (data not shown). Hence, the copolymers $HPMA_{50\%}$-g-$GPMA_{50\%}$ and $HPMA_{50\%}$-s-$GPMA_{50\%}$ were chosen as representatives. Contrary to the results of the APMA-based derivatives, the luciferase expression these polymers induced is proportional to the utilized N/P ratio (best results at N/P 40) without affecting the viability of the cells. In addition, it was observed that the statistical copolymer ($HPMA_{50\%}$-s-$GPMA_{50\%}$) achieved better transfection results, thereby further supporting the hypothesis that copolymers with a statistical charge distribution are superior in terms of transfection efficacy. A possible explanation for the observed phenomenon is that due to the higher charge density in APMA- or GPMA-rich regions, the electrostatic interaction between gradient copolymers and pDNA is too strong, which in turn affects the release. A similar observation was made for cationic block copolymers in Chapter 3. Another reason might lie with the structure of gradient copolymers-based polyplexes. They might, similar to block copolymers, favor micelle-like complexes, where the chain ends with a high positive charge density show towards the condensed DNA in the core region and the chain ends with a low positive charge density form an outer shell.[43] If the shell region is not sufficiently positively charged, the polyplexes are less toxic, but the internalization into cells is hampered.[42] Nevertheless, it is unclear whether these effects are as pronounced in copolymers with high APMA- or GPMA content, due to the overall negligible HPMA content. Hence, the luciferase expression assay provided a clue to the potential of gradient copolymers, since an ideal tradeoff between toxicity and internalization might be feasible, if the co-monomer content is adjusted to the needs.

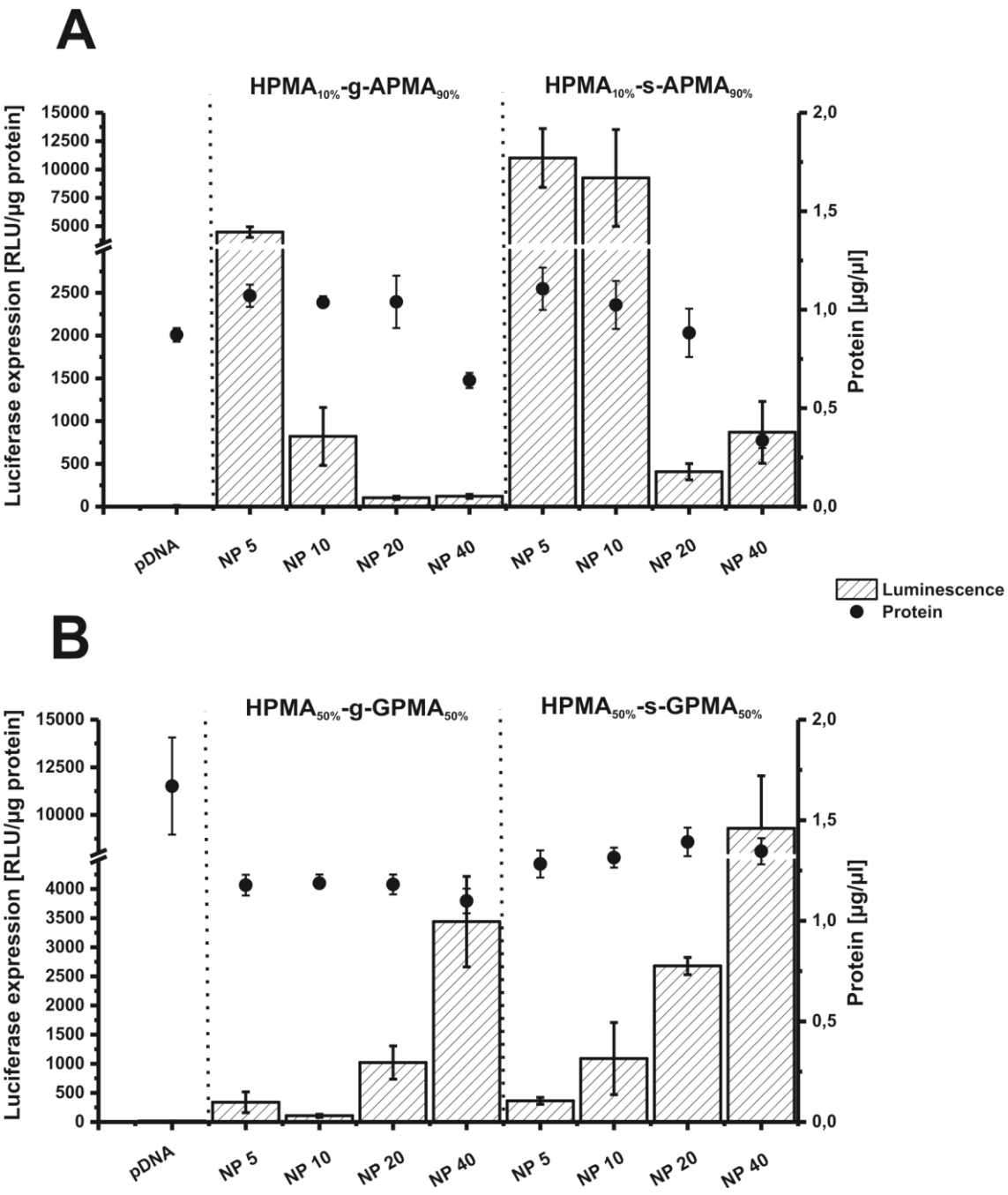

Figure 5.12. Protein content and luciferase expression in CHO-K1 cells after treatment with (A) APMA-based polyplexes or (B) GPMA-based polyplexes

5.4 Cytotoxicity

During the luciferase expression assay toxicity of the polyplexes became an issue for the copolymers $HPMA_{10\%}$-g-$APMA_{90\%}$ and $HPMA_{10\%}$-s-$APMA_{90\%}$. In order to further quantify the polymers' toxicity, a MTT-assay was employed (Table 5.4). Here, CHO-K1 cells were incubated with the polyplexes at different N/P ratios by replicating the transfection conditions, but instead of the luciferase expression readout the toxicity was measured.

A direct correlation was found between the measured cytotoxicity and the employed N/P ratio at which the polyplex was formed. This relationship held true irrespective of the source of the positive charges, but it was significantly more pronounced for APMA-based copolymers. In case of $HPMA_{10\%}$-g-$APMA_{90\%}$ and $HPMA_{10\%}$-s-$APMA_{90\%}$, the monomer arrangement did not affect the overall cell viability, since gradient as well as statistical copolymers, showed increasing toxicity starting at an N/P ratio of 20. These results are in line with the drops in protein concentration, which were observed during the luciferase expression assay. Using uncomplexed copolymers with uncompensated charges led to a slight decrease in viability, but it was expectedly lower than the reference value, where the same polymer concentration was employed (N/P ratio of 5). The toxicity of similar gene carriers has already been linked to the charge density and charge compensation by other researchers.[44] The results of the APMA-based copolymers support the hypothesis that, with respect to the polyplexes' surface charge density, no obvious differences between gradient and statistic polymer structure can be found, if the cationic monomer content reaches the high value of 90 mol%. Contrary to the APMA derivatives, GPMA-based polymers show a distinct difference in toxicity, if a gradient or statistical monomer arrangement is utilized. While both, $HPMA_{50\%}$-g-$GPMA_{50\%}$ and $HPMA_{50\%}$-s-$GPMA_{50\%}$, formed polyplexes that were non-toxic according to DIN ISO 10993-5:2009 at all tested N/P ratios due to the measured relative cell viability of $\geq$ 70%, the gradient derivative exhibited a noticably lower viability at the N/P ratio of 40. In order to determine, whether the absence of toxicity is the consequence of efficient charge compensation, uncomplexed $HPMA_{50\%}$-g-$GPMA_{50\%}$ and $HPMA_{50\%}$-s-$GPMA_{50\%}$ were tested as well, but instead of using the polymer concentrations, which is required for N/P 5, as the reference, the polymer concentration of the N/P ratio of 40 was employed. Here, the statistical copolymer, once again, was deemed non-toxic to the cells, but the gradient copolymer exhibited mild toxicity (68% viability) with a relative viability value slightly below the non-toxic threshold (70% viability). At a GPMA content of

50 mol%, an unequal distribution of GPMA can be assumed in gradient copolymers with regions of concentrated positive charges as well as near-neutral segments. This difference between the statistical and the gradient monomer distribution is expected to affect the structure of the polyplexes. As in section 5.3, polyplexes formed by gradient copolymers are expected to have micelle-like character, where the chain ends with a high positive charge density point towards the condensed DNA in the core region and the chain ends with a low positive charge density form an outer shell.[43] Such a near-neutral shell region is less toxic to cells, but it would not explain the low toxicity of the uncomplexed $HPMA_{50\%}$-g-$GPMA_{50\%}$ and $HPMA_{50\%}$-s-$GPMA_{50\%}$. Although it was expected that these polymers would be tolerated by the cells due to the results of Chapter 3, it is still a remarkable result. Other gene delivery agents are exceedingly toxic, if their charges are not sufficiently compensated.[45]

Table 5.4. Cell viability of CHO-K1 cells in [%]; Thiomersal (0.01% viability) and DNA (103.59 % viability) were used as controls

sample	N/P ratio				free polymer
	5	10	20	40	
$HPMA_{10\%}$-g-$APMA_{90\%}$	98.33	97.45	48.02	5.84	78.83
$HPMA_{10\%}$-s-$APMA_{90\%}$	105.25	99.43	41,65	3.98	81.2
$HPMA_{50\%}$-g-$GPMA_{50\%}$	100.66	101.67	95.14	73.94	68.26
$HPMA_{50\%}$-s-$GPMA_{50\%}$	108.46	111.81	107.50	88.45	99.5

Summarizing the present chapter, a library of statistical and gradient cationic copolymers was synthesized, wherein the content of the protonatable monomers was increased step-wise from 5 to 90 mol% and each polymer sample with a statistical charge distribution had a gradient counterpart. This approach was applied for two different protonatable monomers, namely APMA and GPMA.

The solubilization profile of all polymers was investigated with respect to viscosity and density. For both gradient as well as statistical copolymer a correlation between a polymers' solubility in aqueous media (intrinsic viscosity increases and the apparent Huggins constant decreases) and its content of monomers with basic nitrogen atoms was observed. On the other hand, increasing the content of said monomers influenced the

partial specific volume anti-proportionally and thereby raised the density of the cationic copolymers, which is best visualized by the sedimentation coefficient distributions in Figure 5.8. These effects explain why the evaluation of highly cationic polymers' molar mass by conventional means, such as SEC, is difficult. SEC relies on the correlation between the length of a polymer chain and its hydrodynamic radius in solution. If this relation is affected by other parameters, falsely small or big values of the molecular weight will be estimated. In the present case, although the physico-chemical properties of the macromolecules appear distinct, their actual molar mass, as determined by means of analytical ultracentrifugation, was in all cases shown to be close to the theoretical value, thereby emphasizing the potency of the synthetic approach *via* batch- and semi-batch RAFT polymerization.

Binding- and condensation of pDNA, toxicity and transfection efficacy was investigated for all polymers. Gradient copolymers demonstrated superior binding affinity and denser packing of the polynucleotide in comparison to their statistic counterparts, irrespective of the source of the cationic charges. In addition, gradient copolymers as well as their respective polyplexes were shown to be less toxic to cells. Statistical copolymers, on the other hand, induced higher gene expression and were therefore more effective in terms of transfection. Hence, it was possible to demonstrate that gradient copolymers are an additional design opportunity in gene delivery with their own advantages and disadvantages. The above-mentioned advantages and disadvantage are similar to those of block copolymers, which have been addressed in Chapter 3 of this thesis. Nonetheless, gradient copolymers can be synthesized more easily as well as time-efficiently. In addition, this study represents only the first investigation of gradient copolymers for gene delivery. It cannot be exhaustive with respect to the investigated properties. Hence, further studies for a more distinct differentiation between statistical, gradient and block copolymers are required to draw a more substantial conclusion with respect to their differences. Nonetheless, it needs to be mentioned that in this study it was possible to induce efficient transfection using gradient copolymers. Hence, a strategy other than the post-polymerization modification introduced in Chapter 4, namely the arrangement of cationic monomers in a gradient along the polymer chain, was shown to be effective to resolve the issues of cationic block copolymers described in Chapter 3.

In the present chapter, similar to Chapter 3, the importance of the origin of cationic charges was succinctly demonstrated for not only the binding properties, but also for transfection and cytotoxicity effects. Even low amounts of pendant guanidinium groups

facilitated complete condensation of pDNA. It was not possible to reproduce these results by using polymers bearing primary amines. Additional differences became apparent during the transfection study. GPMA-based copolymers were able to promote luciferase expression at lower cationic charge densities, however, they required high N/P ratios to induce significant luciferase expression. APMA-based copolymers, on the other hand, were only efficient at low N/P ratios.

Conclusively, the distribution and the origin of cationic charges in water soluble copolymers were shown to strongly impact their utility as a pDNA delivery agent. The cationic polymers, which have been the focus of this thesis, possess advantages like a facile synthesis, tunable affinity towards polynucleotides, and the ability to deliver siRNA or DNA into cells. Nevertheless, polymers with pendant guanidinium groups have been repeatedly shown to possess low transfection efficiency. In Chapter 4, post-polymerization functionalization with hydrophobic triphenylphosphonium moieties was shown to alleviate this issue by drastically improving internalization into cells and reducing cytotoxicity of the complexes. This approach aids the transfer of the polyplexes across lipid-phase of the plasma membrane making the commercially available lipid-containing carriers, such as INTERFERin and Lipofectamine 2000 more efficient in delivering siRNA than jetPEI or Metafectene.[46, 47] Even direct conjugation of hydrophobic segments, such as cholesterol[48] or Vitamin E[49] to siRNA was shown to improve uptake.[50] Taking the above-described advantages of statistical copolymers under consideration, it was decided to study statistical cationic terpolymers consisting of hydrophilic as well as hydrophobic monomers as gene delivery agents. Although the copolymerization of monomers with such different solubilization profiles is challenging, circumventing post-polymerization modification, which cannot be guaranteed to be quantitative on all polymer chains, not only simplifies the synthetic approach on the long run, but also provides a higher degree of synthetic precision. Exact structures are essential for medicinal applications.

5.5 References

[1] FR2848557A1 (2004), Atofina, Fr. . inv. O. Guerret;

[2] J. Kim, M. K. Gray, H. Zhou, S. T. Nguyen, J. M. Torkelson, *Macromolecules* **2005**, *38*, 1037.

[3] S. Qin, J. Pyun, J. Saget, S. Jia, T. Kowalewski, K. Matyjaszewski, *Polym. Prepr. (Am. Chem. Soc., Div. Polym. Chem.)* **2002**, *43*, 235.

[4] H. G. Boerner, D. Duran, K. Matyjaszewski, M. da Silva, S. S. Sheiko, *Macromolecules* **2002**, *35*, 3387.

[5] G. T. Pickett, *J. Chem. Phys.* **2003**, *118*, 3898.

[6] B. Gu, A. Sen, *Macromolecules* **2002**, *35*, 8913.

[7] M. K. Gray, H. Zhou, S. T. Nguyen, J. M. Torkelson, *Macromolecules* **2004**, *37*, 5586.

[8] K. Karaky, L. Billon, C. Pouchan, J. Desbrieres, *Macromolecules* **2007**, *40*, 458.

[9] M. D. Lefebvre, M. Olvera de la Cruz, K. R. Shull, *Macromolecules* **2004**, *37*, 1118.

[10] M. D. Lefebvre, C. M. Dettmer, R. L. McSwain, C. Xu, J. R. Davila, R. J. Composto, S. T. Nguyen, K. R. Shull, *Macromolecules* **2005**, *38*, 10494.

[11] J.-S. Park, K. Kataoka, *Macromolecules* **2006**, *39*, 6622.

[12] C. L. H. Wong, J. Kim, C. B. Roth, J. M. Torkelson, *Macromolecules (Washington, DC, U. S.)* **2007**, *40*, 5631.

[13] T. Pakula, *Macromol. Theory Simul.* **1996**, *5*, 987.

[14] P. Gaspard, *Philos. Trans. R. Soc., A* **2016**, *374*, 20160147/1.

[15] J. Brandrup, E. H. Immergut, Editors, "*Polymer Handbook, Fourth Edition*", Wiley, 1998, p. 1920 pp.

[16] C. M. Dettmer, M. K. Gray, J. M. Torkelson, S. T. Nguyen, *Macromolecules* **2004**, *37*, 5504.

[17] G. Chambard, B. Klumperman, *ACS Symp. Ser.* **2000**, *768*, 197.

[18] N. A. A. Rossi, Y. Zou, M. D. Scott, J. N. Kizhakkedathu, *Macromolecules (Washington, DC, U. S.)* **2008**, *41*, 5272.

[19] K. Matyjaszewski, M. J. Ziegler, S. V. Arehart, D. Greszta, T. Pakula, *J. Phys. Org. Chem.* **2000**, *13*, 775.

[20] D. Greszta, K. Matyjaszewski, T. Pakula, *Polym. Prepr. (Am. Chem. Soc., Div. Polym. Chem.)* **1997**, *38*, 709.

[21] R. Duncan, *Nat Rev Cancer* **2006**, *6*, 688.

[22] C. Rodriguez-Emmenegger, E. Brynda, T. Riedel, M. Houska, V. Subr, A. B. Alles, E. Hasan, J. E. Gautrot, W. T. S. Huck, *Macromol. Rapid Commun.* **2011**, *32*, 952.

[23] L. Lybaert, N. Vanparijs, K. Fierens, M. Schuijs, L. Nuhn, B. N. Lambrecht, B. G. De Geest, *Biomacromolecules* **2016**, *17*, 874.

[24] A. W. York, F. Huang, C. L. McCormick, *Biomacromolecules* **2010**, *11*, 505.

[25] N. J. Treat, D. Smith, C. Teng, J. D. Flores, B. A. Abel, A. W. York, F. Huang, C. L. McCormick, *ACS Macro Lett.* **2012**, *1*, 100.

[26] A. C. Holley, W. Wan, G. R. Bishop, F. Huang, C. L. McCormick, "Binding strength of siRNA/copolymer complexes utilizing aqueous RAFT synthesized hydrophilic-block-cationic copolymers and the effects on gene suppression", American Chemical Society, 2014POLY.

[27] A. W. York, Y. Zhang, A. C. Holley, Y. Guo, F. Huang, C. L. McCormick, *Biomacromolecules* **2009**, *10*, 936.

[28] X. Sun, Y. Luo, R. Wang, B.-G. Li, B. Liu, S. Zhu, *Macromolecules* **2007**, *40*, 849.

[29] Y. Chen, H. Chen, M. Feng, Y. Dong, *Eur. Polym. J.* **2016**, *85*, 489.

[30] J. L. Cole, J. W. Lary, T. P. Moody, T. M. Laue, *Methods Cell Biol.* **2008**, *84*, 143.

[31] T. Bronich, A. V. Kabanov, L. A. Marky, *J Phys Chem B* **2001**, *105*, 6042.

[32] I. Insua, A. Wilkinson, F. Fernandez-Trillo, *Eur Polym J* **2016**, *81*, 198.

[33] J. Olmsted, III, D. R. Kearns, *Biochemistry* **1977**, *16*, 3647.

[34] N. A. Jones, I. R. Hill, S. Stolnik, F. Bignotti, S. S. Davis, M. C. Garnett, *Biochim Biophys Acta* **2000**, *1517*, 1.

[35] F. Dai, W. Liu, *Biomaterials* **2010**, *32*, 628.

[36] O. Samsonova, C. Pfeiffer, M. Hellmund, O. M. Merkel, T. Kissel, *Polymers (Basel, Switz.)* **2011**, *3*, 693.

[37] E. Frohlich, *Int J Nanomedicine* **2012**, *7*, 5577.

[38] A. Albert, R. Goldacre, J. Phillips, *J Chem Soc* **1948**, 2240.

[39] H. K. Hall, *Journal of the American Chemical Society* **1957**, *79*, 5441.

[40] D. M. Perreault, L. A. Cabell, E. V. Anslyn, *Bioorgan Med Chem* **1997**, *5*, 1209.

[41] N. M. Luscombe, R. A. Laskowski, J. M. Thornton, *Nucleic Acids Research* **2001**, *29*, 2860.

[42] C. Scholz, E. Wagner, *J Control Release* **2012**, *161*, 554.

[43] M. Ahmed, R. Narain, *Biomaterials* **2011**, *32*, 5279.

[44] D. Fischer, H. Dautzenberg, K. Kunath, T. Kissel, *Int. J. Pharm.* **2004**, *280*, 253.

[45] H. Lv, S. Zhang, B. Wang, S. Cui, J. Yan, *Journal of Controlled Release* **2006**, *114*, 100.

[46] Z. Liu, Z. Zhang, C. Zhou, Y. Jiao, *Prog. Polym. Sci.* **2010**, *35*, 1144.

[47] A. Alshamsan, A. Haddadi, V. Incani, J. Samuel, A. Lavasanifar, H. Uludag, *Mol. Pharmaceutics* **2009**, *6*, 121.

[48] C. Lorenz, P. Hadwiger, M. John, H.-P. Vornlocher, C. Unverzagt, *Bioorg. Med. Chem. Lett.* **2004**, *14*, 4975.

[49] K. Nishina, T. Unno, Y. Uno, T. Kubodera, T. Kanouchi, H. Mizusawa, T. Yokota, *Mol. Ther.* **2008**, *16*, 734.

[50] J. H. Jeong, H. Mok, Y.-K. Oh, T. G. Park, *Bioconjugate Chem.* **2009**, *20*, 5.

6 Terpolymers mimicking cell penetrating peptides

6.1 CADY peptide

Cell-penetrating peptides, as their name suggests, can penetrate biological membranes thereby introducing biomolecules directly into the cytoplasm and can be utilized for intracellular targeting of, for example, mitochondria, nuclei or endosomes.[1] In 2008 Divita et al. developed a secondary amphiphatic cell penetrating peptide named CADY, which forms stable non-covalent complexes with siRNA and accomplishes efficient transfection of adherent and suspension cell lines with high potential for clinical use.[2] CADY is comprised of 20 amino acids (Ac-GLWRALWRLLRSLWRLLWRA-cysteamide, 2723.36 g/mol) and it was derived from the peptide ppTG1[3] by changing Phe^{3}, Leu^{7}, Leu^{18} and Lys^{4}, Lys^{8}, and Lys^{11} to indole-bearing Trp and guanidnium group-bearing Arg. This step was taken to improve the affinity towards siRNA and the interaction with the lipophilic segment of the plasma membrane. CADY adopts a helical conformation, which facilitates the segregation between charged moieties on one side and hydrophobic residues on the other, when interacting with siRNA. This ability allows the peptide to form stable complexes through electrostatic interactions, which enter the cells efficiently independent of the major endocytosis pathways.[4] The cationic charge provided by the guanidinium group of the arginines (GLW**R**AL-W**R**LL**R**SLW**R**LLW**R**A, 5 of 20 ≙ 25%) as well as the hydrophobicity of the incorporated tryptophanes (GL**W**RAL**W**RLLRSL**W**RLL**W**RA, 4 of 20 ≙ 20%) were referred to by the authors as the main reason for the success of CADY, while the remaining amino acids are filler molecules, which allow the peptide to take a helical form or provide solubility in water. While the use of cell-penetrating peptides as vectors for siRNA delivery has its merits, problems need to be acknowledged as well:[5]

(a) The small molar weight of these peptides leads to fast renal clearance from the blood stream.

(b) They are immunogenic due to interactions with serum proteins. They are also easily recognized by mechanisms of the innate as well as the adaptive immune system.

(c) If amino acids with the L-configuration are used as the building blocks, degradation *via* proteases occurs.

(d) Using peptides for the complexation of siRNA can lead to polyplexes with high dispersity.

(e) Solid phase synthesis of peptides allows for exact sequences, however, it requires a multitude of steps and although the process can be automatized, it still requires a long time to prepare the desired peptide.

If the functional peptide sequence can be reproduced in close approximation by a polymer, such issues may be addressed by utilizing the susceptibility of polymer-based scaffolds for additional modification strategies.

6.2 Cationic terpolymers composed of hydrophilic and hydrophobic monomers for gene delivery

Copolymers bearing indole groups have never been used in gene delivery and, based on the results of the CADY peptide, synergistic effects with guanidnium groups for a more efficient delivery of polynucleotides, which could exceed even the results of commercial transfection agents, are expected. Taking inspiration from the CADY peptide and utilizing hydrophobic and cationic monomers as starting materials in a batch copolymerization would circumvent the need for post-polymerization modification, but the statistical copolymerization of monomers with such a divergence in physicochemical properties is challenging. If all chains propagate concertedly due to the chosen polymerization conditions, the resulting polymers are near uniform in size, but a monomer's reactivity (rate of propagation) will affect the polymer's compostion.[6] Monomers with significantly different reactivity ratios, such as styrene and n-butyl acrylate or poly(ethylene glycol) methylether methacrylate and (2,2-dimethyl-1,3-dioxolane)methyl acrylamide, will not copolymerize statistically. Instead they will lead to gradient copolymers.[7-9] Hence, the initial task of this study is finding the reaction conditions, which ensure a controlled polymerization. In order to mimic the CADY peptide the monomers N-(2-hydroxypropyl) methacrylamide (HPMA), 3-guanidinopropyl methacrylamide (GPMA), and N-(2-(1H-indol-3-yl)ethyl) methacrylamide (IEMA) were chosen. Here, HPMA, similar to glycine, alanine and serine of the CADY peptide, functions as a spacer, which does not take part in the electrostatic interactions. GPMA and IEMA, on the other hand, mimic arginine and tryptophan respectively. In addition, HPMA was chosen to improve the solubilization of the polymer in aqueous solutions. This role was fulfilled by the primary amino groups of the lysines in the CADY peptide (G**L**WRA**L**-WR**LL**RS**L**WR**LL**WRA, 7 of 20 ≙ 35%). In future studies it is possible to mimic the

lysines by incorporating N-(3-aminopropyl) methacrylamide (APMA), but this investigation is aimed to attain a better understanding of the interplay between guanidinium groups and the indols.

6.3 Preparation of the desired terpolymers

The monomers IEMA, GPMA and HPMA were polymerized in a batch copolymerization using the RAFT polymerization technique, which not only tolerates all employed functional groups, but was also shown to achieve a high degree of polymerization control. The required monomer- and CTA concentrations were calculated by using the guidelines described in 1.4.

IEMA was synthesized by employing a Schotten-Baumann type reaction between methacryloyl chloride and the amine-bearing 2-(1H-indol-3-yl)ethan-1-amine (Figure 6.1), which allowed quick and facile formation of the necessary monomer. Following purification *via* column chromatography and characterization *via* NMR-spectroscopy, IEMA was used for the polymerization step.

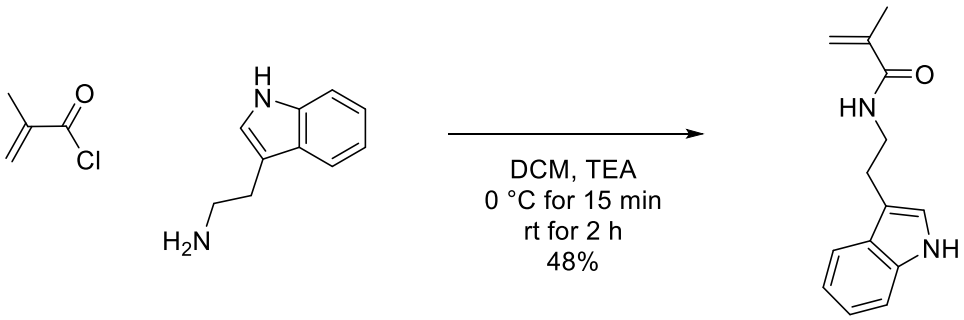

Figure 6.1. Synthesis of N-(2-(1H-indol-3-yl)ethyl)methacrylamide

The following procedure was employed, wherein the polymerization conditions were adjusted in an attempt to improve the results (Table 6.1 and 6.2).

The monomers were dissolved in degassed DMF under argon obtaining a monomer concentration of 1 M. The chain transfer agent and the initiator ACVA, dissolved in DMF, were added to the solution ($[M]_0/[CTA]_0 = 200$, $[CTA]_0/[Ini]_0 = 3$). Polymerization was then performed under argon at 80°C for 5 hours. Subsequent to the polymerization step the solvent was removed *in vacuo* and reaction mixture was washed with DCM before it was further purified *via* dialysis at 4°C and at pH 4 (hydrochloric acid) and

dried by the means of lyophilization. The polymers were then characterized *via* NMR-spectroscopy and SEC_{DMAc}.

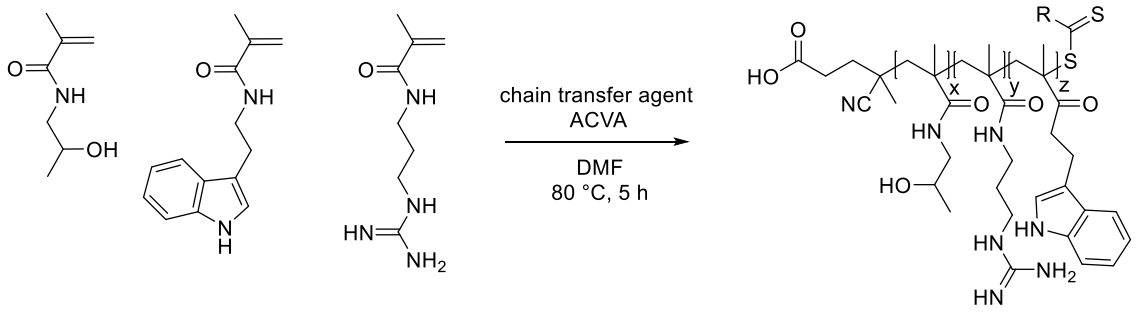

Figure 6.2. Synthesis pathway for HPMA-s-GPMA-s-IEMA

In order to establish the reaction conditions, initially only two monomers (HPMA and IEMA) were used. 4-Cyanopentanoic acid dithiobenzoate (CTP) as the chain transfer agent and pure DMF as the solvent of the polymerization led to well-defined structures (low Đ). However, their experimentally determined molar mass was well below the targeted value of 30 kDa (Table 6.1, blue). HPMA is known to pose problems in water-free RAFT polymerizations, since it stops propagating in such media at low conversions for unknown reasons. To circumvent this problem, water or aqueous buffer was added, which should have re-established propagation by quelling the growing polymers. For the purpose of optimization of the reaction conditions different amounts of water and 1 M acetate buffer were tested. Using a solvent mixture containing 5 vol% water as the medium of the polymerization (Table 6.1, red) did not lead to a significant effect. Increasing this amount to 20 vol% (Table 6.1, green) showed no evident success either, however, replacing the water with the buffer solution (Table 6.1, violet) improved the conversion, which is shown by the rise of the molar mass. Nevertheless, this approach entailed the undesired effect of broadening the dispersity far beyond the range of a controlled polymerizations (Đ > 2.22). Reducing the amount of utilized buffer to 10 vol% (Table 6.1, light blue) reduced the conversion, while still leading to broad distributions. It was not possible to increase the water content of the polymerization solution further, because it lead to precipitation of the IEMA monomer. Hence, the effect of polymerization duration was studied to address the low conversion. Using a solvent mixture containing 10 vol% water as the medium of the polymerization in addition to increasing the reaction time to 24 hours (Table 6.1, orange) showed the best results, where the SEC

determined molar mass was narrowly distributed and also coincided with the theoretical value. These polymerization conditions also allowed control over the amount of the incorporated monomers and the monomer content of the obtained polymers was more in line with the stoichiometry of the reaction. Nevertheless, a distinct difference could still be observed (27 mol% instead of the theoretical 20 mol%). Studying the solubility of the obtained polymers by respectively adding 1 mg of the sample to 5 mL of either water or DPBS solution provided further insights. This investigation demonstrated that IEMA content exceeding 20 mol% leads to the formation of water-insoluble polymers. Polymers, with pendant indole functional groups also seem to be susceptible to forming gels.[10] However, siRNA delivery agents are required to be soluble in water. Hence, 20 mol% IEMA content was set to be the upper limit. Incidentally, this is also the value, which was utilized in the CADY peptide.

Table 6.1. Molar mass, dispersity, monomer composition and solubilization profile (1 mg per 5 ml solvent at 21 °C) for each polymer prepared *via* RAFT polymerization; color-key: (blue) starting conditions, (red) 5 vol% water added, (green) 20 vol% water added, (violet) 20 vol% acetate buffer added, (light blue) 10 vol% acetate buffer added and (orange) 10 vol% water added, reaction time increased to 24 h

polymer[a]	monomer[b] [mol%]		SEC_{DMAc}			Solubility	
	HPMA	IEMA	M_n	M_w	Đ	H_2O	DPBS
$HPMA_{95\%}$-s-$IEMA_{5\%}$	79	21	21500	24000	1.11	+	+
$HPMA_{90\%}$-s-$IEMA_{10\%}$	76	24	21500	24000	1.19	+	+
$HPMA_{80\%}$-s-$IEMA_{20\%}$	65	35	21500	25000	1.17	+	+
$HPMA_{95\%}$-s-$IEMA_{5\%}$	79	21	20000	25000	1.23	+	+
$HPMA_{90\%}$-s-$IEMA_{10\%}$	78	22	20000	23000	1.16	+	+
$HPMA_{80\%}$-s-$IEMA_{20\%}$	56	44	25500	27500	1.22	-	+
$HPMA_{95\%}$-s-$IEMA_{5\%}$	81	19	22000	25000	1.14	+	+
$HPMA_{90\%}$-s-$IEMA_{10\%}$	74	26	19000	23000	1.18	-	+
$HPMA_{80\%}$-s-$IEMA_{20\%}$	66	34	24500	26500	1.10	-	-
$HPMA_{95\%}$-s-$IEMA_{5\%}$	73	27	35000	94000	2.66	+	+
$HPMA_{90\%}$-s-$IEMA_{10\%}$	62	38	27500	61000	2.22	-	-
$HPMA_{80\%}$-s-$IEMA_{20\%}$	45	55	24500	96000	2.32	gel	gel
$HPMA_{90\%}$-s-$IEMA_{10\%}$	42	58	19000	45000	2,23	-	-
$HPMA_{80\%}$-s-$IEMA_{20\%}$	73	27	31000	40000	1.27	gel	-

[a]polymer with the expected monomer composition defined by stoichiometry; [b]experimentally determined monomer composition (NMR);

Considering the large influence of the RAFT agent on the polymerization, since it needs to be compatible with all used monomers (section 1.4), the viability of 4-cyanopentanoic acid dithiobenzoate (Table 6.2, blue) and 4-((((2-carboxyethyl)thio) carbonothioyl) thio)-4-cyanopentanoic acid (Table 6.2, red) to control the RAFT copolymerization of these two largely different monomers, was compared at 10 vol% water and the reaction time of 5 hours. The hydrolytically more stable CTA 4-((((2-carboxyethyl)thio) carbonothioyl) thio)-4-cyanopentanoic acid, which allowed excellent polymerization control in Chapter 5, is poorly suited for these conditions. The detected molar masses remained well under the theoretical value and their distribution was comperatively broad (Đ > 1.33). 4-Cyanopentanoic acid dithiobenzoate, on the other hand, demonstrated its reliability to reproduce excellent polymerization control.

Table 6.2. Molar mass, dispersity, monomer composition and solubilization profile for each polymer prepared *via* RAFT polymerization

polymer[a]	SEC_{DMAc}		
	M_n	M_w	Đ
$HPMA_{95\%}$-s-$IEMA_{5\%}$	19000	21000	1.13
$HPMA_{90\%}$-s-$IEMA_{10\%}$	23500	25500	1.08
$HPMA_{80\%}$-s-$IEMA_{20\%}$	20500	22000	1.08
$HPMA_{95\%}$-s-$IEMA_{5\%}$	15000	20000	1.37
$HPMA_{90\%}$-s-$IEMA_{10\%}$	15000	20000	1.37
$HPMA_{80\%}$-s-$IEMA_{20\%}$	18500	24500	1.33

[a)]polymer with the expected monomer composition defined by stoichiometry;

Having found the reaction conditions (CTP as the CTA, ACVA as the initiator, DMF with 10 vol% water as the solvent, 80 °C reaction temperature and a polymerization duration of 24 h), which facilitate sufficient polymerization control, the synthesis of HPMA-s-GPMA-s-IEMA terpolymers was performed (Table 6.3). Here, the theoretical molar mass was reduced to 15 kDa, to achieve a closer approximation of the CADY peptide. The detected molar masses of the polymers deviated from the theoretical value by 13%, which might have been caused by different reasons. The hydrodynamic characterization of cationic copolymers in Chapter 5 has shown that the incorporation of guanidinium groups leads to an increase in the polymer's density, which in turn changes the elution profile. Therefore, the polymers are observed to be larger. Another reason might

be the partial aminolysis of the terminal dithioester, but since no increase in dispersity was observed, this case can be ruled out.

Table 6.3. Molar mass, dispersity and monomer composition of the terpolymers

polymer[a]	**monomer**[b] **[mol%]**			**SEC_{DMAc}**		
	HPMA	GPMA	IEMA	M_n	M_w	Đ
$HPMA_{85\%}$-s-$GPMA_{5\%}$-s-$IEMA_{10\%}$	83	2	15	17000	19000	1.11
$HPMA_{80\%}$-s-$GPMA_{10\%}$-s-$IEMA_{10\%}$	82	11	7	17000	18500	1.08

[a)]polymer with the expected monomer composition defined by stoichiometry;

The calculation of the monomer composition was less trivial in these terpolymers, since the NMR-peaks of interest are superimposed. To better evaluate the results and properly associate the integrals of the peaks to the respective protons of the polymers a HSQC-NMR spectrum was measured in D_2O (Figure 6.3). Here, it is possible to assign the sharp singlet at 3.92 ppm to the proton geminal to the hydroxyl group of HPMA, while the segment 3.50 – 2.00 ppm encompasses a total of 8 protons. Two of these belong to HPMA, while four could be assigned to GPMA and the remaining ones belong to IEMA. Putting also the aromatic signals belonging solely to IEMA into relation, it is possible to estimate the monomer composition. The used conditions allowed excellent control not only over the polymer molar mass, but also over the monomer composition. Having met the challenge of finding the polymerization protocol, which allows the statistical copolymerization of monomers with such a divergence in physicochemical properties, it is possible to prepare both, a CADY mimic as well as a indole- and guanidinium group containing polymers, which can be then tested in regard to their ability to deliver polynucleotides.

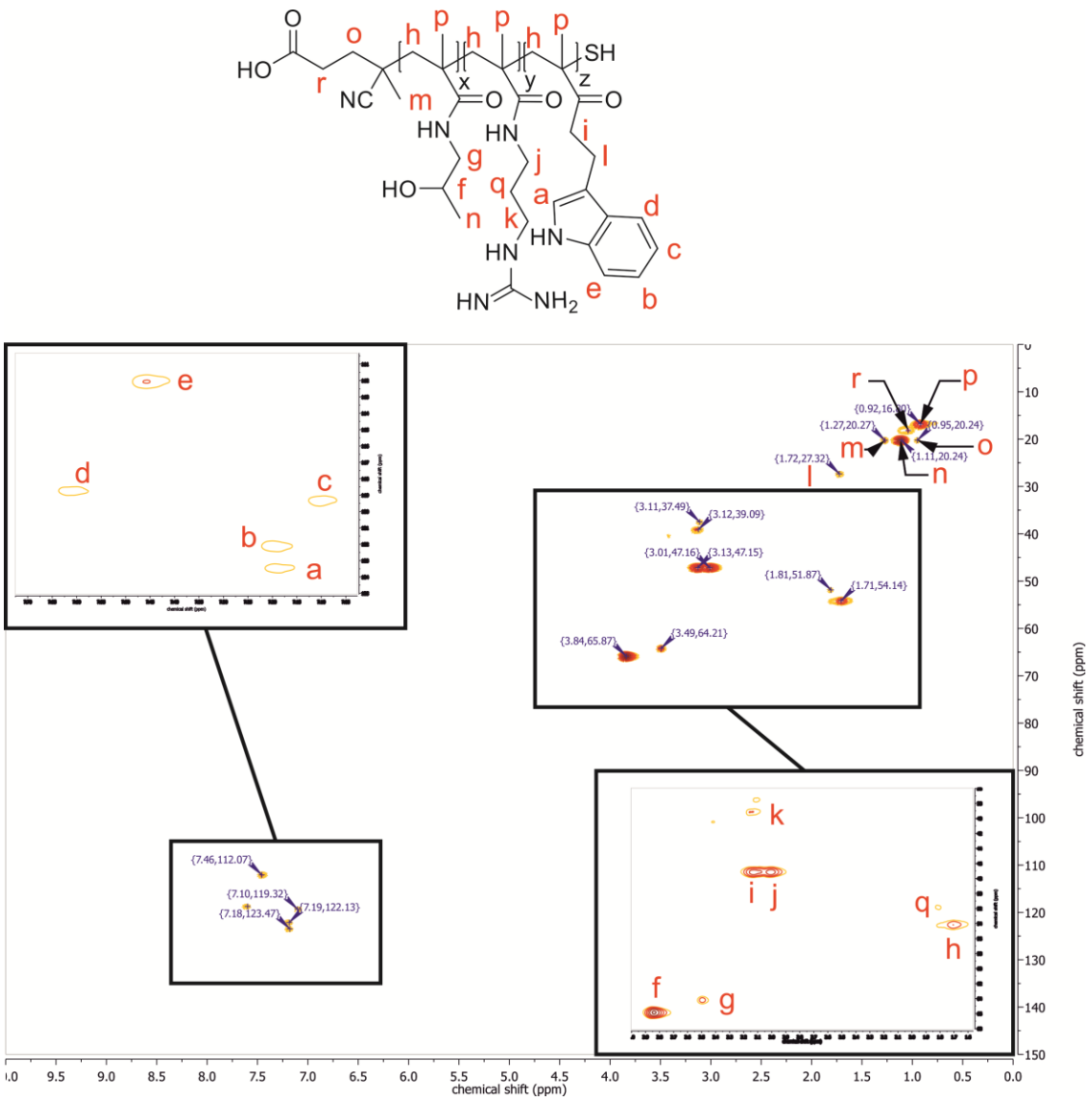

Figure 6.3. HSQC-NMR spectrum of $HPMA_{80\%}$-s-$GPMA_{10\%}$-s-$IEMA_{10\%}$ in D_2O at 313 K (600 MHz) with assigned protons.

6.4 Transfection efficacy based on luciferase expression in CHO-K1 cells

Guanidinium group bearing polymers have been shown in Chapter 3 and 5 to complex polynucleotides even if the polymer in question had a low mol% of the GPMA monomer. It is not expected that the addition of 10 mol% of IEMA will drastically affect or even diminish said capacity for complexation. Hence, it was decided to forgo the binding study and immediately proceed to test the transfection efficacy of the indol group-bearing polymers. For that purpose, a bioluminescence assay according to Chapter 5 was conducted to determine the polymers' ability not only to condense pDNA, but also to deliver its plasmid payload into the cytosol while conserving its integrity and functionality. If the expression of luciferase is not induced, it will not be possible to measure luminescence, which thereby directly correlates to the transfection success.

In Chapter 4 the introduction of lipophilic moieties was shown to drastically improve the ability of the respective polymer to delivery polynucleotides into cells. This modification strategy was even applicable for never before transfected cell lines. Hence, the copolymerization of the lipophilic monomer IEMA is expected to enhance the transfection properties of the polymeric gene delivery agent, in particular, if compared to the results of the statistical copolymers with 5 and 10 mol% GPMA, which were discussed in Chapter 5. They were not able to induce luminescence in CHO-K1 cells.

Figures 6.4 and 6.5 depict the graphical evaluation of the transfection results of the performed transfection study for $HPMA_{85\%}$-s-$GPMA_{5\%}$-s-$IEMA_{10\%}$ and $HPMA_{80\%}$-s-$GPMA_{10\%}$-s-$IEMA_{10\%}$, which was done in cooperation with Leon Zartner (Prof. Dr. Dagmar Fischer, Institute of Pharmacy, Friedrich Schiller University Jena). The protein concentration was incorporated into both of these figures, too, to have a first indication of the toxicity of the polymers and the used N/P ratio. If the viability of the cells were affected by the utilized polymer concentrations, a drop of the protein concentrations would have been observed, since fewer living cells would have remained adherent during the washing steps. None of the investigated samples showed signs of toxicity.

In Figure 6.4 the transfection efficacy of the two terpolymers is compared at different N//P ratios. In case of $HPMA_{85\%}$-s-$GPMA_{5\%}$-s-$IEMA_{10\%}$, at the highest used N/P ratio was it possible to induce luminescence in CHO-K1 cells. Although this result *prima facie* appears to be insignificant, it is nevertheless extraordinary. This terpolymer has only traces of the GPMA monomer (2 mol%) and it is still able to safely deliver its car-

go into the cells. Similar results in respect to luciferase expression were achieved by statistical HPMA-s-GPMA copolymers only at much higher contents of the cationic comonomer (40 mol%). The results of increasing the GPMA content of the terpolymer to 9 mol% and simultaneously reducing the IEMA content from 15 to 7 mol% are immediatelly evident in Figure 6.4. The transfection was improved for all tested N/P ratios due to the higher cationic charge density, but the reduced lipophilicity impacted the transfection reliability, which is linked to the bigger error bars.

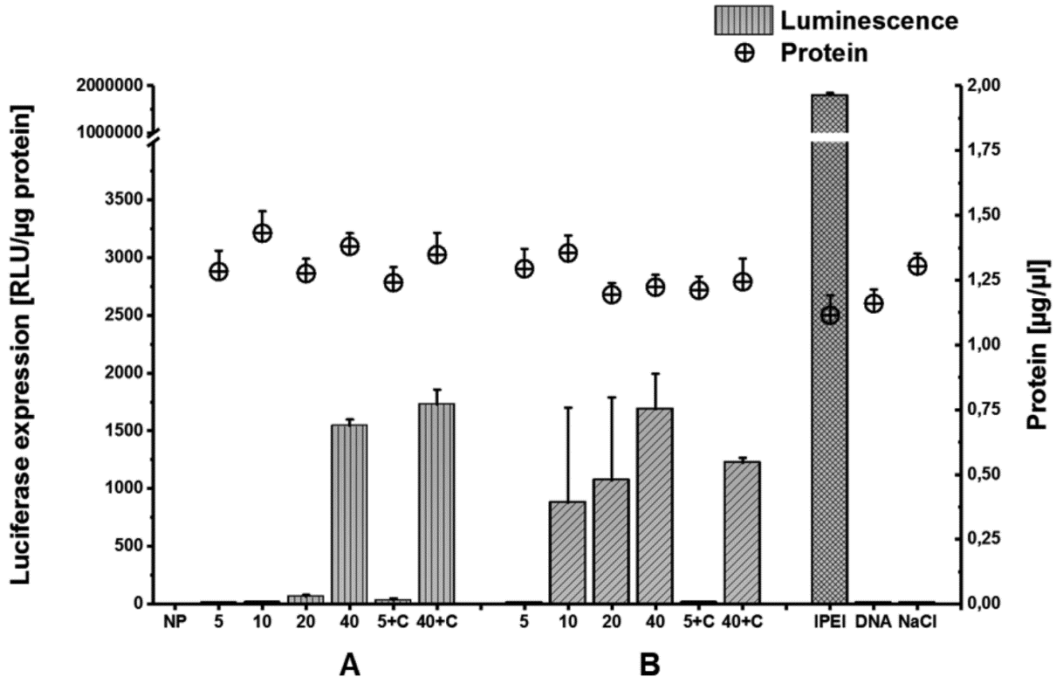

Figure 6.4. Protein content and luminescence due to luciferase expression in CHO-K1 cells after treatment with polyplexes, which were formed at different N/P ratios and wherein either (A) $HPMA_{85\%}$-s-$GPMA_{5\%}$-s-$IEMA_{10\%}$ or (B) $HPMA_{80\%}$-s-$GPMA_{10\%}$-s-$IEMA_{10\%}$ were used as the binding partner for the functional pDNA. The transfection experiments referred to as either "5+C" or "40+C" have been performed using the N/P ratio of either 5 or 40 and in the presence of the endosomal/lysosomal disrupting agent Chloroquine. Linear PEI (lPEI), uncomplexed DNA (DNA) and a sodium chloride solution were used as controls.

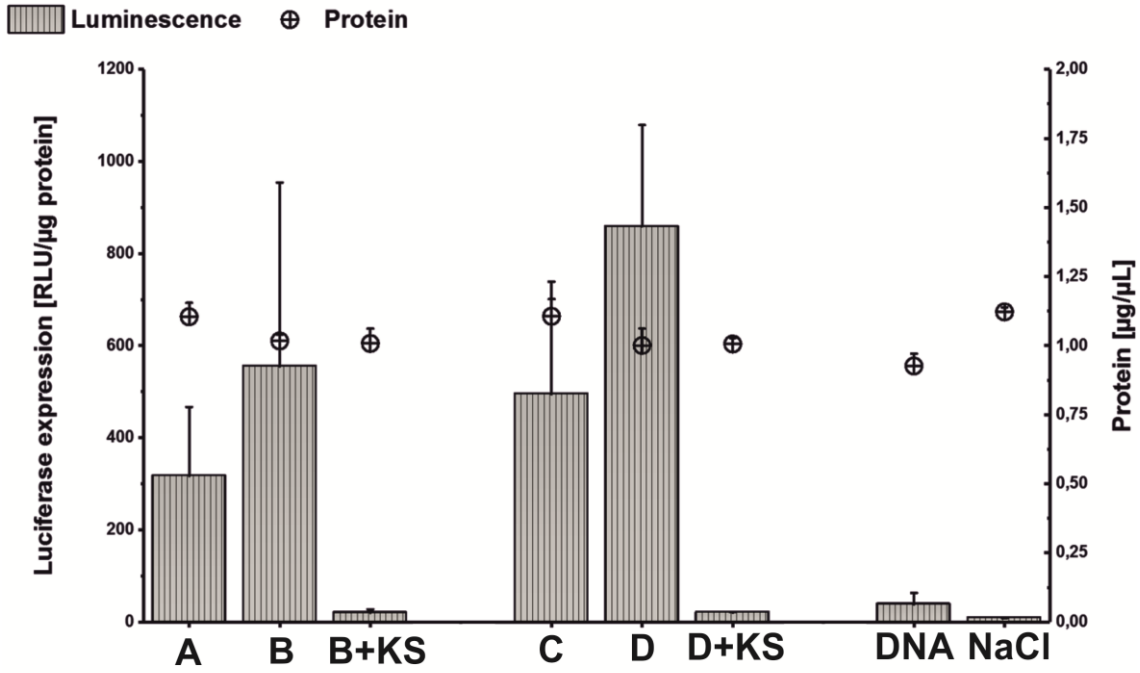

Figure 6.5. Protein content and luminescence due to luciferase expression in CHO-K1 cells after treatment with polyplexes, which were formed between either (A) $HPMA_{95\%}$-s-$GPMA_{5\%}$, (B) $HPMA_{85\%}$-s-$GPMA_{5\%}$-s-$IEMA_{10\%}$, (C) $HPMA_{90\%}$-s-$GPMA_{10\%}$ or (D) $HPMA_{80\%}$-s-$GPMA_{10\%}$-s-$IEMA_{10\%}$ and functional pDNA. The addition of the specification of "+KS" refers to the transfection being conducted at 4 °C. Uncomplexed DNA (DNA) and a sodium chloride solution were used as controls.

Comparing the transfection results of the two terpolymers with the results of the HPMA-s-GPMA copolymers possessing similar cationic charge densities, which have been described in Chapter 5, *i.e.* $HPMA_{95\%}$-s-$GPMA_{5\%}$ and $HPMA_{90\%}$-s-$GPMA_{10\%}$, immediate differences in terms of efficacy were observed. Both terpolymers (Figure 6.5 B and D) induced double or triple values of the luciferase expression, which was observed for the statistical copolymers (Figure 6.5 A and C). In combination with the observations made in Figure 6.4 it can be stated that the introduction of indole group bearing monomers into cationic polymers for gene delivery drastically improves their ability to transfect cells. This strategy can be applied to achieve delivery efficacies observed only for polymers with high cationic charge densities at much lower cationic comonomer contents and thereby address the toxicity issues, which are usually associated with this class of gene delivery agents. The reason for the high transfection efficacy of the terpolymers is their mode of delivery. Contrary to the copolymers, which have been used in Chapters 3 and 5, the two terpolymers, similar to the TPP modified diblock co-

polymer of Chapter 4, were able to cross the plasma membrane without relying on endosomal transport. The known endosomal/lysosomal disrupting agent Chloroquine (Figure 6.4) did not affect the transfection efficacy of the terpolymers significantly. In case of $HPMA_{85\%}$-s-$GPMA_{5\%}$-s-$IEMA_{10\%}$, Chloroquine even appeared to have a positive effect. Only low luminescence was detected, if the transfection experiments were performed at 4 °C (Figure 6.5, samples specified with "+KS"), which blocks fluid-phase pinocytosis and receptor-mediated endocytosis. Hence, it is concluded that the terpolymers are internalized by means of clathrin-mediated, caveolae-mediated, or clathrin and caveolae-independent pinocytosis. Direct transcytosis would have been ascertained, if their transfection efficacy was not affected by the low temperatures.

The luciferase expression assay provided a clue to the potential of indole-functionalized gene delivery agents. Adjusting the molar ratios of the cationic and the lipophilic comonomers will address both the toxicity as well as the uptake efficacy issues, which are inherent to polymeric gene delivery agents.

6.5 Cytotoxicity

Although during the luciferase expression assay toxicity of the polyplexes was *prima facie* not an issue for the either of the two terpolymers, the measured protein concentration after the transfection experiment was only a first indication of the polymers' toxicity. In order to quantify the polymers' cytotoxicity, a MTT-assay was employed (Figure 6.6). Here, CHO-K1 cells were incubated with $HPMA_{85\%}$-s-$GPMA_{5\%}$-s-$IEMA_{10\%}$, $HPMA_{80\%}$-s-$GPMA_{10\%}$-s-$IEMA_{10\%}$, $HPMA_{80\%}$-s-$GPMA_{20\%}$ or $HPMA_{80\%}$-g-$GPMA_{20\%}$ at a concentration of 500 µg/mL. The two copolymers, which had at least twice the amount of cationic charges, were used as a reference. In Figure 6.6 a dotted line at the relative viability of 70% was included. According to DIN ISO 10993-5:2009, samples exhibiting a relative viability equal to or higher than this value, are regarded as non-toxic.

Contrary to the terpolymers, the two copolymers, irrespective of being statistical or gradient copolymers, once again demonstrated a lack of cytotoxicity (Figure 6.6). Due to the low cationic charge density of the terpolymers, they were expected to be even less toxic to cells. Nevertheless, it is apparent that the use of indole-functionalized polymers at high concentrations affects cells adversely. The reason for this effect can only be speculated. For example, it can be hypothesized that the terpolymers reduce the fluidity of the plasma membrane, thereby destabilizing its integrity due to strong interactions

between the lipophilic monomers and the inner segments of the membrane. An extended biochemical characterization is required to make a detailed assessment of the toxicity of the terpolymers. However, the MTT-assay has shown with certainty that the cationic charge density is not the only reason for the high cytotoxicity.

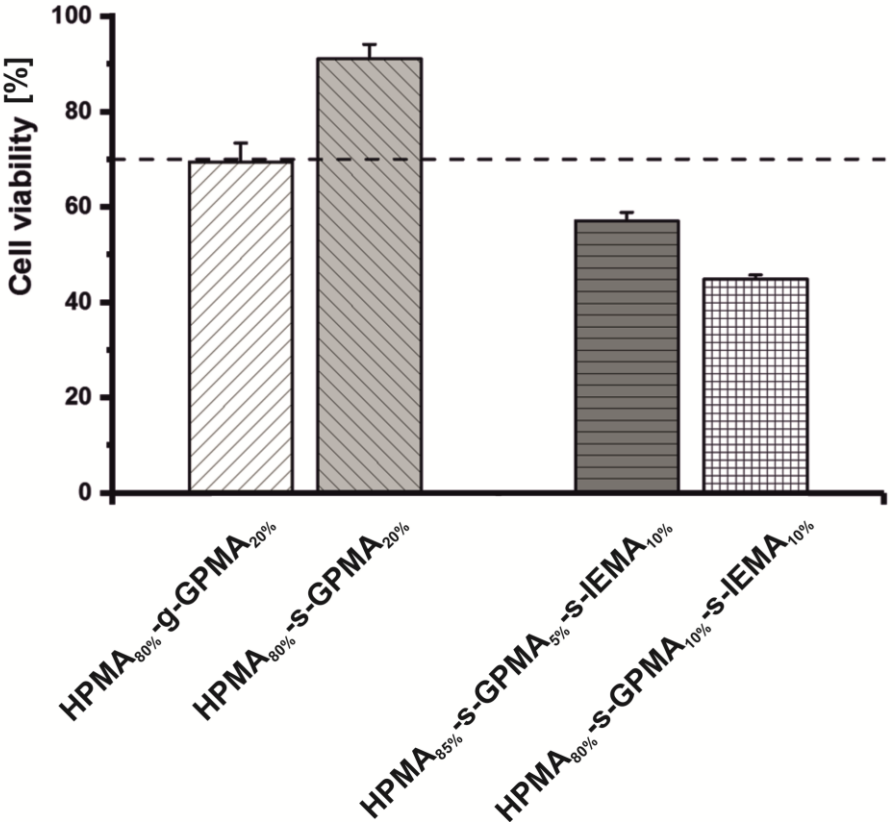

Figure 6.6. Cell viability CHO-K1 cells in [%]. In each case the cells were treated with a polymer concentration of 500 µg/mL. The dotted line refers to the viability value of 70%.

The present chapter concerned gene delivery *via* statistical cationic terpolymers consisting of hydrophilic as well as hydrophobic monomers mimicking the amino acid sequence of the cell penetrating peptide CADY. Since uncharged HPMA, cationic GPMA and lipophilic IEMA, i.e. monomers with different solubilization profiles, were used as building blocks, an extensive trial-and-error approach was necessary to find ideal condi-

tions allowing control over a terpolymers' molar mass and the monomer composition (batch copolymerization *via* RAFT). Following the discovery of ideal polymerization conditions, the indole- and guanidinium group containing polymers were tested in regard to their ability to deliver polynucleotides in a similar fashion described for Chapter 5. With respect to the transfection results three general statements can be made:

(1) The HPMA-s-GPMA-s-IEMA terpolymers possess an improved transfection efficacy in comparison to HPMA-s-GPMA copolymers, i.e. copolymers lacking hydrophobic indole groups, with similar cationic charges.
(2) The cationic charge, similar to the results of Chapter 5, affects the transfection efficacy proportionally. Incorporating more GPMA monomers has led to substantially higher transfection efficacies made visible by higher luminescence values. In addition, similar to the results of the gradient HPMA-g-GPMA copolymers in Chapter 5, low N//P ratios were required.
(3) The terpolymers deliver pDNA by means of fluid-phase pinocytosis. Chloroquine, a known endosomal as well as lysosomal disrupting agent, did not affect the terpolymers' ability to bypass the plasma membrane of CHO-K1 cells. Only shutting down all energy dependent mechanisms in the cell by performing the transfection experiment at 4 °C significantly reduced their ability to transfect CHO-K1 cells.

However, in spite of the exceptional transfection results, the terpolymers are strongly toxic to cells. This property, however, was to be expected, since strong cytotoxicity is common among gene delivery agents, which are not only hydrophobic, but also cationic (e.g. Lipofectamine). In fact, it has been theorized that the efficacy of these delivery agents is improved because they are toxic to cells, for example, by destabilizing the plasma membrane. In spite of the toxicity issue, the terpolymers have been shown to be highly efficient to delivery and release polynucleotides into cells. It is strongly recommended to investigate even higher cationic charge densities. The terpolymers performed better than copolymers described in the previous chapters and the trend indicates that they might even perform better than commercial delivery agents at higher GPMA mol% ratios.

Chapter 6 represents the last one on gene delivery agents. The next chapter does not relate to delivery agents for gene therapy, however, it demonstrates that the findings of this thesis can be applied in other fields of study as well. In particular, it has been re-

peatedly observed that guanidinium group bearing polymers not only facilitate exceptionally strong electrostatic interaction with polynucleotides, but also induce quenching in fluorescent dyes. A sensor based on a complexation cascade for the detection of poisonous compounds with an exceptionally low detection limit was devised, which takes full advantage of both of these properties.

6.6 References

[1] I. Tabujew, M. Lelle, K. Peneva, **2015**, *16*, 59.

[2] K. Konate, A. Rydstrom, G. Divita, S. Deshayes, *Curr. Pharm. Des.* **2013**, *19*, 2869.

[3] K. Rittner, A. Benavente, A. Bompard-Sorlet, F. Heitz, G. Divita, R. Brasseur, E. Jacobs, *Molecular Therapy* **2002**, *5*, 104.

[4] S. Deshayes, M. C. Morris, G. Divita, F. Heitz, *Biochimica et Biophysica Acta (BBA) - Biomembranes* **2006**, *1758*, 328.

[5] E. Koren, V. P. Torchilin, *Trends Mol. Med.* **2012**, *18*, 385.

[6] P. Gaspard, *Philos. Trans. R. Soc., A* **2016**, *374*, 20160147/1.

[7] C. M. Dettmer, M. K. Gray, J. M. Torkelson, S. T. Nguyen, *Macromolecules* **2004**, *37*, 5504.

[8] G. Chambard, B. Klumperman, *ACS Symp. Ser.* **2000**, *768*, 197.

[9] N. A. A. Rossi, Y. Zou, M. D. Scott, J. N. Kizhakkedathu, *Macromolecules (Washington, DC, U. S.)* **2008**, *41*, 5272.

[10] A. Masotti, F. Moretti, F. Mancini, G. Russo, N. Di Lauro, P. Checchia, C. Marianecci, M. Carafa, E. Santucci, G. Ortaggi, *Bioorg. Med. Chem.* **2007**, *15*, 1504.

7 Guanidinium group bearing homopolymers for ultra-sensitive detection of malathion

The use of organophosphorus pesticides (OPs) as insecticides has increased much in agricultural and non-agricultural fields due to their relatively low persistence under natural conditions, low cost and high efficacy in insect eradication. However, the extensive use of OPs led to severe contamination of water, soil and agricultural products, thereby raising food safety issues.[1] The presence of OPs in food and water poses a danger to human health, since these compounds irreversibly inhibit the enzyme acetylcholinesterase, which is essential for the central nervous system. This inhibition leads to cholinergic dysfunction and paralysis.[2] In rural areas of developing countries poisoning with OPs leads to more than 200,000 deaths annually.[3] The broad-spectrum insecticide malathion (Figure 7.1) is one of the most widely employed OPs and its widespread use necessitates the development of detection strategies, which are facile, rapid, selective and highly sensitive, in order to discover contaminations and protect the populace. Although malathion is only mildly toxic to mammals, it is strongly poisonous to aquatic life forms as well as bees, whose population is on the decline.

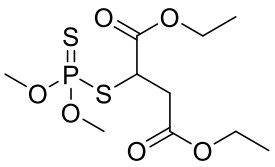

Figure 7.1 Malathion

The conventional methods to detect trace amounts of this compound, which include gas chromatography-mass spectrometry or high performance liquid chromatography, are time consuming, expensive, require sophisticated instrumentation, complex sample preparation and trained personnel. Hence, they are difficult to utilize for field test in rural areas.[4] For the detection of OPs other analytical methods have been suggested. They include electrochemical analysis, immunochips and enzyme-linked immunosorbent assays, which use acetylcholinesterase or organophosphorus hydrolase, as the recognition element.[5, 6] However, these enzyme-based sensors, which are the current standard, are not specific, because other substances including carbamates and heavy metals also inhibit their function leading to falsely positive results. In addition, enzyme-

and antibody-based analytical methods suffer from the short shelf life of their components. Aptamers have emerged as promising biological recognition elements. They are short single-stranded RNA or DNA oligonucleotides with very high as well as specific affinity towards a certain target compound (dissociation constants usually in the pico- to nano-molar range), which can include ions, drugs, toxins, peptides, proteins, viruses, bacteria, and cells.[7] Aptamers possess other advantages, such as high thermal stability and rapid large scale synthesis at low production costs.[8] The commonly used biosensors for the detection of potentially harmful substances usually correlate the binding of the detection unit to fluorescence to indicate the presence of an analyte.[9] Compared to fluorescent proteins or organic dyes, quantum dots (QDs) offer more viability due to their high quantum yields, broad absorption spectra, narrow and symmetric size-tunable emission and strong resistance to photobleaching.[10, 11] The quantum yield and stability of QDs, can be tuned by the introduction of another metal alloy (core-shell QDs)[12] and most of the analytical methods, which are based on QDs, operate by a mechanism of fluorescence resonance energy transfer (FRET)[13], but this makes them susceptible to quenching. Guanidinium group-bearing polymers have been shown to induce strong quenching in FRET-labeled compounds without affecting their stability in solution.[14, 15]

In cooperation with DR. R. K. Sharma (Department of Chemistry & Centre for Advanced Studies in Chemistry, Panjab University) a detection platform with high malathion specificity was developed to address the need of easily accessible strategies for pesticide detection. The concept of this nanoprobe relies on the spectral changes arising in negatively charged CdTe/CdS core-shell QDs in the presence or absence of malathion (Figure 7.2). The electrostatic interactions between the anionic QDs and the positively charged poly(N-(3-guanidinopropyl) methacrylamide) homopolymer (PGPMA) lead to the quenching of the fluorescence signal of the QDs. If malathion is not present, the negatively charged aptamer binds the polymer chains in the solution and, as a consequence of the electrostatic interactions between aptamer and polymer, the fluorescence of QDs remains unaffected. However, in the presence of malathion, PGPMA is released from its polyplex with the aptamer due to the higher affinity of the aptamer towards malathion (formation of Mal-Apt complexes). Consequently, sufficient polymer is available to interact with the QDs and thereby induce quenching. The extent of quenching is proportional to the availability of the polymer, which in turn is dependent on the

concentration of malathion. Thus, the designed platform can be used for the quantitative sensing of malathion depending upon the degree of quenching.

The herein presented sensor, which is based on QDs and a polymer-aptamer nanoprobe for the detection of Ops, is the first of its kind.

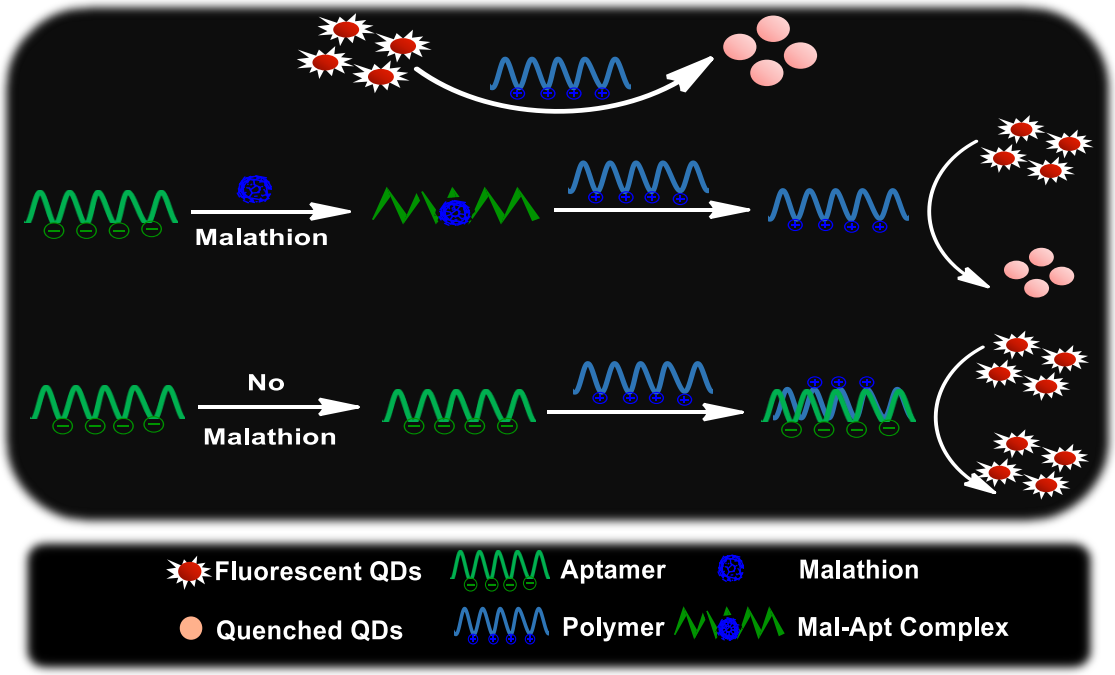

Figure 7.2 Schematic representation of the working principle for the detection of malathion. (top) PGPMA induces quenching of the FRET signal of the QDs, (middle) the fluorescence of the QDs is quenched in the presence of malathion due to the availability of the polymer, (bottom) in the absence of malathion PGPMA is bound to the aptamer and cannot affect the fluorescence of QDs.

7.1 Preparation of the PGPMA homopolymer

To fulfill the requirements of the quencher component, which include solubility in aqueous media as well as a high cationic charge density in a broad pH range, it was chosen to utilize PGPMA. This polymer structure, which has proven FRET-signals quenching properties[14, 15], bears side chain pendant guanidinium groups. These remain charged over a wide pH range, which is reflected in the high pKa value (12.48) of its protonated counterpart.[16] The positive charges provide facile solubilization in water. Therefore, PGPMA homopolymers can ensure the desired quenching of the fluorescence signal of the QDs and pronounced interaction with the aptamer moiety, which in turn can restore the signal of the QDs.

PGPMA was synthesized in analogy to the aRAFT polymerization of PHPMA (section 3.1). However, in this case, longer reaction times as well as a higher propagation temperature were chosen to improve conversion. Rapid decomposition of the conventional chain transfer agent 4-cyano-4-((phenylcarbonothioyl)thio)pentanoic acid in these conditions made its substitution with the hydrolytically stable 4-((((2-carboxyethyl)thio)carbonothioyl)thio)-4-cyanopentanoic acid necessary (Figure 7.3). Size-exclusion chromatography (SEC) with either water or dimethylacetamide (DMAc) as the eluent confirmed a narrow dispersity ($Đ_{DMAc}$ = 1.27, $Đ_{water}$ = 1.04), but, due to the cationic nature of the homopolymer, different polymer lengths were determined depending on the eluent of the SEC ($M_n(SEC_{DMAc})$ = 10 kDa, $M_n(SEC_{water})$ = 5.5 kDa), which reflects the differences in solubilization of the said polymer in different solutions (Table 7.1). Using ^{1}H-NMR spectroscopy complete removal of unreacted monomers was confirmed (section 9.7.3.3).

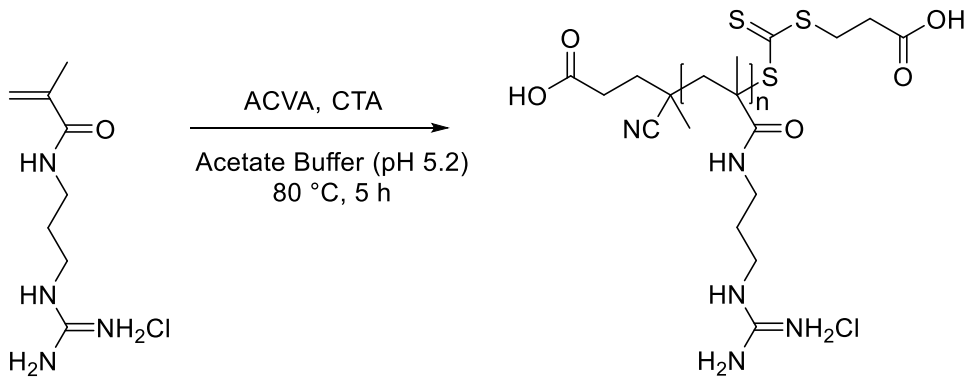

Figure 7.3. Synthesis of PGPMA

Table 7.1. Theoretical and experimentally determined molar mass in [g·mol^{-1}] and dispersity (Đ) of PGPMA

	Mn, theoa	SECDMAc		SECwater	
	[g·mol^{-1}]	Mn [g·mol^{-1}]	Đ	Mn [g·mol^{-1}]	Đ
PGPMA	14000	10000	1.27	5500	1.04

[a)]The theoretical molar mass was calculated using the Formula $M_{n,th} = ([M]_0/[CTA]_0) \cdot M_{w,monomer} \cdot \rho + M_{w,CTA}$, while complete conversion wasassumed

7.2 Composition of the sensor

Having chosen the components of the sensor, it was necessary to determine their optimal composition, on order to ensure functionality. These factors, which are critical to the performance of the biosensor, were examined in cooperation with Dr. R. K. Sharma (Department of Chemistry & Centre for Advanced Studies in Chemistry, Panjab University), who provided the water soluble CdTe/CdS core shell QDs with a sharp fluorescence emission around 575 nm (Figure 7.4).

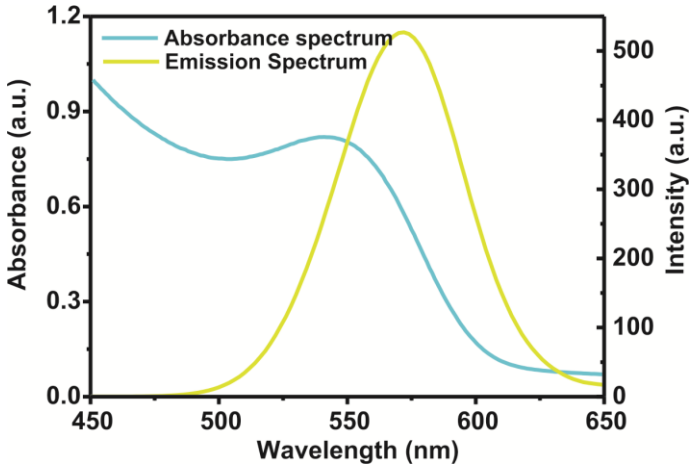

Figure 7.4. Absorbance and emission spectrum of the water soluble CdTe/CdS QDs.

Initially, the optimal PGPMA concentration for efficient quenching of the QDs emission was investigated by incubating a fixed concentration of QDs with increasing amounts of the polymer (0.01 to 1 mg/mL). The correlation between the concentration of PGMA and the decreasing fluorescence signal is depicted in Figure 7.5.

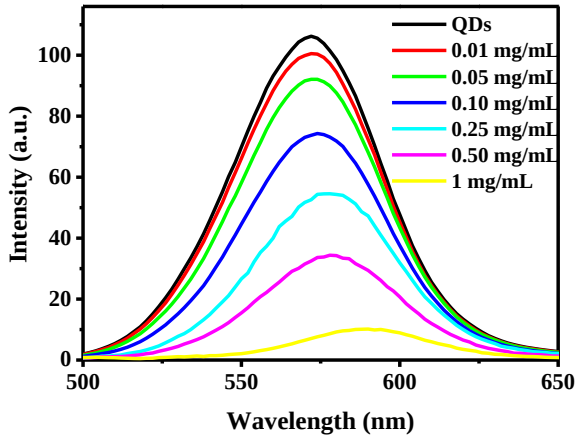

Figure 7.5. Quenching of the fluorescence signal in the presence of different PGP-MA concentrations. The excitation wavelength was 370 nm with excitation and emission slit width 5 nm and 10 nm respectively.

The optimal polymer concentration, which led to sufficient quenching of the signal, was 0.5 mg/mL. Having determined this crucial value, the aptamer concentration, which is required to retain the fluorescence of the QDs, was investigated using the range 0 to 20 µM (Figure 7.6).

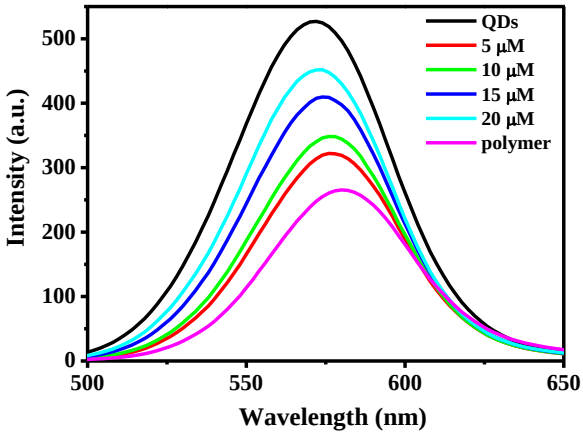

Figure 7.6. Restoration of the fluorescence signal in the presence of PGPMA with a concentration of 0.5 mg/mL by increasing the aptamer concentration.

Employing the aptamer at a concentration of 20 µM almost fully restored the fluorescence signal of the QDs. Hence, it was decided to use this aptamer concentration for assessing the analytical ability of the aptasensor. The detection of malathion was therefore performed by using the following procedure:

10 µL of a 20 µM aptamer solution was mixed with 70 µL of a malathion sample, diluted with 100 µL phosphate buffer and incubated for 40 min at room temperature. Subsequently, 30 µL of the PGPMA solution with a concentration of 0.5 mg/mL was added to the sample solution. Following an incubation period of 20 min at ambient temperature, 200 µL of a QDs solution were added, which was followed by fluorescence measurements. The stock solution of malathion (12 mM) was prepared in acetone and stored at 4 °C. Series dilutions of malathion were then prepared in phosphate buffer (pH 7.32).

7.3 Selectivity

The specificity of the biosensor was assessed in the presence of various non-target pesticides such as atrazine, chlorsulfuron, chlorpyrifos, 2,4-D and diuron, which are also widely employed in agriculture. Here, fluorescence intensities before (F_0) and after the addition of malathion (F) were measured. While the interfering pesticides were used in 1000 times higher concentrations (1µM) than malathion (1 nM), extensive fluorescence quenching was detected only in the case of malathion and no noticeable cross reactivity was seen with non-target pesticides, due to the intrinsic specificity of the aptamer employed in this study (Figure 7.7). These results clearly establish the relevance of proposed strategy for malation detection.

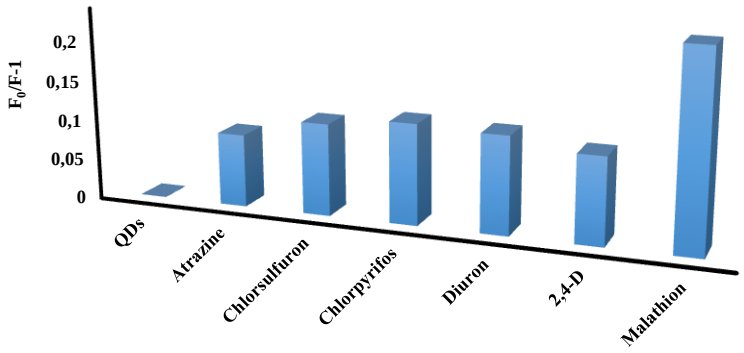

Figure 7.7. Fluorescence response of the nanoprobe towards different non-target pesticides: 1 µM of other pesticides and 1 nM malathion. F_0 is the fluorescence intensity in the absence and F is the fluorescence intensity in the presence of malathion. The concentration of polymer and aptamer was kept constant at 0.5 mg/mL and 20 µM respectively.

7.4 Limit of detection

To determine the sensitivity of the designed malathion sensor, the variation in fluorescence signal of the QDs in the presence of different malathion concentrations ranging from 0.01 nM to 1 µM was investigated with a sample size of n = 3 per concentration. As intended in the concept phase of the sensor design, rising malathion concentrations directly correlate to a decrease in fluorescence intensity (Figure 7.8, A). This relationship was quantified by plotting the relative fluorescence emission (F_0/F) against the used malathion concentration (Figure 7.8, B). Here, F_0 is the measured fluorescence intensity before and F is the one after the addition of malathion. A logarithmic fit with $y = 0.01961 \ln(x) + 1.1572$ best described the found correlation (R^2 = 0.9954). The limit of detection (LOD) was calculated to be 4 pM by using the formula $LOD = \frac{3\alpha}{m}$, where m is the slope of the fit and α is the standard deviation of the blank.[17] This value is considerably lower than the LOD of other techniques, which detect malathion in the nano- or even micro range.[17-21] Hence, this probe was shown to be not only sensitive to malathion, but also ultra-sensitive to even trace amounts.

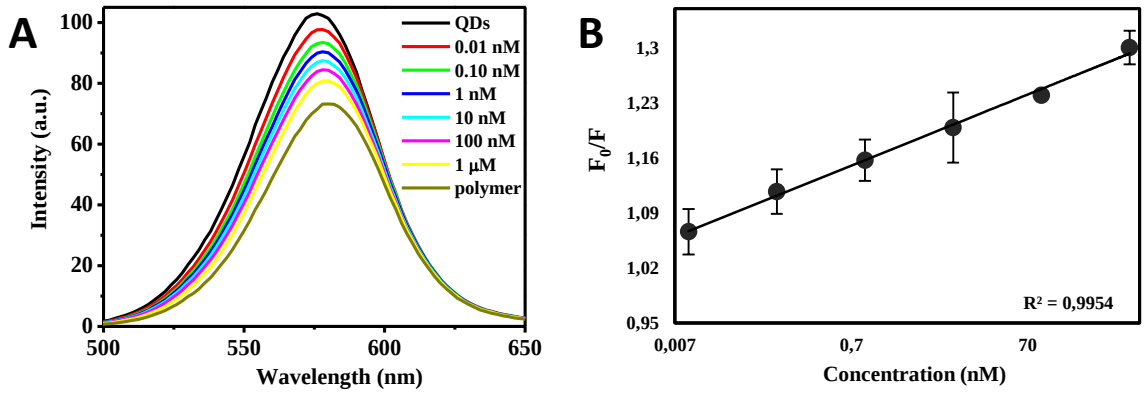

Figure 7.8. Influence of the malathion concentration on the fluorescence signal. The concentration of polymer and aptamer was kept constant at 0.5 mg/mL and 20 µM respectively. (B) Calibration plot of the aptasensor showing a logarithmic correlation. F_0 and F represent the fluorescence intensities in the absence and presence of malathion respectively.

7.5 Applicability in real life situations

The designed sensors must be applicable not only in the laboratory scenario, but also for real samples, which contain a multitude of other components. To make sure that such unrelated chemical compounds do not affect the functionality of the nanoprobe, the sensor was applied to detect the presence of malathion in spiked sample types, which are common in agricultural analytics. Three different water sample types were investigated (tap water, lake water and soil water) and orange juice was chosen to test the viability of the probe for detecting the OP in food. Sample preparation was limited to filtration only, which was followed by spiking with malathion (1 or 100 nM). The results of this study are presented in Table 7.2. The developed sensor detected near exact amounts of malathion in tap water and orange juice (2 - 7% deviation), however, lake and soil water falsified the results by 10 to 22%. Nevertheless, the found malathion concentration are in good agreement with the spiked values. This test clearly ascertained the practicability of the established methodology for environmental monitoring of malathion residues.

Table 7.2. Detection of the malathion concentration in various spiked water and food samples

Source	Spiked Amount [nM]	Found Amount [nM]
Tap water	1	1.02
	100	97.75
Lake water	1	0.86
	100	119.4
Soil water	1	1.10
	100	83.69
Orange juice	1	1.07
	100	99.98

Other than the previous chapters, the present chapter does not focus on gene therapy. Instead, it takes full advantage of the observation that guanidinium group bearing polymers not only strongly interact with polynucleotides, but also induce quenching in fluorescent dyes. Here, GPMA homopolymers were synthesized as a component for highly sensitive for trace-level determination of malathion, wherein detection is reliant on the

polymers interaction with aptamers (binding of polynucleotides) and QD (quenching). Hence, the cationic homopolymer plays the important role of intermediary between detection and data validation. The specificity of the sensor, on the other hand, relies on the aptamer. Although its specificity is stipulated by the used aptamer, where degradation products of the target molecule might interfere with detection, it is simultaneously a huge advantage, since the aptamer is easily interchangeable to achieve specific and ultra-sensitive detection of other pesticides.

The probe was shown to be specific towards malathion and respond negligibly to other pesticides. In addition, the lowest detection limit achieved was found to be 4 pM, which is a substantial improvement if compared to literature known probes. It must also be mentioned that spiking and investigating real samples, such as lake water, soil, and orange juice, indicated that the QD-aptamer-polymer probe possesses applicability outside of laboratory environments. The sensor does not require expensive analytical machinery or even technological education to be used. In addition, the use of aptamers reduces the cost of the biosensor significantly, since they are more affordable in comparison to enzymes or antibodies, which, up until now, are the standard detection component in related biosensors. Thus, it is anticipated that this nanoprobe is highly suitable for pesticide detection in predominantly rural countries, which, in fact, suffer the highest amount of casualties from pesticide-contaminated food and water.

This represents the end of the present thesis. The following chapters will shortly summarize the findings, provide an outlook and describe the experimental procedures in detail.

7.6 References

[1] M. Eddleston, F. Worek, P. Eyer, H. Thiermann, L. Von Meyer, K. Jeganathan, M. H. R. Sheriff, A. H. Dawson, N. A. Buckley, *QJM* **2009**, *102*, 785.

[2] R. Bala, R. K. Sharma, N. Wangoo, *Sens. Actuators, B* **2015**, *210*, 425.

[3] M. Eddleston, N. A. Buckley, P. Eyer, A. H. Dawson, *Lancet* **2008**, *371*, 597.

[4] D. A. Lambropoulou, T. A. Albanis, *Anal. Bioanal. Chem.* **2007**, *389*, 1663.

[5] X. Ji, J. Zheng, J. Xu, V. K. Rastogi, T.-C. Cheng, J. J. DeFrank, R. M. Leblanc, *J. Phys. Chem. B* **2005**, *109*, 3793.

[6] A. P. Periasamy, Y. Umasankar, S.-M. Chen, *Sensors* **2009**, *9*, 4034.

[7] X. Fang, W. Tan, *Acc. Chem. Res.* **2010**, *43*, 48.

[8] R. Bala, S. Dhingra, M. Kumar, K. Bansal, S. Mittal, R. K. Sharma, N. Wangoo, *Chem. Eng. J. (Amsterdam, Neth.)* **2017**, *311*, 111.

[9] C. Zhang, B. Lin, Y. Cao, M. Guo, Y. Yu, *J. Agric. Food Chem.* **2017**, *65*, 3065.

[10] W. C. W. Chan, S. Nile, *Science (Washington, D. C.)* **1998**, *281*, 2016.

[11] K. Zhang, T. Yu, F. Liu, M. Sun, H. Yu, B. Liu, Z. Zhang, H. Jiang, S. Wang, *Anal. Chem. (Washington, DC, U. S.)* **2014**, *86*, 11727.

[12] D. Vasudevan, R. R. Gaddam, A. Trinchi, I. Cole, *J. Alloys Compd.* **2015**, *636*, 395.

[13] A. C. Vinayaka, M. S. Thakur, *Luminescence* **2013**, *28*, 827.

[14] B. Krieg, M. Hirsch, E. Scholz, L. Nuhn, I. Tabujew, H. Bauer, S. Decker, A. Khobta, M. Schmidt, W. Tremel, R. Zentel, K. Peneva, K. Koynov, A. J. Mason, M. Helm, *Pharm. Res.* **2015**, *32*, 1957.

[15] I. Tabujew, C. Freidel, B. Krieg, M. Helm, K. Koynov, K. Muellen, K. Peneva, *Macromol. Rapid Commun.* **2014**, *35*, 1191.

[16] A. Albert, R. J. Goldacre, J. Phillips, *J. Chem. Soc.* **1948**, 2240.

[17] R. Bala, R. K. Sharma, N. Wangoo, *Anal. Bioanal. Chem.* **2016**, *408*, 333.

[18] C. D. L. Albuquerque, R. J. Poppi, *Anal. Chim. Acta* **2015**, *879*, 24.

[19] H. A. Azab, A. S. Orabi, A. M. Abbas, *J. Lumin.* **2015**, *160*, 181.

[20] M. Guler, V. Turkoglu, A. Kivrak, *Environ. Sci. Pollut. Res.* **2016**, *23*, 12343.

[21] S. Singh, P. Tripathi, N. Kumar, S. Nara, *Biosens. Bioelectron.* **2017**, *92*, 280.

8 Summary and Outlook

8.1 Summary

This thesis aimed to improve our understanding of the value guanidinium moeties have in the design of siRNA/DNA carrier systems. In particular, their utility in different linear monomer arrangements, namely diblock copolymers, statistical copolymers, gradient copolymers and homopolymer has been studied with respect to the effects on binding affinity as well as the respective polyplexes' toxicity, internalization into cells and knock-down/transfection efficacy. The observed drawbacks were then addressed by two different approaches, wherein the first one concerned post-polymerization functionalization of the polymers and the second one included the synthesis of terpolymers by copolymerizing the cationic monomers with hydrophilic as well as hydrophobic monomers.

Chapter 3 represents the starting point of this thesis. Therein, a library of twelve positively charged diblock copolymer structures was synthesized to study to what degree (1) the source of the cationic charges (guanidinium groups or primary amines), (2) the length of the cationic block and (3) the charge neutral non-binding block affect the formation of polyplexes as well as the toxicity, the internalization (rate) and the knock-down efficacy of said polyplexes. In addition, the threshold-length of a cationic block required for the formation of stable complexes between siRNA and the respective polymer was investigated.

Herein, polymers **1** to **6** relied on an APMA block for the complexation of siRNA and polymers **7** to **12** used a GPMA block for the same purpose. EMSA and MST analysis showed that changing the length of the cationic block, while keeping the overall molar mass constant, modulates the binding affinity. The rigid rod-like character of siRNA molecules makes condensation by the polymeric carrier more difficult. Hence, it was unexpected to observe a correlation between the measured polyplex size to either the binding efficacy, the charge density, the source of the cationic charges (GPMA or APMA monomers) or even the hydrodynamic radius of the polymer structures. However, it was shown that the length of the cationic block strongly impacts the size of the resulting polyplex. This observation can be explained by the inability of siRNA molecules to adopt bent conformations, thereby allowing only three types of interactions with linear cationic polymers: (1) a longitudinal arrangement, (2) a transversal arrangement, where

a cationic polymer bridges two or more siRNA molecules and (3) an enveloping arrangement, where the cationic polymer coils around the siRNA molecule.

Simulations confirmed that the type of interaction is influenced by the polymer architecture. Specifically, the simulation showed that a shorter guanidinium block - and correspondingly a longer non-binding segment - impedes bridging of multiple siRNA molecules and favors the formation of single siRNA/single polymer chain complexes. Such structures are larger than expected due to the non-binding blocks protruding from the complex's center. Using long binding blocks, on the other hand, leads to polyplexes with multiple bridged siRNA molecules without strongly increasing the overall size. However, the large structures, which were observed by the DLS measuments, could not be explained is this fashion. It is expected that they are either amorphous ill-defined or worm-like polyplexes.

The investigation of the binding properties of each polymer sample also indicated the existence of a threshold length. It was observed that, at the given overall size of the polymer chain of roughly 200 repeat units, a block of more than 22 and less than 27 cationic monomers is required to facilitate efficient complexation of siRNA. Numerical simulations of same-sized block copolymers confirmed these observations and a cationic block with a length of 25 units was calculated as necessary to support the stability of the complex. In other words, a $\text{length}^{\text{binding block}}/\text{length}^{\text{non-biding block}}$ ratio of 1:8.7 (experimental) or 1:7.5 (simulated) was found to be the minimum requirement for the formation of stable polyplexes. This trend was observed irrespective of thhe source of cationic charges.

A systematic analysis of the polyplex structures also highlighted a random relative orientation of the siRNA molecules. The absence (on average) of angular correlation among siRNAs justifies a pictorial representation of the complex as a sphere, which bears consequences for their ability to transport siRNA across plasma membranes. These results of the computational study were confirmed by closely monitoring the internalization of the polyplexes. Polymer **8**-based complexes, for example, were shown to enter HEK293 cells at a fast rate. After only 30 min they were detected inside said cells and after 2 hours of incubation they were found in observable quantities in the cytosol.

The knock-down study revealed that the strong electrostatic interaction between siRNA and GPMA-based diblock copolymers reduces the efficacy of down-regulating gene expression. Although these polymers are able to form nano-sized polyplexes and deliver

siRNA into cells, they are less effective than their APMA counterparts to release their cargo. It was then decided to improve the design *via* post-polymerization modification. Here, the diblock copolymer **8**, which has shown the best results of the guanidinium group bearing copolymers in the knock-down study, was chosen as the candidate. In **Chapter 4**, it was demonstrated that the covalent attachment of triphenylphosphonium moieties can be employed successfully to improve the internalization of the siRNA/polymer polyplexes into cells. In particular, the thusly modified diblock copolymers were shown to be viable carrier systems for the delivery of siRNA even into $CD8^+$ T-cells. Here, the functionalization of cationic diblock copolymers with the uptake-promoting triphenylphosphonium groups caused the formation of exceptionally small polyplexes, thereby allowing this siRNA delivery system to bypass the plasma membrane of $CD8^+$ T-cells, deliver its cargo into the cytosol even at low concentrations. In addition, no cytotoxicity was observed for the uncomplexed modified carrier in spite of bearing uncompensated positive charges. Neither of these feats was achieved by polymer **8**, the precursor polymer of TDBC.

The results of this study not only demonstrated the applicability of the chosen post-polymerization modification to further improve gene delivery agents, but also addressed issues in bioengineering $CD8^+$ T-cells into a treatment tool for currently fatal diseases. Up until now, these cells were viewed to be sheer impossible targets for gene therapy vial polymeric carrier systems. The results of Chapter 4 remove these limitations. Hence, it is vital to investigate the *in vivo* applicability this carrier system. Furthermore, this modification strategy should be tested for different polymeric siRNA delivery agents, which have been deemed impractical before due to their high toxicity or inability to bypass plasma membranes. Nvertheless, the issue of poor siRNA release, which was observed in Chapter 3, was overcome by drastically improving the internalization rate, thereby facilitating high concentrations of the polyplexes in the cytosol and reliable knock-down. To address the poor release and realize efficient transfection, another strategy than the post-polymerization functionalization was envisioned, namely by arranging the cationic monomers in a gradually increasing fashion along the backbone of a linear copolymer, which has never been tested before. For that purpose, a library of statistical and gradient copolymers was synthesized in **Chapter 5** of this thesis. The polymers described and characterized therein, had a content of the protonatable monomers ranging between 5 and 90 mol%, wherein each polymer sample with a statistical

charge distribution had a gradient counterpart. This approach was applied for two different protonatable monomers, namely APMA and GPMA.

Measuring viscosity, density and the partial specific volume of these macromolecules revealed their solubilization profile. Improved solubility in aqueous media due to an overall increase of the intrinsic viscosity and a decrease of the apparent Huggins constant was observed, if the cationic charge density was raised. Increasing the content of the positively charged monomers (APMA or GPMA) influenced the partial specific volume antiproportionally. The thereby increased density of the copolymers altered the sedimentation coefficient distributions accordingly. Hence, it was difficult to evaluate the molar mass by means of SEC and although the physico-chemical properties of the macromolecules appear distinct, their actual molar mass, as determined by means of analytical ultracentrifugation, was shown to be close to the theoretical value.

Binding- and condensation of pDNA, toxicity and transfection efficacy was investigated for all of these polymers. Gradient copolymers were superior in terms of binding affinity and packing density of pDNA if compared to their statistic counterparts, irrespective of the source of the cationic charges. In addition, gradient copolymers formed less toxic polyplexes. Statistical copolymers, on the other hand, induced higher gene expression and were therefore more effective in terms of transfection. Thereby, the monomer arrangement clearly influenced not only their physico-chemical, but also their biological properties. In addition, the importance of the origin of cationic charges was succinctly demonstrated for not only the strength of electrostatic interactions, but also for transfection and cytotoxicity effects. Even sparing amounts of pendant guanidinium groups facilitated complete condensation of pDNA. It was not possible to reproduce these results by using primary amines as the source of cationic charges. Furthermore, GPMA-based copolymers were able to promote luciferase expression at lower cationic charge densities than APMA derivatives. Another difference was found in the required N/P ratios for transfection. While APMA-based copolymers were only efficient at low N/P ratios, copolymers with pendant guanidinium groups induced significant luciferase expression predominantly at high N/P ratios. Conclusively, the distribution and the origin of cationic charges in water soluble copolymers were shown to strongly impact their utility as a pDNA delivery agent. Unveiling the full potential of the (synthetically) easily accessible gradient copolymers, which has been overlooked up until now in pharmaceutical chemistry, will revolutionize the design of gene delivery agents.

Nevertheless, polymers with pendant guanidinium groups have been repeatedly shown to possess low transfection efficiency and the arrangement of the monomers in a gradient along the polymers' backbone was not sufficient to address the issues observed for the diblock copolymers described in Chapter 3. However, in Chapter 4, post-polymerization functionalization with hydrophobic triphenylphosphonium moieties was shown to alleviate this issue by drastically improving internalization into cells and reducing cytotoxicity of the complexes. The conjugation of hydrophobic functional groups was demonstrated to improve the transfer of the polyplexes across lipid-phase of the plasma membrane not only in the present thesis, but also in previous literature known studies. Hence, it was decided to investigate, whether the incorporation of hydrophobic monomers, i.e. the synthesis of statistical cationic terpolymers consisting of hydrophilic as well as hydrophobic monomers, would be sufficient to improve transfection. Hence, **Chapter 6** concerned gene delivery *via* statistical cationic terpolymers consisting of hydrophilic as well as hydrophobic monomers mimicking the amino acid sequence of the cell penetrating peptide CADY.

Excellent batch copolymerization conditions in respect to control over the polymers' molar mass and the monomer composition were found for the synthesis of terpolymers although uncharged HPMA-, cationic GPMA- and lipophilic IEMA monomers were used as building blocks.

The terpolymers containing not only indole moieties, but also and guanidinium groups were then tested in regard to their ability to deliver pDNA into cells. In respect to the transfection results three general statements can be made. Firstly, the HPMA-s-GPMA-s-IEMA terpolymers possess an improved transfection efficacy in comparison to HPMA-s-GPMA copolymers with similar cationic charges. Secondly, the cationic charge, similar to the results of Chapter 5, affects the transfection efficacy proportionally. Here, the addition of only few mol% of GPMA has led to substantially higher luminescence values at lower N/P ratios. Thirdly, the terpolymers deliver pDNA by means of fluid-phase pinocytosis, since the use of Chloroquine, a known endosomal as well as lysosomal disrupting agent, did not affect their ability to bypass the plasma membrane of CHO-K1 cells. Only shutting down all energy dependent mechanisms in the cell by performing the transfection experiment at 4 °C was it possible to significantly reduce the terpolymers' ability to transfect CHO-K1 cells. These polymers, however, are unexpectedly toxic to cells. In order to prove that cationic terpolymers bearing indole moie-

ties can be used to address the prevalent issues of polymeric gene delivery agents, *i.e.* transfection efficacy and high toxicity, further more extensive studies are required.

In conclusion, two viable strategies have been found to address the issue of poor release, thereby solving the only problem found for guanidinium group bearing polymeric gene delivery agents. Applying the results of this thesis, it is now possible to conceive carriers that:

8. complex the polynucleotides
9. are water-soluble
10. are not cytotoxic
11. protect the cargo against nucleases *via* dense packing or shielding
12. transport the polynucleotides across the plasma membrane
13. release the cargo inside the cytosol

Although advancements in the design of gene delivery agents have been made the ideal carrier system has not been found. Targeted delivery to selected tissues as well as the masking of the polyplexes to avoid immunogenicity were not a topic of this thesis. However, continuing the research in even closer collaborations with biochemists in the medical sector might solve even these problems.

Chapter 6 was the last one on the design of gene delivery agents. **Chapter 7** does not relate to gene therapy, however, it demonstrates that the findings of this thesis can be applied in other fields of study as well. Said chapter concerns a highly sensitive and substrate-specific three-component nanoprobe for trace-level determination of malathion.

When investigating the binding strength of the guanidinium group bearing polymers *via* MST, it has been repeatedly observed that they not only facilitate exceptionally strong electrostatic interaction with polynucleotides, but also induce quenching in fluorescent dyes. Hence, a sensor based on a complexation cascade for the detection of poisonous compounds with an exceptionally low detection limit was devised, which takes full advantage of both of these properties. Here, the PGPMA homopolymer, which was provided by me, plays the crucial role of intermediary between detection (specific binding of the aptamer to malathion) and data validation (gradual changes in the fluorescence emission of the QDs due to quenching).

The lowest detection limit achieved was found to be 4 pM, which indicates a substantial improvement in comparison to literature known probes. Spiking and investigating real

samples, including water, soil, and orange juice, indicated that the QD-aptamer-polymer probe possesses huge potential in biosensing. Although its specificity is stipulated by the used aptamer, where, e.g., the degradation products of malathion (isomalathion and malaoxon) might interfere with detection, it is simultaneously a huge advantage, since the aptamer is easily interchangeable to achieve specific and ultra-sensitive detection of other pesticides. In addition, aptamers are more affordable in comparison to enzymes or antibodies, which, up until now, were the standard detection component in related bio-sensors. Thus, it is anticipated that this nanoprobe will serve as the method of choice for pesticide detection in predominantly rural countries, which suffer the highest amount of casualties from contaminated food and water sources.

8.2 Outlook

Throughout this thesis guanidinium groups have been shown to accomplish excellent results in terms of polynucleotide complexation and delivery into cells. Nevertheless, the knock-down study of Chapter 3 and the luciferade expression assay in Chapter 5 have indicated that the release of the cargo is an issue. Tuning the polymers' affinity towards siRNA/DNA by changing the chain length or the charge distribution along the chain (statistical copolymers, gradient copolymers or block co- and terpolymers) helped address this issue to some degree, but the strong electrostatic interactions between the two oppositely charged macromolecules limit the viability of guanidinium group-bearing polymers. The modification strategy of equipping the carrier with triphenylphosphonium moieties helped combat the problem of poor release to a significant degree by improving the uptake. However, utilizing this approach for non-biodegradable polymers, such as the polymethacrylamides, which were employed in this thesis, would lead to problems in a patient's body due to accumulations in organs and cells.[1, 2] Hence, to solve this issue and to further address the problem of release biodegradable polymers are proposed as a new scaffold for the guanidinium groups. Polydepsipeptides, which are copolymers of an α-amino acid and an α-hydroxy acid, fulfill these requirements, since their alternating amide and ester bonds make them susceptible to degradation in natural environments. In addition, they are readily available for modification and they can be made soluble in water by choosing the right substituents.[3] Polydepsipeptides are also known to be non-toxic. Since there are no literature-known derivatives bearing guanidinium groups either on the backbone or on the side chains, their investigation would give us the opportunity to pioneer this field.[4] Nevertheless, polydepsipeptides are not novel. The chemistry of depsipeptides was first reported in 1960[5] and the first polydepsipeptides were synthesized in the mid 70ies.[6, 7] Prof. Goodman and Prof. Ohya contributed most in establishing viable synthesis protocols. Here, the polymerization of the morpholine-2,5-dione derivatives *via* ring opening polymerization in a controlled fashion (Figure 8.1) has been shown to achieve polydepsipeptides at low polydispersities, which is a must for medical applications.[8] However, there are also problems that need to be considered.

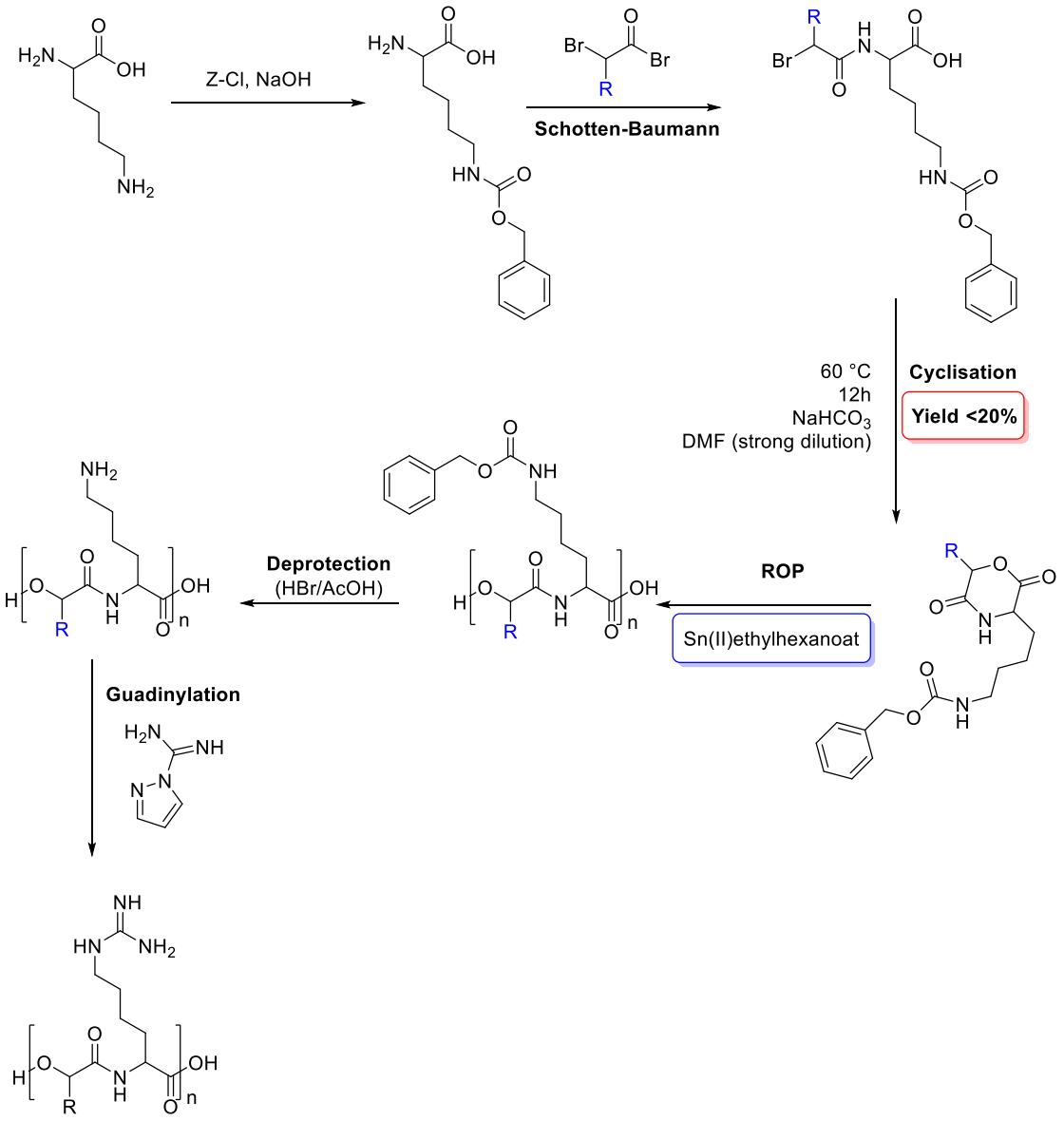

Figure 8.1. Synthetic approach towards novel cationic polydepsipeptide structure – guadinylation subsequent to the polymerization

The first problem (red box, Figure 8.1) is that the functionalized morpholine-2,5-dione monomers are synthesized in poor yields (20%), since uncontrolled polymerization occurs as the competing reaction.[9] The second problem that needs to be considered (blue box, Figure 8.1) is the utilization of metal based catalysts for the polymerization step. Bulky substituents in positions 3 and 6 of the morpholine-2,5-dione derivatives impact the reactivity of the monomers by hindering the interaction of the morpholine based monomers with the catalysts and thereby increasing the polymerization time up to 2 weeks, which has been reported by Feijen et al.[10], Ouchi et al.[9] and Barrera et al.[11] Another explanation for the occurring interference has been provided by Wang et al.,

who associate the formation of intra- or intermolecular interactions with the loss in reactivity of morpholine-2,5-dione-based monomers.[3] The established synthesis protocols rely on $Sn(Oct_2)$ for catalysis. Its contamination makes the resultant samples unsuited for medical applications. Hence, there are two reasons to optimize this process by replacing this catalysator. Polymers structurally related to the polydepsipeptides, such as poly(lactic acid) (PLA) or poly(glycolic acid) (PGA) have been successfully synthesized using enzyme-catalyzed polymerizations.[12] Furthermore, organocatalysis *via* 1,8-Diazabicyclo[5.4.0]undec-7-ene (DBU) or 1,5,7-Triazabicyclo[4.4.0]dec-5-ene (TBD), which are being employed for the polymerization of PLA and PLG for more than a decade, should be pursued as possible alternatives for the $Sn(Oct_2)$-catalysator as well.

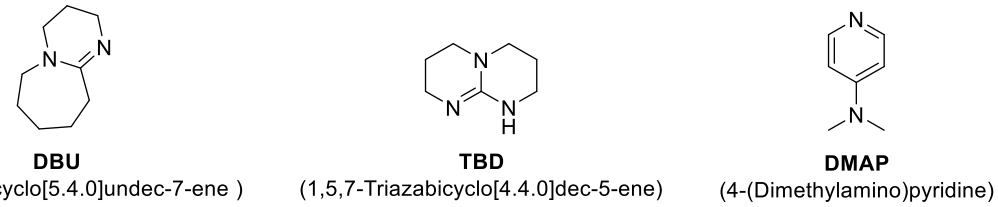

Figure 8.2. Organocatalsts usually utilized for the synthesis of PLA polymers

The synthesis of the desired guanidinium group bearing polymer structure can be facilitated by following two different routes. The first one would be to employ guadinylation subsequent to the deprotection and polymerization steps (Figure 8.1). The polymerization of the morpholine-2,5-dione derivatives *via* ring opening polymerization has been proven viable for the synthesis of poly(Lys-*alt*-Glc), which is the precursor for the guadinylated polymer.[13] However, post-polymerization functionalization is seldom quantitative, which will affect polydispersity. Utilizing protected arginine for the synthesis of the desired poly(Glc-alt-Arg) structure (Figure 8.3) would circumvent this problem, but, due to the increased size of the two Z protective groups, it needs to be considered that the reactivity of the morpholine derivate would drop even further. Both approaches will need to be investigated regarding their applicability before additional substituents (R, Figure 8.1 and 8.3) can be introducing.

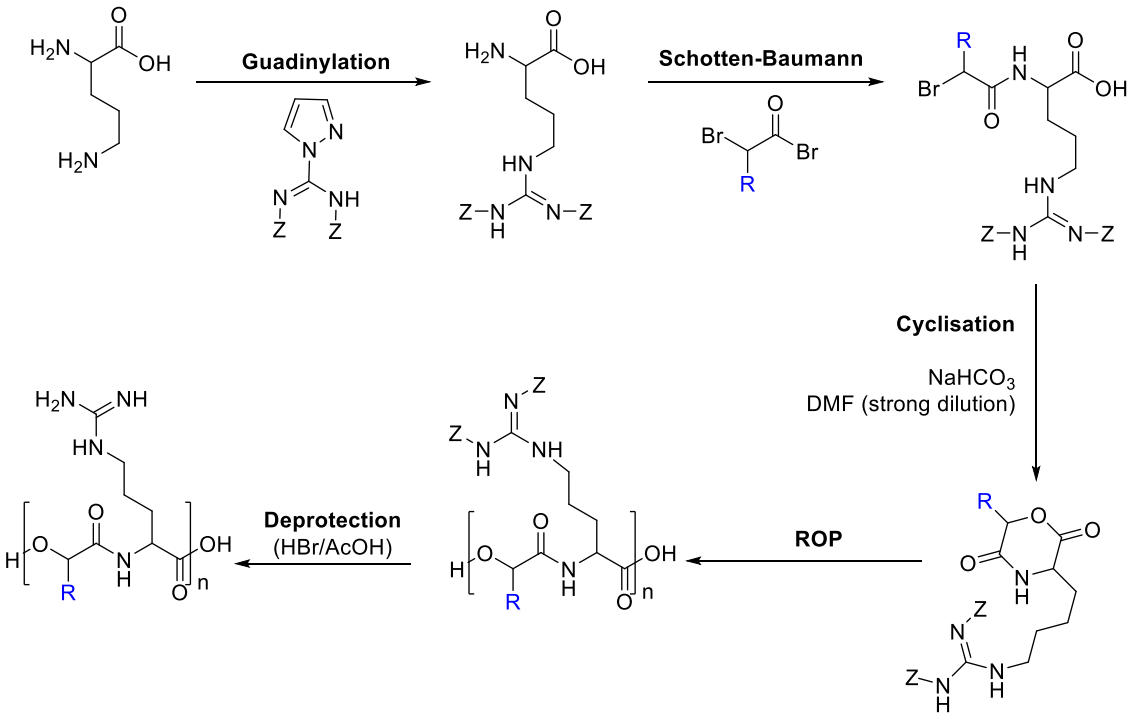

Figure 8.3. Synthetic approach towards the novel cationic polydepsipeptide structure – guadinylation of the monomers

8.3 References

[1] Y. Noguchi, J. Wu, R. Duncan, J. Strohalm, K. Ulbrich, T. Akaike, H. Maeda, *Jpn. J. Cancer Res.* **1998**, *89*, 307.

[2] R. Duncan, L. C. W. Seymour, L. Scarlett, J. B. Lloyd, P. Rejmanova, J. Kopecek, *Biochim. Biophys. Acta, Gen. Subj.* **1986**, *880*, 62.

[3] Y. Feng, J. Lu, M. Behl, A. Lendlein, *Macromol. Biosci.* **2010**, *10*, 1008.

[4] L. S. Nair, C. T. Laurencin, *Prog. Polym. Sci.* **2007**, *32*, 762.

[5] M. M. Shemyakin, *Angew. Chem.* **1960**, *72*, 342.

[6] M. Goodman, C. Gilon, M. Palumbo, R. T. Ingwall, *Isr. J. Chem.* **1974**, *12*, 67.

[7] D. Nissen, C. Gilon, M. Goodman, *Makromol. Chem.* **1975**, *Suppl. 1*, 23.

[8] J. Helder, F. E. Kohn, S. Sato, J. W. Van den Berg, J. Feijen, *Makromol. Chem., Rapid Commun.* **1985**, *6*, 9.

[9] T. Ouchi, T. Nozaki, Y. Okamoto, M. Shiratani, Y. Ohya, *Macromol. Chem. Phys.* **1996**, *197*, 1823.

[10] P. J. A. In't Veld, P. J. Dijkstra, J. Feijen, *Makromol. Chem.* **1992**, *193*, 2713.

[11] D. A. Barrera, E. Zylstra, P. T. Lansbury, Jr., R. Langer, *J. Am. Chem. Soc.* **1993**, *115*, 11010.

[12] Y. Feng, J. Knuefermann, D. Klee, H. Hoecker, *Macromol. Rapid Commun.* **1999**, *20*, 88.

[13] T. Ouchi, T. Nozaki, Y. Okamoto, M. Shiratani, Y. Ohya, *Macromol. Chem. Phys.* **1996**, *197*, 1823.

9 Experimental section

9.1 General methods

9.1.1 Chemicals and Solvents

All chemicals and solvents were purchased from the companies Sigma-Aldrich, ABCR, Acros, Fluka, Lancaster, and Merck at the highest available purity and used as received unless mentioned otherwise. N-(3-aminopropyl) methacrylamide hydrochloride (APMA), which was used for synthesis of N-(3-guanidinopropyl) methacrylamide (GPMA), was purchased from PolySciences, Germany. The chain transfer agent 4-((((2-carboxyethyl)thio)carbonothioyl)thio)-4-cyanopentanoic acid was purchased from Boron Molecular INC, Australia. 4,4′-Azobis(4-cyanovaleric acid) (ACVA), which was used as the radical initiator for RAFT polymerizations, was recrystallized in methanol before use. The ultrapure water ($R < 18.2$ MΩ·cm) was taken from Milli-Q® systems of Merck Millipore.

9.1.2 Chromatography

Preparative column chromatography was performed using silica gel from Merck with a grain size of 0.04-0.63 mm (flash silica gel, Geduran Si 60). Silica gel coated substrates from Macherey-Nagel (ALUGRAM Xtra SIL G/UV254, 4x8 cm) were utilized for analytical thin layer chromatography (TLC). The synthesized low-molecular compounds were detected using fluorescence quenching at 254 nm, by self-fluorescence at 366 nm or by utilizing a glass chamber containing iodine crystals.

9.2 Analytical techniques

9.2.1 Mass spectrometry

FD mass spectra were obtained on a VG Instruments ZAB 2-SE-FPD spectrometer. MALDI-TOF spectrometry was conducted on a Bruker Reflex II-TOF spectrometer, utilizing a 337 nm nitrogen laser. Varying thickness of the prepared sample on the MALDI target reduced the resolution. Therefore, only integers of the molecular peaks are given.

9.2.2 Nuclear magnetic resonance (NMR) spectroscopy

1H-NMR and 13C-NMR spectra were recorded in the listed deuterated solvents on a Bruker WS 300 (controller: Bruker Avance III), Bruker AMX 300 (controller: Bruker Avance II), Bruker WS 400 (controller: Bruker Avance III), Bruker DRX 500 (DSX console), Bruker DRX 700 (Bruker Avance console for double resonance experiments) or a Bruker 850 (Bruker Avance II+ console) spectrometer. The deuterated solvents were used as an internal standard.

The oxidative state of the phosphor atoms contained in the triphenylphosphonium group-modified polymers (Chapter 5) was determined by ^{31}P-NMR using a Bruker Bio-Spin 500 MHz spectrometer (controller: Bruker Avance III) in D_2O.

9.2.3 UV-Vis spectroscopy

Solution UV-Vis spectra were obtained at ambient temperature on a Perkin-Elmer Lambda 100 spectrometer. The samples were measured and compared using different concentrations (10^{-5} to 10^{-7} M) in order to eliminate aggregation phenomena in solution. Thus, the properties of the monomeric species were recorded.

9.2.4 Size exclusion chromatography (SEC)

9.2.4.1 Chapter 3 and Chapter 4

The polymers were characterized using size exclusion chromatography (SEC) with hexafluoroisopropanol (HFIP, +3 g/l K^+TFA^-) as the eluent. SEC was performed with at 40 °C. Modified silica (PFG columns, particle size: 7 µm, porosity: 100 and 1000 Å) was used as the column material. A refractive index detector (G 1362A RID, Jasco) and a UV Detector (UV-2075+, Jasco, wavelength: 230 nm) were used to detect the polymer and the molecular weights were calculated based on a calibration with PMMA standards (Polymer Standards Services GmbH, Mainz). SEC was also used to determine the quantitative removal of the thiocarbonylthio functionality from the block copolymers. Here, the UV signal at 310 nm before and after removal was monitored.

9.2.4.2 Chapter 5, 6 and 7

The molar mass of the polymers was determined by SEC using different eluents (SEC_{DMAc} and SEC_{water}). SEC_{DMAc} was run with dimethylacetamide (DMAc, +0.21% LiCl). The measurement was performed at 40 °C and a flow rate of 1 mL/min using a PSS GRAM guard/1000/30 Å column (particle size: 10 µm). A refractive index detector

(G1362A) and a UV Detector (G1315D, wavelength: 310 nm) were employed to observe the elution behavior of PGPMA. PMMA standards were employed to calculate the relative molar mass. In case of SEC_{water}, water (+0.1 % TFA, +0.1 M NaCl) was used as the eluent and AppliChrom ABOA CatPhil guard/200/350 Å was employed as the column. The flow rate was set to 1 mL/min and the temperature to 30 °C. PGPMA was detected using the refractive index (RI-930) and UV (UV-975, wavelength: 312 nm) and the molar mass was calculated based on PVP standards.

9.2.5 Viscosity

Viscosity was measured with an AMVn viscometer (Anton Paar, Graz, Austria). The capillary/ball combination of the measuring system was used to determine the respective ball times for the solvent (0.01 M PBS), t_0, and for macromolecule solutions of varying concentrations, t_c, at a tilting angle of the capillary of 50°. The viscosity of PBS was determined to be $\eta_0 = 1.03\ mPas$. The measurements were performed at concentrations of the macromolecules resulting in relative viscosities $1.2 < \eta_r = t_c/t_0 < 2.5$. The obtained data points were fitted linearly and the Huggins equation (eq 1) was used to calculate the intrinsic viscosity ([η]) by extrapolating the viscosity to zero concentration:

$$\frac{\eta_r - 1}{c} = [\eta] + k_H[\eta]^2 c$$

9.2.6 Density measurements and partial specific volume (υ) of the macromolecules

The partial specific volume (υ) of a macromolecule is defined as the volume increase of a solution caused by its addition, while the temperature and pressure are kept constant. υ of the macromolecules dissolved in the PBS solution was determined with a DMA4100 density-meter (Anton Paar, Graz, Austria) at $T = 20\ °C$. The density increment ($\rho_c - \rho_0$) measurements were performed in the concentration range $0.1\ w\% \leq c \leq 1\ w\%$. The resultant slope of the curves, i.e. the buoyancy factor ($1 - \nu\rho_0$), was used to calculate ν by considering the measured density of the solvent (PBS, $\rho_0 = 1.0053\ g\ cm^{-3}$).

9.2.7 Analytical ultracentrifugation

These experiments were performed in collaboration with PD Dr. Ivo Nischang using a ProteomeLab XL-I analytical ultracentrifuge (Beckman Coulter Instruments, Brea, CA) with an An-50 Ti eight-hole rotor. The ultracentrifuge cells were equipped with double-sector epon centerpieces with a 12 mm optical path length. One sector was filled with 430 µL of the sample in PBS and the other with 450 µL of PBS as the reference. Interference optics detection was used for observation of the sedimentation boundary in respect to time. The experiments were performed at a rotor speed of 42000 rpm for 24 h and at a temperature of $T = 20\,°C$. Scans were acquired at 5 min intervals. Every third scan was used for data evaluation.

9.2.7.1 Sedimentation-diffusion analysis

Sedimentation velocity data were analyzed with SEDFIT and the $c(s)$ model with a maximum entropy regularization procedure.[1] This model is based on the numerical solution to the Lamm equation, assuming the same apparent translational frictional ratio f/f_{sph} of the sedimenting population of macromolecules. Sedimentation velocity experiments were performed with at least four of up to seven different concentrations. Resultant numerical values of s were obtained as the weight (signal) average of the distributions at varying concentrations. These results were used to determine the values at infinite dilution (s_0) via extrapolation to zero concentration using the relationship $s^{-1} = s_0^{-1}(1 + k_s c)$. f/f_{sph} values were seen to fluctuate around a mean with similar numerical values for each of the macromolecules and without any apparent concentration dependence. $(f/f_{sph})_0$ values for molar mass calculations were therefore assumed as the average of frictional ratios at the different concentrations. The molar mass ($M_{s,f}$) was calculated based on the modified Svedberg equation, where N_a is the Avogadro constant, and $[s] = s_0\eta_0/(1 - \nu\rho_0)$ the intrinsic sedimentation coefficient:

$$M_{s,f} = 9\pi\sqrt{2}N_a([s](f/f_{sph})_0)^{3/2}\sqrt{v}$$

This form of the Svedberg equation for molar mass estimations relies on values of the translational frictional ratios f/f_{sph} that are typically found adequate for ideally behaving random coil conformation macromolecules of narrow unimodal dispersity.[2]

9.2.8 Electrophoretic mobility shift assay (EMSA)

9.2.8.1 Chapter 3 and Chapter 4

0.14 µg of labeled siRNA (either ATTO488 or FRET (ATTO647N (acceptor) and Alexa555 (donor)) labeled, Iba, Göttingen, Germany, anti-EGFP siRNA (sense strand: 5'-GCA AGC UGA CCC UGA AGU UCA U-3', anti-sense strand: 3'- GCC GUU CGA CUG GGA CUU CAA G-5')) were incubated with the polymers at various $mass^{siRNA}/mass^{polymer}$ ratios in 1x PBS for 20 min. Samples were applied onto a 1% agarose gel (1x TBE running buffer), which was analyzed at 120 V for 50 min. The gel was visualized in a dark hood with a Typhoon 9600 (GE Healthcare, Buckinghamshire, UK) at 532 nm excitation wavelength and a 670 nm BP 30 emission filter for detecting the FRET signal.

9.2.8.2 Chapter 5

Preparation of pDNA: The pGL3 plasmid (Promega, Madison, WI, USA) encoding for luc+ luciferase reporter gene was amplified in E. coli TG1 (kind gift of Hans-Knoell-Institute, Jena, Germany), and isolated with E.Z.N.A.® Plasmid DNA Maxi Kit (OMEGA bio-tek, GA, USA), according to the manufacturer's protocol.

The N/P ratios were calculated based on a literature known approach. Here, the phosphate content of the polynucleotide was estimated by assuming an average molar mass per nucleotide of 330 $g \cdot mol^{-1}$ and 3,03 nmol phosphate per µg DNA.[3] The nitrogen ratio, on the other hand, was calculated under the assumption that using physiological conditions both primary amines and guanidine groups can be protonated only once. Hence, these functional groups were treated as providers of one basic nitrogen.

Preparation of polymer/DNA polyelectrolyte complexes: DNA/polymer polyplexes were prepared by following the literature known procedure with minor modifications.[4] 2 µg of pDNA and the appropriate amounts of polymer for the desired N/P ratios were each diluted in 50 µl of saline solution (0.15 M sodium chloride, Carl Roth, Germany, in bidistilled water, pH 7.2-7.4) and vortexed for 10 seconds (MS1 Minishaker, IKA GmbH & Co. KG, Germany). After 10 minutes of equilibration at room temperature, all of the polymer solution was added to the pDNA solution and vortexed for 10 seconds. Subsequently, the complex formation was allowed to take place during 10 minutes at room temperature.

Binding assay: Agarose gel electrophoresis was conducted with polyplexes prepared with pDNA to visualize the DNA binding ability of the polymers. For this, 50 µl of the polyplex solution were mixed with 5 µl of loading buffer (40 mM Tris-base (Carl Roth GmbH, Germany), 50 vol% glycerol (Caesar & Loretz GmbH, Germany), 1 mM EDTA (Carl Roth GmbH, Germany), pH 7.4) and loaded onto a 1% agarose gel (peqGOLD universal agarose, PEQLAB Biotechnologie GmbH, Germany) containing 1.25 µg/l ethidium bromide (SERVA Electrophoresis GmbH, Germany). Electrophoresis was performed at 80 V (Biorad PowerPac 1000, Bio-Rad Laboratories, CA, USA) for 60 minutes in TAE buffer (40 mM Tris-base, 1 vol% acetic acid (Merck KGaA, Germany), 1 mM EDTA). Gels were photographed (DOC-PRINT VX5, Vilber, France) under UV transillumination (UV-transilluminator, Intas, Germany) at 312 nm.

9.2.9 Fluorophore exclusion assay

The ability of the polymers to condense pDNA was quantified by using the AccuBlue™ High Sensitivity dsDNA Quantitation Kit (Biotinum, Inc., Fremont, CA, USA) according to the manufacturer's protocol with minor modifications. The respective polyplex solutions were prepared in accordance with the procedure described in 9.2.8.2. 5 µl of these solutions, which is equivalent to 100 ng of pDNA, followed by 200 µl of working solution were then pipetted onto a 96 well microplate (FLUOROTRAC™ 200, Greiner Bio-One, Germany) and incubated on an orbital shaker (Titramax 100, Heidolph Instruments GmbH & Co.KG, Germany) for 10 minutes at 300 rpm. Fluorescence was measured at 485 nm excitation wavelength and 530 nm emission wavelength (SPARK 10M, TECAN Group AG, Austria). As controls, polyplexes formed between linear polyethylenimine (lPEI, 2,500 g·mol^{-1}, Polysciences Europe GmbH, Germany) and pDNA at an N/P ratio of 20, polymer diluted in saline solution, as well as uncomplexed pDNA dissolved in saline solution were used. Relative fluorescence units (RFU) were calculated as follows:

$$RFU = \frac{F_{sample} - F_{blank}}{F_{pDNA\ uncomplexed} - F_{blank}} \cdot 100$$

9.2.10 Microscale thermophoresis (MST)

Measurements were performed on a NanoTemper Monolith NT.115 instrument using the blue (absorption: 455 - 485 nm, emission: 510 - 530 nm) or the red filter (absorption: 600-650 nm, emission: 675 – 690 nm) for excitation and detection of fluorescence. The measurement was performed in standard capillaries at varying percent LED and IR-

Laser power with a Laser-On time 30 sec between Laser-Off times of 5 sec in the beginning and the end. To determine the affinity of a binding reaction, a titration series of one binding partner was performed. Analysis and fitting of the detected signals was performed with the software NT Analysis 1.4.27 based on the theoretic calculations described by Jerabek-Willemsen *et al*. and Baaske *et al*.[5, 6] While the fluorescently labelled binding partner siRNA (either ATTO488 or FRET (ATTO647N (acceptor) and Alexa555 (donor)) labeled, Iba, Göttingen, Germany; sense strand: GCA AGC UGA CCC UGA AGU UCA U, antisense strand: GAA CUU CAG GGU CAG CUU GCC G) was kept at a constant concentration of 400 nM. Binding of the polymer particles to fluorescently labeled siRNA was quantified in Dulbecco's phosphate-buffered saline (1xDPBS, with Ca^{2+}/Mg^{2+}, Life Technologies) and the same medium was used to prepare stock-solutions of the polymer structures (2 $mg \cdot mL^{-1}$). Shortly prior to the measurement the complexes were prepared by mixing both components and incubated for 20 minutes at ambient temperature. Here, the $mass^{polymer}$/$mass^{siRNA}$ ratio for the polyplex formation was varied in a titration series between 1 and 100 (1, 5, 7.5, 10, 12, 15, 17.5, 20, 25, 50, 100).

9.2.11 Fluorescence correlation spectroscopy (FCS)

FRET-labeled siRNA: A commercial FCS setup (Zeiss, Germany) was employed consisting of the module ConfoCor2 and an inverted microscope model Axiovert 200 with a Zeiss C-Apochromat 40x/1.2 W water immersion objective. The Atto647N acceptors on the FRET-labeled siRNAs were directly excited by a helium-neon laser (633 nm), and the emission was detected after filtering by a LP650 long pass filter, and the emission was detected after filtering by a LP650 long pass filter. For detection, an avalanche photodiode that enables single-photon counting was used.

ATTO488-labeled siRNA: A LSM 880 confocal fluorescence microscopy system (Carl Zeiss, Jena, Germany) was employed. The excitation laser light was strongly focused into the studied samples by a Zeiss C-Apochromat 40×/1.2 W water immersion objective. The ATTO488-labeled siRNA were excited with the 488 nm line of an Argon laser and the emission was detected in the range of 500 - 562 nm. Emission was collected after passing through a confocal pinhole, directed to a spectral detection unit (Quasar, Carl Zeiss). In this unit, the emission is spectrally separated by a grating element onto a 32 channel array of GaAsP detectors operating in a single photon counting mode.

In all cases an eight-well polystyrene chambered cover glass (Nunc™ Lab-Tek™, Thermo Fisher Scientific) was used as a sample cell. The solutions containing the polyplexes, which were prepared in accordance with 9.2.8.1 at the $weight^{polymer}/weight^{siRNA}$ ratio of 100:1 and a concentration of the fluorescent species of 5 µM. For each sample series of measurements with a total duration of 150 s were performed. The time-dependent fluctuations of the fluorescent intensity $\delta I(t)$ were recorded and analyzed by an autocorrelation function to evaluate the hydrodynamic radii of the studied fluorescent species. Solutions containing either solely labeled siRNA or mixtures of siRNA molecules and nano carrier were studied. The appearance of fluorescent species with significantly larger hydrodynamic radii confirmed the complexation of the siRNA by the nano carriers.

9.2.12 Dynamic light scattering (DLS)

Dynamic light scattering (DLS) measurements were performed on an ALV spectrometer consisting of a goniometer and an ALV-5004 multiple-tau full-digital correlator (320 channels), which allows measurements over an angular range from 30° to 150°. A He-Ne Laser (wavelength of 632.8 nm) was used as the light source. For temperature controlled measurements, the light scattering instrument was equipped with a thermostat from Julabo. Aggregate formation of the polymers needed to be suppressed in order to clearly differentiate complex formation. For that purpose, the polymers were dissolved in aqueous 0.15 M sodium chloride (NaCl) solutions and filtered at 0.2 µm cut-off. The filter removed formed aggregates and the salt solution inhibited their rearrangement for the duration of the measurement. Having measured the hydrodynamic radius of the single polymer molecules, unlabeled siRNA (Iba, Göttingen, Germany; Nucleic Acids Synthesis, annealed, unlabeled sense strand: GCA AGC UGA CCC UGA AGU UCA U, unlabeled antisense strand: GAA CUU CAG GGU CAG CUU GCC G) was added at the $mass^{siRNA}/mass^{polymer}$ ratio of 100:1 ensuring complete complexation, incubated for 20 min at ambient temperature and measured again.

9.2.13 Detection of malathion

The utility of the quantum dots-polymer based fluorescence aptasensor was investigated in collaboration with Prof. Dr. Rohit K. Sharma. A stock solution of malathion (12 mM) was prepared in acetone and stored at 4 °C. It was used as the basis for a concentration series utilizing phosphate buffer (pH 7.32) for dilution. The sample preparation for mal-

athion detection performed as follows: 10 µL of a 20 µM aptamer solution (sequence: 5′ATCCGTCACACCTGCTCTTATACACAATTGTTTTTCTCTT AACTTCTT-GACTGCTGGTGTTGGCTCCCGTAT-3′, Sigma-Aldrich, India) were mixed with 70 µL of varying malathion concentrations. This solution was further diluted with 100 µL phosphate buffer and incubated for 40 min at ambient temperature. Subsequently, 30 µL of a polymer solution with the concentration of 0.5 mg/mL were added and the solution was again incubated for 20 min. Finally, 200 µL of the quantum dot solution were added and fluorescence measurements were performed. The specificity of the biosensor was assessed in the presence of various non-target pesticides such as atrazine, chlorsulfuron, chlorpyrifos, 2,4-D and diuron.

9.2.14 Cryogenic transmission electron microscopy

Cryogenic transmission electron microscopy (cryo TEM) measurements were performed on a FEI Tecnai G^2 20 cryo-Transmission Electron Microscope (Philipps, Eindhoven, The Netherlands). Acceleration voltages were set to 120 kV. Samples were prepared on Quantifoil grids (3.5/1) after cleaning by argon plasma treatment for 120 s. 9.5 µL of the solutions were blotted by using a Vitrobot Mark IV. Samples were plunge-frozen in liquid ethane and stored under nitrogen before being transferred to the microscope utilizing a Gatan transfer stage. TEM images were acquired with a 200 kV FEI Tecnai G^2 20 equipped with a 4k x 4k Eagle HS CCD and a 1k x 1k Olympus MegaView camera .

9.3 Biochemical characterization

The biochemical characterization was performed in close collaboration with Dr. Bettina Krieg (Prof. Dr. Mark Helm), Dr. Marleen Willig (Prof. Dr. Volker Mailänder), Dr. Lars Tebbe (Prof. Dr. Uwe Wolfrum) and Leon Zartner (Prof. Dr. Dagmar Fischer).

9.3.1 Cell culture

HeLa (human cervical carcinoma cell line, ATCC CCL-2), Kelly wt (human neuroblastoma cell line, ACC 355), HEK293 (human embryonic kidney cell line, ACC 305) and MCF7 cells (human breast cancer cell line, ATCC HTB-22) were cultured in Dulbecco´s modified Eagle´s medium (DMEM, Live Technologies), which was supplemented with 10% fetal calf serum (FCS, GIBCO), 2 mM L-Glutamine (Life Technologies), and 100 units·mL^{-1} Penicillin-Streptomycin (ThermoFischer Scientific). C2C12 cells (mu-

rine myoblast cell line, ACC 565) were cultured in DMEM containing 4 mM L-glutamine, 4500 mg·L^{-1} glucose, 1 mM sodium pyruvate, and 1500 mg·L^{-1} sodium bicarbonate. This medium was further supplemented with 10% fetal calf serum (FCS, GIBCO). All cell lines were grown and incubated in a humidified incubator at 37 °C and 5% CO_2.

PBMCs (peripheral blood mononuclear cells) were isolated from buffy coats of healthy donors (according to the ethics committee guidelines from the Blood transfusion center, University Medical Center of the Johannes Gutenberg University Mainz) by density gradient centrifugation. Subsequently, the $CD8^+$ T-cells were purified by MACS Separation and afterwards stimulated with an anti-CD3 antibody (OKT3) and recombinant human IL-2. PBMCs and $CD8^+$ T-cells were cultured in RPMI-1640 media (Gibco, Thermo Fisher Scientific) supplemented with 10% FBS (Gibco, Thermo Fisher Scientific) and 1% PenStrep (Gibco, Thermo Fisher Scientific). The cells were weekly restimulated with 30 ng/ml OKT3 antibody (provided by the group of Prof. Dr. T. Wölfel, University Medical Center of the Johannes Gutenberg University Mainz) and 600 I.E of recombinant human IL-2 (Proleukin S, Novartis) whereas, 400 I.E IL-2 were added for medium change and for the experiments.

Chinese hamster ovary cells (CHO-K1, German Collection of Microorganisms and Cell Cultures, DSMZ, Germany) were incubated in Hams F12 nutrient mixture with L glutamine containing 10 vol% fetal bovine serum (both GE Healthcare Europe GmbH, Germany) at 37° C, 5% CO2 and 95% relative humidity (CB150 Incubator, BINDER GmbH, Germany).

9.3.2 Luciferase expression

CHO-K1 cells were seeded on 12 well plates (CELLSTAR®, Greiner Bio-One GmbH, Germany) with $5*10^4$ cells per well and incubated for 24 hours. Subsequently, cells were washed once with phosphate buffered saline solution (PBS, 8.2 mM Na_2HPO_4, 1.47 mM KH_2PO_4, 0.137 NaCl, 2.68 mM KCl, pH 7.4, all Carl Roth GmbH, Germany), and 2 mL of fresh medium containing as well as 200 µl polyplex solution, which equals to 4 µg pDNA, were added. This polyplex solution was prepared by respectively diluting 4 µg of pDNA and the appropriate amounts of polymer for the desired N/P ratios in 100 µl of saline solution and vortexing them for 10 seconds. After 10 minutes of equilibration at room temperature, the polymer solution was added to the pDNA solution and vortexed for 10 seconds. Subsequently, the complex formation was allowed to take

place for 10 minutes at room temperature. As controls, 200 µl of saline solution, free plasmid in saline solution and lPEI/pDNA polyplexes at an N/P ratio of 20 were added to the cells. After 4 hours of incubation, cells were washed once with PBS, fresh medium was added, and incubation was continued for 44 hours. Subsequently, cells were washed twice with PBS before they were lysed. Ensuing, a luciferase assay was performed according to the manufaturer's protocol (Luciferase Assay System, Promega, USA). In addition, to normalize the detected luminescence, the protein content of the cell lysate was quantified by bicinchoninic acid assay (Pierce BCA Protein Assay Kit, Thermo Fisher Scientific Inc., USA) with minor modifications: 25 µl of cell lysate were treated with 10 µl iodoacetamide (AppliChem GmbH, Germany) for 20 minutes at 37° C to inactivate dithiothreitol (DTT) in the lysis reagent. Having added the working reagent, samples were incubated again at 37° C for 40 minutes. Both measurements for luciferase expression assay and BCA assay were carried out on a multidetection microplate reader (FLUOstar OPTIMA, BMG LABTECH GmbH, Germany). The luciferase expression was then calculated as luminescence (RLU) per µg protein.

9.3.3 Knock-down study

The siRNA against Kif2a (J-041075-07-0005, ON-Targetplus Mouse Kif2a: CUA CAC AAC UUG AAG CUA U) and non-targeting control siRNA (D-001810-10-05, ON-TARGETplus Non-targeting Pool: UGG UUU ACA UGU CGA CUA A, UGG UUU ACA UGU UGU GUG A, UGG UUU ACA UGU UUU CUG A, UGG UUU ACA UGU UUU CCU A) were purchased from Dharmacon (Lafayette, CO, USA). IMCD3 cells (mouse inner medullary collecting duct cells) were seeded with a density of 162,500 cells per well in a 6-well plate and incubated in Dulbecco's modified Eagle's medium F12 (DMEM-F12) (Thermo Fisher Scientific, Waltham, USA) containing 10% heat-inactivated fetal calf serum (FCS) overnight. The DMEM-F12 was removed on the next morning and after washing the cells with 1x PBS buffer (phosphate-buffered saline; 140 mM NaCl, 2.7 mM KCl, 10 mM $Na_2HPO_4 \times 2H_2O$, 1.8 mM KH_2PO_4, pH 7.3), reduced serum medium (Opti-MEM) (Thermo Fisher Scientific) was added. In all cases, the siRNAs were employed in final concentrations of 50 nM for the transfection of the IMCD3 cells. The commercially available transfection reagent LTX RNAiMAX (Thermo Fischer Scientific) was used as the positive control. For the negative control, the cells were incubated with siRNA molecules lacking a transfection reagent. The polymer samples, which have been shown to complex siRNA effectively by means of

electrophoretic mobility shift assay and microscale thermophoresis, were dissolved in 1xPBS to gain stock solutions. The complexes were then prepared by mixing the siRNA with the respective polymer structures (1 $mg \cdot mL^{-1}$ stock solution) in $weight^{polymer}/weight^{siRNA}$ ratios guaranteeing complete complexation and incubating the solution for 20 min at ambient temperature. The complexes were then added to the cells, before incubating them for 72h in Opti-MEM at 37°C and 5% CO_2. Subsequently, the cells were harvested and lysed using Triton-X100 lysis buffer (50 mM Tris–HCl pH 7.5, 150 mM NaCl, 0.5% Triton X-100) that contained the protease inhibitor cocktail (PI-mix; Roche Diagnostics, Mannheim, Germany). Lysis was performed for 10 min on ice with a vortexing step every 2 min and a final centrifugation (14000 xg, 10 min, 4 °C). The lysates were analyzed with SDS-PAGE electrophoresis and western blot in order to determine the knockdown efficiency according to: $\left(1 - \frac{\text{"siRNA" sample}}{\text{"pool" sample}}\right) * 100\% = knock - down\ in\ [\%]$.

9.3.3.1 BCA protein assay

A protein quantification assay was performed to determine the protein concentration for each cell lysate, which is necessary to ensure a uniform loading of the SDS-PAGE gels. Here, 4 µl of the lysate and 96 µl of a 1M HEPES buffer (4-(2-hydroxyethyl)-1-piperazineethanesulfonic acid, Thermo Fischer Scientific) were mixed with 2 mL of the BCA working reagent, which was prepared according to the user's manual of the Pierce™ BCA Protein Assay Kit (Thermo Fischer Scientific). The resulting solution was vortexed and incubated at 37 °C for 30 min. All samples were then cooled to ambient temperature and their absorbance at 562 nm was analyzed using the protein quantitative mode of the GENESYS 30 Vis Spectrophotometer (Thermo Fischer Scientific). Their protein content was calculated based on a linear calibration fit, which was obtained by investigating the absorbance of a dilution series with known amounts of BSA (Thermo Fisher Scientific), ranging between 0 and 750 µg/mL, under identical conditions.

9.3.3.2 SDS-PAGE

A 5% stacking gel (H_2O [60 vol%], 0.5M Tris-HCl buffer at pH 6.8 [25 vol%], 30% (w/v) acrylamide [13.9 vol%], 10% (w/v) SDS [1 vol%], 10% (w/v) ammonium persulfate (AP) [1 vol%] and N,N,N′,N′-tetramethylethylenediamine (TEMED) [0.1 vol%]) and a 12% separation gel (H_2O [32 vol%], 1.5M Tris buffer at pH 8.8 [26 vol%], 30%

(w/v) acrylamide [40 vol%], 10% (w/v) SDS [1 vol%], 10% (w/v) ammonium persulfate (AP) [1 vol%] and N,N,N′,N′-tetramethylethylenediamine (TEMED) [0.1 vol%]) were used for protein separation. Having determined the protein concentration (µg/µl) of each sample using the Bradford assay, volumes corresponding a total protein content of 30 µg were pipetted into 0.5 mL Eppendorf tubes, mixed with an equal volume of 2x Laemmli sample buffer (Sigma-Aldrich) and then loaded onto the gel. Electrophoresis was performed for 1.5 h using a current of 100 V (Biorad PowerPac 1000, Bio-Rad Laboratories, CA, USA). PageRuler™ Prestained Protein Ladder with a rage of 10 to 180 kDa (Thermo Fischer Scientific) was used as a molecular weight marker.

9.3.3.3 Western blot

The transfer of the proteins from the SDS-PAGE gel to the PVDF membrane (Immobilon®, Sigma-Aldrich), which facilitates their detection via antibodies, was performed using western blot procedure in a Mini Trans-Blot® Cell from Bio-RAD. For that purpose the PVDF membrane was activated prior to the procedure by incubating it in methanol for 1 min. The membrane was subsequently rinsed for 5 min in the transfer buffer (Towbin buffer: 25 mM Tris, 192 mM glycine, pH 8.3), which contained 20% (v/v) methanol and 0.01% (w/v) SDS. Similarly, the SDS-PAGE separation gel was immersed in the transfer buffer for 30 min. Complete protein transfer was accomplished within 2 h by using a current of 75 V (Biorad PowerPac 1000, Bio-Rad Laboratories, CA, USA) and a cooling unit. The following primary antibodies were used for the detection of the proteins that were transferred to the membrane: anti-actin (MA5-11869; Thermo Fisher Scientific) and anti-Kif2a (ab37005; Abcam, Cambridge, UK). The following fluorescently labeled secondary antibodies were utilized for staining: IRDye800 donkey anti-mouse (610-732-124; Rockland Immunochemicals, Limerick, PA, USA) and Alexa Fluor 680 donkey anti-rabbit (A10043; Thermo Fisher Scientific). Detection of the stained protein bands was performed by means of the Odyssey Infrared Imaging System from Licor. The raw images were cropped and processed using Photoshop CS5 before quantifying the stained protein bands *via* ImageJ.

9.3.4 In vitro toxicity

9.3.4.1 Chapter 3

100 mM stock solutions of the polymers were prepared in 1xDPBS and diluted in a cell line-suitable medium to the final working concentrations. Here, the molarity was calcu-

lated by using the molecular weights of the polymers that were obtained by the HFIP-SEC. The respective cells were seeded into black-walled 96-well plates with a clear bottom (Corning™ 3603) in a density of 1 * 104 cells per well in 100 µl of suitable medium and incubated for 24 h to allow attachment. Then, after washing the cells with 1xDPBS, the medium was replaced against one containing the polymer structures at set concentrations (100 µM, 50 µM, 30 µM, 20 µM, 10 µM, 5 µM, 2.5 µM, 1 µM, 0.5 µM) and the cells were incubated for 72 h. The cell viability was determined by following the protocol of the CellTiterGlo® Assay (Promega Corporation), which is a luciferase-based method for ATP quantitation. Luminescence of each well was measured on the Tecan plate reader (Tecan, Austria). Untreated cells were used to determine the value for 100% cell viability and wells containing only medium were used as negative controls. The IC_{50} values [µM] were determined from survival curves (OriginPro 8.5.1G).

9.3.4.2 Chapter 4

The toxicity of the modified block copolymers was studied using an FITC-Annexin V Apoptosis Detection Kit with 7-AAD (Biolegend). Here, $2*10^5$ $CD8^+$ T-cells per well in 500 µL RPMI medium were seeded in flat transparent 48 well plates and incubated with the unlabeled as well as uncomplexed TDBC at different concentrations (75, 150, 200, 300, 400, 600, 800 µg/mL) for 72 h in a humidified incubator. Subsequently, FITC-Annexin V and 7-AAD staining was performed following the manufacturer's protocol and the samples were directly analysed with the flow cytometer. Untreated cells were used as the negative control, whereas 5 % DMSO treated T-cells were used as the positive control. Double negative cells were alive, Annexin V positive cells were early apoptotic, 7-AAD positive cells were necrotic, double positive cells were late apoptotic.

Other cell lines (HeLa [cervical cancer cells, human], MCF-7 [breast cancer cells, human], C2C12 [myoblast cells, murine], HEK293 [embryonic kidney cells, human]): 100 mM stock solutions of the TPP-modified block copolymers were prepared in 1xDPBS and diluted in a cell line-suitable medium to the final working concentrations. Here, the molarity was calculated by using the molecular weights of the polymers that were obtained by the HFIP-GPC. The respective cells were seeded into black-walled 96-well plates with a clear bottom (Corning™ 3603) in a density of $1 * 10^4$ cells per well in 100 µl of suitable medium and incubated for 24 h to allow attachment. Then, after washing the cells with 1xDPBS, the medium was replaced against one containing the polymer structures at set concentrations (720 $\mu g \cdot ml^{-1}$, 360 $\mu g \cdot ml^{-1}$, 216 $\mu g \cdot ml^{-1}$, 144 $\mu g \cdot ml^{-1}$, 72

$\mu g \cdot ml^{-1}$, 36 $\mu g \cdot ml^{-1}$, 18 $\mu g \cdot ml^{-1}$, 7.2 $\mu g \cdot ml^{-1}$, 3.6 $\mu g \cdot ml^{-1}$) and the cells were incubated for 72 h. The cell viability was determined by following the protocol of the CellTiter-Glo® Assay (Promega Corporation). Luminescence of each well was measured on the Tecan plate reader (Tecan, Austria). Untreated cells were used to determine the value for 100% cell viability and wells containing medium only were used as negative controls. The IC_{50} values [µM] were determined from survival curves (OriginPro 8.5.1G).

9.3.4.3 Chapter 5

The cytotoxicity of the DNA/polymer polyplexes was determined by an 3-(4,5-dimethylthiazol-2-yl)-2,5-diphenyltetrazolium bromide (MTT) assay.[7-10] For that purpose, 200 µl of polyplex solution were prepared with htDNA. Here, 4 µg herring testes DNA (htDNA, type XIV, Sigma-Aldrich Inc., MO, USA), and the appropriate amounts of polymer for the desired N/P ratios were each diluted in 100 µl of saline solution and vortexed for 10 seconds. After 10 minutes of equilibration at room temperature, all of the polymer solution was added to the pDNA solution and vortexed for 10 seconds. Subsequently, the complex formation was allowed to take place during 10 minutes at room temperature and it was further diluted with 2 mL of cultivation medium. CHO-K1 cells were seeded on 96 well microplates (polystyrene, clear, F-bottom, Greiner Bio-One GmbH, Germany) with identical cell density as in luciferase experiments and incubated for 24 hours. Following this, 191.8 µl of polyplex solution diluted in medium were added to the cells. As negative and positive controls, 191.8 µl of pure medium and 191.8 µl of medium containing 0.02 wt/vol% thiomersal (Carl Roth GmbH, Germany) were added. 191.8 µl of medium without cells was used as blank control. After 4 hours of incubation, cells were washed once with PBS, fresh medium was added and incubation of cells was continued for another 44 hours. Following this, the medium was aspirated and the blue formazan crystals were dissolved with 200 µl of dimethyl sulfoxide (DMSO, Carl Roth GmbH, Germany). Subsequently, the absorbance was measured at 570 nm (SPARK 10M, TECAN Group AG, Austria) and the relative cell viability was calculated. According to DIN ISO 10993-5:2009, samples exhibiting a relative viability of $\geq$ 70% were regarded as non-toxic.

9.3.4.4 Chapter 6

The cytotoxicity of the polymers was determined by an 3-(4,5-dimethylthiazol-2-yl)-2,5-diphenyltetrazolium bromide (MTT) assay.[7-10] For that purpose, polymer concentrations of 500 µg/mL were tested. CHO-K1 cells were seeded on 96 well microplates

(polystyrene, clear, F-bottom, Greiner Bio-One GmbH, Germany) with identical cell density as in luciferase experiments and incubated for 24 hours. Following this, 191.8 µl of polymer solution diluted in medium were added to the cells. As negative and positive controls, 191.8 µl of pure medium and 191.8 µl of medium containing 0.02 wt/vol% thiomersal (Carl Roth GmbH, Germany) were utilized. 191.8 µl of medium without cells was used as blank control. After 4 hours of incubation, cells were washed once with PBS, fresh medium was added and incubation of cells was continued for another 44 hours. Following this, the medium was aspirated and the blue formazan crystals were dissolved with 200 µl of dimethyl sulfoxide (DMSO, Carl Roth GmbH, Germany). Subsequently, the absorbance was measured at 570 nm (SPARK 10M, TECAN Group AG, Austria) and the relative cell viability was calculated. According to DIN ISO 10993-5:2009, samples exhibiting a relative viability of ≥ 70% were regarded as non-toxic.

9.3.5 Confocal laser scanning microscopy (cLSM)

9.3.5.1 Chapter 3 and Chapter 4

Staining of cells: For fluorescence microscopy imaging, HEK293 cells were seeded at a concentration of $1*10^4$ cells per cm^3 in a volume of 200 µL on 8-well chambered cover glasses (# 1.0 Borosilicate Coverglass System, Lab-Tek, Nunc) and grown for 24 h to allow attachment to the surface. The block copolymer was dissolved in Dulbecco's phosphate-buffered saline (1xDPBS, with Ca^{2+}/Mg^{2+}, Life Technologies) to give a stock solution of 2 mg/mL, which was stored at 4 °C. The complexes were prepared shortly prior to the transfection experiments by mixing the labeled siRNA with the respective polymer structures in $weight^{polymer}/weight^{siRNA}$ ratios guaranteeing complete complexation (deducted from the results of the electrophoretic mobility shift assay) and incubating the solution in 1xDPBS for 20 min at ambient temperature. Here, siRNA was chosen to carry the fluorescent label, in order to minimize falsely positive results originating from the fact that for the complex formation an excess of the polymers were used (free available polymer molecules in solution). The complexes were further diluted in phenol red-free cell culture medium to achieve a 50 nM final concentration of siRNA. Before staining, the cells were washed once with 1xDPBS, which was then replaced by 200 µL of the staining solution and incubated at 37 °C and 5% CO_2 for the indicated duration. During incubation, cells could be directly imaged without washing.

Imaging: The internalization of the polyplexes consisting of the block copolymer structures (or TDBC) and ATTO488-labelled siRNA double helix (IBA Nucleic Acids Syn-

thesis, annealed, 3'-labelled sense strand: GCA AGC UGA CCC UGA AGU UCA U (ATTO488), unlabelled antisense strand: GAA CUU CAG GGU CAG CUU GCC G) was tested in live HEK293 cells at 37°C and 5% CO_2. Fluorescence confocal laser scanning microscopy (cLSM) images were acquired with a TCS SP5 (Leica) equipped with a 63x/1.4 and 100×/1.4 oil plan apochromatic objective and an incubation chamber for live cell imaging (37°C, 5% CO_2). The acquisition was performed either in an automated way every 10 min for 15 h (time lapse study) or Z-scans were taken manually after the indicated incubation times. The ATTO488 label was excited by an argon laser at λ_{ex} = 488 nm (power set to 20%, AOTF transmission set to 5-10 %) and the emission range was set to λ_{em} = 520 - 600 nm. Fluorescence signals were detected by hybrid detectors (HyD) with fixed gain values that were set to 100. Fluorescence image acquisition and processing was performed with the LAS AF 4.0 software (Leica) and Fiji. In order to rule out the possibility that the staining of the cells was caused by free dye molecules, the cells were also incubated with uncomplexed ATTO488-labeled siRNA, in which case no internalization could be observed.

9.3.5.2 Chapter 4

Intracellular localization of the polyplexes was imaged using Leica TCS SP5 II, which was equipped with a HCX PL APO CS 63x/1.4-0.6 oil-immersion objective. Image processing was done via the Leica LAS AF Software. All experiments were performed in µ-Slide 8 well glass bottom dishes, in which $CD8^+$ T-cells were seeded in concentrations of $8*10^4$ cells per well in a total volume of 200 µl medium. The complexes between the modified diblock copolymers and siRNA were prepared by following the described procedure in 8.2.8.1 at the $weight^{polymer}/weight^{siRNA}$ ratio of 100:1 shortly prior to the cLSM experiment. The cells were then stained using a final polymer concentration of 150 µg/mL. cLSM-imaging was performed after 3 h of incubation in a humidified incubator (37 °C, 5% CO_2), which was done subsequently to the staining of the cells via CellMask™ Green plasma membrane stain (Thermo Fisher Scientific; diluted 1:1000 with 1x phosphate buffered saline, incubation time of 15 min at 37 °C and 5% CO_2).

The same conditions were used to follow the internalization of uncomplexed polymers. In these cases, co-staining using MitroTracker® Green FM (Thermo Fisher Scientific) was performed in accordance to the manufacturer's protocol.

9.3.6 Flow cytometric analysis

The fluorescence-activated cell sorting (FACS) was performed with a Partec CyFlow ML flow cytometer equipped 4 different laser (375, 488, 561 and 640 nm) and Flowmax 3.0. For data analysis FCS4express (De Nova Software) was employed. $CD8^+$ T-cells were seeded in 48 well plates at a concentration of $2*10^5$ cells/well in 200 µl medium. The cells were incubated for 3 h with polymer-siRNA complexes, which were prepared at a $mass^{siRNA}/mass^{polymer}$ ratio of 1:100. Here, final polymer concentrations of 200 µg/mL were utilized. Following the incubation period in a humidified incubator, the cells were stained with Zombie Aqua™ Fixable Viability Kit (Biolegend) according to the manufacturer's protocol. Subsequently, cells were fixed with 4% Histofix (Carl Roth) and analyzed with the flow cytometer. The same approach was used for uncomplexed polymer structures. To investigate the influence of serum proteins on the uptake, alterations to the setup were implemented. Here, the concentrations of fetal bovine serum (2%, 10% or 100%) in the RPMI-1640 medium were altered to simulate polyplex/protein aggregation and its effects on membrane penetrability. In addition, the samples were stained at different time points (0 min, 30 min, 1 h, 3 h, 6 h, 18 h, 24 h) with Zombie Aqua™ Fixable Viability Kit (Biolegend) according to the manufacturer's protocol and before they were fixed with 4 % Histofix and analyzed via flow cytometer.

9.4 Simulation

The simulation was performed in collaboration with Maziar Heidari and Prof. Dr. Raffaello Potestio, who operated the computational devices and software.

The LAMMPS[11] simulation package was used to simulate the system composed of copolymers and siRNAs. For the polymers a semi-flexible bead-and-spring model was employed and for the siRNA coordinates of a segment (21 base pairs) of RNA we extracted from the protein data bank. All simulations were performed in canonical ensemble (NVT), i.e. the temperature (T), volume (V) and the number of particles (N) of the system are kept constant during the simulations. To compare the stability of the complex, simulations were carried out with equal time of $10^6\,\tau$, where τ is the characteristic time scale and it is defined by the mass unit m, energy unit ϵ and the length unit σ; $\tau = \sqrt{\epsilon/m\sigma^2}$. The simulation time step is set to $\Delta t = 0.002\tau$. The time averaging is perfomed over the last $5 \times 10^5\tau$. The illustrations showing polymers and siRNAs were prepared using the VMD[12] visualization package.

9.5 Synthesis

9.5.1 Ubiquitously used compounds

These compounds were synthesized repeatedly for the duration of my PhD work, since they were utilized as materials in all chapters. The used amounts of starting compounds and the corresponding yields are representative for the performed synthesis.

9.5.1.1 4-Cyano-4-((phenylcarbonothioyl)thio)pentanoic acid (CTP)

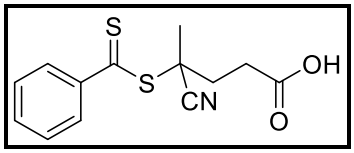

4,4′-Azobis(4-cyanovaleric acid) (3.33 g, 7.90 mmol) and 1.5 equivalents of di(thiobenzoyl)disulfide (2.43 g, 11.88 mmol) were dissolved in 50 mL dry ethylacetate. The reaction mixture was refluxed under argon for 18 h at the temperature of 80 °C. The solvent was removed *in vacuo* and the raw product mixture was then worked up via column chromatography with ethylacetate/n-hexane (2:3) as the eluent. Recrystallization in toluene yielded the required purity for its use as a chain transfer agent in RAFT polymerizations.

Yield: 1.52 g, 46%, red solid

The analytical data agrees with that published by Thang *et al.*.[13]

9.5.1.2 N-(3-Guanidinopropyl) methacrylamide (GPMA)

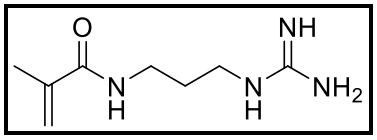

N-(3-Aminopropyl) methacrylamide hydrochloride (APMA) was dissolved in DI H_2O. The pH was adjusted by drop wise adding an aqueous NaOH solution (50 wt%) until a pH of 11 was reached. The de-acidified APMA was extracted using dry dichlormethane. The dichlormethane was then removed in vaccuo leaving a transparent yellow oil, which was added drop wise to a mixture of 2-ethyl-2-thiopseudourea hydrobromide and triethylamine in dry acetonitrile. The reaction was performed at ambient temperature by continuous stirring for 40 hours. The product was purified via flash chromatography (50:50 EtOH/EtOAc).

Yield: 120 mg, 15%, colorless oil

The analytical data agrees with that published by Treat *et al.*.[14]

9.5.1.3 N-(2-Hydroxypropyl) methacrylamide (HPMA)

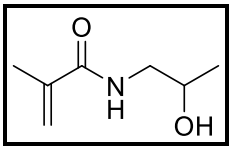

N,N-Diisopropylethylamine (12.5 mL, 71.75 mmol) was dissolved under argon in dry dichlormethane and the mixture was cooled to -10 °C. Then, 1-amino-2-propanol (5.54 mL, 71.75 mmol) was added. Subsequently freshly distilled methacryloyl chloride (5 g, 47.83 mmol), which was dissolved in dry dichlormethane, was added dropwise over 3h under vigorous stirring while keeping the reaction temperature at -10 °C. The mixture was then allowed to attain room temperature and stirred for another 30 min. Following filtration to remove the precipitate, the filtrate was concentrated *in vacuo* until formation of crystallization seeds was observed. The product was allowed to crystalize overnight and further purified by using column chromatography (200-400 mesh, 40-75 µm) with DCM:EtOH (10:1) as the solvent.

Yield: 6.24 g, 91%, colorless solid

The analytical data agrees with that published by Apostolovic *et al.*[15] and Scales et al.[16]

9.5.2 Chapter 3

9.5.2.1 Macromolecular chain transfer agents (MacroCTAs)

The macromolecular chain transfer agents were prepared in sets of two (21 and 28 kDa) to prepare diblock copolymers with altered block size without affecting the final polymer length (30 kDa). These structures were prepared using ACVA as radical initiator and 4-Cyano-4-((phenylcarbonothioyl)thio)pentanoic acid (CTP) as the chain transfer agent of the RAFT polymerization.

Poly(N-(2-hydroxypropyl) methacrylamide) MacroCTA (PHPMA MacroCTA)

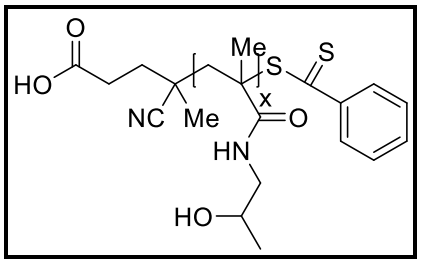

CTP, HPMA (3.00 g, 21 mmol) were added to a 50 mL Schlenk flask and dissolved in acetate buffer (pH 5.2, 0.27 M acetic acid and 0.73 M sodium acetate) achieving a monomer concentration of 1 M. Afterwards ACVA was added and the reaction was carried out under argon at 70 °C for 3 h 30 min. The HPMA homopolymer was prepared with a $[M]_o/[CTA]_o$ ratio of 390/1 (long block) or 290/1 (short block), while the $[CTA]_o/[I]_o$ was kept at 3/1. The macroCTA was dialyzed at pH 4 (hydrochloric acid) at 4 °C and dried via lyophilization. The product polymers were then characterized using NMR-spectroscopy and size exclusion chromatography with hexafluoroisopropanol (HFIP) as the eluent.

(N-(2-Hydroxypropyl) methacrylamide)-stat-(N-(3-aminopropyl) methacrylamide) MacroCTA (HPMA-s-APMA MacroCTA)

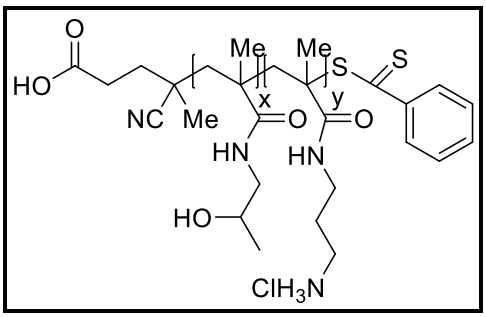

CTP, HPMA (3.00 g, 21 mmol, 90 mol%) and APMA (0.348 g, 2.1 mmol, 10 mol%) were added to a 50 mL Schlenk flask and dissolved in acetate buffer (pH 5.2, 0.27 M acetic acid and 0.73 M sodium acetate) achieving a monomer concentration of 1 M. Afterwards ACVA was added and the reaction was carried out under argon at 70 °C for 3 h 30 min. The HPMA-s-APMA copolymer was prepared with a $[M]_o/[CTA]_o$ ratio of 380/1 (long block) or 285/1 (short block), while the $[CTA]_o/[I]_o$ was kept at 3/1. The copolymer was dialyzed at pH 4 (hydrochloric acid) at 4 °C and dried via lyophilization. The product polymers were then characterized using NMR-spectroscopy and size exclusion chromatography with hexafluoroisopropanol (HFIP) as the eluent.

(N-(2-Hydroxypropyl) methacrylamide)-stat-(N-(3-guanidinopropyl) methacrylamide) MacroCTA (HPMA-s-GPMA MacroCTA)

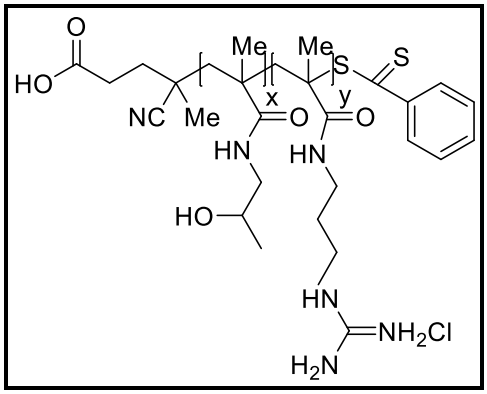

For the preparation of the desired polymers with the diblock copolymer structure (HPMA-*s*-GPMA)-*b*-APMA and (HPMA-*s*-GPMA)-*b*-GPMA (HPMA-s-GPMA) macroCTAs had to by synthesized (Step 1, Scheme S3). CTP, HPMA (3.00 g, 21 mmol, 90 mol%) and GPMA (0.462 g, 2.1 mmol, 10 mol%) were added to a 50 mL Schlenk flask and dissolved in acetate buffer (pH 5.2, 0.27 M acetic acid and 0.73 M sodium acetate) achieving a monomer concentration of 1 M. Afterwards ACVA was added and the reaction was carried out under argon at 70 °C for 3 h 30 min. The HPMA-s-GPMA copolymer was prepared with a $[M]_o/[CTA]_o$ ratio of 370/1 (long block) or 275/1 (short block), while the $[CTA]_o/[I]_o$ was kept at 3/1. The copolymer was dialyzed at pH 4 (hydrochloric acid) at 4 °C and dried via lyophilization.

9.5.2.2 Diblock copolymer structures

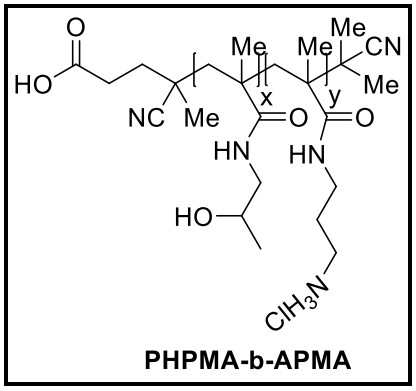

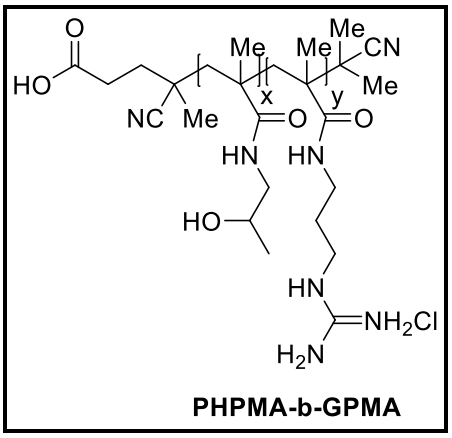

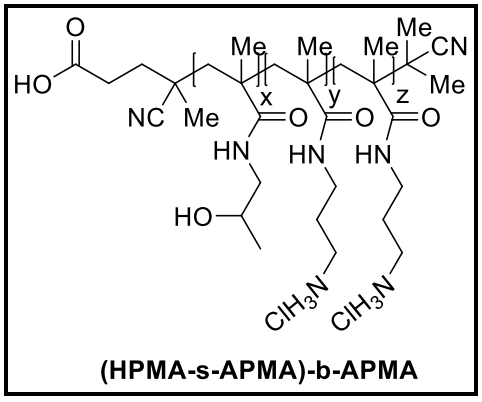

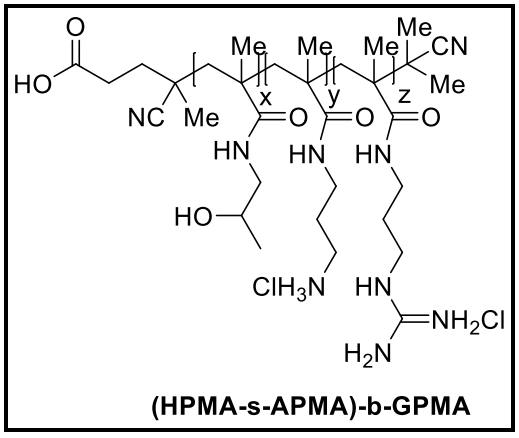

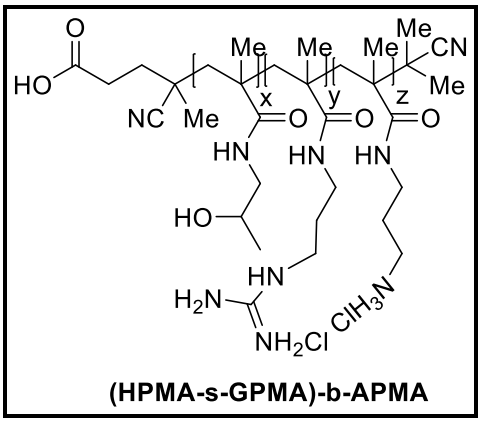

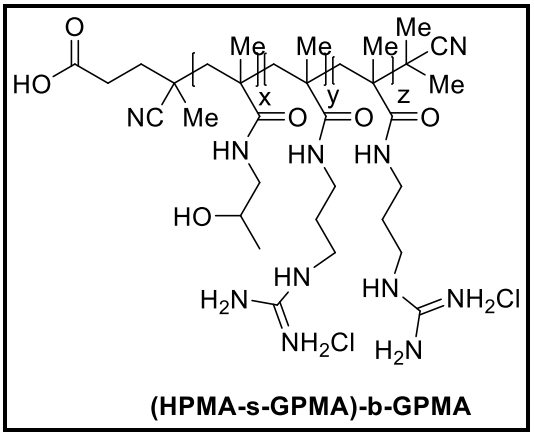

The addition of the second block was performed in analogy to the synthesis of the macroCTAs. The respective macroCTA and the GPMA (or APMA) monomer were dissolved in acetate buffer (pH 5.2, 0.27 M acetic acid and 0.73 M sodium acetate) diluting the monomer concentration to $[M]_0$ = 1.0 M. Then the radical initiator ACVA was added. The reaction mixture was stirred under argon at 70 °C for 10 h. The polymer was prepared with a $[M]_o/[CTA]_o$ ratio, which would ensure the final polymer size of 30

kDa, while the $[CTA]_o/[I]_o$ ratio was kept at 3/1. The work-up was done by dialyzing the reaction mixture in water at pH 4 (hydrochloric acid) and a temperature of 4 °C. Subsequent lyophilization yielded the polymer as a pink powder.

In the next step the terminal thiocarbonylthio functionalities were removed. Here, the approach of using azobisisobutyronitrile (AIBN) was chosen. The diblock copolymers still possessing their CTA function were dissolved together with AIBN in degased DMF (molar ratio of polymer/AIBN of 1:30). This solution was heated to 70 °C and stirred for 3 h under argon. Precipitation in in cold anhydrous diethyl ether, repeated washing with ether and filtering gave the pure polymer. Two reaction cycles were performed to ensure complete conversion.

9.5.3 Chapter 4

9.5.3.1 N-(2,6-Diisopropylphenyl)-1,6,7,12-tetraphenoxyperylene-3,4:9,10-tetra carboxy-9,10-monoanhydride-3,4-monoimide

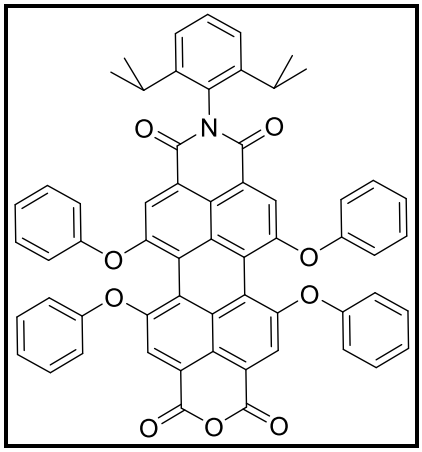

To a solution of N,N´-bis(2,6-diisopropylphenyl)-1,6,7,12-tetraphenoxyperylene-3,4:9,10-tetracarboxy diimide (8.00 g, 7.44 mmol) in 2-propanol (1040 mL) an aqueous solution of KOH (156.4 g, 2.801 mol, 144 mL H_2O) was added. The reaction took place under argon at 110 °C. Reaction progress was controlled using TLC-plates. Having observed complete conversion of the starting compound, the reaction solution was cooled to room temperature, precipitated in an aqueous solution of HCl (64 mL 13 M HCL in 4 L H_2O), filtered and dried under vacuum at 60 °C. The solid was dissolved in acetic acid (145 mL), which was then refluxed at 80 °C for 30 min. The desired product was obtained *via* precipitation in water, filtration and purification using column chromatography with dichlormethane as the eluent.

Yield: 2.14 g, 31%, red solid

The analytical data agrees with that in the Ph.D. Thesis of K. Peneva.[17]

9.5.3.2 N-(2,6-Diisopropylphenyl)-N'-(4-aminoethyl)-1,6,7,12-tetraphenoxyperylene-3,4:9,10-tetracarboxydiimide

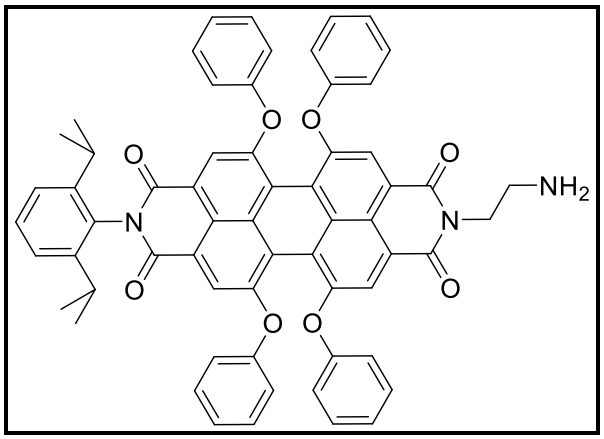

N-(2,6-diisopropylphenyl)-1,6,7,12-tetraphenoxyperylene-3,4:9,10-tetra carboxy-9,10-monoanhydride-3,4-monoimide (665 mg, 0.72 mmol) and 1,2-ethylenediamine (429 mg, 7.02 mmol) were dissolved in toluene (70 mL). The mixture was stirred under argon at 60 °C for 3 h. Following the removal of the solvent in vacuo, the material was purified using column chromatography with (first) dichlormethane/acetone (9/1) and (second) dichlormethane/ethanol (10/3) as eluent systems.

Yield: 492 mg, 71%, red solid

The analytical data agrees with that in the Ph.D. Thesis of K. Peneva.[17]

9.5.3.3 N-(2,6-Diisopropylphenyl)-N'-(4-aminoethyl)-1,6,7,12-tetra(4-sulfophenoxy)-perylene-3,4:9,10-tetracarboxydiimide

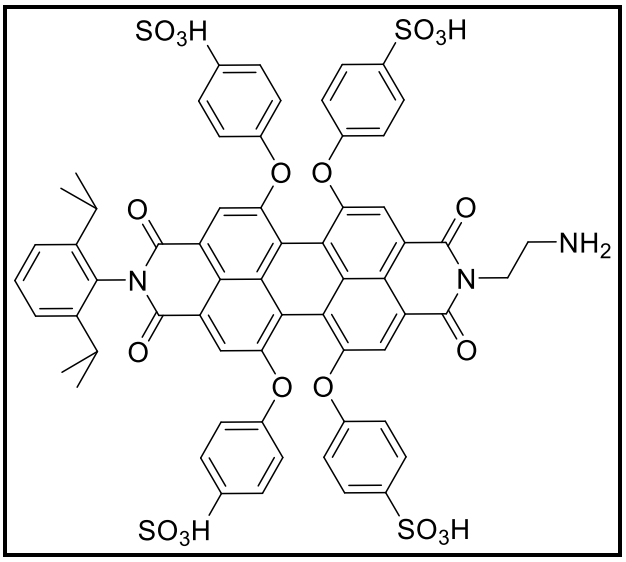

N-(2,6-Diisopropylphenyl)-N'-(4-aminoethyl)-1,6,7,12-tetraphenoxyperylene-3,4:9,10-tetracarboxydiimide (172 mg, 0.179 mmol) was dissolved in concentrated sulfuric acid (4 mL). The flask was sealed and the mixture was stirred at ambient temperature for 20 h. Then, water was slowly added to the flask while keeping the temperature of the reaction mixture at 0 °C. The resulting solution was dialyzed in water and lyophilized to give the product as a red solid.

Yield: 152 mg, 67%, red solid

The analytical data agrees with that in the Ph.D. Thesis of K. Peneva.[17]

9.5.3.4 (5-Carboxypentyl) triphenylphosphonium bromide (TPP)

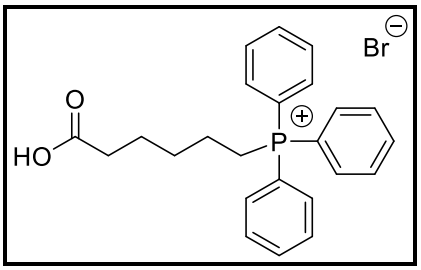

An equimolar mixture of 6-bromocaproic acid (3 g, 15.38 mmol) and triphenylphosphine (4.03 g, 15.38 mmol) was dissolved in 15 mL toluene and refluxed for 48 h. The reaction was stopped by cooling the solution to ambient temperature. The precipitate, which formed during the reaction, was filtered as well as repeatedly washed with diethyl ether. The crude product mixture was then recrystallized from ethylacetate to give the purified compound as a colorless solid.

Yield: 3.51 g, 60%, colorless solid

The analytical data agrees with that published by Cuchelkar *et al.*.[18]

9.5.3.5 (HPMA-s-APMA) MacroCTA (21 kDa)

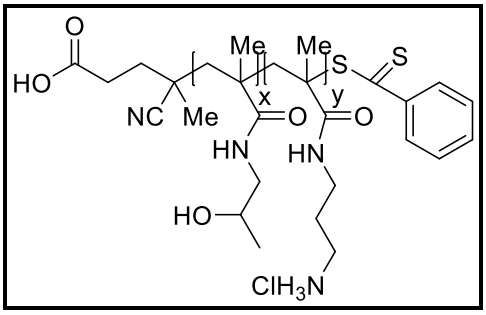

CTP, HPMA (3.00 g, 21 mmol, 90 mol%) and APMA (0.348 g, 2.1 mmol, 10 mol%) were added to a 50 mL Schlenk flask and dissolved in acetate buffer (pH 5.2, 0.27 M acetic acid and 0.73 M sodium acetate) achieving a monomer concentration of 1 M. Afterwards ACVA was added and the reaction was carried out under argon at 75 °C for 3 h 30 min. The HPMA-*s*-APMA copolymer was prepared with a $[M]_o/[CTA]_o$ ratio of 140/1, while the $[CTA]_o/[I]_o$ was kept at 3/1. The copolymer was dialyzed at pH 4 (hydrochloric acid) at 4 °C and dried via lyophilization to give a pink powder.

9.5.3.6 ((N-(2-Hydroxypropyl) methacrylamide)-stat-(N-(3-aminopropyl) methacrylamide))-block-(N-(3-guanidinopropyl) methacrylamide) ((HPMA-s-APMA)-b-GPMA) diblock copolymer with a terminal thiol

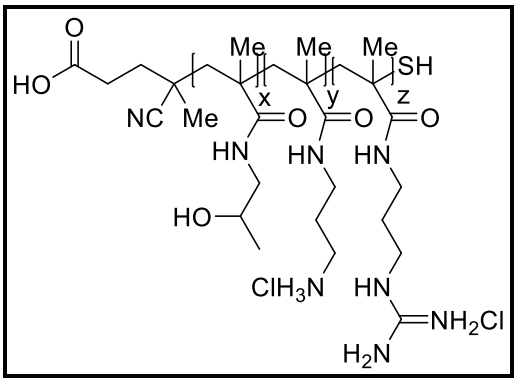

HPMA-*s*-APMA macroCTA (0.3 g) and the GPMA monomer (0.116 g, 0.628 mmol) were dissolved in acetate buffer (pH 5.2, 0.27 M acetic acid and 0.73 M sodium acetate) achieving a monomer concentration of $[M]_0$ = 1.0 M. Then the radical initiator ACVA was added. The block copolymer was prepared with a $[M]_o/[MacroCTA]_o$ ratio of 45/1, while the ratio of $[MacroCTA]_o/[I]_o$ was kept at 3/1. The reaction mixture was stirred in an argon atmosphere at 75 °C for 5 h. (HPMA-*s*-APMA)-*b*-GPMA MacroCTA was obtained as a pink powder after worked-up, which included dialysis of the reaction solution at pH 4 (hydrochloric acid) and a temperature of 4 °C and subsequent lyophilization.

(HPMA-*s*-APMA)-*b*-GPMA MacroCTA (0.1 g) and 1,2-ethylenediamine (0.002g, 0.03 mmol) were dissolved in 2 mL DMF. The reaction mixture was sealed with a septum, purged with argon and stirred at ambient temperature for 2 hours. The polymer was precipitated in cold anhydrous diethyl ether, washed twice with ether and filtered off before it was briefly dialyzed at pH 4 (hydrochloric acid) and a temperature of 4 °C giving the desired polymer structure as a colorless powder subsequent to lyophilization.

9.5.3.7 (HPMA-*s*-APMA)-b-GPMA – TPP conjugate

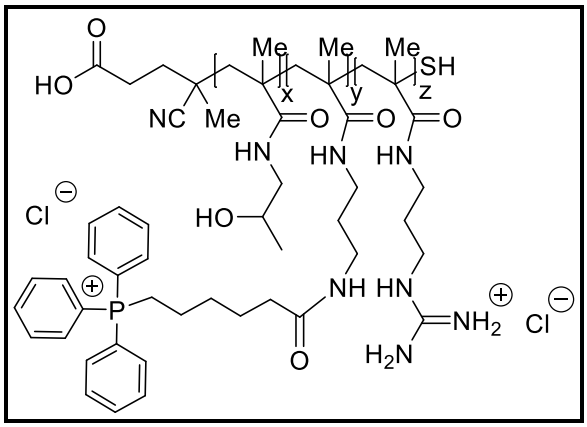

TPP (0.032 g, 0.084 mmol) was dissolved in 1 mL of the solvent mixture DMF/dioxane in the volume ratio of 1:1. Diisopropylethylamin (DIPEA, 0.014 g, 0.109 mmol) as well as N,N,N',N'-tetramethyl-O-(N-succinimidyl)uronium tetrafluoroborate (TSTU, 0.033 g, 0.109 mmol) were then added to the reaction mixture, which was stirred at ambient temperature for 30 min. (HPMA-*s*-APMA)-*b*-GPMA with a terminal thiol (0.1 g), which was dissolved in 1 mL DMF and made basic (pH 9) by DIPEA (0.0039 g, 0.03 mmol), was then added to the reaction mixture. The solution was stirred at ambient temperature for two hours. DMF and dioxane were removed *in vacuo* and the crude product mixture was purified by means of a column packed with BIO-RAD Bio-Gel® P-6 Gel using an aqueous 25 mM triethylamonium acetate buffer solution as the solvent. Dialysis at pH 4 (hydrochloric acid) and a temperature of 4 °C gave the desired polymer structure following lyophilization.

9.5.3.8 Perylene-labeled (HPMA-*s*-APMA)-b-GPMA – TPP conjugate

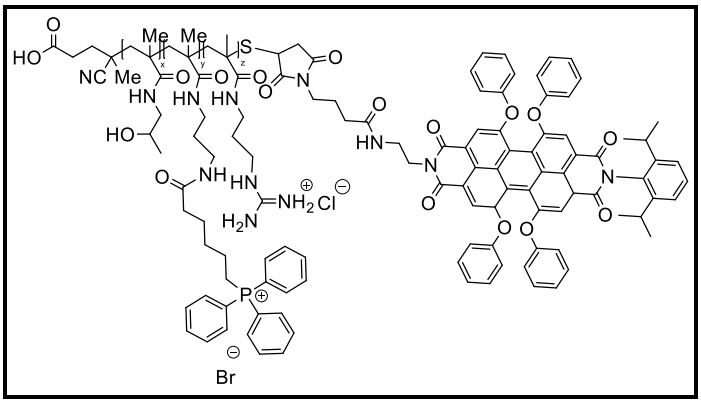

N-(2,6-Diisopropylphenyl)-N'-(4-aminoethyl)-1,6,7,12-tetraphenoxyperylene-3,4:9,10-tetracarboxydiimide (10 mg, 0.01 mmol) was dissolved in 1 mL DMF and DIPEA was added drop wise until the solution reached a pH of 11. N-γ-maleimidobutyryl-oxysuccinimide ester (GMBS, 2.2 mg, 0.008 mmol), dissolved in 100 µL DMF, was added to the reaction mixture, which was then stirred at ambient temperature for 2h. The Process of the reaction was checked via HPLC every 45 min until complete conversion of the dye was observed. Then the (HPMA-s-APMA)-b-GPMA – TPP conjugate (0.1 g) was dissolved in DMF containing a 10 mM concentration of EDTA. The polymer solution was made basic by drop wise addition of DIPEA until the pH of 8 was reached and both solutions were combined. The reaction mixture was stirred at ambient temperature overnight. DMF was removed *in vacuo* and the addition of water dissolved the crude product mixture, while the hydrophobic free dye could be removed via filtration. The labeled polymer structure was dialysed at pH 4 (hydrochloric acid) and a temperature of 4 °C to give the desired product as a red powder.

9.5.4 Chapter 5

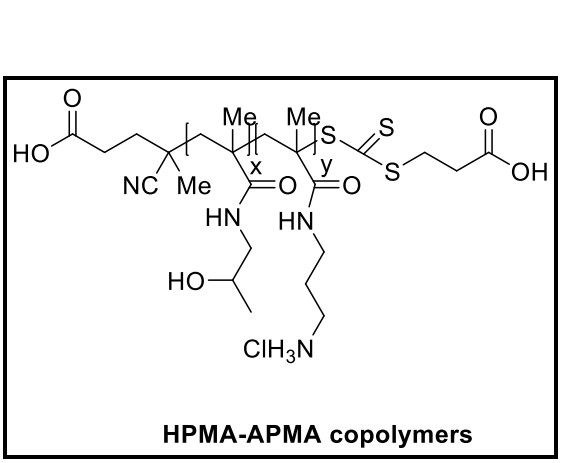

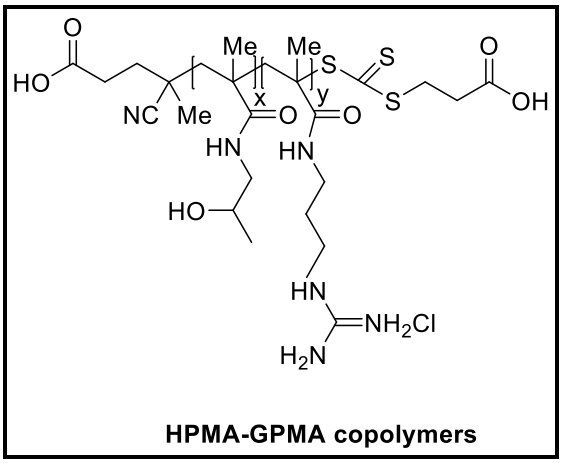

9.5.4.1 Statistical copolymers

The statistical copolymer structures (N-(2-hydroxypropyl) methacrylamide)-stat-(N-(3-aminopropyl) methacrylamide) (HPMA-*s*-APMA) and (N-(2-hydroxypropyl) methacrylamide)-stat-(N-(3-guanidinopropyl) methacrylamide) (HPMA-*s*-GPMA) with varying monomer composition (APMA or GPMA content in mol%: 5, 10, 20, 40, 50, 60, 75 and 90) were prepared using the aqueous reversible addition-fragmentation chain transfer polymerization. The general procedure is follows the procedure in 9.5.2.1, however, 4-((((2-Carboxyethyl)thio)carbonothioyl)thio)-4-cyanopentanoic acid was used as the chain transfer agent instead of the otherwise employed 4-cyano-4-((phenylcarbonothioyl)thio)pentanoic acid. In addition, polymerization run-time and propagation temperature were increased. The procedure is described using the structure HPMA-s-APMA with an APMA-content of 10 mol% as the example:

4-((((2-Carboxyethyl)thio)carbonothioyl)thio)-4-cyanopentanoic acid, HPMA (0.50 g, 3.49 mmol, 90 mol%) and APMA (0.63 g, 0.35 mmol, 10 mol%) were added to a 50 mL Schlenk flask and dissolved under argon in acetate buffer (pH 5.2, 0.27 M acetic acid and 0.73 M sodium acetate) achieving a monomer concentration of 1 M. Afterwards ACVA was added and the reaction was carried out under argon at 80 °C for 5 h. The HPMA-s-APMA copolymer was prepared with a $[M]_0/[CTA]_0$ ratio of 80/1, while $[CTA]_0/[I]_0$ was kept at 3/1. Dialysis in acidic water (pH 4, hydrochloric acid) at 4 °C and lyophilisation gave the product polymer as a yellow powder.

9.5.4.2 Gradient copolymers

The aRAFT semi-batch copolymerization method was used for the synthesis of the gradient copolymer structures (N-(2-hydroxypropyl) methacrylamide)-grad-(N-(3-aminopropyl) methacrylamide) (HPMA-*g*-APMA) and (N-(2-hydroxypropyl) methacrylamide)-grad-(N-(3-guanidinopropyl) methacrylamide) (HPMA-*g*-GPMA) with varying monomer ratios (APMA or GPMA content in mol%: 5, 10, 20, 40, 50, 60, 75 and 90). For the calculation of the desired molar mass and monomer composition, the comonomers APMA or GPMA were treated as if fully present at the start of the reaction. The general procedure is described using the structure HPMA-g-APMA with an APMA-content of 10 mol% as the example:

A Schlenk flask was charged with HPMA (0.50 g, 3.49 mmol, 90 mol%) and dissolved under argon in acetate buffer (pH 5.2, 0.27 M acetic acid and 0.73 M sodium acetate) obtaining a 1 M monomer concentration. 4-((((2-carboxyethyl)thio)carbonothioyl)thio)-4-cyanopentanoic acid and the initiator ACVA, which were dissolved in DMF, were added to the reaction mixture. APMA (0.63 g, 0.35 mmol, 10 mol%) was dissolved in the acetate buffer to give a 1 M solution, filled into a syringe, and placed into a syringe pump. The polymerization was performed under argon at 80 °C for 5 hours, while the syringe pump was set to add the APMA-solution continuously into the reaction mixture over the set period of time (Table 8.4). The ratio of $[M]_0/[CTA]_0$ was set to 80/1 and $[CTA]_0/[Ini]_0$ to 3/1. The obtained copolymer was purified via dialysis at 4°C/pH 4 (hydrochloric acid) and dried by means of lyophilisation, which yielded a yellow powder.

Table 9.1 Monomer addition rates in [mmol/h] of APMA and GPMA throughout the semi-batch copolymerization

Gradient copolymer with x mol% APMA/GPMA	monomer addition rate [mmol/h]
5%	0,097
10%	0,150
20%	0,276
40%	0,653
50%	0,954
60%	1,407
75%	2,764
90%	8,193

9.5.5 Chapter 6

9.5.5.1 2-(3-Indol-yl)ethyl methacrylamide (IEMA)

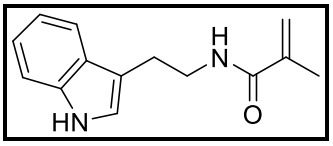

Tryptamine (5 g, 31.21 mmol) and triethylamine (4,35 mL, 31.21 mmol) were dissolved in 40 mL dry dichlormethane and cooled to 0 °C. Then freshly distilled methacryloyl chloride (2.77 mL, 28.37 mmol), dissolved in an equal volume of dichlormethane, was added drop wise under continuous cooling and stirring. The reaction mixture war subseuqnetly stirred at 0 °C for 1 h and for 2 h at ambient temperature before it was washed with a saturated aqueous natrium hydrogen carbonate solution and brine. The organic phase was dried over magnesium sulfate. Removal of the solvent *in vacuo* gave the crude product mixture, which was further purified by means of column chromatography using EtOAc/hexane in a ratio of 1:1 as the eluent. The colorless product was initially of an oily consistence, but crystalized overnight.

Yield: 3.11 g, 48%, pale yellow solid

The analytical data agrees with that published by Ilgin *et al.*.[19]

9.5.5.2 (N-(2-Hydroxypropyl) methacrylamide)-stat-(N-(2-(3-indol-yl)ethyl methacrylamide) (HPMA-s-IEMA)

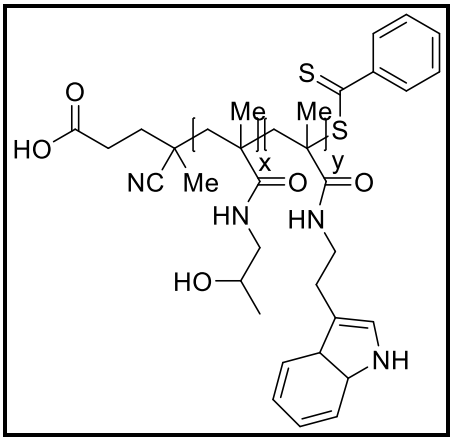

A Schlenk flask was charged with IEMA and HPMA giving the desired stoichiometric ratio (mol%) of the monomers ($HPMA_{95\%}$-s-$IEMA_{5\%}$, $HPMA_{90\%}$-s-$IEMA_{10\%}$ or $HPMA_{80\%}$-s-$IEMA_{20\%}$). The monomers were dissolved in degassed DMF containing 10 vol% MilliQ water under argon obtaining a monomer concentration of 1 M. The chain transfer agent 4-Cyano-4-((phenylcarbonothioyl)thio)pentanoic acid and ACVA, which were dissolved in DMSO, were added to the reaction mixture. The $[M]_0/[CTA]_0$ ratio was set to 200/1 and $[CTA]_0/[Ini]_0$ was adjusted to 3/1. Polymerisation was then performed under argon at 80°C for 24 hours. Subsequent to the polymerization step the solvent was removed *in vacuo* and raw product mixture was washed with DCM before it was further purified via dialysis at 4°C and at pH 4 (hydrochloric acid). Lyophilisation gave the polymer as a pink powder.

9.5.5.3 (N-(2-HHydroxypropyl) methacrylamide)-stat-(N-(3-guanidinopropyl) methacrylamide)-stat-(N-(2-(1H-indol-3-yl)ethyl) methacrylamide) (HPMA-s-GPMA-s-IEMA)

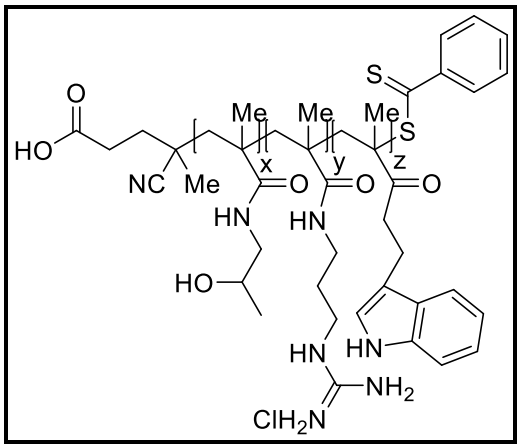

A Schlenk flask was charged with IEMA, GPMA and HPMA giving the desired stoichiometric ratio (mol%) of the monomers ($HPMA_{90\%}$-s-$GPMA_{5\%}$-s-$IEMA_{5\%}$ or $HPMA_{80\%}$-s-$GPMA_{10\%}$-s-$IEMA_{10\%}$). The monomers were dissolved in degassed DMF containing 10 vol% MilliQ water under argon obtaining a monomer concentration of 1 M. The chain transfer agent 4-Cyano-4-((phenylcarbonothioyl)thio)pentanoic acid and ACVA, which were dissolved in DMSO, were added to the reaction mixture. The $[M]_0/[CTA]_0$ ratio was set to 200/1 and $[CTA]_0/[Ini]_0$ was adjusted to 3/1. Polymerisation was then performed under argon at 80°C for 24 hours. Subsequent to the polymerization step the solvent was removed *in vacuo* and raw product mixture was washed with DCM before it was further purified via dialysis at 4°C and at pH 4 (hydrochloric acid). Lyophilisation gave the polymer as a pink powder.

9.5.6 Chapter 7

9.5.6.1 Poly(N-(3-guanidinopropyl) methacrylamide) (PGPMA)

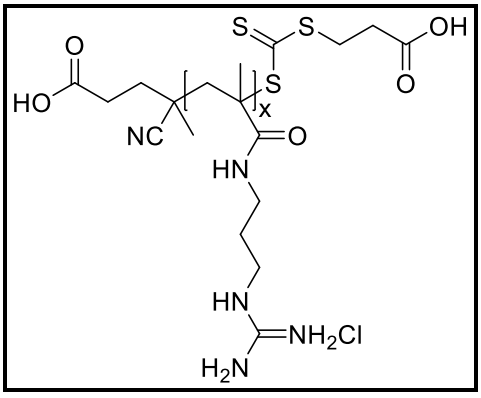

GPMA (1.20 g, 6.51 mmol) and 4-((((2-Carboxyethyl)thio)carbonothioyl)thio)-4-cyanopentanoic acid (26.4 mg, 0.085 mmol) were dissolved under argon in acetate buffer (pH 5.2, 0.27 M acetic acid and 0.73 M sodium acetate) achieving a monomer concentration of 1 M. Recrystallized 4,4'-azobis(4-cyanopentanoic acid) (ACVA, 8.01 mg, 0.0286 mmol) was then added to the mixture and the polymerization was carried out at 80 °C for 5 h. Dialysis in acidic water (pH 4, hydrochloric acid) at 4 °C and subsequent lyophilisation gave PGPMA as a yellow powder.

9.6 References

[1] P. Schuck, *Biophys J* **2000**, *78*, 1606.

[2] I. Nischang, I. Perevyazko, T. Majdanski, J. Vitz, G. Festag, U. S. Schubert, *Anal Chem* **2017**, *89*, 1185.

[3] P. L. Felgner, Y. Barenholz, J. P. Behr, S. H. Cheng, P. Cullis, L. Huang, J. A. Jessee, L. Seymour, F. Szoka, A. R. Thierry, E. Wagner, G. Wu, *Human Gene Therapy* **1997**, *8*, 511.

[4] D. Fischer, H. Dautzenberg, K. Kunath, T. Kissel, *Int. J. Pharm.* **2004**, *280*, 253.

[5] M. Jerabek-Willemsen, C. J. Wienken, D. Braun, P. Baaske, S. Duhr, *Assay Drug Dev. Technol.* **2011**, *9*, 342.

[6] P. Baaske, C. J. Wienken, P. Reineck, S. Duhr, D. Braun, *Angew. Chem., Int. Ed.* **2010**, *49*, 2238.

[7] T. Mosmann, *J Immunol Methods* **1983**, *65*, 55.

[8] C. L. Gebhart, A. V. Kabanov, *Journal of Controlled Release* **2001**, *73*, 401.

[9] S. Ochrimenko, A. Vollrath, L. Tauhardt, K. Kempe, S. Schubert, U. S. Schubert, D. Fischer, *Carbohydr Polym* **2014**, *113*, 597.

[10] D. Fischer, Y. Li, B. Ahlemeyer, J. Krieglstein, T. Kissel, *Biomaterials* **2003**, *24*, 1121.

[11] S. Plimpton, *J. Comput. Phys.* **1995**, *117*, 1.

[12] W. Humphrey, A. Dalke, K. Schulten, *J. Mol. Graphics* **1996**, *14*, 33.

[13] S. H. Thang, Y. K. Chong, R. T. A. Mayadunne, G. Moad, E. Rizzardo, *Tetrahedron Lett.* **1999**, *40*, 2435.

[14] N. J. Treat, D. Smith, C. Teng, J. D. Flores, B. A. Abel, A. W. York, F. Huang, C. L. McCormick, *ACS Macro Lett.* **2012**, *1*, 100.

[15] B. Apostolovic, S. P. E. Deacon, R. Duncan, H.-A. Klok, *Biomacromolecules* **2010**, *11*, 1187.

[16] C. W. Scales, Y. A. Vasilieva, A. J. Convertine, A. B. Lowe, C. L. McCormick, *Biomacromolecules* **2005**, *6*, 1846.

[17] K. Peneva, "Design, Synthesis and Application of Ultrastable Rylene Dyes for Fluorescent Labeling of Biomolecules", Johannes-Gutenberg University, 2008.

[18] V. Cuchelkar, P. Kopeckova, J. Kopecek, *Mol. Pharmaceutics* **2008**, *5*, 776.

[19] P. Ilgin, O. Selcuk Zorer, O. Ozay, G. Boran, *J. Appl. Polym. Sci.* **2017**, *134*, n/a.

9.7 Spectra

9.7.1 Microscale Thermophoresis

9.7.1.1 Chapter 3

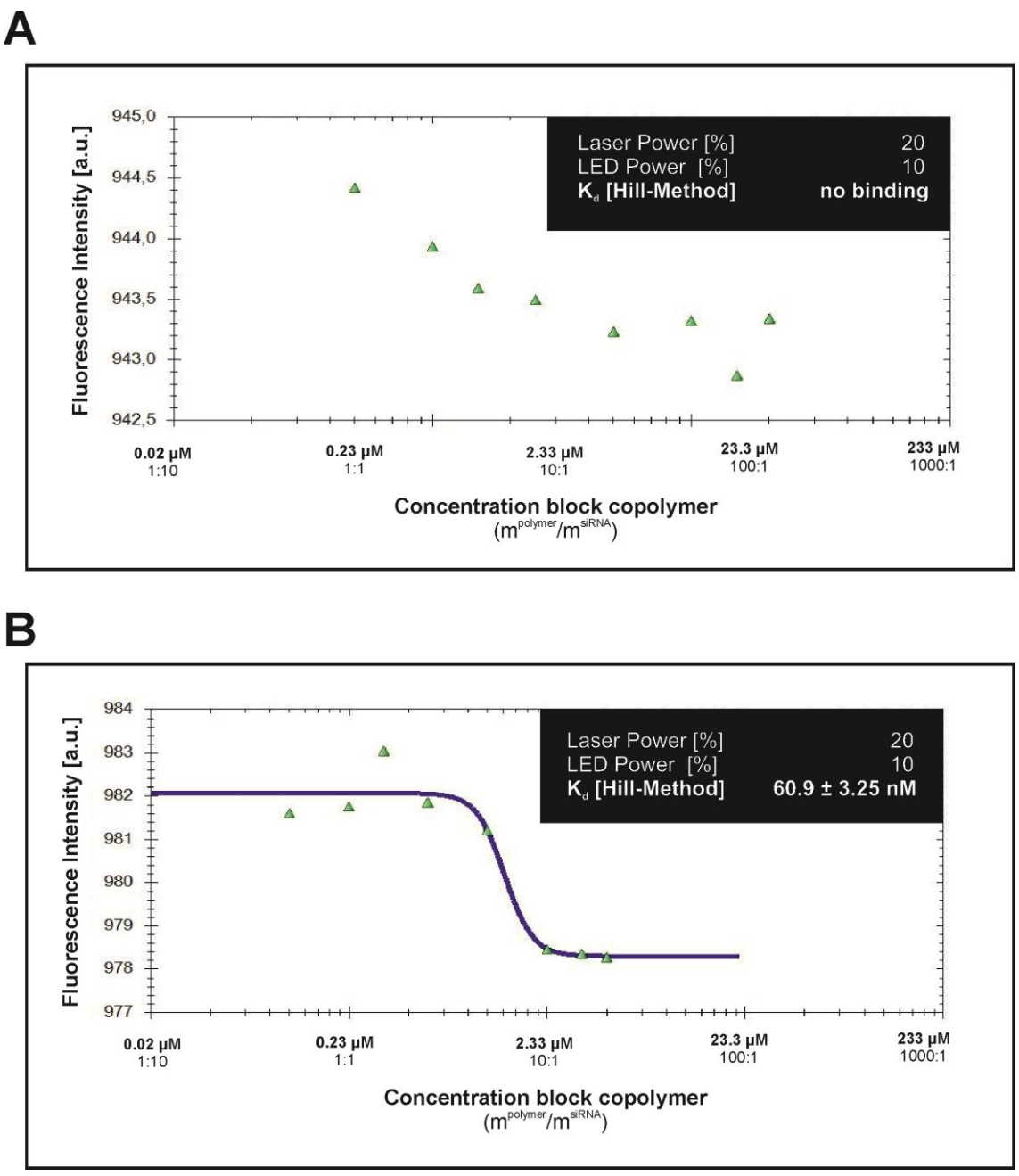

Figure 9.1. Fluorescence mode-evaluated Microscale Thermophoresis results (Hill method fit) for (A) HPMA$_{199}$-*b*-APMA$_{10}$ and (B) HPMA$_{147}$-*b*-APMA$_{45}$

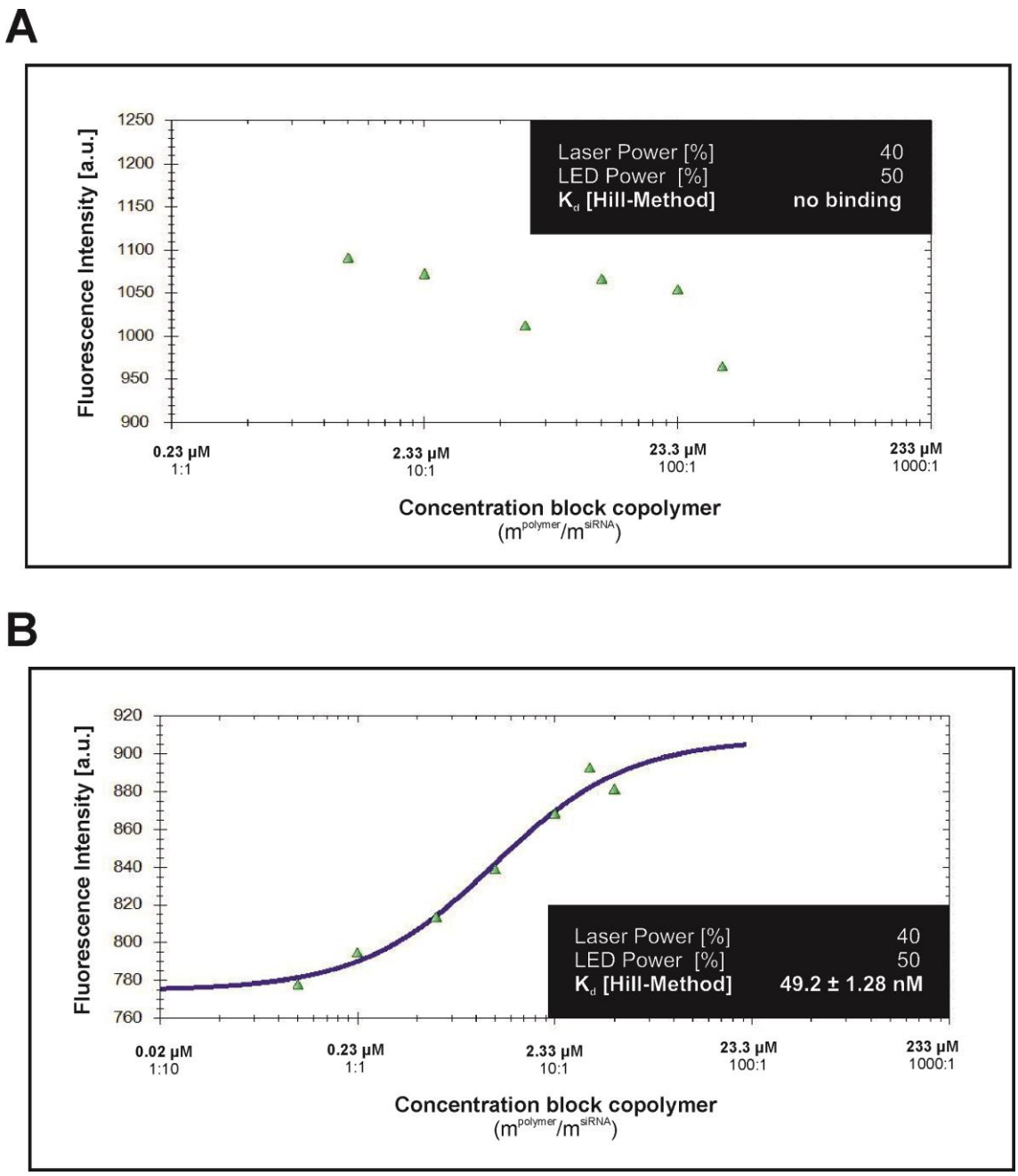

Figure 9.2. Fluorescence mode-evaluated Microscale Thermophoresis results (Hill method fit) for (A) HPMA$_{196}$-*b*-GPMA$_{16}$ and (B) HPMA$_{150}$-*b*-GPMA$_{58}$

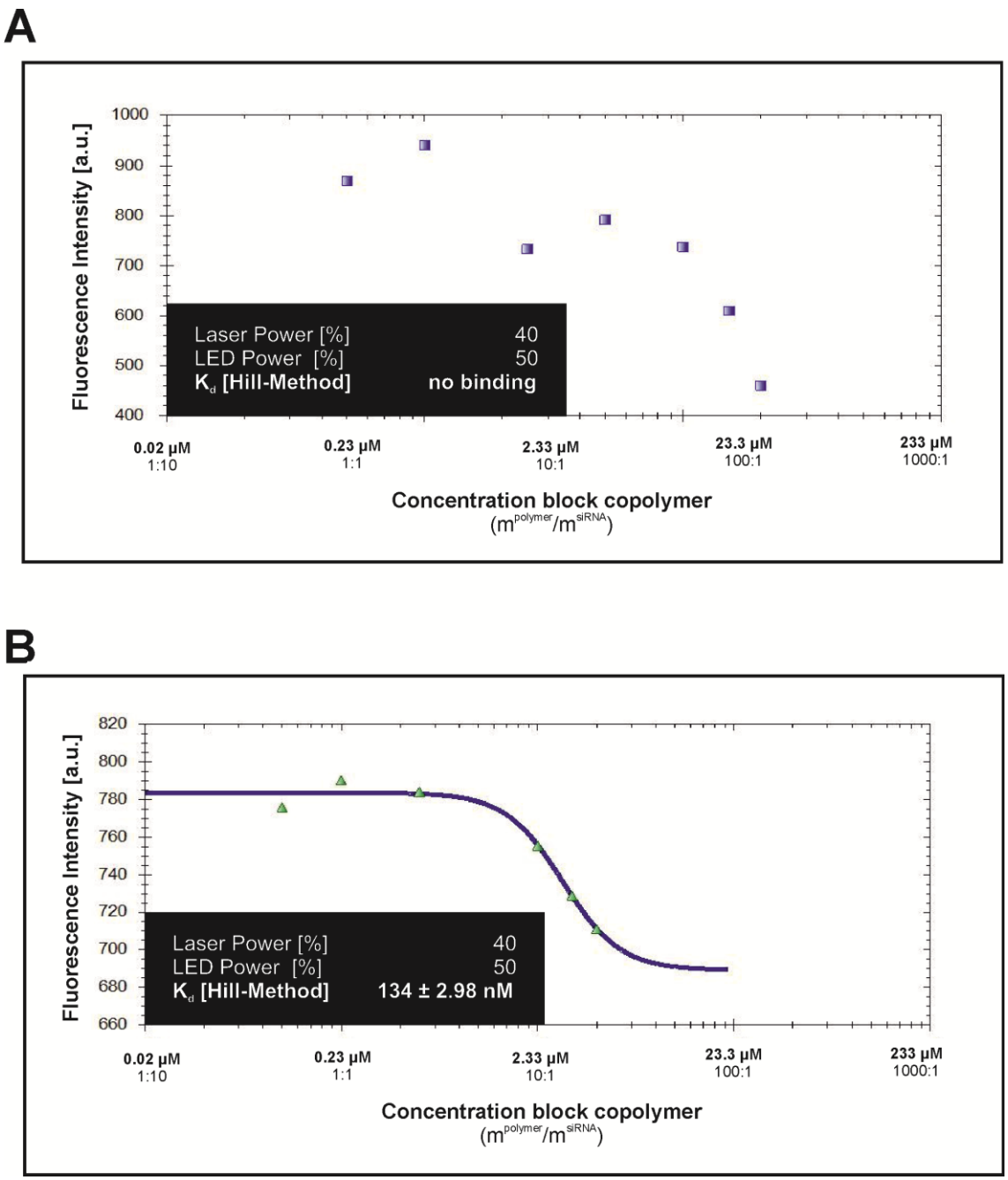

Figure 9.3. Fluorescence mode-evaluated Microscale Thermophoresis results (Hill method fit) for (A) ($HPMA_{180}$-*s*-$APMA_{20}$)-*b*-$APMA_{14}$ and (B) ($HPMA_{126}$-*s*-$APMA_{14}$)-*b*-$APMA_{64}$

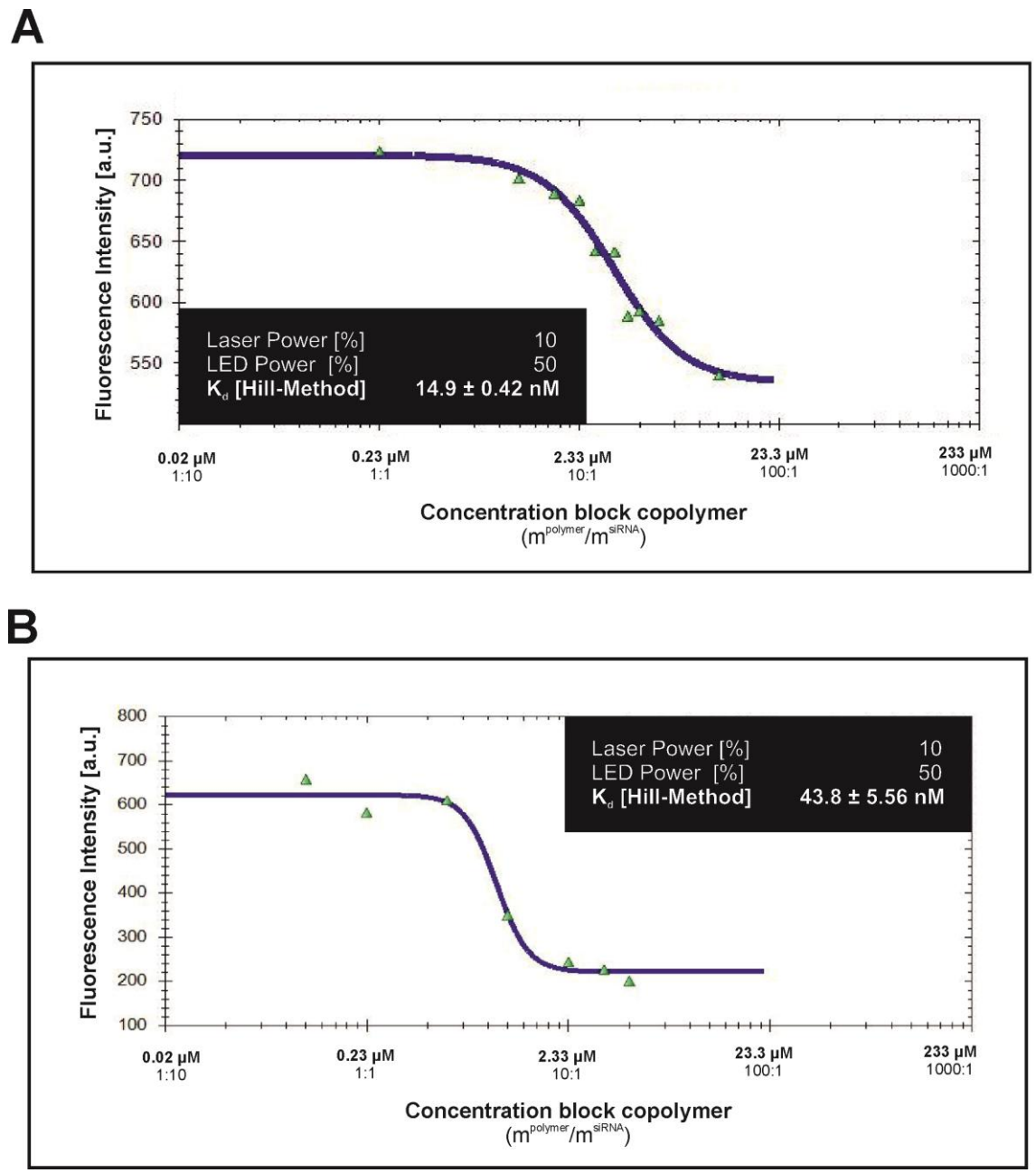

Figure 9.4. Fluorescence mode-evaluated Microscale Thermophoresis results (Hill method fit) for (A) ($HPMA_{180}$-*s*-$APMA_{20}$)-*b*-$GPMA_{11}$ and (B) ($HPMA_{126}$-*s*-$APMA_{14}$)-*b*-$GPMA_{49}$

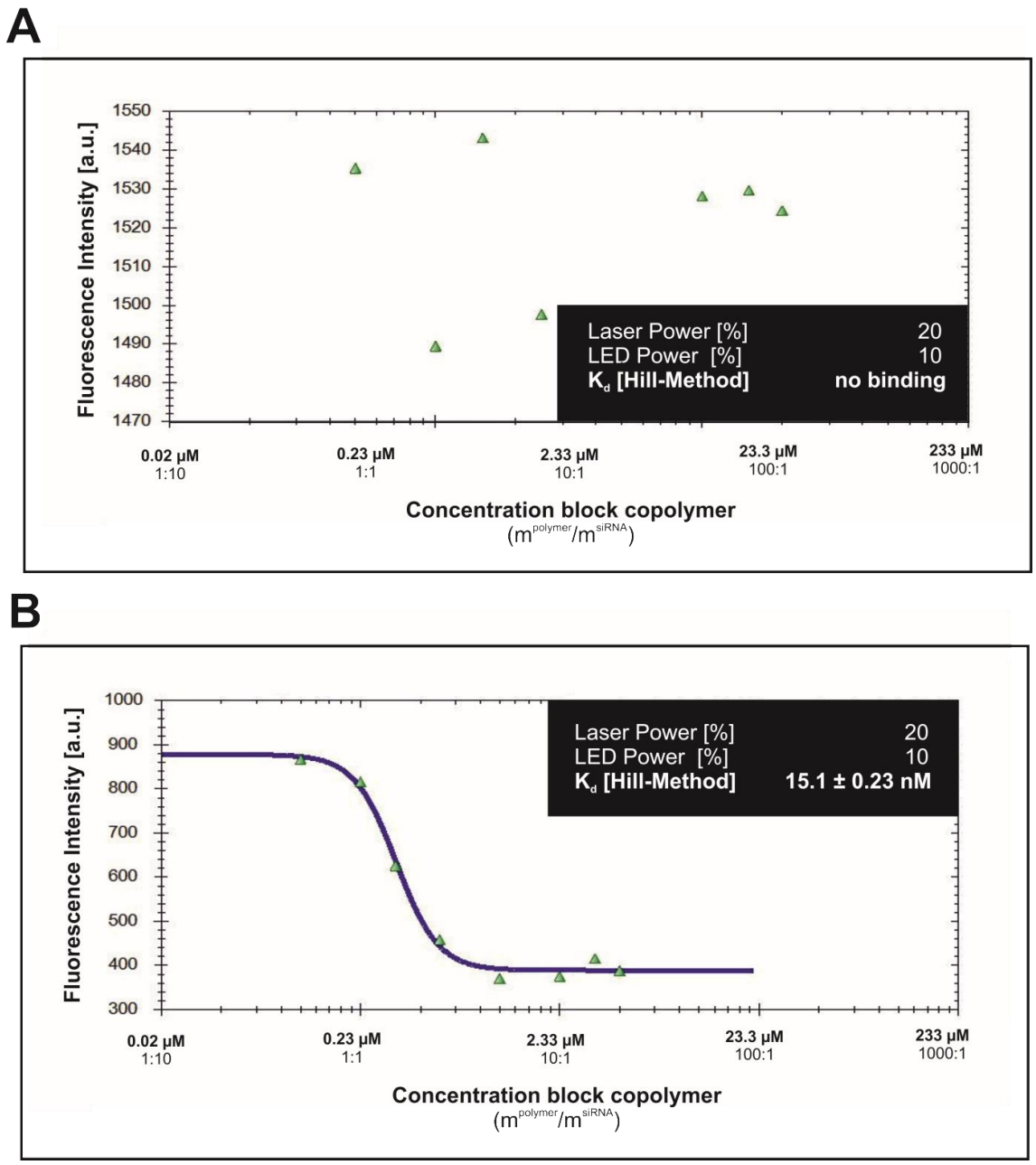

Figure 9.5. Fluorescence mode-evaluated Microscale Thermophoresis results (Hill method fit) for (A) ($HPMA_{180}$-*s*-$GPMA_{12}$)-*b*-$APMA_{22}$ and (B) ($HPMA_{157}$-*s*-$GPMA_{13}$)-*b*-$APMA_{28}$

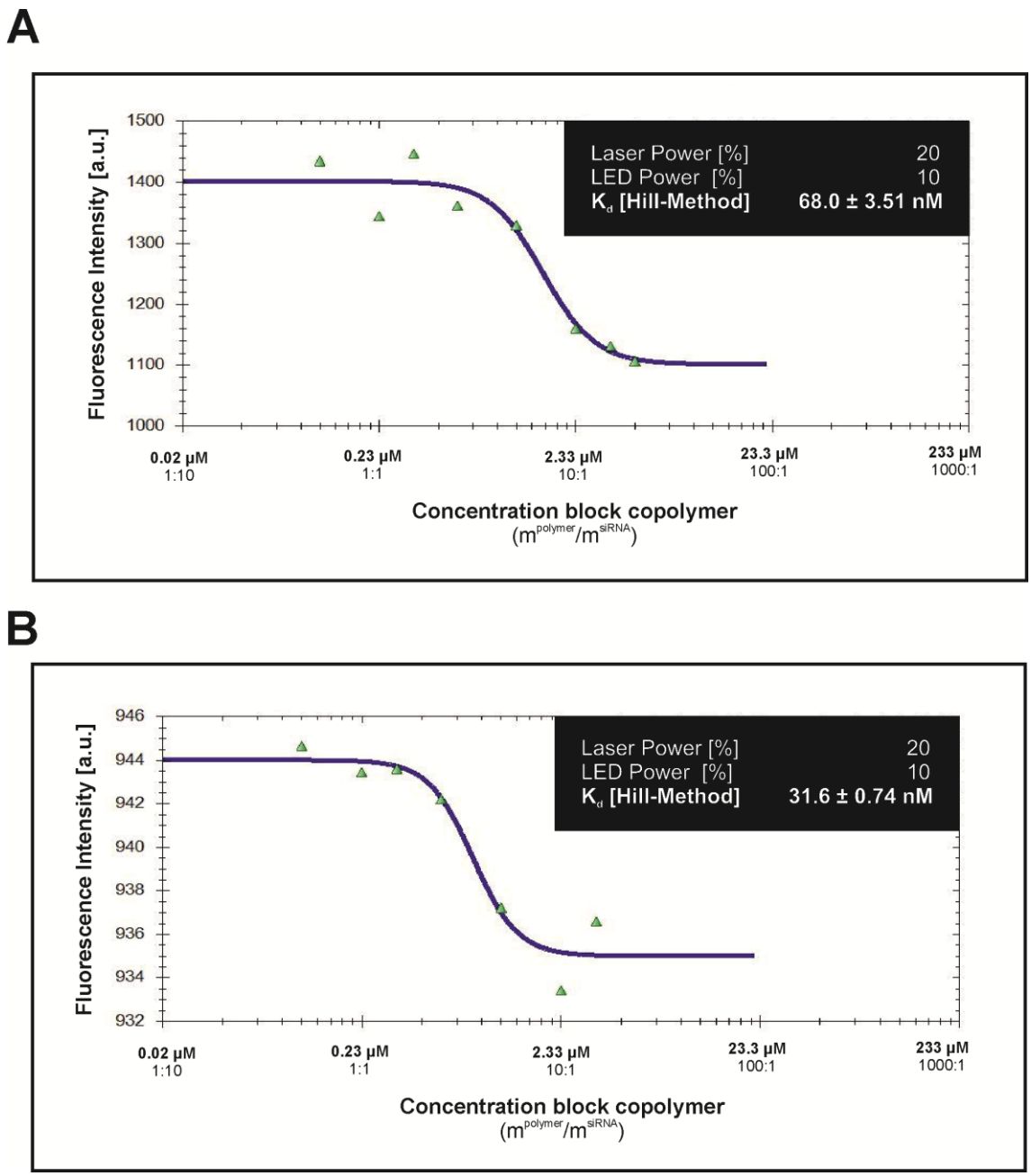

Figure 9.6. Fluorescence mode-evaluated Microscale Thermophoresis results (Hill method fit) for (A) ($HPMA_{180}$-*s*-$GPMA_{12}$)-*b*-$GPMA_{22}$ and (B) ($HPMA_{157}$-*s*-$GPMA_{13}$)-*b*-$GPMA_{27}$

9.7.1.2 Chapter 4

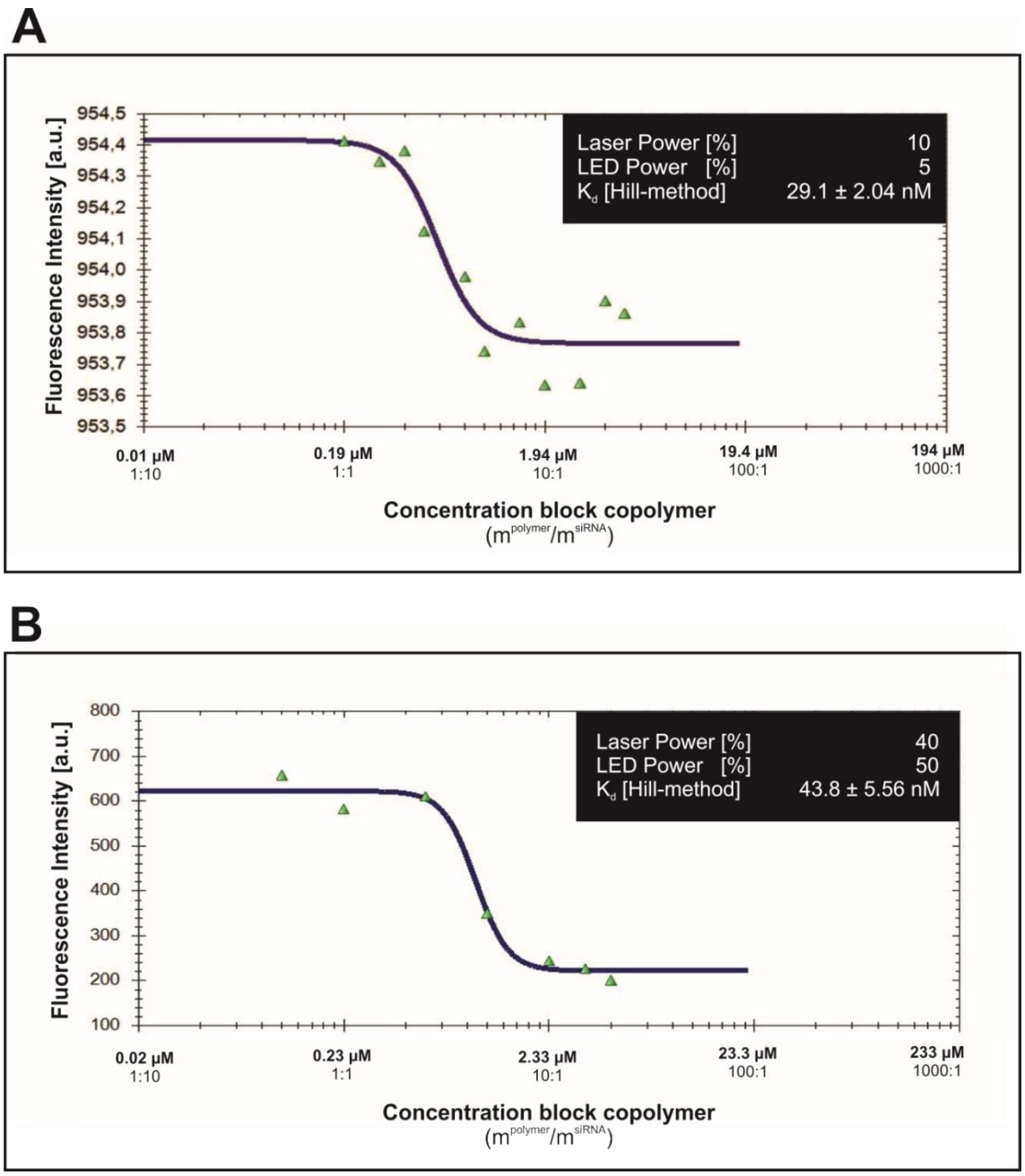

Figure 9.7. Fluorescence mode-evaluated Microscale Thermophoresis results (Hill method fit - ratio of polymer/siRNA (1:10) - (50:1)) for (A) ($HPMA_{126}$-*s*-$APMA_{14}$)-*b*-$GPMA_{49}$-TPP conjugate and (B) the unmodified ($HPMA_{126}$-*s*-$APMA_{14}$)-*b*-$GPMA_{49}$

9.7.2 Dynamic light scattering

9.7.2.1 Chapter 3

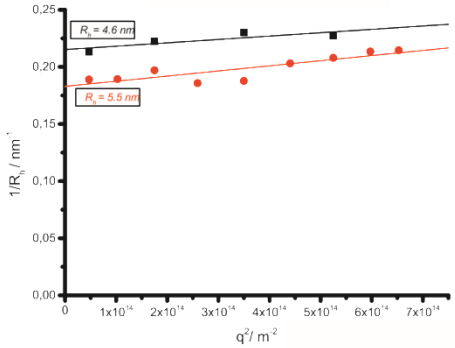

Figure 9.8. Plotted dynamic light scattering results to determine the hydrodynamic radius of the polymer 1 ($HPMA_{180}$-*s*-$APMA_{20}$)-*b*-$APMA_{14}$ before and after the addition of siRNA in a $mass^{siRNA}/mass^{polymer}$ ratio of 1:100.

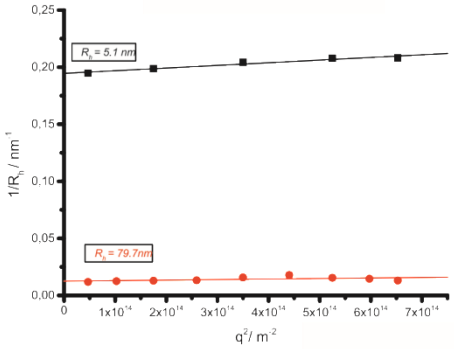

Figure 9.9. Plotted dynamic light scattering results to determine the hydrodynamic radius of the polymer 2 ($HPMA_{126}$-*s*-$APMA_{14}$)-*b*-$APMA_{64}$ before and after the addition of siRNA in a $mass^{siRNA}/mass^{polymer}$ ratio of 1:100

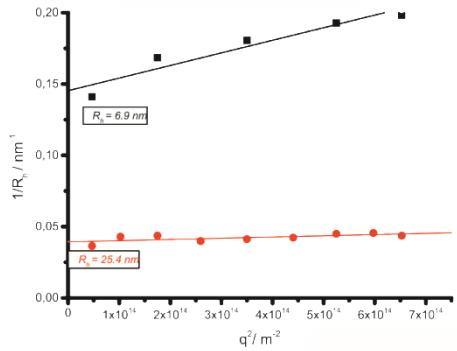

Figure 9.10. Plotted dynamic light scattering results to determine the hydrodynamic radius of the polymer 3 $HPMA_{147}$-*b*-$APMA_{45}$ before and after the addition of siRNA in a $mass^{siRNA}/mass^{polymer}$ ratio of 1:100.

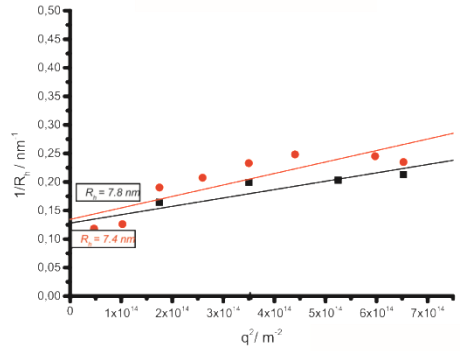

Figure 9.11. Plotted dynamic light scattering results to determine the hydrodynamic radius of the polymer 4 $HPMA_{199}$-*b*-$APMA_{10}$ before and after the addition of siRNA in a $mass^{siRNA}/mass^{polymer}$ ratio of 1:100.

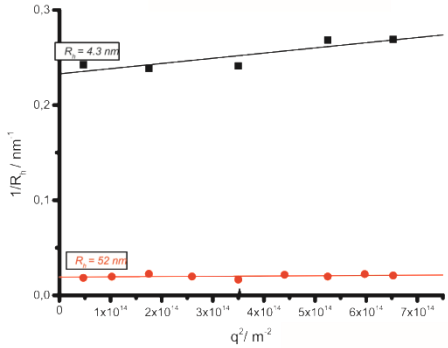

Figure 9.12. Plotted dynamic light scattering results to determine the hydrodynamic radius of the polymer 5 ($HPMA_{157}$-*s*-$GPMA_{13}$)-*b*-$APMA_{28}$ before and after the addition of siRNA in a $mass^{siRNA}/mass^{polymer}$ ratio of 1:100.

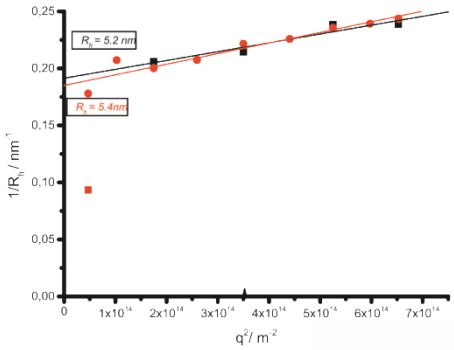

Figure 9.13. Plotted dynamic light scattering results to determine the hydrodynamic radius of the polymer 6 (HPMA$_{180}$-*s*-GPMA$_{12}$)-*b*-APMA$_{22}$ before and after the addition of siRNA in a mass^{siRNA}/mass^{polymer} ratio of 1:100.

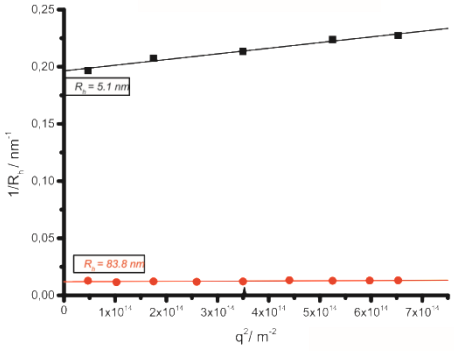

Figure 9.14. Plotted dynamic light scattering results to determine the hydrodynamic radius of the polymer 7 (HPMA$_{180}$-*s*-APMA$_{20}$)-*b*-GPMA$_{11}$ before and after the addition of siRNA in a mass^{siRNA}/mass^{polymer} ratio of 1:100.

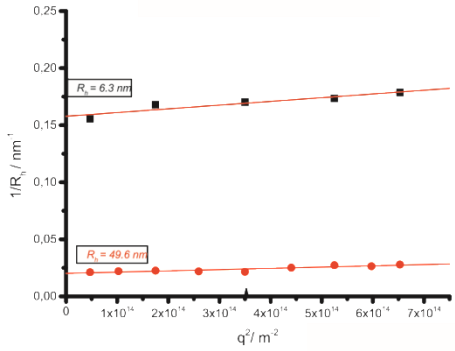

Figure 9.15. Plotted dynamic light scattering results to determine the hydrodynamic radius of the polymer 8 (HPMA$_{126}$-*s*-APMA$_{14}$)-*b*-GPMA$_{49}$ before and after the addition of siRNA in a mass^{siRNA}/mass^{polymer} ratio of 1:100.

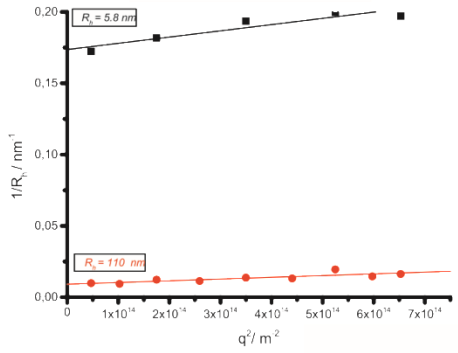

Figure 9.16. Plotted dynamic light scattering results to determine the hydrodynamic radius of the polymer 9 $HPMA_{150}$-*b*-$GPMA_{58}$ before and after the addition of siRNA in a mass^{siRNA}/mass^{polymer} ratio of 1:100.

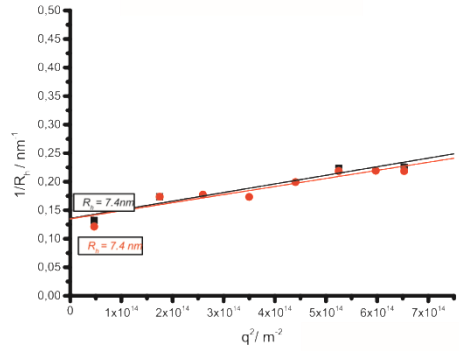

Figure 9.17. Plotted dynamic light scattering results to determine the hydrodynamic radius of the polymer 10 $HPMA_{196}$-*b*-$GPMA_{16}$ before and after the addition of siRNA in a mass^{siRNA}/mass^{polymer} ratio of 1:100.

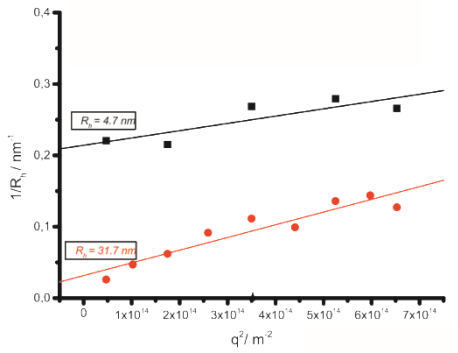

Figure 9.18. Plotted dynamic light scattering results to determine the hydrodynamic radius of the polymer 11 ($HPMA_{157}$-*s*-$GPMA_{13}$)-*b*-$GPMA_{27}$ before and after the addition of siRNA in a mass^{siRNA}/mass^{polymer} ratio of 1:100.

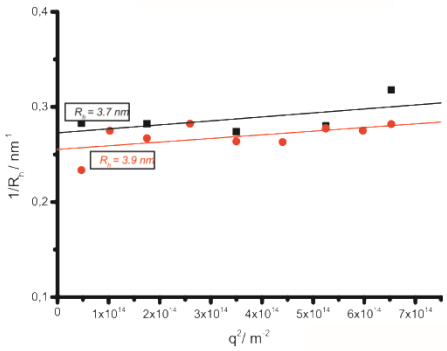

Figure 9.19. Plotted dynamic light scattering results to determine the hydrodynamic radius of the polymer 12 ($HPMA_{180}$-*s*-$GPMA_{12}$)-*b*-$GPMA_{22}$ before and after the addition of siRNA in a $mass^{siRNA}/mass^{polymer}$ ratio of 1:100.

9.7.2.2 Chapter 4

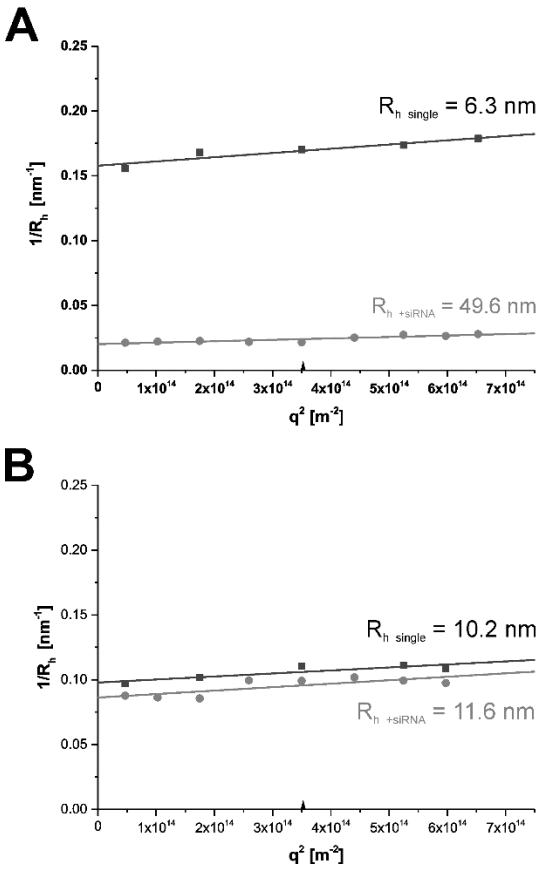

Figure 9.20. Plotted Dynamic Light Scattering results for the determination of the hydrodynamic radii of (A) ($HPMA_{126}$-*s*-$APMA_{14}$)-b-$GPMA_{49}$, (B) the TPP conjugate of ($HPMA_{126}$-*s*-APMA14)-b-$GPMA_{49}$ and the hydrodynamic radii of the complexes formed between the respective polymer structures and siRNA

9.7.3 NMR Spectroscopy

9.7.3.1 Chapter 3

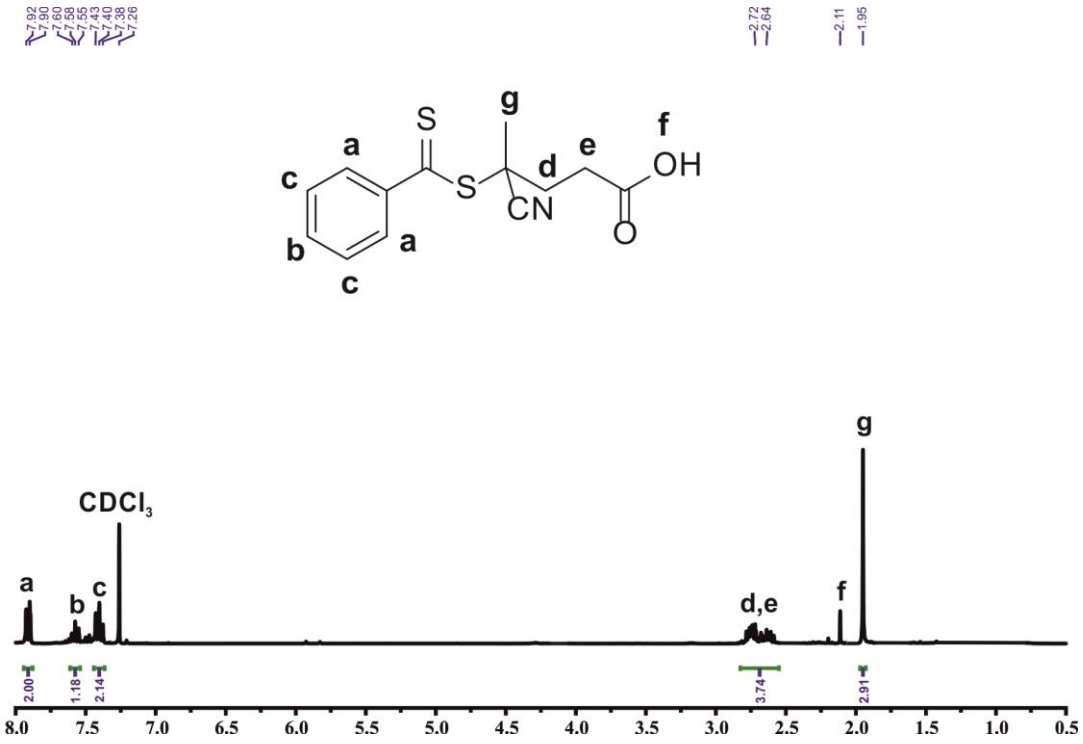

Figure 9.21. ^{1}H-NMR spectrum (300 MHz) of 4-cyano-4-((phenylcarbonothioyl)thio)pentanoic acid in $CDCl_3$ at ambient temperature

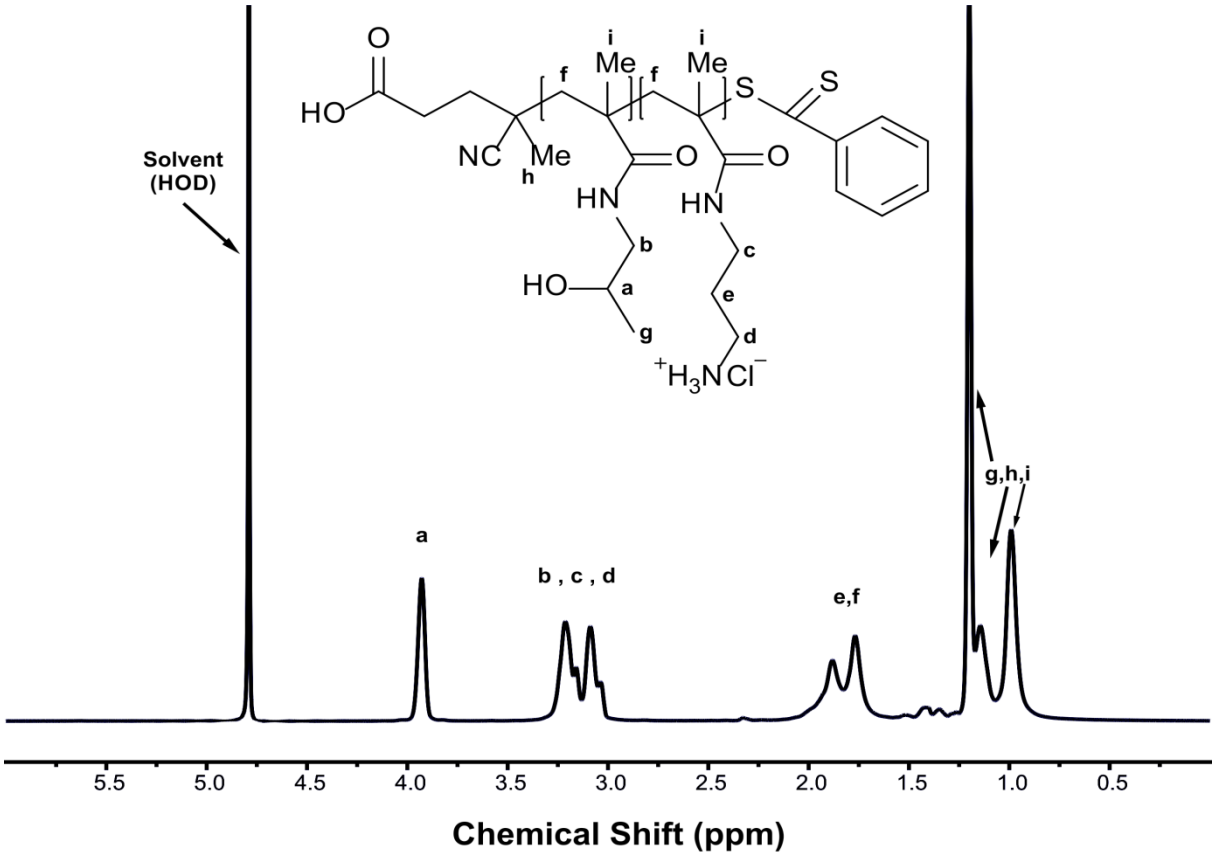

Figure 9.22. ^{1}H-NMR spectrum of ($HPMA_{180}$-s-$APMA_{20}$) in D_2O at 20 °C (700 MHz)

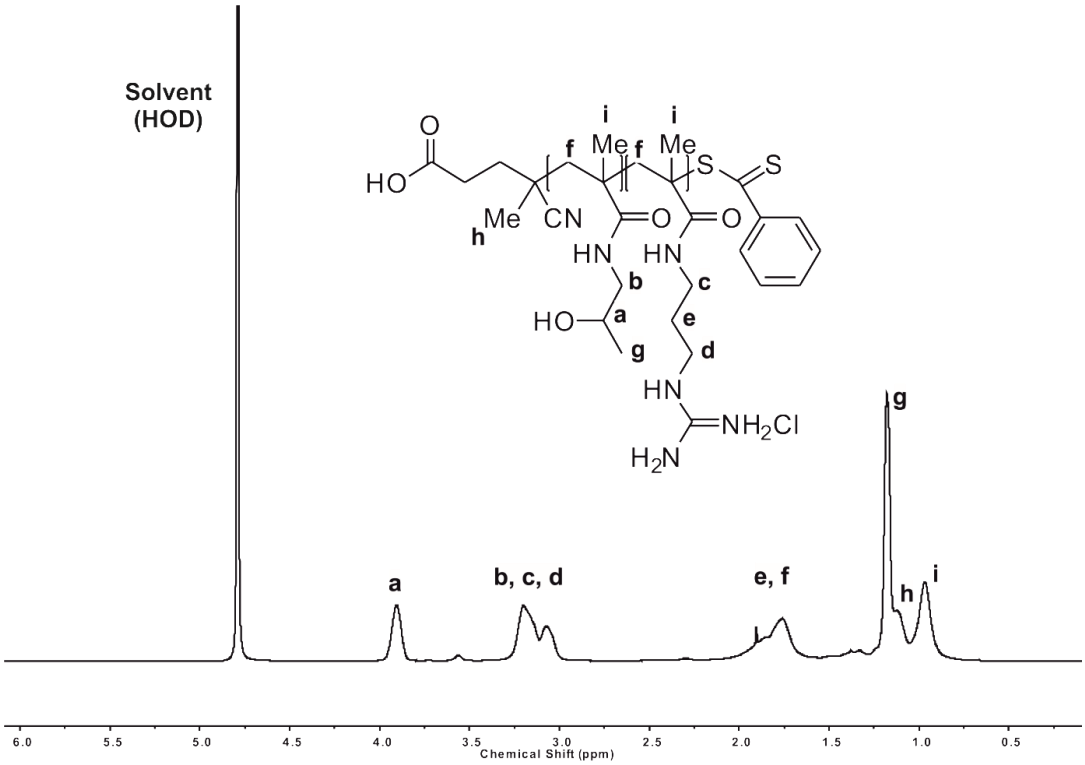

Figure 9.23. ^{1}H-NMR spectrum of ($HPMA_{157}$-s-$GPMA_{13}$) in D_2O at 25 °C (400 MHz)

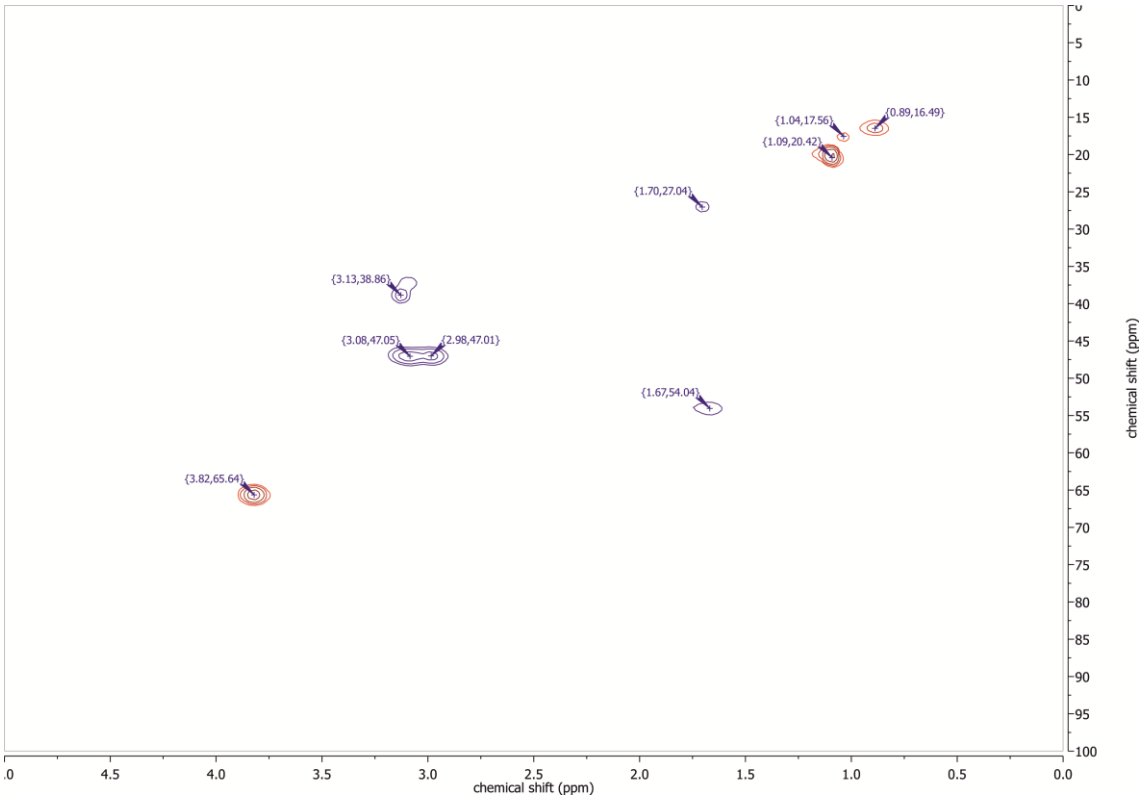

Figure 9.24. HSQC-NMR spectrum of ($HPMA_{157}$-s-$GPMA_{13}$) in D_2O at 297 K (400 MHz)

9.7.3.2 Chapter 4

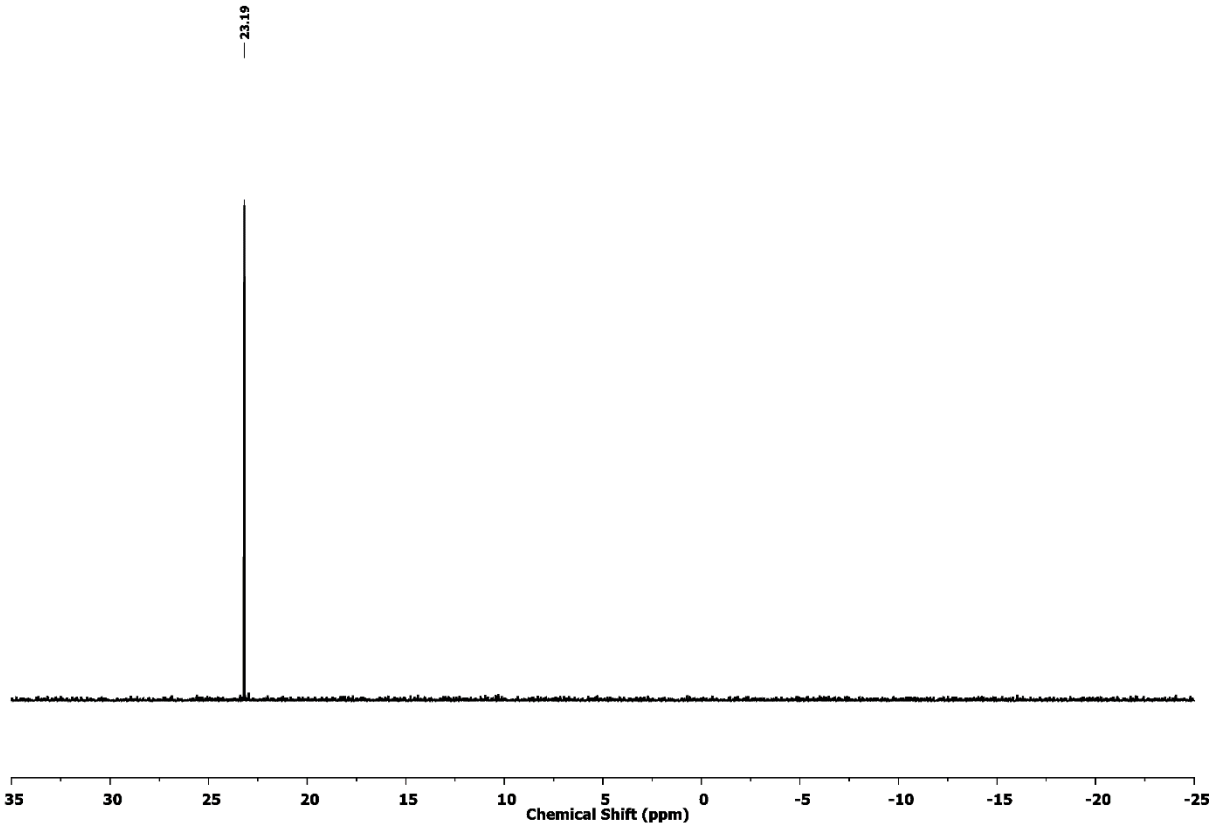

Figure 9.25. ^{31}P-NMR spectrum of (HPMA$_{126}$-s-APMA$_{14}$)-*TPP conjugate* in D_2O at 20°C (500 MHz)

9.7.3.3 Chapter 6

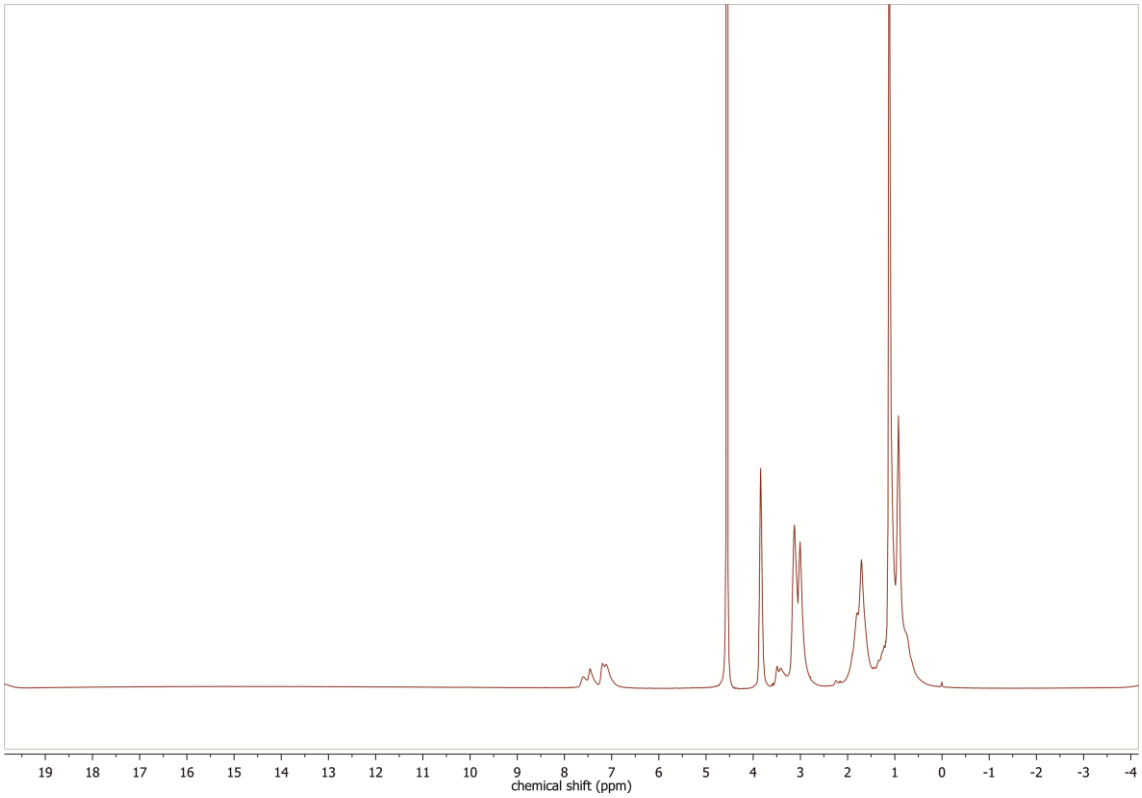

Figure 9.26. ^{1}H-NMR spectrum of HPMA$_{80\%}$-s-GPMA$_{10\%}$-s-IEMA$_{10\%}$ in D_2O at 313 K (600 MHz)

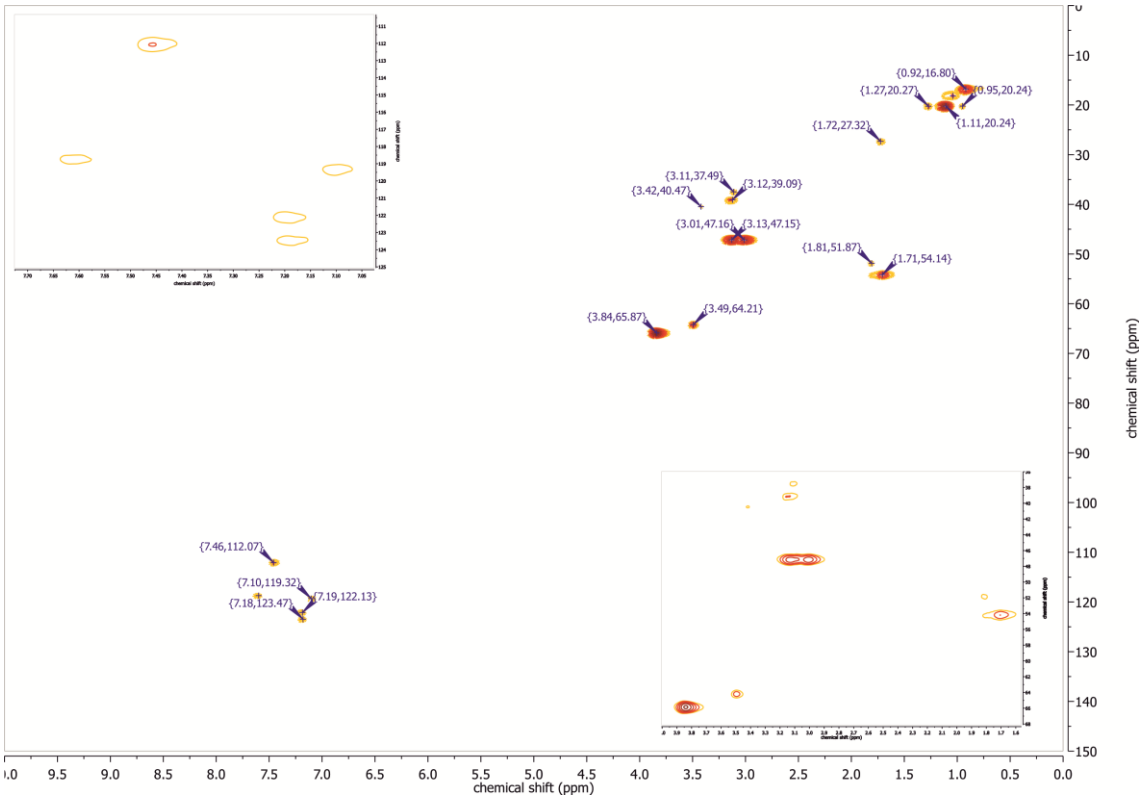

Figure 9.27. HSQC-NMR spectrum of $HPMA_{80\%}$-s-$GPMA_{10\%}$-s-$IEMA_{10\%}$ in D_2O at 313 K (600 MHz)

9.7.3.4 Chapter 7

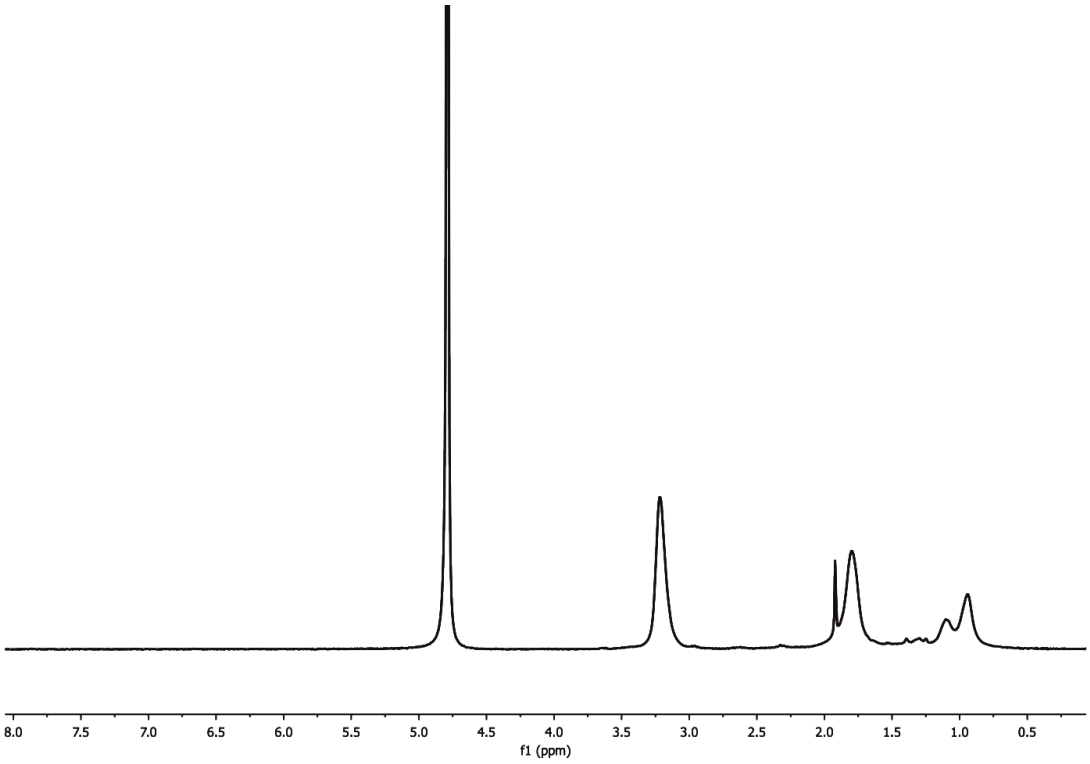

Figure 9.28. ^{1}H-NMR spectrum of PGPMA in D_2O at 298 K (300 MHz)

9.8 List of publications

1. The Guanidinium Group as a Key Part of Water-Soluble Polymer Carriers for siRNA Complexation and Protection against Degradation, **Ilja Tabujew**, Christoph Freidel, Bettina Krieg, Mark Helm, Kaloian Koynov, Klaus Müllen, Kalina Peneva, *Macromolecular Rapid Communications*, 2014, 35, 1191-1197.
2. CHAPTER 1 : Functionalization of Cationic Polymers for Drug Delivery Applications, **Ilja Tabujew** and Kalina Peneva, *Cationic Polymers in Regenerative Medicine* 2015, 1-29.
3. New Techniques to assess in vitro release of siRNA from nanoscale polyplexes, Bettina Krieg, Markus Hirsch, Erik Scholz, Lutz Nuhn, **Ilja Tabujew**, Heiko Bauer, Sandra Decker, Andriy Khobta, Manfred Schmidt, Wolfgang Tremel, Rudolf Zentel, Kalina Peneva, Kaloian Koynov, A. James Mason, Mark Helm, *Pharmaceutical Research* 2015, 32, (6), 1957-1974.
4. Cell-penetrating peptides for nanomedicine – how to choose the right peptide, **Ilja Tabujew**, Marco Lelle and Kalina Peneva, *BioNanoMaterials*, 2015, 16, (1), 59-72.
5. Overcoming drug resistance by cell-penetrating peptide- mediated delivery of a doxorubicin dimer with high DNA- binding affinity, Marco Lelle, Christoph Freidel, Stefka Kaloyanova, **Ilja Tabujew**, Alexander Schramm, Michael Musheev, Christof Niehrs, Klaus Müllen, and Kalina Peneva, *European Journal of Medicinal Chemistry*, 2017, 30, 336-345.
6. Ultra-sensitive detection of malathion using quantum dots-polymer based fluorescence aptasensor, Rajni Bala, Anuradha Swami, **Ilja Tabujew**, Kalina Peneva, Nishima Wangoo, Rohit K. Sharma, *Biosensors & Bioelectronics*, 2018, 104, 45-49.
7. Tackling the limitations of copolymeric siRNA delivery agents by a combined experimental-computational approach, **Ilja Tabujew**, Maziar Heidari, Christoph Freidel, Mark Helm, Lars Tebbe, Uwe Wolfrum, Kerstin Nagel-Wolfrum, Kaloian Koynov, Raffaello Potestio, Kalina Peneva, in preparation
8. Overcoming the Barrier of CD8+ T Cells: Two types of Nano-Sized Carriers for siRNA Transport, **Ilja Tabujew**, Marleen Willig, Nadine Leber, Christoph Freidel, Inka Negwer, Kaloian Koynov, Mark Helm, Katharina Landfester, Rudolf Zentel, Kalina Peneva, Volker Mailänder, in preparation
9. The influence of gradient and statistical arrangements of guanidinium or primary amine groups for poly(methacrylate) copolymers on their DNA binding affinity, **Ilja Tabujew**, Ceren Cokca, Leon Zartner, Ivo Nischang, Ulrich S. Schubert, Dagmar Fischer, Kalina Peneva, in preparation

List of figures

List of tables

Danksagung

Mein Dank gilt zuallererst meinem Doktorvater Prof. Dr. Klaus Müllen, der es mir ermöglichte in seiner Gruppe am Max-Planck-Institut für Polymerforschung auf diesem fordernden und faszinierenden Forschungsgebiet zu arbeiten. Seine stete Suche nach Perfektion und die hilfreichen Ratschläge waren für mich ein Quell der Motivation.

Ein herzlicher Dank gebührt ebenso meiner Betreuerin Prof. Dr. Kalina Peneva, die mir immerzu die nötigen Freiräume zur Umsetzung von Ideen gewährte. Die hier erreichten Ergebnisse wären ohne ihre motivierenden Worte und konstruktive Kritik nicht möglich gewesen.

Ich bin allen Kooperationspartnern für die ertragreiche Zusammenarbeit und die vielen unterstützenden Diskussionen dankbar. Mein Dank gilt besonders Prof. Dr. Mark Helm und Dr. Bettina Krieg vom Institut für Pharmazie und Biochemie der Johannes Gutenberg-Universität in Mainz; Prof. Dr. Uwe Wolfrum, Dr. Kerstin Nagel-Wolfrum und Dr. Lars Tebbe vom Fachbereich Biologie der Johannes Gutenberg-Universität in Mainz; Prof. Dr. med. Volker Mailänder und Dr. Marleen Willig, die sowohl an der Universitätsmedizin der Johannes Gutenberg-Universität als auch am Max-Planck-Institut für Polymerforschung wirkten; Prof. Dr. Dagmar Fischer und Leon Zartner von der biologisch-pharmazeutischen Fakultät der Friedrich-Schiller-Universität in Jena; Dr. Raffaello Potestio und Maziar Heidari, die die Computersimulationen in der Arbeitsgruppe von Prof. Dr. Kurt Kremer am Max-Planck-Institut für Polymerforschung durchführten. In diesem Zusammenhang möchte ich auch Prof. Dr. Rohit Kumar Sharma vom Fachbereich Chemie der Panjab Universität in indischen Chandigarh für die ergebnisreiche Zusammenarbeit danken.

Des Weiteren gilt mein Dank all jenen, die mich bei der Analyse und Charakterisierung der isolierten Substanzen unterstützt haben und mir beratend zur Seite standen. Hierbei sind besonders zu nennen: Dr. Hans-Joachim Räder und Stefan Türk von der Massenspektrometrie-Abteilung; Ceren Cokca und Dr. Ivo Nishang, die im Zentrum für Angewandte Forschung in Jena Molmassenbestimmungen mit der analytischen Ultrazentrifuge durchführten; Dr. Kristin Mohr und Christine Rosenauer für die Größenbestimmungen mittels dynamischer Lichtstreuung; Dr. Kaloian Koynov und Andreas Best für die Fluoreszenzkorrelationsspektroskopiemessungen; Friederike Pielenz, Gabriele Sentis, Dr. Peter Bellstedt, Stefan Spang, Petra Kindervater für die zahlreichen NMR-Messungen und Dr. Manfred Wagner, der viele lustige Stunden beim Fußball ermöglichte.

Ebenso bedanke ich mich bei allen Studenten, die durch Forschungspraktika einen unterstützenden Beitrag geleistet haben.

Zuletzt möchte ich mich beim gesamten jetzigen und früheren Arbeitskreis für die herzliche Atmosphäre sowie die schöne Zeit am Max-Planck-Institut bedanken. Besonderer Dank gebührt dabei Dr. Christoph Freidel und Dr. Stefka Kaloyanova für die anregenden fachlichen als auch nicht-fachlichen Gespräche vor dem Abzug und im Büro.